Guided Functional Re-Engineering of the Mitral Valve Leaflet

Lucrezia Morticelli
MEng

Submitted in accordance with the requirements for the degree of
Doctor of Philosophy

The University of Leeds

School of Mechanical Engineering
December 2013

The candidate confirms that the work submitted is her own, except where work which has formed part of jointly authored publications has been included. The contribution of the candidate and the other authors to this work has been explicitly indicated below. The candidate confirms that appropriate credit has been given within the thesis where reference has been made to the work of others.

Part of the work in Chapters 3 and 4 of the thesis has appeared in publication as follows:

Investigation of the suitability of decellularised porcine pericardium in mitral valve reconstruction (2013) Lucrezia Morticelli, Daniel Thomas, Nicholas Roberts, Eileen Ingham, Sotirios Korossis.

I was responsible for the majority of the experimental work described in the publication and also drafted the manuscript. The contribution of the other authors was to conception of the study (Korossis), experimental data on the biocompatibility and cell seeding of the decellularised pericardium (Thomas), technical training, guidance and assistance (Thomas; Roberts), advice on experimental design and analysis (Ingham) and final review and advice on the manuscript (Korossis and Ingham).

Acknowledgements

I would like to express my sincere gratitude to my supervisor Professor Eileen Ingham, thanks for being such a wise and talented scientist, and thanks for your endless guidance, friendship and moral support throughout my study. The same applies to Dr Sotirios Korossis; thanks for your invaluable knowledge, support and friendship, and thanks for giving me the opportunity of continuing my work in the tissue engineering field in your laboratory in Germany.

My deepest thanks go also to Dr Daniel Thomas, my lab tutor; thanks for your endless moral support and guidance and thanks for answering my continuous questions. The time you spent helping me with my work with the bioreactor is unforgettable, you never left me alone during that challenging and hard time!

Professor Eileen Ingham, Dr Sotirios Korossis and Dr Daniel Thomas have been like a family to me, during my nice time spent at Leeds.

My sincere thanks also go to Professor John Fisher, thanks for the precious instructions and advice you gave me during my work with the bioreactor, your support has been crucial for the completion of the final experiments.

This thesis would not have been possible without the help, support and patience of these great four scientists mentioned above!

I would like to thank Dr Nagitha Wijayathunga and Mr Irvin Homan for their continuous support with the ordering of the tissue needed for my experiments; my deepest thanks also go to Mr Lee Wetherill, Mr Philip Wood and Mr Keith Dyer for their constant technical support, especially with the mechanical design and manufacture of the equipment I needed. Thanks also to Mrs Amisha Desai and Dr Nicholas Roberts for their support when working with the mechanical testing device.

My deepest thanks also go to our great technicians at Professor Ingham's lab, Fiona, Natalie and Laura, (now PhD student), thanks for your help and support during the last experiments with the bioreactor, your help has been essential for the completion of the work for my PhD.

Thanks to everybody from Professor Ingham's lab, especially thanks to Iraklis, Blessing, Ji and Tay for answering my questions and for their kind assistance during this project.

Thanks to all the friends and collegues at iMBE: Raman, Vassilis, Eirini, Carly, Hazel, Caroline, Nic, Jahid, Normalina, Lindsey, Silvia, Serena, Halina and many others, you have been like a big family to me and you made my time at Leeds special! Special thanks to Carly for introducing me to the great world of UK culture and for being a friend during hard and good times!

I would like to thank my amazing Italian friends both at Leeds and in Turin, my hometown, thanks for your moral support, I would not have enjoyed my time at Leeds as much as I did without your support. I would like to extend my thanks to my new friends and collegues in Germany, thanks for supporting me during the writing up of my PhD thesis.

I would like to thank Vj, my flatmate, for being such a great friend, you were always there, in the hard and happy times!

I wish to thank my family, my mother and my father for their moral and financial support and in particular my sister Annalisa, thanks for being such a great sister, a great and wise woman and thanks for your constant moral support, without you all this would never have been possible!

I also would like to thank my wonderful boyfriend, Daniele, your love and encouragement allowed me to finish this journey. Thanks for being there sharing my tears and my joy, in every moment!

Also, I would like to thank Marisa, Pia and Professor Mario Calderale, our family friends for their moral support and motivation.

Thanks to all of you for sharing the hard and the happy moments, you made this experience wonderful and possible! Thank you!

Abstract

Valvular heart disease is a major cause of mortality worldwide. Mitral valve regurgitation represents the second major valvular disorder in the western world. Current strategies for mitral valve reconstruction are imperfect. The aim of this study was to investigate the tissue engineering of mitral valve leaflets for mitral valve leaflets reconstruction. The approach taken was to utilise decellularised porcine pericardium seeded with porcine mesenchymal stem cells (pMSCs) and to mechanically condition the cell seeded constructs using biaxial strain in a bespoke bioreactor.

The biomechanical and biological properties of porcine mitral valve leaflets and native and decellularised porcine pericardium were studied for comparative purposes. The porcine pericardium was decellularised using a propriety method based upon low concentration sodium dodecyl sulphate (SDS) and proteinase inhibitors. Histological characterisation showed the four and three layered structure of leaflets and fresh/decellularised pericardium, respectively. Histological analysis of decellularised pericardium did not reveal any remaining cells. Moreover, the histoarchitecture of collagen and elastic fibres appeared to be well preserved. Biochemical analysis showed that the mitral valve leaflets and the fresh pericardium had hydroxyproline and glycosaminoglycan (GAG) contents similar to those reported in the literature. Decellularised pericardium had higher hydroxyproline content than that of fresh pericardium but lower GAG content. The levels of deoxyribonucleic acid (DNA) in fresh and decellularised pericardium were determined and this showed that there was a 99% reduction in the DNA content following decellularisation. *In vitro* biocompatibility studies showed that the decellularised pericardium was not cytotoxic to porcine skin fibroblasts and pMSCs. Biomechanical properties were determined using low strain rate uniaxial loading to failure. Both fresh and decellularised pericardium demonstrated rather isotropic behaviours, possessing similar mechanical properties along the two orthogonal directions studied. Anterior leaflet specimens cut circumferentially were stiffer than those cut radially and the posterior leaflets. This anisotropic mechanical behaviour of the anterior leaflet was related to the main orientation of the collagen fibres along the circumferential direction. Conversely, the posterior leaflets were more isotropic.

The optimum seeding density for culturing decellularised pericardial samples was 1×10^5 cells$\cdot$cm^{-2} for pMSCs and the ideal time for culturing prior to loading the reseeded scaffold in

the bioreactor stations was 3 days. With regards to fibroblasts and porcine smooth muscle cells (pSMCs), the optimum seeding density was 2×10^5 cells·cm^{-2} at 1 week culture for fibroblasts, whereas pSMCs had the tendency of forming agglomerates on the surface of tissue rather than penetrating throughout the thickness of the scaffold, thus, they were not considered ideal for remodelling the histoarchitecture of tissue during dynamic experiments.

The actuator of the bioreactor was calibrated and the general set up of the system was completed. Suitable conditions to apply during static culture in the bioreactor, in terms of oxygen and pH control, in order to maintain the ECM integrity and cell viability in the bioreactor, were initially determined using fresh pericardium, however this proved problematic due to the variability in the tissue that was available.

One day static experiment performed with the bioreactor by using decellularised pericardium reseeded with pMSCs showed that there was no difference in terms of viability when keeping the tissue statically in the tissue holders and in the bioreactor stations. Thus, tissue holders could be used as positive static controls during dynamic experiments.

One day dynamic experiments (10% strain) performed with the bioreactor by using decellularised pericardium reseeded with pMSCs showed that cells were viable both when kept dynamically in the bioreactor and statically in the tissue holders. Cells started aligning along specific directions when kept dynamically in the bioreactor.

Overall porcine mitral valve leaflets and porcine fresh/decellularised pericardium shared similar histoarchitectures, but had different biochemical composition and biomechanics. Decellularised pericardium was shown to be an optimum material for cell repopulation, delivering the necessary biological and biomechanical cues to seeded cells. The bioreactor was optimised for both static and dynamic culture and is now ready for further investigation at longer time points. This research provided the basics into the optimal strategy for mechanostimulation of cell-seeded pericardial scaffolds *in vitro* in order to generate heart-valve like tissue.

Table of Contents

List of Tables

List of Figures

List of Abbreviations

aVICs	Activated valve interstitial cells
ATP	Adenosine triphosphate
Alcian blue-PAS	Alcian blue-periodic acid-Schiff
ANOVA	Analysis of variance
LA	Anterior mitral valve leaflets
AV	Atrioventricular
α-SMA	α-smooth muscle actin
CVS	Cardiovascular system
cm	Centimetre
CHAPS	3-[(3-cholamidopropyl)dimethylammonio]-1-propanesulfonate
C.I.	Confidence interval
DPO	Decellularised pericardium orthogonal to the collagen fibres alignment
DPP	Decellularised pericardium parallel to the collagen fibres alignment
DNAse	Deoxyribonuclease I
DNA	Deoxyribonucleic acid
DMSO	Dimethyl sulfoxide
DMEM	Dulbecco's Modified Eagle Medium
ECs	Endothelial cells
EPCs	Endothelial progenitor cells
EMT	Endothelial-to-mesenchymal transformation
ESEM	Environmental scanning electron microscopy
EDTA	Ethylenediaminetetraactic acid
ePTFE	Expanded polytetrafluoethylene
ECM	Extracellular matrix
FBS	Foetal bovine serum
FBA	Fresh blood agar
FP	Fresh porcine pericardium
FTE	Functional tissue engineering
α-gal	Galα1,3-Galβ1-4GlcNAc-R
GAG	Glycosaminoglycan

GFs	Growth factors
H&E	Haematoxylin & eosin
h	Hour
HEPES	Hydroxyethyl-piperazineethane-sulfonic acid buffer
HXP	Hydroxyproline
iPCs	Induced pluripotent stem cells
ICs	Interstitial cells
LAC	Leaflet anterior along the circumferential direction
LAR	Leaflet anterior along the radial direction
LPC	Leaflet posterior along the circumferential direction
LPR	Leaflet posterior along the radial direction
LV	Left ventricular
MIT	Massachusetts Institute of Technology
MMPs	Matrix metalloproteinases
MS	Mean square
MSCs	Mesenchymal stem cells
ml	Millilitre
mm	Millimiter
MSD	Minimum significant difference
min	Minute
MV	Mitral valve
MVP	Mitral valve prolapse
MVR	Mitral valve regurgitation
MVS	Mitral valve stenosis
M	Molarity
MTT	3-(4,5-Dimethylthiazol-2-yl)-2,5-diphenyltetrazolium bromide
NBF	Neutral buffer formalin
NA	Nutrient agar
obVICs	Osteoblastic valve interstitial cells
PAA	Peracetic acid
PO	Pericardium orthogonal to the collagen fibred alignment
PP	Pericardium parallel to the collagen fibres alignment

PBS	Phosphate buffered saline
P4HB	Poly 4-hydroxybutyrate
PGLA/PGA	Poly(lactide-co-glycolide)/polyglycolic acid
PGA	Polyglycolic acid
PGA/PLLA	Polyglycolic acid/ poly L-lactic acid
PGA/PLA	Polyglycolic acid/ polylactic acid
PLA	Polylactic acid
PDVF	Polyvinylidene fluoride
PERV	Porcine endogeneous retrovirus
pMSCs	Porcine mesenchymal stem cells
pSMCs	Porcine smooth muscle cells
LP	Posterior mitral valve leaflets
lb. sq. in.	Pound per square inch
pVICs	Progenitor valve interstitial cells
qVICs	Quiescent valve interstitial cells
r	Radius
RNAse	Ribonuclease I
RNA	Ribonucleic acid
SAB	Sabouraud agar
SVR	Saddle height ratios
SEM	Scanning electron microscopy
s	Second
SA	Sinoatrial
SMCs	Smooth muscle cells
SDS	Sodium dodecyl sulphate
SE	Standard error
SB-10	Sulfobetaine-10
SB-16	Sulfobetaine-16
3D	Three dimensional
TE	Tissue engineering
TIMPs	Tissue inhibitors of metalloproteinases
TGF-β1	Transforming growth factor beta-1

TVPs	Transvalvular pressures
TBS	Tris buffered saline
UTS	Ultimate tensile strength
VECs	Valve endothelial cells
VICs	Valve interstitial cells

Chapter 1

Introduction & literature review

1.1 Introduction

Valvular disease represents one of the major causes of mortality worldwide, causing disability, reduced quality of life, and early mortality (Chockalingam *et al*., 2004; Otto and Bonow, 2009). Valvular disease is most commonly manifested by two dysfunctional effects; valvular stenosis, which occurs when the valve opening is smaller than normal due to stiff or fused leaflets, and valvular deficiency, also called regurgitation, which occurs when a valve leaflets do not close tightly. In the United States alone, there are roughly 100,000 valve replacement or repair operations each year, and 20,000 valvular-disease-related deaths (Otto and Bonow, 2009). Mitral valve (MV) regurgitation represents the second major valvular disorder in the Western world, after aortic valve dysfunction (Otto and Bonow, 2009). Current treatment strategies for MV dysfunction include MV repair and replacement. Repair is the gold standard and usually employs synthetic biomaterials, such as expanded polytetrafluoethylene (ePTFE), for chordal reconstruction, or chemically-treated xenograft tissue, such as pericardium, for annular, cuspal or chordal reconstruction (Salati *et al*., 1997; Bevilaqua *et al*., 2003; Acar *et al*., 2004; David et al., 2013). Both approaches only deliver inert or biocompatible material solutions that cannot regenerate or grow with the patient. In addition, glutaraldehyde-treated tissue with cell remnants will calcify, become rigid and eventually degenerate (Boskey, 1981). Ideally, surgeons would prefer autologous tissue since it will retain viability and regenerate. In most cases, however, autologous tissue is not available, and even if it is available, this is not an ideal solution since it involves the sacrifice of the patient's healthy pericardium. Although less advantageous than repair, valve replacement with bioprosthetic, mechanical or homograft valves have also been employed for MV dysfunction (Moon *et al*., 2001). However, this approach is associated with limited durability of the bioprostheses, the need for anticoagulation with the mechanical valves and the limited availability and immunogenicity of the homograft mitral apparatus (Chauvaud *et al*., 2003).

The disadvantages associated with the current strategies for MV repair and replacement, have motivated the investigation of new approaches for the treatment of MV dysfunction.

Tissue engineering (TE) has recently emerged as an exciting alternative to conventional strategies for valvular repair and replacement. The ultimate goal of TE is to develop implants, which will not only be fully compatible, but will also be able to grow (in the young patient), remodel and regenerate *in vivo*. In general, there are two main TE strategies, namely *in vivo* TE and *in vitro* TE. *In vivo* TE involves the use of bioresorbable scaffolds that rely on the patient's cellular response *in vivo*, with the intention of developing functionality after implantation. *In vitro* TE, or functional TE (FTE), employs scaffolds that are seeded with autologous cells *in vitro*, and physically conditioned with a view to producing *in-vivo*-equivalent functionality prior to implantation. In this fashion, FTE simulates the type of physical environment that native tissues encounter in the body with a view to engineering functional constructs in the laboratory. The development of FTE simulation systems for the growth of tissues in response to physiological mechanical stimulation has the potential not only to provide alternative strategies for tissue reconstructions, but also important model systems for the enhancement of understanding into mechanotransduction, the process by which the cells transduce mechanical stresses into biochemical signals to regulate their function (Ulbricht *et al.*, 2013).

The aim of this study was to develop, optimise and evaluate FTE simulation models for the future development of MV-leaflet-equivalents for MV reparative surgery. The approach adopted was to utilise decellularised porcine pericardium seeded with porcine mesenchymal stem cells (pMSCs). The long term strategy was envisaged as the production of decellularised xenogeneic donor pericardial scaffolds seeded with the patient's own MSCs, isolated from the bone marrow, and mechanically conditioned in the bioreactor, to allow for the remodelling of the scaffold in order to obtain a MV-leaflet-equivalent tissue prior to implantation. Human cells were not used in this study due to the limited availability of human tissue.

The biomechanical and biological properties of porcine MV leaflets were studied with a view to understanding the histoarchitectural, biomechanical and functional requirements of the TE constructs. The properties of native and decellularised porcine pericardium were also studied to assess the effects of decellularisation on the histoarchitecture, biomechanics and function of the pericardium, as well as to assess the suitability of pericardium for MV leaflet repair. Subsequently, the optimum conditions for seeding the pericardial scaffolds with pMSCs were investigated in static cultures. The pMSCs-seeded scaffolds were then dynamically cultured in

the bioreactor, with a view to investigating the effect of MV-relevant stimuli on the function and morphology of the pMSCs, and on the histoarchitecture of the TE constructs.

1.2 Literature review

1.2.1 The cardiovascular system

The cardiovascular system (CVS) consists of the heart and the blood vessels; from the arteries, arterioles, and capillaries, to the venules and veins. The heart and blood vessels transport nutrients to and remove waste products from the cells. In particular, the CVS is responsible for the rapid convective transport of oxygen, glucose, amino acids, fatty acids, vitamins, drugs and water to the tissues, and the rapid washout of metabolic waste products such as carbon dioxide, urea (soluble compound) and creatinine (the anhydride of creatine).

The heart consists of two intermittent muscular pumps; the right and left ventricles. Each pump is filled from a contractile reservoir; the right or left atrium. The right ventricle pumps deoxygenated blood through the pulmonary artery to the lungs. The pulmonary veins return oxygenated blood from the lungs to the left side of the heart, completing the pulmonary circulation. The left ventricle pumps out an equal volume of oxygenated blood to the rest of the body. Deoxygenated blood returns to the right atrium of the heart via the two main veins, the superior and inferior vena cava, to complete the systemic circulation (Figure 1.1), (Levick, 2003; Martini and Nath, 2009; Tortora and Nelsen, 2009).

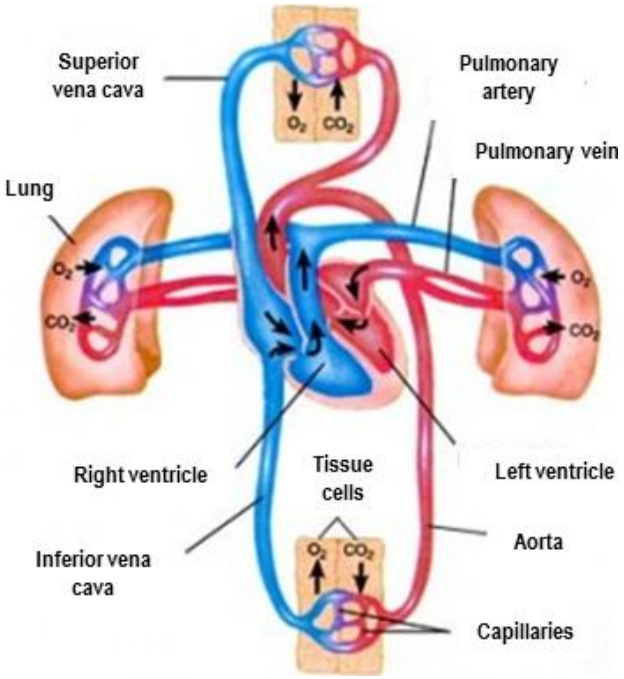

Figure 1.1: The pulmonary and systemic circulation. From http://nursingcrib.com/nursing-notes-reviewer/maternal-child-health/from-fetal-circulation-to-pulmonary-circulation/ (accessed on 05/11/2013).

1.2.2 Anatomy, structure & function of the heart

The human heart is a cone-shaped muscle of around 12 cm long and 9 cm wide (Levick, 2003). Unlike most other muscles in the body, the heart never rests. It beats approximately 100,000 times each day pumping roughly 8000 litres of blood (Martini and Nath, 2009). The heart consists of four muscular chambers; the left and right atrium, and the left and right ventricle (Figure 1.2). It lies obliquely across the midline of the chest, with the tip of the cone (apex) located directly posterior to the sternum. The apex moves mainly during the contraction producing the heartbeat (apex beat) that is felt through the chest wall.

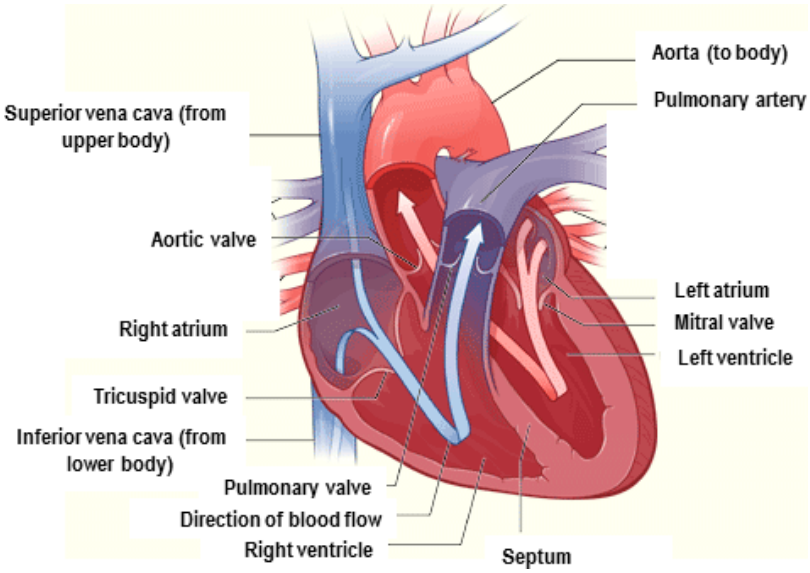

Figure 1.2: The human heart. Adapted from: http://planetearth.nerc.ac.uk/news/story.aspx?id=369 (accessed on 05/11/2013).

The atria and the ventricles are separated by muscular partitions, called septa; the atria by the inter-atrial septum, and the ventricles by the much thicker inter-ventricular septum. The atria and ventricles of each side of the heart communicate via the atrioventricular (AV) valves (tricuspid valve and mitral valve). The AV valves permit the unidirectional blood flow from the atria to the ventricles (Martini and Nath, 2009). Blood passes from the right atrium into the right ventricle through the tricuspid AV valve, which is composed of three fibrous cusps or leaflets. The tricuspid valve closes when the right ventricle contracts, preventing the backflow of blood into the right atrium. The blood exits the right ventricle into the pulmonary circulation through the pulmonary valve, or pulmonary semilunar valve, which is located at the superior part of the right ventricle. The left atrium receives blood from the lungs via the pulmonary veins. The left AV valve, or bicuspid valve, or mitral valve (MV), regulates the blood inflow from the pulmonary circulation into the left heart, allowing blood from the left atrium into the left ventricle and also preventing the backflow of blood to the left atrium during systole.

The left ventricle is the thickest part of the heart (averaging 10 - 15 mm thickness) and it forms the apex of the heart. Similarly to the right ventricle, the left ventricle accommodates the papillary muscles, which are active muscular extensions in the internal wall of the ventricles, and anchor the AV leaflets via the chordae tendineae. The latter are tendinous structures that act in a similar manner to the strings of a parachute, preventing the AV leaflets from overshooting (prolapse) into the atria during ventricular contraction. The blood exits the left

ventricle through the aortic valve, entering the largest artery of the body, the ascending aorta. Some of the blood in the aorta flows into the coronary arteries, carrying blood to the myocardium (Tortora and Nelsen, 2009). The four heart valves are illustrated in Figure 1.3.

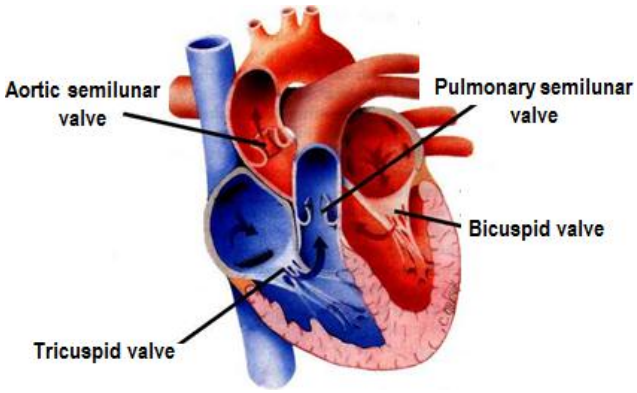

Figure 1.3: The four heart valves acting in the human heart. Modified from http://www.indiana.edu/~nimsmsf/P215/p215notes/LabManual/Lab10.pdf (accessed on 05/11/2013).

1.2.3 The pericardium

The pericardium is the membrane that surrounds and protects the heart. It restricts the heart in its position, allowing at the same time sufficient freedom of movement for strong and rapid contraction. The pericardium can be divided in two main portions: the fibrous and serous pericardium (Figure 1.4). The superficial fibrous pericardium is a tough, inelastic, dense and irregular connective tissue, which resembles a bag attached to the diaphragm. The fibrous pericardium prevents overstretching of the heart, and provides protection and anchoring of the heart to the mediastinum.

The deeper serous pericardium is a thinner and more delicate membrane that forms a double layer around the heart. The serous pericardium is in turn divided into three main components; the parietal layer, pericardial cavity and visceral layer. The outer parietal layer is fused to the fibrous pericardium. The inner visceral layer, also called the epicardium, adheres tightly to the heart and consists of the mesothelium (cell layer of mesodermal origin) and an underlying layer of areolar connective tissue, attached to the myocardium. Between the parietal and visceral layers is the pericardial cavity that contains a thin film of lubricating fluid. This fluid is known as pericardial fluid and it is secreted by the pericardial cells (Tortora and Nelsen, 2009).

The differentiation among the layers varies in the literature. In a study by Mirsadraee (2005), the parietal pericardium is referred to as the fibrous layer and the parietal layer considered together. The study described the parietal pericardium as a sac consisting microscopically of three layers (Figure 1.5). These layers included: the serosa, consisting of a layer of mesothelial cells and a narrow submesothelial space, the middle thick fibrosa, containing variously oriented layers of collagen fibrils and small elastic fibres, and the outer epipericardial layer, containing mainly large bundles of collagen (Ishihara *et al.*, 1980). In this thesis, the definition of parietal pericardium described by Mirsadraee (2005) is used.

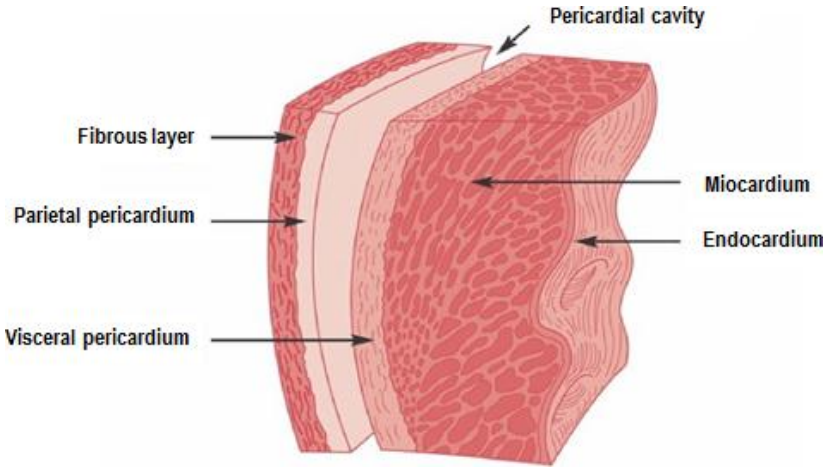

Figure 1.4: The human pericardium. Adapted from Martini and Nath (2009).

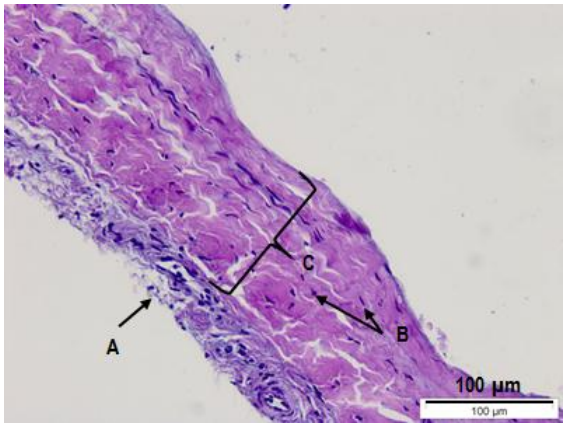

Figure 1.5: Alcian blue-periodic acid-Schiff (PAS) staining of a human parietal pericardium sample isolated along the direction of the collagen fibres. A: Mesothelial layer and cells; B: Connective tissue cells; C: Fibrosa and epipericardial layers. Scale bar indicates 100 µm.

1.2.4 Heart physiology & the cardiac cycle

Every heart beat is a single cardiac contraction during which the entire heart contracts in series (first the atria and then the ventricles). The heart beat is initiated by an electrical system within the heart called the sinoatrial (SA) node which discharges spontaneously at regular intervals (Figure 1.6). This system is composed of modified cardiomyocytes, not nervous tissue (Levick, 2003). The electrical discharge reaches the atrioventricular (AV) node from which, the electrical impulse reaches the ventricular wall. The period between the start of one heartbeat and the start of the next is called the cardiac cycle. The cardiac cycle includes alternating periods of contraction and relaxation. For each chamber of the heart, the cardiac cycle can be described into two phases; systole and diastole (Figure 1.7).

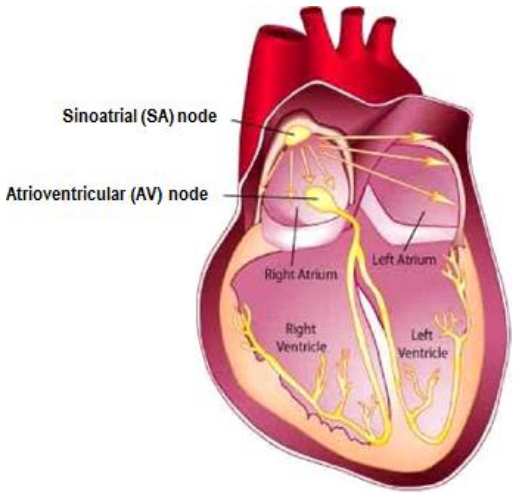

Figure 1.6: The conducting system of the heart. The stimulus is generated in the SA node, then it is propagated to the AV node via the atria and then spreads into the ventricles. Adapted from: http://www.mda.org/publications/quest/q123edmd.html (accessed on 05/11/2013).

Systole represents the contraction during which the chamber contracts and pushes blood into the adjacent artery (pulmonary or aorta). Diastole represents the relaxation during which the ventricles fill with blood from the atria and prepare for the next cardiac cycle. During the cardiac cycle the pressure within each chamber rises during systole and falls during diastole. The valves between adjacent chambers ensure the unidirectional flow of blood from one chamber to the next when the pressure in the first chamber exceeds the one in the second. Although the pressure is lower in the right atrium and right ventricle, both sides of the heart contract at the same time, and they eject equal volumes of blood.

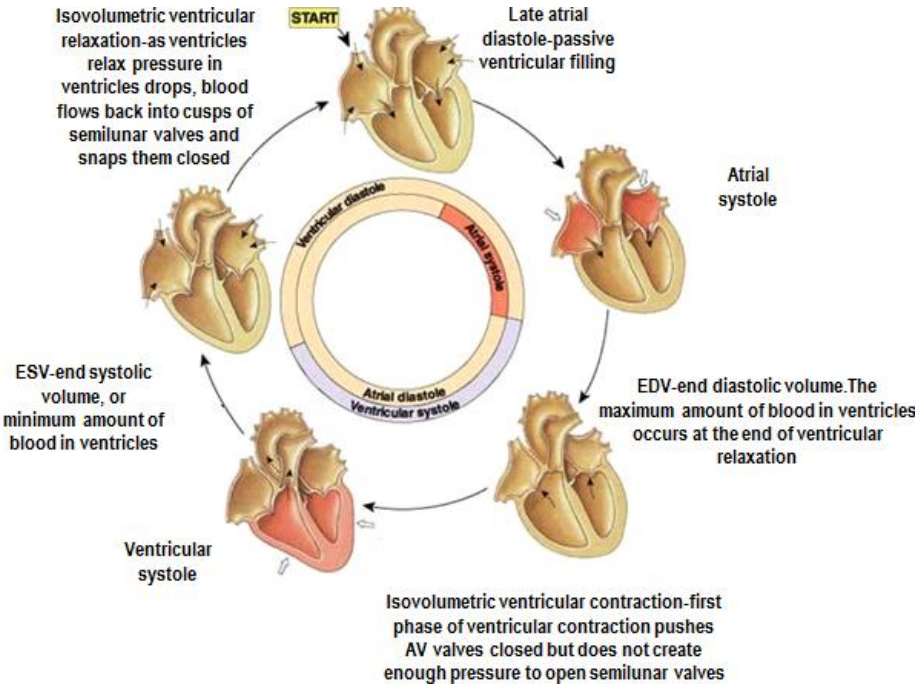

Figure 1.7: The cardiac cycle. Description of the four phases of the cardiac cycle: atrial systole, atrial diastole, ventricular systole and ventricular diastole. Modified from Martini and Nath (2009).

The cardiac cycle begins with the atrial systole, during which the atrial pressure raises pushing blood into the ventricles through the open AV valves. At start of atrial systole, the ventricles are already filled to about 70 per cent of their normal capacity, due to the passive blood flowing during the end of the previous cardiac cycle. Following the atrial systole, the atrial diastole and the ventricular systole begin. During ventricular systole, the pressure in the ventricles rises above the one in the atria, causing the AV valves to close. When the ventricular pressure exceeds that in the arterial trunks, the semilunar valves open and blood flows into the pulmonary and aortic trunks. At the end of the ventricular systole, there is a rapid fall of the ventricular pressure. Blood in the aorta and pulmonary trunk flows back towards the ventricles, causing the semilunar valves to start closing, and a gradual decrease in the aortic and pulmonary pressure. Subsequently, the ventricular diastole starts and is followed by the atrial systole of the next cycle.

1.2.5 The mitral valve

The MV is situated between the left atrium and left ventricle and its function is to direct the blood flow from the left atrium towards the left ventricle. Its orifice is smaller than the tricuspid

orifice, with a mean circumference of 9 cm in males and 7.2 cm in females. When the leaflets of the MV close, they form a single coaptation zone.

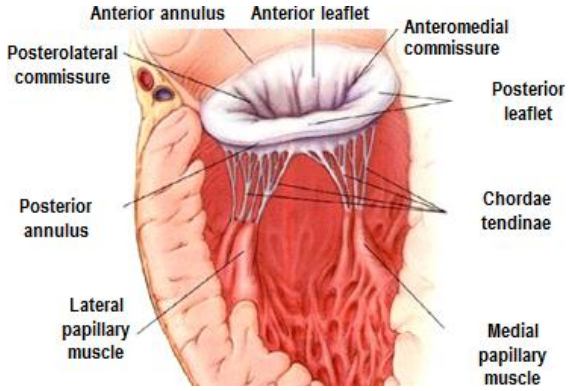

Figure 1.8: Anatomy of the mitral valve. Adapted from http://www.heart-valve-surgery.com/heart-surgery-blog/2008/09/02/mitral-valve-annulus-definition-diagrams-prolapse-calcification-treatment/ (accessed on 05/11/2013).

There are two valve commissures, or junctional zones, between the leaflets of the normal MV, which resemble deep folds in the leaflets. These include the anteromedial and the posterolateral commissures (Figure 1.8). The MV annulus is made of fibrocollagenous elements of varying consistency from which the fibrous core of the leaflet (fibrosa) originates. This architecture allows for significant changes in the shape and dimensions of the annulus at different stages of the cardiac cycle, which ensure valve competence (Gray, 2008). The two MV leaflets constitute a veil, which is attached around the circumference of the mitral annulus. Although the MV leaflets are more like a single continuous leaflet, they are usually referred to as the anterior and posterior leaflets. On the ventricular side, the leaflets have a “rough” zone which includes the insertions of the chordae tendinae to the leaflet tissue. Between the “rough” zone and the annulus, there is a macroscopically “smooth” leaflet zone, free of chordae insertions, whose fibrous core incorporates extensions attached to the rough zone. During passive ventricular filling and atrial systole, the smooth atrial surface of the anterior leaflet is important in directing the blood towards the ventricle body and apex. The posterior leaflet has a longer attachment to the annulus than the anterior leaflet. From the papillary muscle, the chordae attach to the free edge of the leaflets. The two MV papillary muscles vary in length and width and may be bifid. The chordae tendinae usually arise from the tip and apical zone of each papillary muscle, but sometimes originate from near their base.

The principal components of the extracellular matrix (ECM) of the MV leaflets are collagen (60%), elastin (10%) and proteoglycans (20%) (Kunzelman *et al.*, 1993a). Each component contributes to the valve's unique physical properties. Collagen provides mechanical strength and it is predominantly type I and III (74% and 24%) with 2% of type V (Cole *et al.*, 1984). The collagen fibres are surrounded by an elastin matrix, which provides interconnections between the collagen (Scott and Vesely, 1995). These fibres can withstand high tensile forces, with low torsional and flexural stiffness. The fibres are oriented along the circumferential direction in which the tissue is able to withstand the greatest tensile stresses (Sacks and Yoganathan, 2007). The glycosaminoglycan (GAG) side-chains of proteoglycans are negatively charged leading to a significant water-binding capacity and the formation of a porous gel. An important function is the ability to resist compressive forces (Culav *et al*., 1999). These components constitute the four layers of the leaflet, including the atrialis, spongiosa, fibrosa and ventricularis (Gross and Kugel, 1931; Kunzelman *et al*., 1993a; Flanagan and Pandit, 2003). The arrangement of these layers is different between the semilunar and AV valves. In particular, the AV valves possess an additional layer called atrialis (Flanagan and Pandit, 2003), (Figure 1.9).

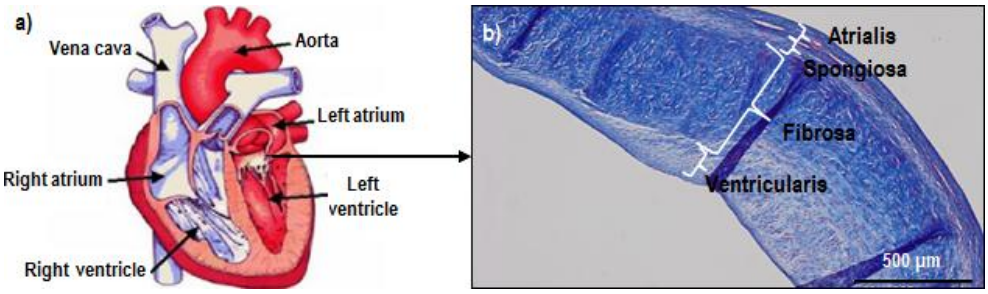

Figure 1.9: MV location (a) and Masson's trichrome staining of anterior leaflet (radial) (b). Collagen stained blue, blood vessels and cytoplasm stained red). Scale bar indicates 500 µm. (a) Modified from: http://www.drugdevelopmenttechnology.com/projects/xarelto/xarelto1.html (accessed on 05/11/2013).

The fibrosa of the MV leaflet is the central layer and it forms the load- bearing backbone, consisting of sheets of collagen bundles (Kunzelman *et al.*, 1993a) aligned mainly along the circumferential direction and arranged in a crimped manner to allow expansion during valve closure (ventricular systole). This layer is continuous with the collagen core of the chordae

tendineae. The atrialis layer is mainly made of well organised multiple layers of elastin fibres, whereas the spongiosa is formed by loose connective tissue, including proteoglycans and randomly oriented collagen. The atrialis and spongiosa are able to absorb stresses generated during valve closure (ventricular systole) through GAG presence. The ventricularis is the inferior layer and thinnest one. It is abundant of elastin, allowing the leaflets to withstand cyclic deformation/reformation during the cardiac cycle (Culav *et al.*, 1999; Kunzelman *et al.,* 1993a).

At the cellular level, heart valves are sheathed by a layer of valve endothelial cells (VECs). These cells are aligned circumferentially with the collagen architecture. Valve interstitial cells (VICs) are spread throughout the three layers of the leaflets, and their purpose is to remodel the valve ECM. They respond to the deformation of the leaflets during the cardiac cycle, repairing the damage occurred in the lealfets during cyclic loading. VICs also act as signal transduction sites, transducing the mechanical information from the ECM to chemical signals to regulate their function, a process that is known as mechanotransduction (Weber *et al.*, 2002). The key components of the heart valves and their function is summarised in Table 1.1.

Element	Sub-structure	Function
ECM	Collagen	Provides strength and stiffness to maintain coaptation during diastole, when leaflet has maximal area.
	Elastin	Extends in diastole; contracts in systole to minimize leaflet area.
	GAGs	Accommodates shear of cuspal layers, cushions shock during valve cycle.
Cells	Interstitial	Synthesize ECM; express MMPs and TIMPs that mediate matrix remodelling.
	Endothelial	Maintain non-thrombogeneicity; blood-tissue interface;
Blood vessels	-	Few and focal; valve leaflets and leaflets sufficiently thin to be nourished by diffusion from the heart's blood.
Nerves	-	Present, with uncertain function.
Anisotropy	-	Permits differences in radial and circumferential extensibility.

Table 1.1: Key elements of the heart valves. MMPs: matrix metalloproteinases; TIMPs: tissue inhibitors of metalloproteinases. Modified from Mendelson and Schoen (2006).

1.2.6 Biomechanics of the heart valves

Understanding the interaction between the heart valves and the local haemodynamic and biomechanical environment is critical to understanding native valve function and structure. During the cardiac cycle, the valves undergo large dynamic deformations. One of the best methods to understand the key characteristics of valve deformation is to examine it in relation

with the transvalvular pressures (TVPs). The maximum physiological TVPs of a heart at rest, for the tricuspid, pulmonary, mitral and aortic valves are 25, 10, 120 and 80 mm Hg, respectively (Guyton, 1976). Therefore, the valves in the left side of the heart experience higher TVPs. Owing to this, the mitral and aortic valves are more prone to disease. Sacks *et al*. (2009a) reported large changes in anterior MV leaflet area (30 %) under minimal TVP, (Figure 1.10), followed by a sharp transition to a highly stiff region. This stiff region corresponded to the fully coapted state of the MV when it is closed. A peak areal strain rate of 1000 % per second was observed during the MV closing phase. Other studies reported that the anterior MV leaflet experienced large, anisotropic strains during closure and that once closed, during systolic ejection, further leaflet deformation ceased (Sacks *et al.*, 2002; 2007). Mean peak strain rates of 300-400 % per second were observed along the radial direction and 100-130 % per second along the circumferential direction. The authors reported that the closing deformation behaviour was symmetrically reversed during valve opening (Sacks *et al*., 2002, 2007).

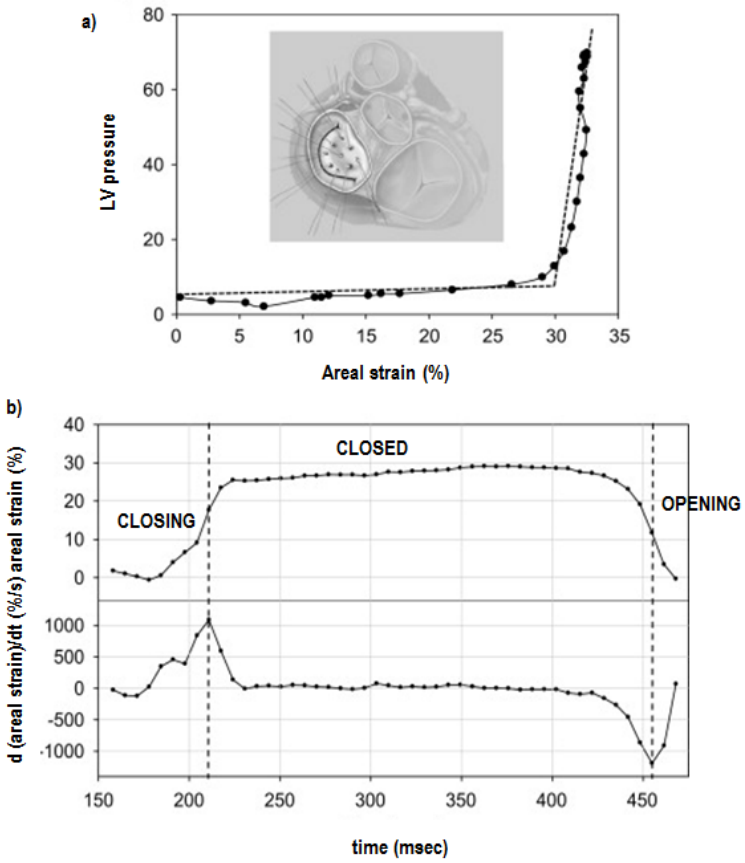

Figure 1.10: Area changes of the anterior MV leaflet during the cardiac cycle. (a) Relationship between left ventricular (LV) pressure and MV areal strain. (b) Representative areal strain traces, with the corresponding strain rate. From Sacks *et al.* (2009a).

During the cardiac cycle, the MV leaflets experience tension, shear, and flexure (Sacks *et al.*, 2009a). These loading modes are imposed cyclically during valve opening and closing (flexure), during blood flow through the valve (shear), and when the valve is fully closed (tension) (Mendelson and Schoen, 2006; Merryman *et al.*, 2006). These macroscopic forces are translated to the microscale level, and then transduced by VICs at the cellular level. Heart valves respond in normal and pathological conditions to the surrounding environmental stimuli, especially mechanical loading, by cell activation (VICs switch to their activated myofibroblast phenotype) and consequent ECM remodelling and synthesis. This interrelation between the physical environment of the heart valves and the function of their cellular populations has an inevitable effect on the constitution of their ECM. This in turn affects the mechanical behaviour of the tissue. Mechanical behaviour is concerned with the deformation that occurs under loading. The simplest experiment that can be carried out to determine the mechanical behaviour of a tissue, and to understand the relation between mechanics and histoarchitecture, is the uniaxial tensile test. During such a test, the stress as a response to the straining of the tissue sample is recorded. The typical stress-strain behaviour of soft tissue under uniaxial tensile loading to failure is shown in Figure 1.11.

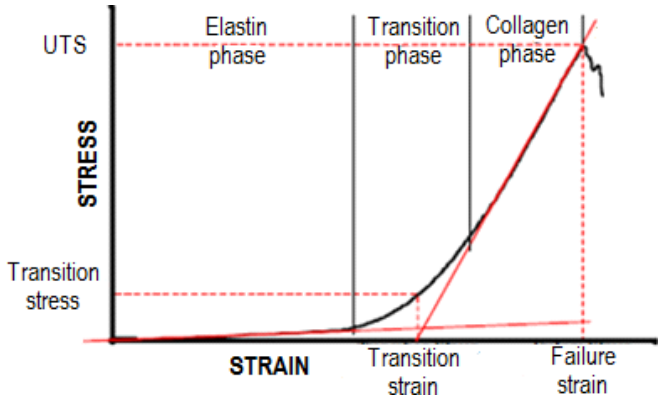

Figure 1.11: A typical stress-strain behaviour of soft tissue. UTS: ultimate tensile strength. Adapted from Fung (1984).

Such a behaviour has three distinct phases before failure, including an initial linear phase (elastin phase), an intermediate transition phase and a final linear phase (collagen phase) (Fung, 1984). During the elastin phase, the tissue offers little resistance to elongation since force transmission and load bearing is provided mainly by the elastin fibres. During this phase the tissue behaves almost as a Hookean elastic solid with the stress increasing linearly with

the strain. In the transition phase, collagen uncrimping occurs and gradually more collagen fibres become uncoiled and aligned (recruited), increasingly contributing to force transmission. In the collagen phase, all the collagen fibres are uncoiled and the load is entirely borne by them. The slope of the stress-strain curve for this phase is steep and almost constant, reflecting the material properties of the collagen fibres, which allow limited elongation to fracture (Korossis, 2002). The collagen phase of a tissue usually continues well beyond the physiological range, corresponding to its reserve strength. At the end of the collagen phase the slope starts decreasing and a further increase of the load will finally result in tissue failure. This stress-strain behaviour varies among tissues, depending on the structure and quantity of the various tissue components, (Fung, 1984; Auricchio, 2003). Moreover, the stress-strain behaviour of biological tissue shows non-linear viscoelasticity, so that when the tissue is subjected to cyclic loading, the stress-strain response demonstrates a hysteresis between loading and unloading (Figure 1.12). With succeeding cycles the hysteresis loop decreases, tending to a steady state after a number of cycles. This period of adjustment is common to all tissues, and it is called preconditioning. The reason that preconditioning occurs is that the internal structure of the tissue changes during the cycling. By repeated cycling, a steady state is reached at which no further change will occur unless the cycling routine is changed.

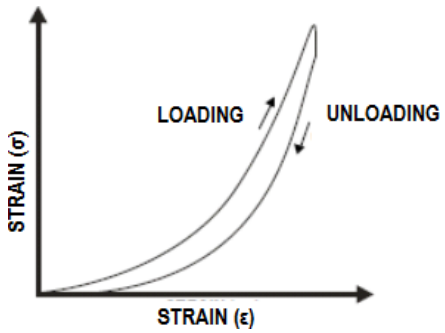

Figure 1.12: Hysteresis loop between loading and unloading. From Fung (1984).

1.2.7 Valvular cells

Two types of cells are found in valve leaflets, including VECs, which cover the surfaces of the leaflets, and VICs, which populate the ECM of the leaflets. Both cell types exhibit unique functions that are different from those of other endothelial (ECs) and interstitial (ICs) cells found throughout the body. VECs are located on the outflow and inflow surfaces of the valve, and they differ from one surface to another since they are influenced by different pressure and

flow patterns (Sacks *et al.,* 2009b). Chester and Taylor (2007) reported that although valvular cells play an important role in maintaining the integrity of the leaflets, in cases where inappropriate stimuli occurs, VICs and VECs may also participate in processes that lead to valve degeneration and calcification. The VECs form a continuous layer with the endocardium of the heart and they are involved in the regulation of vascular tone, inflammation, thrombosis and remodelling (Leask *et al.*, 2003). At a basic structural and functional level, VECs resemble ECs present elsewhere in the circulation. The primary role of the ECs is to form a semi-permeable membrane able to exclude the plasma and other biomolecules of the blood while allowing nutrients to move rapidly (Levick, 2003). ECs have an important role in the maintenance of a non-thrombogenic blood-tissue interface, the regulation of immune and inflammatory reactions, and in the regulation of the function of other cell types. In fact VECs are part of the EC family, but since they are subjected to the valvular mechanical environment, they assume different phenotypes to other ECs (Rabkin-Aikawa *et al*., 2005).

VICs comprise different cell populations, which are able to synthesize several types of ECM molecules and degrading enzymes, such as matrix metalloproteinases (MMPs), as well as their inhibitors (TIMPs), which allow for the ECM remodelling and repair (Rabkin-Aikawa *et al.*, 2005). The different functions of VICs are illustrated in Figure 1.13. VICs are present throughout the leaflet and express three different phenotypes of VICs; fibroblasts, smooth muscle cells (SMCs) and myofibroblasts (Taylor *et al*., 2003; Sacks and Yoganathan, 2007). These different VIC phenotypes are believed to be plastic and reversible (Rabkin *et al.*, 2002; Rabkin-Aikawa *et al.*, 2004). Contractile VICs (expressed by the SMC phenotype) may have a function in aiding adaptation to altered haemodynamic forces via the generation of valvular forces (Rabkin-Aikawa *et al.*, 2004). The myofibroblastic phenotype is thought to be involved in the rapid remodelling of the ECM, whereas the fibroblastic phenotype is thought to be important in regulation and stabilisation of the ECM structure. Rabkin-Aikawa *et al.* (2005) reported that under mechanical equilibrium the majority of the VIC population is composed of quiescent fibroblast-like cells. When stimulated by mechanical loading or other environmental stimuli (during valve development, adaptation, pathology and substitution), the fibroblastic phenotype becomes activated (myofibroblastic) and mediates rapid connective tissue remodelling through collagen biosynthesis and other cellular activities (Rabkin-Aikawa *et al.*, 2005).

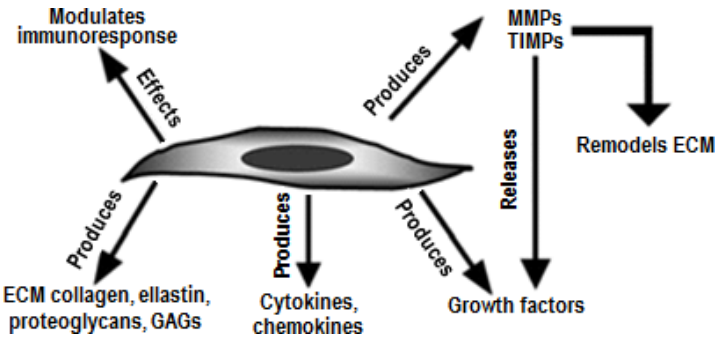

Figure 1.13: Cellular functions of valve interstitial cells. From Taylor *et al.* (2003).

The ability of fibroblasts to readily adapt to their environment could be very useful in tissue engineering. These cells synthesise collagen, elastin, proteoglycans, fibronectin, growth factors, cytokines, chemokines, MMPs and TIMPs. MMPs play a vital role in ECM remodelling and maintenance in health and disease (Segura *et al.*, 1998). They also control the release of growth factors. Myofibroblasts are unique mesenchymal cells found in many tissues and have both fibroblast and SMC characteristics (Schmitt-Graff *et al.*,1994). Studies of organ cultures of valves, as well as animal studies, have demonstrated that although VICs play an important role in repair, they may also have a detrimental role in mediating valve calcification (Mohler *et al.*, 1999).

In addition, and in studies by Liu *et al.* (2007) and Schoen (2008), five identifiable VIC phenotypes were suggested. These include embryonic progenitor endothelial/mesenchymal cells, quiescent VICs (qVICs), activated VICs (aVICs), progenitor VICs (pVICs), and osteoblastic VICs (obVICs). The embryonic progenitor endothelial/mesenchymal cells undergo endothelial-to-mesenchymal transformation (EMT) that initiate the process of valve formation in the embryo to give rise to qVICs and/or aVICs. The qVICs are at rest in the adult valve and maintain normal valve physiology. In the case of haemodynamic/mechanical stress or pathological injury, qVICs become aVICs that participate in repair and remodelling of the valve. In conditions promoting valve calcification, such as in the presence of osteogenic and chondrogenic factors, qVICs can undergo osteoblastic differentiation into obVICs.

1.2.8 Heart valve dysfunction

The most common aetiologies of heart valve disease are classified to congenital abnormalities (disruption in the formation of the valve architecture due to incorrect gene expression),

myxomatous valve degeneration (damage to or inadequate collagen leading to weakness of the leaflets), acquired disease (such as valve calcification or endocarditis) or a mixture of congenital and acquired disease (such as calcification or endocarditis of a congenitally malformed valve) (Schoen, 2005a, 2008; Otto and Bonow, 2009). Calcification involves the impregnation of the leaflets or surrounding tissue with calcium or calcium salts, which harden the tissue. Endocarditis is the inflammation of the endocardium due to an infectious or non-infectious cause. Acquired valvular heart disease can be either of rheumatic or non-rheumatic origin (Otto and Bonow, 2009). Valve pathology is often mediated through abnormal and complex interactions between the VICs, VECs, ECM and their environment (Schoen, 2008).

During the last century, there has been a dramatic decline in the incidence of rheumatic fever in developed countries to less than 1 per 100,000, whereas in developing countries, rheumatic heart valve disease still remains one of the major clinical conditions. Rheumatic fever is an acute inflammatory disease that induces a progressive immune reaction and causes the thickening and fibrosis of the valve with fusion of the commissures, reduced leaflet mobility and a small orifice. Moreover the chordae may be matted together with heavy calcification of the valve (Otto and Bonow, 2009). Although the incidence of rheumatic fever has declined in the developed countries, the overall burden of valvular heart disease has not followed the same trend due to the increase in age-related degenerative valve disease (World Health Organization, 2004; Carapetis, 2007). Over the last 30 years there has been a considerable change in the frequency of various valvular disorders in the Western world. Currently, MV regurgitation represents the second major valvular disorder, after aortic valve dysfunction. Other common types of MV disease include MV prolapse and MV stenosis (Otto and Bonow, 2009).

1.2.8.1 Mitral valve regurgitation

Mitral valve regurgitation (MVR) is one of the most common valvular disorders and it may be caused by a wide variety of aetiologies (Otto and Bonow, 2009). MVR occurs when the MV is not capable of closing completely during left ventricle contraction, causing blood flowing back into the atrium (Turi, 2004; Figure 1.14). MVR can be caused by the malfunction of the valve leaflets, valve annulus, chordae, papillary muscles or ventricular myocardium.

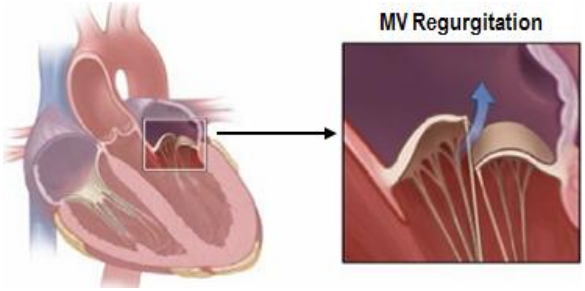

Figure 1.14: Pathology of MV regurgitation. Blue arrow indicates blood regurgitating back to the atrium. From: http://www.uofmhealth.org/health-library/zm6291 (accessed on 05/11/13).

MVR can be caused by mitral valve prolapse (Turi, 2004), or rheumatic fever. The latter causes distortion the leaflets and shortening of the chordae (Buchbinder and Roberts, 1972; Arnett and Roberts, 1976; Turi, 2004). Other types of MVR include ischaemic MVR, which can be either acute (due to papillary muscle rupture or myocardial infarction), or chronic (due to shape alterations of the left ventricular; Otto and Bonow, 2009). MVR may also be caused by endocarditis, which involves damage of the leaflets or rupture of the chordae, producing acute or chronic MVR (Otto and Bonow, 2009), and by cardiomyopathy (Virmani, 1980; Ross and Roberts, 1986; Roberts *et al.*, 1987; Klues *et al.*, 1992). Moreover, the enlargement of the left ventricle can cause dilation of the mitral annulus, resulting in inadequate closing of the valve orifice by the leaflets and, consequently leading to MVR (Turi, 2004).

1.2.8.2 Mitral valve prolapse

Mitral valve prolapse (MVP), also called “click murmur syndrome” or “Barlow's syndrome”, represents the displacement of enlarged, thickened, mitral leaflets back into the left atrium during ventricular systole (Hayek *et al.*, 2005; Figure 1.15). Owing to this, the valve does not close tightly during systole, allowing blood back to the left atrium. MVP is equally common in men and women and has an occurrence in the general population of about 2-3%. MVP can be classified as classic (when the thickening is greater than 5 mm), or non-classic prolapse (Freed *et al.*, 1999). The underlying cause of MVP can be histological abnormalities in the valvular tissue, geometric disparities between the left ventricle and the MV, or various connective tissue disorders, such as myxomatous degeneration (Schoen, 2008). Myxomatous degeneration, which is the most common cause of MVP, is associated with inadequate chordal support (elongation or rupture), excessive leaflet tissue and annular dilatation in conjunction with leaflet thickening (Otto and Bonow, 2009). Leaflet thickening is usually

caused by excessive deposition of proteoglycans in the spongiosa (Schoen, 2008). In addition, there is an attenuation of the collagen-rich fibrosa layer of the valve, together with development of structurally abnormal chordae (Hayek *et al.*, 2005). As a result, a decrease in stiffness and an increase in extensibility occur in the valvular tissue (Barber *et al.*, 2001a, 2001b). In myxomatous degeneration, the VICs alter the synthesis and/or remodelling of the ECM by increasing the expression of MMPs and other enzymes responsible for ECM protein degradation (Rabkin *et al.*, 2001), and by increasing GAG synthesis (Hayek *et al.*, 2005; Schoen 2008). MVP causes chest pain, palpitations, fatigue, weakness, anxiety and panic attacks (Turi, 2004; Hayek *et al.*, 2005). One of the most serious complications of MVP is severe MVR.

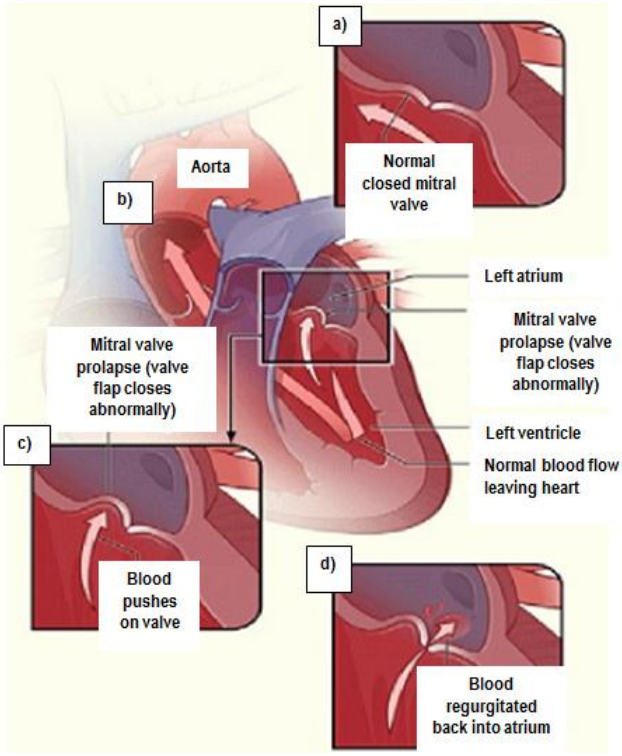

Figure 1.15: MV prolapse. From: http://www.nhlbi.nih.gov/health/health-topics/topics/mvp/ (accessed on 05/11/13).

1.2.8.3 Mitral valve stenosis

Mitral valve stenosis (MVS) involves the narrowing of the MV orifice (Figure 1.16), which reduces the efficiency of the heart to filling the left ventricle during diastole (Turi, 2004). The most usual cause of MVS is rheumatic heart disease (Roberts *et al.*, 1973, 1987; Otto and Bonow, 2009), whereas less common, non-rheumatic causes include severe calcification of

the mitral annulus and leaflets (Hammer *et al.*, 1978; Theleman *et al.*, 2006), congenital anomalies (Roberts *et al.*, 1973, 1987), infective endocarditis (Roberts *et al.*, 1967), neoplasms (particularly myxoma) protruding through the mitral orifice (Roberts, 2001), and a mismatched prosthesis used to replace the native MV (Roberts *et al.*, 1973). MVS is uncommon in most industrialized nations, due to the dramatic decrease of rheumatic fever. However, it remains relatively common in developing countries (Turi, 2004).

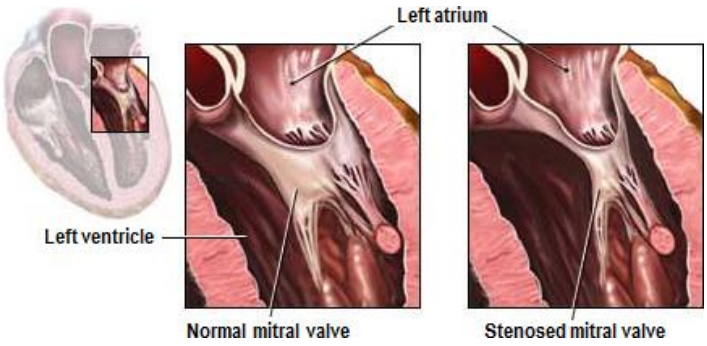

Figure 1.16: Pathology of MV stenosis: the MV orifice is narrowed during stenosis. From: http://www.heart-valve-surgery.com/mitral-valve-disorders-symptoms.php (accessed on 05/11/13).

The symptoms of MVS include breathlessness and palpitations. The latter are caused by a dysfunction in the stability of the heart beat (Turi, 2004; Otto and Bonow, 2009). Other symptoms may include fatigue, chest pain and occasional coughing up of blood (Turi, 2004). In patients with MVS the valve has a domed appearance, restricted opening, and is thickened with an enlarged left atrium (Turi, 2004).

1.2.9 Conventional mitral valve reconstruction strategies

Current surgical interventions for MV dysfunction include MV repair and replacement (Otto and Bonow, 2009). Similarly to the case of the other heart valves, reconstruction strategies for MV dysfunction need to employ materials and devices that are non-thrombogenic, provide resistance to infection, have adequate mechanical properties and structural integrity and, ideally, support cell infiltration and viability (Mendelson and Schoen, 2006).

1.2.9.1 Mitral valve repair

Currently, repair of the MV is the gold standard for treating MV dysfunction and involves open heart surgery. In the last 50 years, MV repair techniques have undergone many modifications and improvements (Spiegelstein *et al.*, 2007). Depending on the underlying cause of MV

dysfunction, different types of MV repair techniques are applied. MV repair in degenerative MVR is associated with very good short- and long-term outcomes (Gillinov *et al.*, 1998; Spiegelstein *et al.*, 2007). Repair techniques used to treat this condition include quadrangular (Figure 1.17), trapezoid, or triangular resection of the segment of the posterior leaflet demonstrating prolapse or ruptured chords (Carpentier *et al.*, 1983; Deloche *et al.*, 1990; Braunberger *et al.*, 2001; Daimon *et al.*, 2006; Spiegelstein *et al.*, 2007). The posterior leaflet is repaired with either plication of the annulus, or with sliding plasty. The former involves the suturing of the annulus at the level of the resection in order to make the two leaflet remnants come in close apposition with a little overlap. The latter is associated with excess tissue, as in the case of Barlow's diseases, and involves the detachment of part of the two remnants of the posterior leaflet from the annulus, followed by the reattachment of the segments to the annulus, allowing the close apposition of the leaflet remnants with a little overlap (Perier, 2005). Commonly, after a quadrangular resection the insertion of a ring completes the repair. MV repair in rheumatic disease remains controversial due to the high possibility of re-operation after repair, and the risks associated with the advanced age of the patients and the presence of active rheumatic endocarditis (Duran *et al.*, 1991).

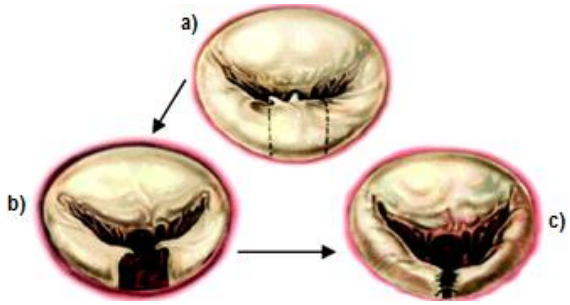

Figure 1.17: Quadrangular resection in MV repair. Part of the posterior leaflet is resected (a, b); final suturing involving either plication of the annulus or sliding plasty (c). From Otto and Bonow (2009).

In anterior leaflet prolapse or ruptured chords, ePTFE chord replacements have become quite popular in the past decade (Von Oppel and Mohr, 2000; David, 2004; Dreyfus *et al.*, 2006; Lawrie, 2006). Chordal transfer is performed in patients with myxomatous disease and involves the transfer of chords from a healthy portion of the leaflet to the prolapsing one. This technique has demonstrated excellent clinical outcomes (Smedira *et al.*, 1996; Salati *et al.*,

1997; Duran *et al.*, 1999; Gillinov *et al.*, 2005a). Shortening of the anterior leaflet (Quigley *et al.* 2005), or anterior leaflet chord (Dreyfus *et al.*, 2006), have also been used.

Annuloplasty of the posterior part of the annulus has been performed using untreated (Salati *et al*., 1991) and glutaraldehyde-treated (Borghetti *et al.*, 2000) autologous pericardium. Comparative studies with rigid prosthetic rings have shown that autologous pericardium provided more favourable annulus dynamics (Borghetti *et al.*, 2000). Prosthetic annuloplasty rings have also been used in conjunction with glutaraldehyde-treated autologous pericardium for the augmentation of the anterior leaflet (Acar *et al*., 2004; Chavaud *et al*., 1998). Studies have shown that this technique is associated with decreased re-operation risk compared to using an annuloplasty ring alone. Further studies with glutaraldehyde-treated autologous pericardium used in MV leaflet extension, have shown late deterioration and calcification of the tissue with minimal risk of thromboembolic events (Chauvad *et al*., 1991; 2001). Autologous pericardium has the most favourable characteristics for cardiovascular implantation since it is a low-cost biomaterial, free of donor derived pathogens, non-immunogenic, easily accessed (Duran and Gometza, 1993; Mirsadraee *et al*., 2006) and may remodel in the patient. However, it is not an ideal solution since it requires sacrifice of the pericardium of the patient, and involves inflammatory changes after pericardiotomy (Duran and Gometza, 1993). Glutaraldehyde-treated bovine pericardium has also been used to close MV leaflet perforations (Muhercke *et al*., 1997). However, glutaraldehyde-treated tissue with cell remnants can cause calcification. The calcific deposits enlarge and coalesce, leading to the formation of mineralized nodules, which can cause tissue stiffening and weakening, ultimately leading to deterioration of the bioprosthesis (Boskey *et al*., 1981).

In the case of chronic ischemic MVR, the most commonly used surgical procedure is restrictive mitral annuloplasty (Dion *et al.*, 1995; Bolling *et al.*, 1998; Daimon *et al.*, 2006; Spiegelstein *et al.*, 2007; Braun *et al.*, 2008). Generally, almost all MV repairs are completed with annuloplasty, which involves the reconstruction of the annulus. Its role is to reduce the size of the annulus and the tension caused by the repairing sutures (Tuladhar *et al.*, 2006). Different types of annuloplasty rings have been employed clinically. These include rigid or flexible and complete or incomplete rings (Spiegelstein *et al.*, 2007). Additional MV repair techniques include the edge-to-edge, or Alfieri technique, and commisuroplasty. The former involves the localised suturing of the two leaflets at the site of regurgitation (Alfieri *et al.*, 1999, 2004; Spiegelstein *et al.*, 2007) (Figure 1.18). The latter is used for patients with small leaflet

prolapse, adjacent to the commissure, and provides a localised closure of the commissure without altering the valve orifice (Gillinov *et al.,* 2005b; Aubert *et al.,* 2005). The recently-developed Mitraclip system, which has been adapted to the edge-to-edge technique (Gaemperli *et al*., 2013), and has been shown to be less invasive by employing a catheter inserted in the femoral vein to reach the heart.

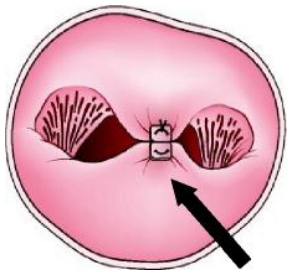

Figure 1.18: Edge-to-edge technique; single suture on the free edges. From Otto and Bonow (2009).

MV repair has many advantages over mitral replacement including, lower operative mortality, reduced incidence of thromboembolism and reduced need for anticoagulation (Perier *et al.*, 1984; Gillinov *et al.*, 1998; Yau *et al.*, 2000), lower risk of endocarditis (Galloway *et al.*, 1988; Duran, 1993), and improved long-term results (Galloway *et al.*, 1989; Akins *et al.*, 1994). Nevertheless, there are several cases of recurrent MV dysfunction following MV repair, which require reoperation. Failed repair can be divided into two groups, namely early failure and late failure. Early failure is caused by factors related to the procedure used. These factors include rupture of shortened chordae, haemolysis, and incomplete repair with residual mitral regurgitation. Late failure is caused by new valvular pathologic lesions and progressive disease (Otto and Bonow, 2009). Overall, less than half of MV repair reoperations have a successful outcome (Shekar *et al.*, 2005; Dumont *et al.*, 2007).

1.2.9.2 Mitral valve replacement

Although MV repair is generally the most common choice for degenerative MVR, MV replacement is still preferred for some specific conditions of MV dysfunction. Specifically, replacement is preferred in patients with rheumatic MV disease, degenerative disease with annulus and leaflet calcification, and endocarditis with extensive valve deterioration and repair (Gillinov *et al.*, 2001; Jokinen *et al.*, 2007; Fedak *et al.*, 2008). Heart valve replacement involves the substitution of the diseased valve with either a mechanical or a tissue valve. Mechanical prostheses are made entirely of artificial components. Based on their design,

these valves are classified into three types (Figure 1.19), including ball and cage, tilting disc and bileaflet valves. Mechanical valves are associated with enhanced durability, but generate large regurgitation volumes during valve closing and require life-long anticoagulation treatment (Warfarin). The latter is necessary in order to avoid thromboembolic complications associated with blood clotting caused by turbulent-flow-induced high fluid stresses (Edmunds *et al.*, 1987; Wurzinger and Schmid-Schönbein, 1990; Korossis *et al.*, 2002). Owing to the need of anticoagulation, one of the major problems with mechanical heart valves are haemorrhagic disorders (Grunkemeier and Rahimtoola, 1990; Schoen *et al.*, 1992). The use of mechanical valves in children and young adults is problematic due to their inability to grow with the patient, leading to costly re-operations. In addition, patients with mechanical prosthesis are prone to increased incidence of endocarditis (Otto and Bonow, 2009).

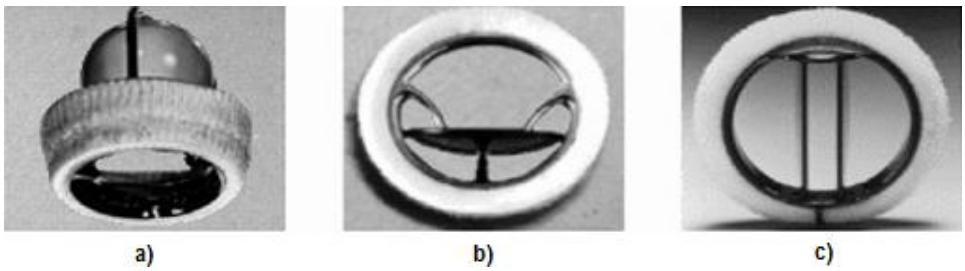

Figure 1.19: Mechanical valves: (a) ball & cage; (b) tilting disc; (c) bileaflet. From Korossis (2002).

Tissue valves include bioprosthetic valves, made of chemically-treated porcine or bovine tissue (xenografts), and cadaveric valves (allografts or homografts). Tissue valves are associated with significantly lower thromboembolic risks, thus they do not require anticoagulation treatment, and have a haemodynamic performance comparable to that of the native valve (Russo *et al.*, 2008). However, tissue deterioration and structural dysfunction, due to both calcification and non-calcific mechanisms, represent serious drawbacks with tissue valves (Hammermeister *et al*., 1993). In addition, valve infection and non-structural dysfunction affect both tissue and mechanical valves almost equally (Korossis, 2002).

Bioprosthetic valves are cross-linked with low-concentration glutaraldehyde solutions in order to reduce their antigenicity and to stabilise the tissue against structural degradation (Korossis, 2002). In addition, studies have described treatment of these valves with anticalcific agents to minimize the risk of calcification (Schoen *et al.*, 2005a, 2005b). Porcine bioprosthetic valves are usually made from intact pig aortic valves (with or without the valve root). These valves

are cross-linked under various boundary conditions (degree of valve pressurisation), which have shown to affect the haemodynamic performance of the prostheses (Korossis *et al*., 2002). Stinson *et al*. (1974, 1977) reported that the use of glutaraldehyde-treated porcine aortic valves for MV replacement provided overall durability comparable to that of mechanical prostheses. Other works reported on the use of porcine and bovine xenografts for MV replacement and concluded that bovine pericardial valves were associated with lower risk of thromboembolism, due to their superior haemodynamics (Gonzalez-Lavin *et al.,* 1984).

Bioprosthetic valves are subjected to structural deterioration due to chemical, mechanical, and morphological changes occurring during cross-linking and fabrication. This, in conjunction with the lack of a regeneration mechanism makes these valves prone to structural dysfunction. In addition, the lack of an endothelial barrier, causes increase permeability of the xenograft tissue (Schoen *et al.*, 2008), whereas internal rearrangements, involving collagen crimp and alignment, are not possible due to the fixation of the ECM proteins (Vesely *et al.*, 1988; Fisher and Davies, 1989). Moreover, cell remnants in the tissue act as foci for calcification. However, new generation bioprostheses have demonstrated 64 - 98 % freedom from structural valve deterioration after 10 years (Marchand *et al*., 1998; Masters *et al*., 2004). In addition, recent studies have suggested that development of improved GAG cross-linking techniques, to limit GAG degradation, may improve valve longevity (Lovekamp *et al.*, 2006; Shah *et al.*, 2008).

Homografts are usually intact mitral, aortic and pulmonary valves, obtained from human donors and cryopreserved. Chauvaud *et al*. (2003) reported on MV homografts and showed that papillary muscle in the subvalvular apparatus caused an increased immunogenic reaction. The authors concluded that this kind of replacement was not suitable for young patients. Doty *et al*. (2001) used homograft MVs and reported that successful replacement requires secure fixation to the papillary muscles. Moreover, mismatch between the homograft and the patient's valve can cause early dysfunction (Ali *et al*., 2004). Homografts have been reported to demonstrate good haemodynamics, low thrombogeneicity and low infection rates. However, although homografts are subject to decreased degeneration compared to bioprostheses, their long-term performance is limited by progressive degeneration due to absence of a repair mechanism.

According to Schoen *et al.* (1982), the criteria for an ideal valve substitute is ease of implantation, quick healing in the implanted position, long life cycles with minimal wear or degenerative change, high flow with minimal turbulence when opened and no regurgitation

when closed, limited risk of thrombosis and biocompatibility. None of the currently available valve substitutes meet all these criteria. In addition, none of the current valve replacements, or indeed valve repair materials (with the exception of autologous pericardium), have an inherent remodelling/repair mechanism and thus, they cannot regenerate or grow with the patient.

1.2.10 The tissue engineering concept

Tissue engineering (TE) has emerged as a promising alternative for tissue reconstructions. The ultimate goal of TE is to provide tissue-equivalents, which will not only be fully compatible, but will also remodel, regenerate and ultimately grow with the patient. TE involves the development of biological or synthetic substitutes for implantation into the body with the purpose of fostering remodelling and regeneration of diseased tissue. In the past few years, a number of different TE strategies have been developed (Rabkin and Schoen, 2002). These are summarised in Figure 1.20. *In vivo* TE involves the use of bioresorbable scaffolds that rely on the patient's cellular response *in vivo*, with the intention of developing functionality after implantation. This approach has been investigated for a range of tissues (Brown *et al.*, 2013; Del Gaudio *et al*., 2013; Manassero *et al*., 2013). However, this approach is limited by the patient response in terms of scaffold recellularisation and regeneration. This can lead to the development of inappropriate properties of the implant *in vivo*. Utilisation of passive *in vitro* recellularisation prior to implantation has also been attempted but its success is limited since cell differentiation and tissue matrix remodelling may not progress physiologically.

In vitro TE, or functional TE (FTE), employs scaffolds that are recellularised with appropriate autologous cells *in vitro*, and physically conditioned with a view to producing *in-vivo*-equivalent functionality prior to implantation. In this fashion, FTE simulates the type of physical environment that native tissues encounter in the body with a view to generating functional tissue-engineered constructs in the laboratory, prior to implantation (Langer and Vacanti, 1993; Vacanti and Langer, 1999; Rabkin and Schoen, 2002). Compared to *in vivo* transplantation of dissociated cells and/or biodegradable scaffolds alone, the implantation of functional tissue has the potential to promote graft fixation and survival.

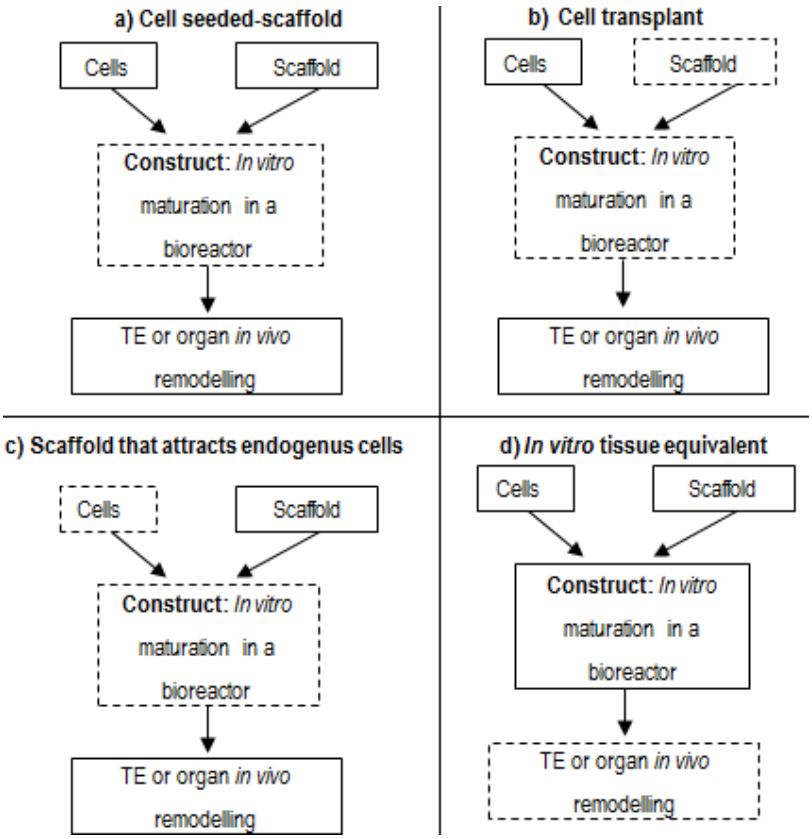

Figure 1.20: The four main different TE approaches: (a) The cell-seeded scaffold is implanted without *in vitro* conditioning/maturation; (b) Cells introduced directly into the host without a scaffold; (c) Scaffolds attract endogenous cells *in vivo* to repopulate and remodel; (d) Functional tissue-equivalents are engineered *in vitro*, prior to implantation. Modified from Rabkin and Schoen (2002).

1.2.10.1 Progress in valvular tissue engineering

Tissue engineering approaches emerged 20 years ago, as a potential solution to overcome the problems associated with the limited availability of human donor tissues (Fuchs *et al*., 2001). The term TE was coined by Fung in 1987, although early attempts appear to originate as early as in the 1960s, in an attempt to propagate skin cells *in vitro*, and in the 1970s with the work of Rheinwald and Green at Massachusetts Institute of Technology (MIT), who successfully developed skin grafts using sheets of cultured keratinocytes, and dermal cells (Rheinwald and Green, 1975). Over the past few years, there has been a considerable interest in the TE of heart valves, especially for the aortic and pulmonary positions. Rabkin-Aikawa *et al.* (2005) reported that to achieve the challenge of heart valve TE, a deep

understanding of both normal and pathological tissue function is necessary, including mechanisms of embryological development and functional tissue biomechanics.

To date, there have been two main strategies for the development of TE heart valves. These include the transplantation of unseeded scaffolds, with a view to attracting endogenous cells, and cell-seeded scaffolds, which have been physically conditioned *in vitro*, with a view to developing valve-equivalent functionality prior to implantation.

Decellularised scaffolds have been implanted to investigate the *in vivo* autologous regeneration potential of the unseeded scaffolds. Theodoridis *et al.* (2013) compared the recellularisation potential of decellularised pulmonary valves, unseeded or seeded, prior to implantation into elderly sheeps. Ovine pulmonary valves decellularised unseeded and decellularised re-endothelialized with autologous endothelial cells, were implanted in the orthotopic position in sheep. Explantation after six and twelve months showed no signs of degradation of the ECM, minimal calcification and cell repopulation, but to various degrees. Only one valve showed complete repopulation, and a slight tendency of better repopulation was observed in the re-endothelialized pulmonary valves implants, however no significant difference in the cell densities was found among the groups. Elkins *et al.* (2001) decellularised human and sheep pulmonary valves using the SynerGraft treatment process and implanted these in human patients and sheeps, respectively. The decellularised sheep allograft valves were monitored echocardiographically and histologically at 3 and 6 months; they became functional during the implantation period, and were progressively repopulated with recipient cells. The decellularised human allografts implanted in humans did not seem to provoke reactive antibody response.

According to the cell-seeded scaffolds approach, mechanical loading has been considered to be necessary to stimulate the growth and maturation of the seeded cells and the formation of the ECM. As such valvular constructs have been conditioned using dynamic flow or strain, or a combination of both (Filova *et al.,* 2009). Engelmayr *et al*. (2006) reported that mechanical stimulation had fundamental effects on the differentiation of sheep bone-marrow-derived stem cells on polyglycolic acid/ poly L-lactic acid (PGA/PLLA) valvular scaffolds. Moreover, fibrin-based valvular constructs cultivated with porcine VICs under 15% cyclic distension were shown to have increased collagen content and ultimate strength (Syedain *et al.,* 2008). In a study by Ku *et al*. (2006), VICs and MSCs stretched on collagen-coated substrates increased their collagen synthesis. In general, mechanical conditioning has been demonstrated to

improve the properties of valvular constructs when compared to static cultures (Hoerstrup *et al*., 2002; Mol *et al*., 2003; Engelmayr *et al*., 2005). Moreover, cell-seeded and *in-vitro*-conditioned valvular scaffolds were shown to be fully functional in the pulmonary position in the study of Hoerstrup *et al.* (2000a). They seeded ovine myofibroblasts and ECs onto fabricated bioresorbable polymeric scaffolds and cultured them in a pulse duplicator prior to implantationt. They reported the formation of a layered leaflet tissue structure and efficient functionality after 20 weeks in lambs.

1.2.10.2 Valvular tissue engineering scaffolds

Typically, a TE scaffold is a porous, bioresorbable polymer of either synthetic or natural origin, which can support appropriate cell function (Bianco and Robey, 2001; Blau et al., 2001). Depending on the approach used, degradation and remodelling of the scaffold starts either *in vitro* or *in vivo*. Three main types of scaffolds have been used in valvular TE. These include: decellularised xenogeneic or allogeneic valvular scaffolds, synthetic scaffolds, and scaffolds fabricated from reconstituted ECM proteins, such as collagen and elastin. Decellularised xenogeneic or allogeneic scaffolds together with scaffolds fabricated from reconstituted ECM proteins are considered natural scaffolds. The advantages and disadvantages of the different scaffold types are presented in Table 1.2.

	Synthetic scaffolds	**Natural scaffolds**
Advantages	Control over structure and properties (pore size, stability, and degradation rate); Easily reproduced; Potentially resorbable.	Natural histoarchitecture; Maintain biological cues (reactive sites, growth factors); Resorbable.
Disadvantages	Difficulty in controlling cell adhesion and tissue reorganisation; Inflammation due to incomplete polymer degradation; Limited diffusion in thick scaffolds (> 2mm)	Decellularisation may alter physical properties; May induce immunologic reaction; Calcification potential; Limited diffusion in thick scaffolds (> 2mm).

Table 1.2: Advantages and disadvantages of synthetic and natural scaffolds. Adapted from Mendelson and Schoen 2006.

Ideally, a valvular scaffold should closely mimic the ECM of the native valve and have the following characteristics: 1) have mechanical and biological integrity; 2) allow and support cell attachment and migration; 3) transfer appropriate mechanical and biochemical cues to the cells; 4) allow sufficient diffusion of nutrients and cell metabolites; 5) allow dynamic changes

in its architecture (Dohmen and Konertz, 2009). Moreover, the scaffold should be biocompatible, and biodegradable into non-toxic products. Scaffolds may be combined with growth factors (GFs), cytokines (regulatory proteins) and hormones, which can regulate cell function and tissue formation (Flanagan and Pandit, 2003). Moreover, cell adhesion onto the scaffold can be improved by modifying its surface with covalently attached adhesion peptide sequences, such as arginine-glycine-aspartic (RGD; Hubbell, 1995). These peptide sequences allow the formation of a physical link between the scaffold and the cells via integrin cell surface receptors (Van der Flier and Sonnenberg, 2001).

Natural materials

Natural scaffolds are usually made of reconstituted ECM proteins, such as fibrin, elastin and collagen, or decellularised homograft or xenograft tissue. Decellularisation was first used as a means of reducing the cell-debris-induced immunogenicity and calcification of bioprosthetic valves. Decellularised xenogeneic or homogeneic tissue scaffolds have been used in a number of studies over the past few years. The commercially available SynerGraft valve (CryoLife Inc., USA) was a decellularised porcine valve, which was used in clinical trials (O' Brien *et al.,* 1999). However, early failure in humans resulted in the withdrawing of this implant (Simon *et al*., 2003). Specifically, the decellularised valve caused a strong inflammatory response, which was non-specific and was followed by a lymphocyte response, and rapid structural failure within one year. This failure was attributed to incomplete decellularisation of the graft. Rieder *et al*. (2005) compared decellularised porcine and cryopreserved decellularised human pulmonary valves to investigate whether decellularisation was more effective on xenograft or homograft valves. The authors reported that decellularisation was more effective on human tissue. Indeed, a considerable amount of antigenic content was still detectable within xenogeneic tissue after decellularisation. This acute immunogeneic reaction induced by the SynerGraft implant was associated to the presence of the α-gal (Galα1,3-Galβ1-4GlcNAc-R) epitope. This epitope represents the major xenogeneic antigen which causes hyperacute rejection of animal tissue in Man.

A decrease in immunogeneic response for decellularised homografts, compared to cryopreserved homografts, was observed *in vivo* in human patients with good short-term results (Hawkins *et al*., 2003; Sievers *et al*., 2003). Da Costa et al. (2009) reported that the Ross operation completed with decellularised pulmonary valves homografts in the pulmonary position was associated with good functional recovery and low incidence of reoperation up to

13 years. An important consideration with decellularised scaffolds is the fact that the decellularisation treatment itself most likely causes alteration in the biomechanical properties of the scaffolds compared to the starter tissue (Korossis, 2002). The potential toxicity of the decellularisation agents is another important factor that needs to be taken into account in the development of such scaffolds.

The reconstituted ECM protein-based scaffolds are probably the least explored approach. Collagen based constructs seeded with vascular SMCs and/or ECs have been used for the generation of tubular blood vessels (Weinberg and Bell, 1986), aortic valve leaflets (Tranquillo and Girton, 2003), and chordae tendineae (Shi and Vesely, 2003, 2004). Shi and Vesely (2003) fabricated MV chordae through collagen gel contraction by casting a collagen-cell suspension into silicone rubber wells. The authors reported that gel contraction increased with increasing cell-seeding density, whereas fibril density increased with culture time as the gel contracted. The authors also reported that insufficient mechanical properties have been the main limitation for the application of collagen-based constructs, and that the mechanical strength of the constructs can be enhanced by optimizing the cell type, seeding density, culture time, and initial collagen concentration. Ye *et al*. (2000) used a similar approach by encapsulating cells in autologous fibrin gel, and reported the generation of new ECM. Ramamurthi and Vesely (2005), used crosslinked hyaluronan (GAG) gels, seeded with neonatal rat aortic SMCs, and reported that these gels are useful as substrates to induce elastin synthesis in culture to obtain structures that resemble the elastin matrix of the native aortic valve. Flanagan *et al.* (2006) investigated a type I collagen-GAG (chondroitin sulphate) hydrogel for the creation of MV tissue. They isolated porcine MV VICs and VECs, and they co-cultured them for 4 weeks in the hydrogels. The authors reported that both collagen alone and collagen-GAG constructs contracted to form tissue-like structures *in vitro*. They also noted that the addition of GAGs resulted in a more porous construct, positively influencing the bioactivity of the seeded cells and tissue remodelling. They also reported that further optimisation was necessary to improve construct structure and mechanical strength. In addition to inadequate mechanical properties, other limitations associated with reconstituted protein scaffolds include excessive shrinkage of the construct and the possibility of necrosis and apoptosis of the entrapped cells (Mendelson and Schoen, 2006).

Synthetic materials

Synthetic polymer scaffolds have the advantage of possessing well controlled and reproducible properties. In addition, they are bioresorbable, serving as temporary ECMs until the seeded cells are capable of producing their own ECM proteins. Synthetic, biodegradable polymers most widely used in valvular TE include PGA, polylactic acid (PLA) and their copolymers. PGA was used as the first totally synthetic resorbable suture, commercially available under the name of Dexon. PGA has been used by Hoerstrup *et al*. (2002) to produce trileaflet valvular scaffolds for pulmonary valve replacement. These scaffolds were coated with poly 4-hydroxybutyrate (P4HB) and seeded with human bone-marrow-derived MSCs. Following 14 days of dynamic culture in a bioreactor, the cellular tissue was organised in a layered fashion, in contrast to the static controls that looked loose and less organized. However, PGA is rapidly resorbable and loses its mechanical strength rapidly (Grayson *et al.*, 2004). Copolymers formed by the polymerisation of PGA with the much more hydrophobic PLA, have been shown to possess a lower rate of degradation, due to the decreased rate of hydrolysis and, therefore, better mechanical properties. These polymers are considered biocompatible, and they have been used successfully in a number of FDA-approved implants (Grayson *et al.*, 2004). Sutherland *et al.* (2005) seeded ovine bone-marrow-derived MSCs onto 50:50 poly(lactide-co-glycolide) (PGLA)/PGA blend biodegradable scaffolds to create semilunar valves, which were implanted into the pulmonary position in sheep. The explanted TE valves (4 and 8 months) demonstrated ECM deposition and cell distribution similar to the native pulmonary valves.

Nevertheless, in spite of the positive results there are a number of disadvantages associated with the use of scaffolds made of these polymers. These disadvantages are mainly related to cell regulation and 3D tissue reorganization, since such materials are usually isotropic whereas native valves present a significant anisotropy in their structure and mechanical properties (Merryman *et al.*, 2006). Towards this end, many studies have focused on overcoming the problem with the isotropy of these scaffolds by producing PGA/PLA electrospun scaffolds that resemble the structural anisotropy and fibre orientation of the native valve leaflets (Roy, 2004). Further disadvantages include potential tissue inflammation due to the foreign body reaction and slow or incomplete polymer degradation. Moreover, while the scaffold degrades, the free space formed is progressively filled by cells and ECM, which may cause fibrosis (scar tissue) leading to excessive contraction and distortion during maturation.

In addition, polymeric valvular scaffolds lack the elaborate histoarchitecture and biochemical cues of the native valvular ECM. However, their main disadvantage is their poor mechanical properties, which make them unlikely candidates for direct implantation (without cells and *in vitro* conditioning) to the demanding valvular environment in the body (Rabkin and Schoen, 2002).

1.2.10.3 Tissue decellularisation techniques

Decellularised xenogeneic or allogeneic biological scaffolds are an attractive approach in valvular TE since they possess natural histoarchitectures and biochemical cues, which favour cell adhesion, migration and proliferation. Decellularisation involves the removal of cells and their immunogenic components, including lipid membranes, membrane-associated antigens and soluble proteins, whilst retaining the integrity and architecture of the ECM proteins (GAGs, elastin and collagen; Korossis *et al.*, 2002). Over the years, there have been a number of treatments developed for tissue decellularisation, employing physical treatments or chemical agents. Among the latter, non-ionic detergents, ionic detergents, zwitterionic detergents (which combine the properties of both ionic and non-ionic), biologic agents (such as enzymes), or a combination of these have been used (Dohmen and Konertz, 2009). Among the physical treatments, freeze-thawing, direct pressure, sonication and agitation, have been reported in the literature (Dohmen and Konertz, 2009). These physical treatments have been successful in achieving cells lysis, but cellular debris remains unless removed by subsequent processing with chemicals.

Decellularisation treatments with non-ionic detergents aim at disrupting the lipid-lipid and lipid-protein interactions of the cells, without interfering with structural protein-protein interaction of the ECM (Seddon *et al*., 2004). The most common non-ionic detergent used is Triton X-100, which removes almost all nuclear material, but not all cellular debris (Grauss *et al.*, 2005). Moreover, it causes an almost complete loss of GAGs, affecting the histoarchitecture and mechanical properties of the tissue. Ionic detergents have been shown to be effective in removing cytoplasmic and nuclear material. The most commonly used ionic detergents include sodium dodecyl sulphate (SDS) and sodium-deoxycholate. Booth *et al.* (2002), reported on a number of different methods used to decellularise porcine aortic valve leaflets. The study used different detergents, including Triton X-100, SDS, and sodium deoxycholate at different concentrations. They reported that only the protocols that utilised SDS or sodium deoxycholate could achieve decellularisation, whilst maintaining the major ECM proteins.

However, sodium deoxycholate was effective only when used in high concentrations, raising concerns about the cytotoxicity of the produced scaffolds. On the other hand, SDS achieved complete decellularisation using much lower concentrations, which enabled the effective removal of the detergent, as confirmed by cytotoxicity studies (Wilcox *et al*., 2005). The same group also investigated the effects of different concentrations of SDS in hypotonic or isotonic buffer on the mechanical integrity of aortic valve leaflets, and reported increased extensibility of the decellularised leaflets due to the hypotonic buffer. Nevertheless, the strength of the decellularised tissue was comparable to the native aortic valve (Korossis *et al.,* 2002).

Zwitterionic detergents combine the properties of ionic and non-ionic detergents. These detergents have a greater capability to denature proteins than non-ionic detergents. Two different zwitterionic detergents have been used in decellularisation treatments, including 3-[(3-cholamidopropyl)dimethylammonio]-1-propanesulfonate (CHAPS; blood vessels) (Dahl *et al.,* 2003), and sulfobetaine-10 (SB-10) and -16 (SB-16) (nerves) (Hudson *et al.*, 2004a; 2004b). CHAPS-treated arteries showed histological properties similar to the native control, but significantly decreased burst pressure and maximum stress. Nevertheless the decrease was similar to the decrease obtained using Triton X – 100 and hypotonic/hypertonic solutions (Dahl *et al.,* 2003). CHAPS has been shown to be most effective for cell removal from thinner tissues (Petersen *et al.*, 2010) and less effective for thicker tissues (Du *et al.*, 2011).

Another method used in tissue decellularisation involves enzymatic digestion with proteases and nucleases (Ruoslahti and Pierschbacher, 1987). Nucleases, such as endonucleases and exonucleases, degrade ribonucleic acid (RNA) and deoxyribonucleic acid (DNA) (Tarone *et al.*, 1982). The most commonly used proteolytic enzyme is trypsin. Although enzymatic digestion with trypsin has been used as a means of decellularisation, it has been shown to be ineffective in producing acellular tissues (Korossis *et al*., 2002). Grauss *et al*. (2005) reported that the use of trypsin to decellularise porcine aortic valves caused distortion of elastic fibres, changes in collagen distribution, and washout of GAGs, chondroitin sulphate, laminin and fibronectin.

Hypertonic and hypotonic solutions have been used in decellularisation treatments due to their capabilities of dissociating DNA from proteins and causing cell lysis through osmotic effects with minimal changes in the ECM architecture (Cox and Emili, 2006; Xu *et al*., 2007). Mirsadraee *et al.* (2006) used a decellularisation protocol incorporating an ionic detergent (SDS), in combinations with hypotonic and hypertonic solutions, and enzymatic digestion.

They reported successful decellularisation of human pericardium, which retained its histoarchitecture and was void of cells and cell debris. The mechanical strength of the decellularised tissue was not significantly different compared to the native tissue.

1.2.10.4 Mechanotransduction in tissue engineering

Once implanted in the body, engineered constructs will be subjected to a complex biomechanical environment, potentially consisting of time varying changes in stresses, strains, fluid pressure, fluid flow, and cellular deformation (Guilak *et al.*, 1995). These physical factors influence the synthetic capabilities of the cells in the engineered tissues when implanted, determining the success or failure of the engineered grafts. Indeed, the cells convert mechanical stimuli into biochemical responses, which eventually lead to ECM protein production and cell differentiation, through a process called mechanotransduction (Ingber *et al*., 2006). Therefore, elucidating and understanding the mechanisms of mechanotransduction (Williams *et al.*, 1999) is of paramount importance in FTE. Many studies have suggested that physical factors may improve and accelerate tissue regeneration and repair *in vitro*. Mechanical stretch has been shown to increase cellular alignment, proliferation and protein synthesis in many different cell types (Buckley *et al.*, 1988). Mechanically interactive bioreactors have been used to increase matrix deposition in tissue engineered cartilage by using cyclic compression (Buschmann *et al.*, 1995). Other studies have shown improved success of tissue engineered constructs such as blood vessels by preconditioning grafts with pulsatile fluid flow and pressure (Niklason, 1999). It has been observed that forces transmitted bi-directionally between the cytoskeleton and the extracellular matrix (ECM) can switch hepatocytes between growth and differentiation (Mooney *et al*., 1992), and mechanically stressed dermal fibroblasts differentiate into myofibroblasts (Grinnell, 1994). Moreover, fluid-induced shear stress has a well-known impact on vascular cell morphology, proliferation, and orientation. The long term application of cyclic strain has been shown to increase organisation of engineered smooth muscle tissue *in vitro* (Kim *et al*., 1999), whereas exposing cartilage constructs to dynamic compression at physiological frequencies has been shown to enhance ECM synthesis rates in chondrocytes (Eschenhagen *et al*., 1997).

The elements involved in the mechano-chemical transduction include ECM, cell-ECM, and cell-cell adhesions, membrane components, specialized surface processes, cytoskeletal filaments, and nuclear structures. The ECM reacts when the whole tissue or organ is stressed, changing its original stress distribution. The cells in the tissue sense the distortion or

the change in the stress of the ECM through transmembrane adhesion receptors, such as integrins, which are connected to the cytoskeletal network of the ECM (Wang *et al*., 1993; Choquet *et al*., 1997; Ingber, 1997). Integrins are connected to the cytoskeleton through focal adhesion proteins; when they transfer the forces from the ECM to the cells, the cytoskeleton rearranges its interlinked actin microfilaments, microtubules and intermediate filaments, as well as associated organelles (e.g., mitochondria), to strengthen the whole cell against mechanical distortion (Wang *et al*., 1993; Ralph *et al*., 2002). The mechanical force transferred inside the cell can guide its differentiation. Cells need to attach to the ECM to divide; when the ECM rigidity increases, the cytoskeletal tension increases causing cell flattening, whereas, when the ECM rigidity decreases the force is transferred to internal microtubules causing cell rounding which can switch off cell division, turning on differentiation or even apoptosis. Depending on the level of the forces exerted on the cells, the stresses can be concentrated on specific molecules within the cells, affecting the change of specific biochemical activities (Ingber, 2006).

The complex mechanisms underlying mechanotransduction need to be fully determined, however, the basis of this process is beginning to be unravelled. The majority of research has been carried out in simple two-dimensional culture systems in which the cells are subjected to fluid flow and/or stretch. Most cell types *in vivo* exist in 3D and there are as yet, few studies of mechanotransduction in 3D systems. Moreover, the type and appropriate amount of mechanical stimuli needed to improve tissue formation remains unknown. The development of functional simulation systems for the study of tissues in response to physiological mechanical stimulation will provide important model systems for the enhancement of understanding into mechanotransduction, and the relationship between physical conditions, cellular function, matrix remodelling and tissue properties.

1.2.10.5 Cells in valvular tissue engineering

One of the main issues in the application of TE heart valves is appropriate cell sourcing since the patient's cells that are required to create autologous TE constructs are associated with a number of limitations. The most important of these include: the long time required for cell expansion to sufficient numbers, which may affect patient survival, and the decreased proliferative ability of cells from older patients. In general, two main cell type have been used in valvular TE, including differentiated stromal cells (such as ECs and/or SMCs), and stem cells (Mendelson and Schoen, 2006). Stem cells, which can be generally divided into two

main types, including adult and embryonic stem cells, have unique properties such as multipotency (adult), pluripotencey (embryonic), and capacity of self-renewal. Adult stem cells include hematopoietic stem cells (forming blood cells), endothelial progenitor cells (EPCs), and mesenchymal stem cells (MSCs). Adult stem cells are an attractive cell source since they can be easily isolated from bone marrow biopsies of the patients, and have extensive proliferation capacity *in vitro* (Vesely, 2005).

Endothelial progenitor cells (EPCs) are capable of differentiating into ECs. Since EPCs also circulate in the blood, they can be attracted by scaffolds coated with appropriate cell-signalling molecules, with a view to encouraging EPC adhesion and differentiation (Schoen, 2008). Cultured MSCs show spindle shape morphology, characteristic of myofibroblasts, and express cell markers characteristics of VICs. Studies have shown that MSCs injected in a mouse after infarction, have been able to differentiate into cardiac myocytes, ECs and vascular SMCs (Orlic *et al*., 2001). Other studies have reported that human MSC-derived cells showed a myofibroblastic phenotype expressing α-smooth muscle actin (α-SMA) and vimentin. Kadner *et al.* (2002) investigated the feasibility of using human bone-marrow-derived MSCs in the TE of heart valves. These cells were shown to express α-SMA and vimentin, and to produce collagen type I and III.

Embryonic stem cells generated a great interest in the tissue engineering field due to their high differentiation potential into all the three germ layers. However, there are ethical concerns associated with their harvesting which is embryo-destructive; in addition to this, embryonic stem cells derived cells may be rejected by the patient and undifferentiated embryonic stem cells may be tumorogenic (Forsberg and Hovatta, 2012).

Takahashi and Yamanaka (2006) successfully investigated the reprogramming of terminally differentiated cells in order to provide them with the capacities of pluripotent stem cells, including the capability of differentiating to any tissue of the body. These reprogrammed cells were called induced pluripotent stem cells (iPCs), and these cells, in contrast to embryonic stem cells, do not raise ethical concerns and may overcome the issue of immunological rejection. To date, no studies about heart valve engineering using iPCs have been reported in the literature. A few studies have, however, investigated the use of this cell type for vascular tissue engineering (Samuel *et al*., 2013; Hibino *et al.* 2012).

With regards to stromal cells, Shinoka *et al.* (1995) used a mixed population of SMCs and fibroblasts isolated from ovine femoral arteries and subsequently seeded onto PGLA and PGA

scaffolds. Unfortunately, femoral artery does not represent the ideal cell source due to the medical complications related to cells transplant. Schnell *et al.* (2001) cultured myofibroblasts, derived from human saphenous vein, on polyurethane scaffolds. This source represents a more clinically realistic cell source, since saphenous veins are already being used as heterotopic grafts in coronary artery bypass surgery, thus they can be harvested with minimally invasive surgery. Although promising results have been obtained using the aforementioned cell types, the ideal cell type for heart valve TE would be VICs and VECs, even though it would be very difficult to obtain them without damaging the valve of the patient (Flanagan and Pandit, 2003). Masoumi *et al.* (2013a) cultured porcine aortic and pulmonary VICs on anisotropic, micro-moulded poly(glycerol sebacate) scaffolds, and reported retention of the mechanical properties of the scaffolds and high collagen deposition after 14 and 28 day cultures.

1.2.10.6 Bioreactors for heart valve tissue engineering

Different types of bioreactors have been developed for the mechanical stimulation and conditioning/maturation of tissue-engineered cardiovascular constructs, including vascular grafts (Niklason *et al*., 1999; Seliktar *et al*., 2000), myocardial patches (Sodian *et al*., 2001), and heart valves (Zeltinger *et al*., 2001). The optimum TE bioreactor should provide simple modes of mechanical/hydrodynamic stimulation, accommodate multiple samples, and provide sterile and physiological temperature, oxygen and pH environment to the conditioning samples. In addition, the bioreactor should be able to replicate the biomechanical/hydrodynamic environment experienced by the native heart valves *in vivo*. Native heart valves *in vivo* are subjected to cyclic circumferential stretch, shear stress, and flexure during valve opening and closing (Berry *et al*., 2010).

In the field of valvular TE, the most commonly used bioreactors are pulse duplicators (Hoerstrup *et al.*, 2000a, 2000b; Dumont *et al.*, 2002; Hildebrand *et al.*, 2004), even though simple bioreactors exerting uniaxial tensile strain have been used for engineering mitral valve chordae (Shi and Vesely, 2004). Hoerstrup *et al.* (2000b) created one of the first heart valve bioreactors to culture/condition PGA valvular scaffolds seeded with carotid ECs and carotid myofibroblasts under gradually increased medium flow and pressure conditions. The cultured tricuspid valve leaflets were subsequently implanted into lambs and showed poor hemodynamic performance (Hoerstrup *et al.*, 2000a). Lichtenberg *et al.* (2006) developed a pulsatile flow bioreactor, which featured flow rate, pressure and temperature monitoring, and

this was used to condition decellularised human pulmonary valves seeded with human autologous EPCs for up to 21 days. The conditioned valves were then implanted at the pulmonary position of two paediatric patients. The 3.5 years follow-up showed normal patient growth and normal valve growth (Cebotari *et al*., 2006).

Flanagan *et al.* (2007) used a pulsatile flow bioreactor to condition fibrin-based tissue-engineered valves seeded with ovine carotid artery-derived cells for up to 12 days. The dynamically-conditioned valves showed enhanced deposition of ECM proteins, lower shrinkage and higher cell attachment and alignment, compared to control valves cultured in a beaker with stirring. Lee *et al.* (2009) also used a pulsatile bioreactor for the endothelialisation of decellularised pulmonary valves seeded with epithelial progenitor cells. The seeded valves demonstrated complete endothelialisation after 7 days of dynamic conditioning. Dohmen *et al.* (2011) reported on the clinical application of decellularised pulmonary allografts, seeded with autologous vascular ECs in a bioreactor system prior to implantation. Ten years postoperatively, the implanted valves showed no calcification and excellent haemodynamics.

Accumulating evidence suggests that bioreactors are important for the culture/conditioning/ maturation of tissue-engineered heart valves. However, even though the duplication of the physiological conditions experienced by native valves *in vivo* for the conditioning of the valvular TE constructs represents a plausible starting point, there is still a significant need for further research in optimising the conditioning/maturatrion of TE valves in terms of magnitude and frequency of the mechanical/haemodynamic stimulus. Along these lines, it would be beneficial to decouple the complex synergistic mechanical/haemodynamic stimuli experienced by heart valves, especially those with the more complex geometries (such as the AV valves), with a view to understanding the specific effect of different forces on cell function and construct remodelling and maturation.

1.2.10.7 Computational modelling for tissue engineering

Information on the mechanical/hydrodynamic environment of tissues is crucial in FTE. Many of the tissues and organs that require replacement, such as the heart valves, have an important biomechanical function. Thus, *in vivo* stress-strain mechanical histories need to be measured in order to provide the appropriate mechanical properties to the constructs. For tissues such as heart valves, there is a lack of experimental information on the *in vivo* mechanical environment due to the inability or limitations of physically measuring it. For such cases, *in vivo* strain can only or more easily be estimated by analytical and computational

methods. The information provided through computational modelling can then be used for the maturation/conditioning of TE constructs *in vitro*. Computational modelling has also been used to estimate the dynamic strain magnitude after *in vitro* conditioning (Mol *et al*., 2005), to optimise tissue growth in bioreactor culture (Wick and Farooque, 2009) and to investigate the impact of fluidic forces and stresses on cells and tissue engineered constructs during growth *in vitro* (Hutmacher and Singh, 2008).

The bioreactor used in this study was a cyclic strain simulator, which was designed to subject the pericardial samples to biaxial stretching, similar to the circumferential and radial stretching experienced by the MV leaflets *in vivo*. The deformation of the scaffolds in the bioreactor stations used in this study was designed to duplicate the deformation of the MV leaflets *in vivo*, characterised by inflation during systole and deflation during diastole. Dynamic flexure induced by cyclic inflation/deflation has been reported as being the major mode of deformation of heart valve leaflets (Vesely and Boughner, 1989). A strain value of 10% was chosen to be applied on the pericardial scaffold, representing the maximum physiological strain experienced by the MV anterior leaflets during the cardiac cycle, obtained through computational modelling of the MV apparatus performed by Roberts (2012). Roberts (2012) investigated the deformations experienced by the MV leaflets using mathematical models. He studied the geometry and a constitutive model to describe the mechanical properties and behaviour of the MV leaflets, and then he brought them together to finally create the finite element model. Roberts then modelled the annular deformation using different annular configurations (fixed annulus and elastic boundary method to obtain 15% and 25% saddle height ratios (SVR)). The model showed highly regional characteristics of the strains.

Little work has been focused on the modelling of the MV compared to the aortic valve. The reason for this is related to the fact that the MV is non-symmetrical and anatomically more complex than the aortic valve. Finite element model analysis of the MV leaflets was performed by a few groups (Kunzelman *et al*., 1993b; Einstein *et al*., 2005; Dal Pan *et al.* 2005; Lim *et al.* 2005; Votta *et al.* 2008). A number of published *in vitro* experimental studies into anterior leaflet deformation at physiological pressures can be found in the literature (Sacks et al., 2002; Chen et al., 2004a; He et al., 2005; Jimenez et al., 2007). In particular, Sacks *et al.* (2002) placed three- dimensional spatial positions of markers in the central region of the MV anterior leaflet in a left ventricle-simulating flow loop to investigate the strains in the leaflet; they reported mean peak strain values ranging from 2.5 to 3.3% in the circumferential

direction and between 16 to 22% for the radial direction. Jimenez et al. (2007) used a similar experimental approach; the values of the peak strain in the radial direction ranged between 13.52 and 29.72% depending on the annular configuration, whereas the peak strain for the circumferential direction was 11% and was not affected by the change in annular configuration. Several approaches have been taken to attempt to quantify MV dynamics through *in vivo* experiments; in a study by Sacks and Yoganathan (2007), sonomicrometry was used for the quantification of the strains of the anterior leaflets. Their finding showed areal strain values (defined as the changes in the area) ranging from 15 to 20% throughout the cardiac cycle. Nevertheless, the highly dynamic motions, large anisotropic deformations, complex surface geometries of the MV represent an obstacle for currently available imaging technologies; thus, the quantification of the magnitudes of strains on the valve have proven difficult to measure.

1.3 Aims and objectives

Aims:

The aim of this study was to investigate the tissue engineering of MV leaflets for MV leaflets reconstruction. The experimental approach involved the use of decellularised porcine pericardium seeded with porcine MSCs and mechanically conditioned in a biaxial strain bioreactor.

The underpinning hypothesis was that a MV leaflet-relevant biomechanical and biochemical environment *in vitro* could selectively guide recellularisation of decellularised pericardial scaffolds in order to produce MV leaflet equivalents.

The biomechanical and biological properties of porcine MV leaflets and decellularised and native porcine pericardium were studied for comparative purposes. The cell type, seeding density and time for seeding decellularised pericardial samples were assessed. Finally, the decellularised constructs seeded with MSCs were cultured in a bioreactor, under dynamic conditioning for up to 1 day to investigate the effects of biaxial strain on cell viability and alignment of the cell-seeded constructs.

Objectives:

- To compare the biological, biochemical and biomechanical properties of porcine MV leaflets and pericardium.
- To assess the effects of decellularisation of porcine pericardium on the histoarchitecture, the total amount of DNA, the presence of specific matrix proteins and on the mechanical properties of the tissue by comparison with fresh pericardium.
- To determine the *in vitro* biocompatibility of the decellularised porcine pericardium.
- To investigate the seeding density and time for culturing different cells types (porcine dermal fibroblasts, SMCs, MSCs) on the decellularised porcine pericardium under static conditions prior to loading on the bioreactor.
- To calibrate the bioreactor, in terms of the frequency and strain level to apply during mechanical conditioning of the decellularised porcine pericardial samples seeded with pMSCs.
- To investigate the function of the bioreactor under static conditions in terms of sterility maintenance and cell culture medium circulation using fresh porcine pericardial samples.
- To investigate the static culture of the cell-seeded pericardial scaffolds in the biaxial bioreactor under sterile conditions.
- To investigate the effects of the dynamic conditioning on the viability and spatial arrangement of cells as well as on the histoarchitecture of the cell-seeded scaffolds cultured in the bioreactor.

Chapter 2

General Materials and Methods

This chapter describes the general materials and methods used to investigate the histological, immunohistochemical, biochemical and biomechanical properties of fresh and decellularised porcine pericardium and fresh mitral valve (MV) leaflets, both anterior and posterior. In addition, it describes cell culture techniques and cell viability assays used throughout this study.

2.1. Equipment

The laboratory equipment used in order to carry out the experiments in this project is listed in Table 2.1.

Equipment	Model	Supplier
Actuator	Superpump	Vivitro system
Actuator controller	Smart step microstepping smartdrive PCW-5008	Industrial Devices Corporation
Autoclavable bag	-	Westfield limited
Automatic Pipettes	Gilson P2-P1000	Anachem Ltd
Automatic Pipettes	Finnipipette® P2-P1000	Thermo Fisher Scientific Inc
Balances (Accuracy: 0.01g/0.0001g)	GR200/GX2000	Jencons PLC
Bench top centrifuge	5415R	Eppendorf
Blood tissue spinner	SB3	Stuart
Cell counter	-	ENM
Cell medium aspirator	Vacusafe comfort	Integra Biosciences
Centrifuge tube	-	Fisher Scientific
Chemostat	Bioconsole ADI 1025	Applikon biotechnology
Chemostat controller	Biocontroller ADI 1010	Applikon biotechnology
Class II safety cabinet	Herasafe	Heraeus
Class II safety cabinet	11518/85	Heraeus
CO2 Incubator	MCO-20AIC	SANYO Biomedical Europe BV

Culture tubs (500 ml)	-	Nalgene
Freezer (-20°C)	Electrolux 3000	Jencons Plc
Fridge	Electrolux ER8817C	Jencons Plc
Fume cupboard/fume hood	-	Whiteley
Heater controller	-	Electrical Engineering, University of Leeds
Flexible silicone rubber heaters	020100C2 100 (Watts)	Watlow
Histology cassettes	CMB-160-030R	Thermol Fisher Scientific Ltd
Histology water bath	MH8515	Barnstead Electrothermal
Hot forceps	Speci-leps	BIOS EUROPE
Hot plate	E18.1 hotplate	Raymond A Lamb
Hot wax dispenser	E66 wax dispenser	Raymond A Lamb
Light box	KL003	Kermo limited
Luer (stainless steel)	(Various)	Cole parmer
Magnetic stirrer	Stuart SB161	Scientific Laboratory Systems Ltd
Micro plate spectrophotometer	Multiskan spectrum	Thermo Scientific
Microscope (upright)	Olympus BX51	Microscopes, medical Diagnostic Systems and Olympus Patient systems Ltd
Microscope (inverted phase contrast)	Olympus CK40	Microscopes, medical Diagnostic Systems and Olympus Patient systems Ltd
Microscope (inverted phase contrast)	Olympus IX71	Microscopes, medical Diagnostic Systems and Olympus Patient systems Ltd
Microtome	RM2125 RTR	Leica Microsystems
Microwave KM19W, 800w PROLINE	KM19W, 800w	PROLINE
Monitor for the actuator	B8961	Industrial Devices Corporation
Nanodrop Spectrophotometer	ND-1000	Labtech Int
Orbital shaker	POS300	Grant-bio

Orbital shaker	IKA KS130 basic	Jencons Plc
Oven (hot air)	OMT225	SANYO Biomedical Europe BV
Peristaltic pump	Easy load II77200-50	Cole parmer
Peristaltic pump	Multichannel pump 7536-04	Cole parmer
pH meter	Jenway 3010	VWR International
Plastic histology cassettes Ltd	CMB-160-030R	Thermo Fisher Scientific
Plate reader	Multiskan Spectrum 1500	Thermo Fisher Scientific
Plate shaker	IKA KS130 basic	Jencons Plc
Pipette boy	Acu	Intergra Biosciences
Quick connectors	(Various)	Cole parmer
Silicone o rings	(Various)	Thomson Bros. Limited
Silicone tubes	-	Masterflex
Slide holder	E102	Raymond A Lamb
Sterile filter	Midisart 2000	Sartorius stedium biotech
Sterile gloves	-	Kimberly-Clark
Stopcock	Luer fittings, nickel-plated brass three-way stopcocks	Cole parmer
Temperature probe	-	RS
Tensile testing machine	3365	Instron® tensile tester
Thickness gauge	-	Mitutoyo
Tissue processor	TP11020	Leica Microsystems
Vortexer 2	MS2 minishaker	IKA
Water bath	Grant	Jencons Plc
Wax oven	Windsor E18/31	Scientific Laboratory Supplies

Table 2.1: Equipment used throughout the study.

2.2 Chemicals

The chemicals used during this project are listed in Table 2.2.

Chemical/Reagent	Supplier
Acetic acid	Thermo Fisher Scientific Ltd
Acetone	European Bios
Alcian blue	Raymond A Lamb
Alpha-SMA	Sigma
Amphotericin B	Lonza
Antifoam	Sigma
Aniline blue (Masson trichrome staining)	Bios Europe
Aprotinin 10 KIU.ml^{-1}	Nordic pharma
Biebrich scarlet acid fuchsin (Masson trichrome staining)	Bios Europe
Bovine serum albumin	Sigma-Aldrich
Calcium chloride	VWR International
Chloramine T	Sigma-Aldrich
Citric acid	VWR International
Collagenase	Sigma
Collagen I	Millipore MAB3391
Collagen III	Abcam, ab7778
Collagen IV	Dako M0785
Chondroitin sulphate	Sigma
Chondroitin sulphate B	Sigma-Aldrich
DABCO	Sigma-Aldrich
p-dimethylaminobenzaldehyde	Sigma-Aldrich
1,9 dimethylene blue	Sigma-Aldrich
Dimethyl sulfoxide (DMSO)	Sigma-Aldrich
DNeasy blood & tissue kit	QIAgen
DNAse	Sigma-Aldrich
DPX mountant	Thermo Fisher Scientific Ltd
Dulbecco's PBS tablets	Oxoid Microbiology Products, Thermo Scientific

Eosin	Biostain
Ethanol	Thermo Fisher Scientific Ltd
Ethylenediaminetetraactic acid (EDTA)	Fisher Scientific
Fibronectin	Dako A0245
Foetal calf serum	Biosera
Formaldehyde	Biostain
Formic acid	Sigma-Aldrich
Gentamicin	Biochrom
Giemsa solution	VWR International
Glacial acetic acid	VWR International
Glycerol	Sigma-Aldrich
Hank's balanced salt solution (HBSS)	Lonza
Haematoxylin (for H&E)	Lamb
Haematoxylin solution, Gill No. 3 (for Alcian blue-PAS)	Sigma-Aldrich
HEPES buffer (1M)	Lonza
Hydrochloric acid (12M)	VWR International
Hydrogen peroxide (30%, v/v)	Sigma-Aldrich
Isotype control	DAKO
Isotype control	GeneTex
Laminin	Sigma L8271
L-glutamine	Invitrogen
Live/Dead assay kit	Invitrogen
Magnesium chloride	Thermo Fisher Scientific Ltd
Methanol	Vichers Laboratories
Miller's elastin	Raymond A Lamb
MTT reagent	Sigma-Aldrich
Neutral buffered formalin	Biostain Ready Reagents
Nuclease free water	Fermentas
Nutrient agar	University of Leeds

Oxalic acid	VWR International
Paraffin wax	Thermo Fisher Scientific Ltd
PBS with Ca and Mg	Lonza
PBS without Ca and Mg	Lonza
Penicillin	Invitrogen Ltd
Peracetic acid	Sigma-Aldrich
Perchloric acid (60%)	BDH
Percoll	Sigma-Aldrich
Picric acid	Sigma-Aldrich
Picro sirius red	VWR International
pH standards (4,7,10)	Scientific Laboratory Supplies Ltd
Polymyxin B	Fluka analytical
Potassium permanganate 5% (w/v)	Bios Europe
Propan-1-ol	VWR International
RNAse	Sigma-Aldrich
SAB agar	University of Leeds
Schiffs reagent (Alcian blue-PAS)	Sigma-Aldrich
Sodium acetate	Thermo Fisher Scientific Ltd.
Sodium azide	Sigma-Aldrich
Sodium chloride	Thermo Fisher Scientific Ltd
Sodium di-hydrogen orthophosphate	VWR International
Sodium dodecyl sulphate (SDS)	Sigma Life Science
Sodium formate	VWR International
Sodium hydroxide	VWR International
Streptomycin	Invitrogen
Trans-4-hydroxy-L-proline	Sigma-Aldrich
Trigene Scientific	Laboratory Supplies Ltd
Tripsin	Sigma-Aldrich
Trizma base	Sigma-Aldrich

Trypan blue	Sigma
Trypsin (0.25% w/v)/EDTA	Lonza
Tyrode's balanced salt solution	Sigma-Aldrich
Tween 20	Sigma-Aldrich
Vancomycin hydrochloride	Aldrich chemistry
Vimentin	Leica
Virkon	Scientific Laboratory Supplies Ltd
Von Willebrand	Dako A0082
Weigert's iron hematoxylin (Masson trichrome staining)	Bios Europe
Xylene	Genta medical

Table 2.2: Chemicals and reagents used throughout the study.

2.3 Consumables

The consumables and plasticware used during this project are listed in Table 2.3 and Table 2.4, respectively.

Item	Model/Size	Supplier
Glass coverslips Scientific	MIC3228	Laboratory Supplies
Filter paper	Whatman® Grades 1-5	Whatman International Ltd
ImmEdge Hydrophobic Barrier Pen	H-000	Vector Laboratories
Microtome blades	SD3050835	Fisher Scientific
Parafilm M	-	Sigma-Aldrich Ltd
Scalpel blade	Size 22	Fisher Scientific
Superfrost Microscope Slide	MIC3040	Scientific Laboratory Supplies
Superfrost Plus Microscope Slide	MIC3022	Scientific Laboratory Supplies
Syringe needles	-	Thermo Fisher Scientific Ltd

Table 2.3: General consumables used throughout the study.

Item	Model/Size	Supplier
Bijous	5 ml	Scientific Laboratory Supplies Ltd
Cell culture flasks	75 cm^2	Thermo Fisher Scientific Ltd
Disposable plastic syringes	1ml, 2ml, 5ml, 10ml, 20ml, 50ml	Scientific Laboratory Supplies
Eppendorf	1.5ml	Sigma-Aldrich
Pipette tips (non-filtered)	10µl, 20µl, 200µl, 1000µl, 5000µl	Star Labs
OptiplateTM	96-well	PerkinElmerTM
Universals	25ml	Scientific Laboratory Supplies
Well plates, Nunc® (flat and round bottomed)	6-well, 12-well, 96-well plates	Thermo Fisher Scientific Ltd

Table 2.4: Plasticware used throughout the study.

2.4 Cells

Porcine skin fibroblasts, porcine mesenchymal stem cells (pMSCs) and porcine smooth muscle cells (pSMCs) were used in this study. The cells had been previously isolated, cryopreserved and stored in the in-house cell bank. Specifically, dermal fibroblasts were isolated from porcine skin by collagenase digestion by Dr. Iraklis Papageorgiou; pSMCs were isolated by Dr. Helen Wilcox from porcine aorta according to the explant method described by Wilcox *et al*. (2005) and pMSCs were isolated from porcine bone marrow by Dr. Rick Knight and Dr. Daniel Thomas using the Percoll gradient method described by Knight (2003). Cells were resurrected from frozen. Dermal fibroblasts and pSMCs were cultured for phenotyping by immunofluorescence. pMSCs were phenotyped using flow cytometry by Dr Daniel Thomas.

2.5 General stock solutions

2.5.1 Phosphate buffered saline (PBS)

PBS was prepared by dissolving 1 tablet of Oxoid Dulbecco PBS in 100 ml of distilled water using a magnetic stirrer and stirrer bar. The pH was adjusted to 7.2 – 7.4 by adding 6 M

hydrochloric acid or 6 M sodium hydroxide while stirring. The solution was autoclaved at 121°C and 15 lb sq. in. for 20 min and stored for up to 1 month at room temperature.

2.5.2 Tris buffered saline (TBS)

Tris solution (2 M) was prepared by dissolving 242 g of trizma base into 500 ml of distilled water. The pH was adjusted to 7.6 by adding 6 M hydrochloric acid or 6 M sodium hydroxide. The volume was made up to 1 L with distilled water. A volume of 25 ml of the Tris solution was mixed with 50 ml of 3 M sodium chloride solution. The volume was made up to 1 L with distilled water and the pH was adjusted to 7.6. Finally, the solution was autoclaved at 121°C and 15 lb. sq. in. for 20 min and stored for up to 1 month at room temperature.

2.5.3 TBS containing 0.05% (w/v) Tween 20

Tween 20 (500 µl) was added to 1 L of TBS. The pH was adjusted to 7.6 and the solution was stored at room temperature for up to 3 months.

2.5.4 Complete cell culture medium

Dulbecco's modified Eagle's medium (DMEM) was supplemented with 10% (v/v) foetal bovine serum (FBS), 100 $U \cdot ml^{-1}$ penicillin, 100 $U \cdot ml^{-1}$ streptomycin, and 2 mM L-glutamine. This was stored for up to two weeks at 4°C.

2.6 Preparation, cleaning, and sterilisation of glassware

Reusable glassware, such as bottles and measuring cylinders, were washed with detergent, rinsed and whenever necessary, sterilised. Immediately after use, the glassware was washed manually using Decon in tap water with brushes.

2.6.1 Dry heat sterilisation

All glassware and metal surgical instruments that could be sterilised by dry heat were covered with aluminium foil and placed in an oven and kept at 190°C for 4 hours.

2.6.2 Moist heat sterilisation (autoclaving)

Solutions and plasticware, not suitable for dry heat sterilisation, were sterilised by autoclaving at 121°C and 15 lb. sq. in. for 20 minutes.

2.6.3 Filter sterilisation

Solutions not suitable for autoclaving were sterilised using single use 0.2 µm filters (Scientific Lab Supplies, UK) and a disposable syringe.

2.7 Measurement of pH

A Jenway 3010 pH meter was used to measure the pH of the solutions. The pH meter was calibrated using pH standard solutions at pH 4, 7 and 10. The solutions were gently stirred during measurements using a magnetic stirrer. The values were taken when the reading reached a steady state. To adjust the pH of the solution, 1-6 M hydrochloric acid or 1-6 M sodium hydroxide was added drop-wise while stirring.

2.8 Dissection of porcine pericardium and mitral valve leaflets

Porcine hearts were obtained from 24-26 weeks old pigs from a local abattoir and dissected within 3-4 hours of slaughter. The dissected tissues were either frozen, or used immediately for the biomechanical and biological testing. Loose pericardium (parietal layer) was separated from the heart and gently stripped of the adherent layer of fatty tissue (Figure 2.1). Excess tissue (fat and connective tissue) was carefully trimmed from the pericardium using scissors.

Figure 2.1: Dissection of porcine pericardium. Separation of the parietal layer from the heart.

Following isolation of the pericardium, the heart was exposed and the MV leaflets were dissected (Figure 2.2). During MV leaflet dissection, the heart was separated in two parts by cutting along the inter-ventricular septum, in order to isolate the left side of the heart. The left

atrium was then removed, and the left ventricle was opened in order to access the MV leaflets. The leaflets were separated from the chordae tendineae and the annulus fibrosus, leaving a small bar (around 0.5 - 1 cm) of the annulus fibrosus attached to the leaflets (Figure 2.2c).

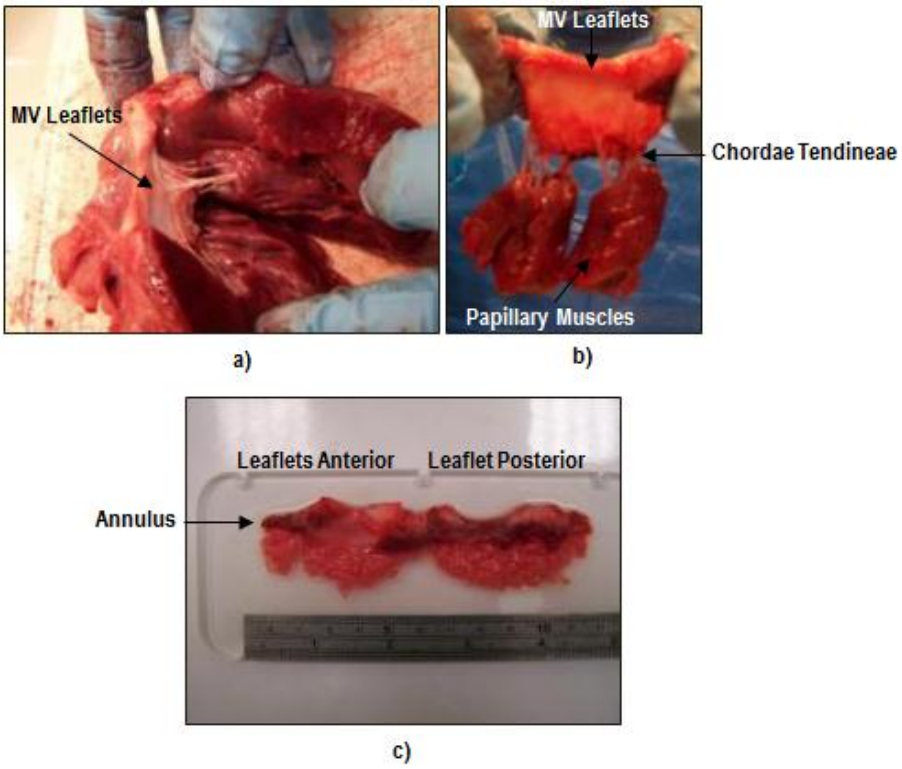

Figure 2.2: Dissection of porcine mitral valve leaflets. (a) Open view of the left ventricle, after removal of the left atrium. (b) The mitral valve apparatus consisting of the leaflets, chordae tendineae and papillary muscles. (c) Anterior and posterior leaflets with a small bar (around 0.5-1 cm) of annulus fibrosus. MV: mitral valve.

2.9 General experimental approach

Six pericardia were isolated from six different hearts and were decellularised according to the in-house decellularisation protocol. Fresh pericardia were also used for the biomechanical and biological testing (6 in each case). Decellularised and fresh pericardial samples, measuring 5 mm width by 10 mm length, were cut across and along the collagen fibre alignment, (Fig. 2.3a, b) and tested biomechanically, histologically and immunohistochemically. Fibre alignment was visualized using a light box and two polarized light filters. Fresh and decellularised samples with no particular fibre orientation were used for biochemical analysis.

Anterior and posterior MV leaflet strips measuring 5 mm width by 10 mm length were cut along the circumferential and radial direction (Fig. 2.3c) and tested biomechanically, histologically and immunohistochemically. Due to the small size of the leaflets, it was only possible to isolate one sample per leaflet per heart. Anterior and posterior leaflet samples with no particular fibre orientation were used for biochemical analysis. The test groups used for biomechanical and histological analysis, together with their abbreviations are summarised in Table 2.5.

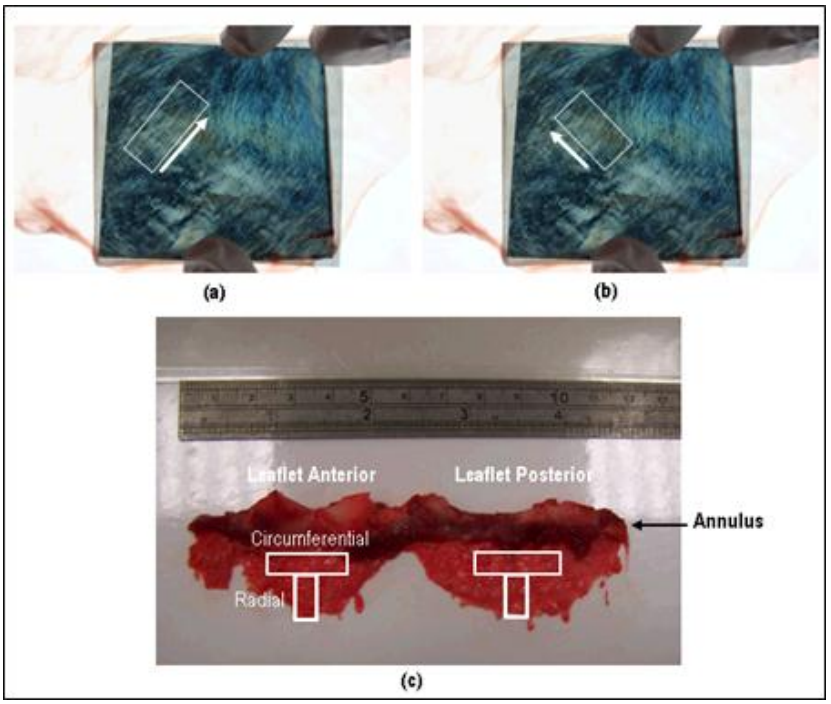

Figure 2.3: Orientation of pericardial and MV leaflet samples used in the biomechanical and histological testing: Fresh pericardial samples were isolated parallel (a) and orthogonally (b) to the collagen fibre alignment. Leaflet samples were isolated along the circumferential and radial directions of the leaflets (c).

Abbreviation	Description
PO	Pericardium orthogonal to the collagen fibred alignment
PP	Pericardium parallel to the collagen fibres alignment
DPO	Decellularised pericardium orthogonal to the collagen fibres alignment
DPP	Decellularised pericardium parallel to the collagen fibres alignment
LAR	Leaflet anterior along the radial direction
LAC	Leaflet anterior along the circumferential direction

LPR	Leaflet posterior along the radial direction
LPC	Leaflet posterior along the circumferential direction

Table 2.5: Abbreviations of the test groups used throughout the project.

2.10 Sample preparation for histology & immunohistochemistry

2.10.1 Tissue fixation

Tissue samples were placed into individual histological cassettes. The tissues were fixed in 10% (v/v) neutral buffered formalin (NBF), for 1 to 2 hours prior to tissue processing.

2.10.2 Tissue processor and paraffin embedding

Dehydration, clearing and infiltration were performed using an automated tissue processor. The cassettes containing the tissue blocks were sequentially immersed in 10% (w/v) neutral buffered formalin, 70% (v/v) ethanol, 90% (v/v) ethanol, 100% ethanol, 100% ethanol, 100% ethanol, three pots of xylene, and three final steps of paraffin waxing. The samples were immersed in each solution for 1 hour under vacuum at room temperature except the waxing which was carried out at 50°C. Subsequently, the histology cassettes were removed and transferred to fresh molten wax. The tissues were removed from the cassettes and correctly oriented in wax block moulds containing molten wax. The samples were positioned so that they were cut along the thickness of the tissue; in this way the different layers of the leaflets and the pericardium could be clearly observed by microscopy following histological staining and immunohistochemistry. The samples were left to cool and harden at room temperature. The wax blocks were removed from the mould, with the block left attached to the cassette base, and the excess wax was trimmed.

2.10.3 Sectioning and slide preparation

The paraffin embedded tissue samples were sectioned using a microtome at a thickness of 6 μm. The isolated sections were carefully transferred to a 45 - 50°C water bath before they were transferred onto Superfrost microscope slides for histological staining or Superfrost Plus slides for immunohistochemistry labelling. The tissue sections were then dried using a 60°C hotplate.

2.10.4 Tissue section dewaxing and rehydration

The slides were immersed into 2 pots of xylene for 10 min each, inside a fume hood, before they were sequentially immersed in three pots of 100% ethanol for 3, 2 and 2 min, respectively, in a pot of 70 % (v/v) ethanol for 2 min and finally into running tap water for 3 minutes.

2.10.5 Dehydration and mounting

Following staining, all sections were immersed into 70 % (v/v) ethanol for 5 sec, followed by immersion in 3 different pots of 100 % ethanol for 1, 2, 3 min, respectively. Finally, the sections were immersed sequentially into 2 different pots of clean xylene (clearing solvent) for 10 min each inside a fume hood. The sections were then mounted using DPX mountant and were left to air dry for a minimum of 4 hours inside a fume hood.

2.11 Histological Staining

2.11.1 Haematoxylin & eosin

Rehydrated sections were placed in Mayer's hematoxylin solution for 1 min. Subsequently, the slides were rinsed until clear under running tap water, and then immersed in eosin solution for 3 min. The stained sections were then dehydrated and mounted as described in Section 2.10.5.

2.11.2 Alcian blue- periodic acid and Schiffs reagent (PAS)

Rehydrated sections were immersed in Alcian blue solution for 15 min and rinsed in running tap water for 1 min. The sections were then treated in periodic acid and Schiffs reagent (PAS) for 5 and 15 min, respectively. Subsequently, the sections were rinsed in running tap water for 5 min and counterstained in hematoxylin for 90 sec to stain the cell nuclei. Finally, the slides were dehydrated and mounted as described in Section 2.10.5.

2.11.3 Sirius red and Millers elastin

Rehydrated sections were treated for 5 min with potassium permanganate 5 % (w/v), rinsed in distilled water and immersed into 1 % (w/v) oxalic acid for 2 min. The slides were then rinsed well using distilled water and then immersed in 70 % (v/v) and 95 % (v/v) ethanol. Following this, the slides were stained using Miller's stain for 1 h. The slides were then rinsed in 70 %

(v/v) and 95 % (v/v) ethanol and tap water. The sections were counterstained with Weigerts hematoxylin for 10 min, and then rinsed in tap water and distilled water. Finally, the slides were stained using picro Sirius red for 1 h and rinsed in distilled water before blotting dry. The slides were dehydrated and mounted as described in Section 2.10.5.

2.11.4 Masson's trichrome

Rehydrated sections were fixed by immersion in Bouin's solution overnight. This type of fixation enhanced trichrome intensity and brilliance. Following this, the slides were rinsed sequentially in running tap water and distilled water in order to wash out the Bouin fixative. The slides were immersed for 7 min in Weigert's iron hematoxylin solution to stain the cell nuclei. The sections were then stained in Biebrich Scarlet acid fuchsin for 7 min (cell cytoplasm and muscle staining), rinsed in distilled water and placed in phosphotungstic acid solution for 10 min to allow for a better staining of the collagen fibres during the subsequent immersion in aniline blue solution for 7 min. The sections were rinsed briefly and dehydrated and mounted as described in Section 2.10.5.

2.12 Immunohistochemistry

2.12.1 Antigen retrieval methods

Antigen retrieval is useful in order to unmask the antigens that can be masked due to the tissue fixation procedure. Antigen retrieval reagents were used to pretreat the tissue sections in order to break the protein cross-links formed by formalin fixation and thereby uncover hidden antigenic sites.

Citric acid microwave treatment

Reagents

- Citric acid buffer solution (10mM) was adjusted to pH 6.0 using NaOH (6 M).

Method

The slides were laid out on a pyrex dish so that they did not overlap, and with the tissue sections facing upwards. Citric acid was added in the pyrex dish in order to cover the tissue

sections. The pyrex dish was then covered with cling film and microwaved on full power for 10 min. After the dish was cooled, the slides were removed.

Proteinase k

Reagents

- Proteinase k (Dako) was used for the proteolytic digestion of the tissue sections.

Method

The sections were treated with one drop of proteinase k for 7 min before they were rinsed in running tap water for 5 min.

Trypsin retrieval method 1 (0.1 % w/v trypsin)

Reagents

- Trypsin solution was prepared by dissolving 0.1 g trypsin and 0.1 g calcium chloride in 100 ml TBS (pH 7.6). The trypsin solution was then warmed to 37°C, and the pH was adjusted to 7.8 by adding drops of 1 M sodium hydroxide.

Method

The sections were incubated at 37°C for 10 min in prewarmed distilled water before they were digested in trypsin at 37°C for 30 min. The sections were then rinsed in running tap water for 5 min.

Trypsin retrieval method 2 (0.5 % w/v trypsin)

This method was the same as the trypsin retrieval method 1, but in this case the trypsin solution was prepared by dissolving 0.5 g trypsin instead of 0.1 g.

2.12.2 Antibodies

The primary antibodies, isotypes and antigen retrieval methods are illustrated in Table 2.6. The protein concentration used for the isotype control was the same as the specific primary antibody.

Antigen	Suppli-er	Clone	Isotype	Antigen retrieval method	Diluted concentration	Antibo-dy dilution	Isotype dilution
Alpha-SMA	Sigma A2547	1A4	Mouse IgG2a (Dako X0943)	Trypsin (Method 1)	15.25 $mg \cdot L^{-1}$	1:400	1:6
Collagen I	Millipore MAB3391	5D8-G9	Mouse IgG1 (Dako X0931)	Trypsin (Method 1)	10 $mg \cdot L^{-1}$	1:50	1:5
Collagen III	Abcam, ab7778	-	Rabbit IgG (GeneTex, GTX35035)	Proteinase k	20 $mg \cdot L^{-1}$	1:50	1:750
Collagen IV	Dako M0785	CIV 22	Mouse IgG1 (Dako X0931)	Proteinase k	1.6 $mg \cdot L^{-1}$	1:50	1:3
Fibronectin	Dako A0245	-	DAKO rabbit immunoglo-bulin Fraction, code X0936	Trypsin (Method 2)	49 $mg \cdot L^{-1}$	1:100	1:300
Laminin	Sigma L8271	LAM-89	Mouse IgG1 (Dako X0931)	Proteinase k	9 $mg \cdot L^{-1}$	1:800	1:10
Chondroitin sulphate	Sigma	CS-56	Mouse IgM (Dako X0942)	Proteinase k	3 $mg \cdot L^{-1}$	1:200	1:33
Vimentin	Leica	NCL-L-VIM-V9	Mouse IgG1 (Dako X0931)	Citric acid microwave	78 $mg \cdot L^{-1}$	1:50	2:3
Von Willebrand	Dako A0082	-	DAKO rabbit immunoglo-bulin Fraction, code X0936	Proteinase k	15.5 $mg \cdot L^{-1}$	1:200	1:1000

Table 2.6: Primary antibodies, isotypes and antigen retrieval methods used.

2.12.3 Immunohistochemistry protocol

Reagents

The reagents used for the immunohistochemistry were:

- TBS pH 7.6;
- TBS containing 0.05 % (v/v) Tween 20, pH 7.6;
- Antibody diluent: 100 ml TBS (pH 7.6) supplemented with 0.01 % (w/v) sodium azide and 0.01 % (w/v) bovine serum albumin (BSA). The pH was adjusted to pH 7.6 and the solution was stored at 4 °C and used within 1 month;
- PBS pH 7.2 - 7.4;
- 3 % (v/v) hydrogen peroxide (H_2O_2), prepared by diluting 30 % (v/v) H_2O_2 10× using PBS at pH 7.6;
- Ultravision Detection kit (only with mouse and rabbit primary antibodies).
- Substrate chromagen: 20 µl of liquid DAB + chromagen was added to 1 ml of substrate buffer and mixed thoroughly.

Method

Paraffin embedded tissue sections were dewaxed and rehydrated as described in Section 2.10.4. Antigen retrieval was carried out according to the manufacturer's instructions. The sections were incubated in 3 % (v/v) H_2O_2 to block endogenous peroxidase activity present in the tissue. The sections were then washed in running tap water for 3 min and the tissue samples on each slide were circled using a hydrophobic marker. The sections were washed using TBS and 1 drop of dual endogenous enzyme block was added to each section (10 min of incubation). The sections were then washed twice for 10 min using TBS. The primary monoclonal antibody was applied at a suitable dilution (according to manufacturer's instructions) and incubated in a moist atmosphere (humid chamber) at room temperature for 60 min (overnight at 37°C for collagen I).

Two negative controls were used; the primary antibody was replaced by the isotype control (at a suitable concentration) in one section and by no antibody in another section. Following the application of the primary antibody or the isotype control, the sections were washed twice for 10 min using TBS containing 0.05 % (w/v) Tween, followed by another 2 washes in TBS of 10 min each. Subsequently, 20 µl of labelled polymer-HRP was applied onto each section and incubated for 30 min at room temperature in the dark. The Polymer-HRP had the same

function as a secondary antibody, thus, it attached to the primary antibody and to the substrate chromagen in order to allow the final coloured reaction. The sections were then washed twice for 10 min using TBS containing 0.05 % (w/v) Tween 20, followed by another 2 washes in TBS of 10 min each. Excess buffer was tapped off. Finally, 15 µl of substrate chromagen was added from the Envision kit to each section, in order to visualise the labelling of the sections, and incubated for 10 min at room temperature. After 4 washes in distilled water, the sections were counterstained through immersion into hematoxylin for 10 s. The sections were then rinsed using tap water until the water ran clear. Finally, the sections were dehydrated and mounted as described in Section 2.10.5.

Data analysis

Images of the tissue sections treated for histology and immunohistochemistry were captured using an Olympus BX51 microscope.

2.13 Electron Microscopy

Tissue for scanning electron microscopy (SEM) was fixed overnight with 2.5 % (w/v) glutaraldehyde and post-fixed overnight with 1 % (w/v) osmium tetroxide and then dehydrated using an ascending alcohol gradient. Following dehydration, critical point drying was carried out using a Polaron E3000. The tissue samples were then coated with gold and mounted on 13 mm diameter stubs. Fresh specimens prepared for environmental scanning electron microscopy (ESEM) analysis were imaged immediately after mounting on pin stubs. The samples were imaged for both SEM and ESEM analysis in an FEI Quanta 200F FEG ESEM.

2.14 Biochemical Assays

2.14.1 Freeze-drying

Tissue samples were frozen overnight at -20°C for subsequent biochemical assays. The wet weights for the different tissues used in the biochemical assays are reported in Table 2.7. The samples were lyophilised at -40°C for up to 3 days. The tissue samples were weighed after 24 hours, 48 hours and 52 hours to ensure a constant weight in order to have complete dehydration.

Tissue and abbreviations	Hydroxyproline (mg)	Hydroxyproline denatured (mg)	Glycosaminoglycans (mg)
Anterior leaflet (LA) Posterior leaflet (LP)	60	-	60
Fresh pericardium (FP)	60	60	60
Decellularised pericardium (DP)	60	90	90

Table 2.7: Wet weights used in the biochemical assays. The values are expressed as mg of wet weights.

2.14.2 Hydroxyproline assay

Reagents

The following reagents were used for the hydroxyproline assay:

- Hydroxyproline buffer: 13.3 g citric acid, 32 g sodium acetate ($3H_2O$), 9.1 g sodium hydroxide in 3.2 ml glacial acetic acid and 80 ml propan-1-ol (n-propanol). The volume was made up to 300 ml using distilled water. The pH was adjusted to between 6.0 – 6.5 by adding drops of 6 M hydrochloric acid while stirring. The final volume was adjusted to 400 ml using distilled water. The solution was kept for up to 2 months in a dark bottle at 4°C.
- Ehrlich's reagent: 7.5 g p-dimethylaminiobenzaldehyde in 30 ml propan-1-ol and 13 ml 62 % (v/v) perchloric acid, with the final addition of 7 ml of distilled water. The solution was stirred until fully dissolved and then used within 1 h.
- Oxidizing solution prepared by dissolving 1.41 g chloramine T in 100 ml distilled water. The solution was used immediately.

Method

The method used was based on the method reported by Edwards and O' Brien (1980). Prior to running the final biochemical analysis, the tissue sample was freeze dried, as described in Section 2.14.1, and then acid hydrolysed.

Acid hydrolysis

Freeze dried tissue was weighed, macerated and placed in 15 cm glass test tubes. Hydrochloric acid (6 M, 4 ml for each individual sample) was added to the test tubes and the tissues were autoclaved at 121°C for 2, 4, 5 and 6 h. After cooling and prior to biochemical

analysis, 6 M sodium hydroxide was added to the tissue to adjust the pH to 7. The final volume in each test tube was recorded.

Biochemical analysis

Trans-4-hydroxy-L-proline was diluted in hydroxyproline buffer at the concentrations of 2, 4, 6, 8, 10, 15, 20, 25 and 30 $\mu g \cdot ml^{-1}$, in order to produce working calibrator solutions. Hydroxyproline buffer was used as the blank control for the assay. Triplicates of test and standard solutions were added in a volume of 50 µl to a flat-bottomed 96 well plate. Chloramine T (100 µl) was added to each well and the plate was gently shaken for 5 min. Ehrlich's reagent (100 µl) was then added to each well and the plate was incubated for 45 min in a water bath at 60°C. The optical densities were measured using a micro plate reader spectrophotometer at 570 nm. The concentration of hydroxyproline in the acid-hydrolysed tissue samples was calculated by interpolation from the standard absorbance curve (Figure 2.4).

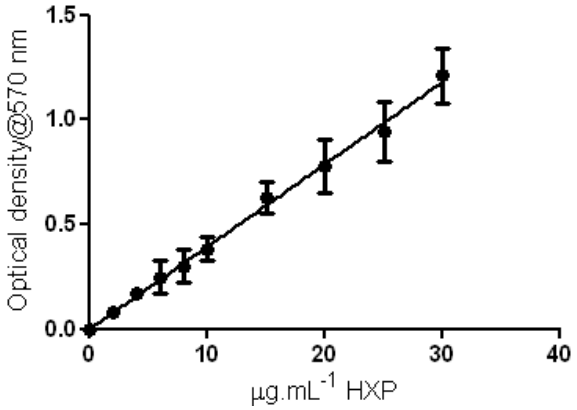

Figure 2.4: Standard curve for hydroxyproline. Data expressed as means (n=6) ± 95% confidence limits.

2.14.3 Collagen denaturation assay

Only the fresh and decellularised pericardial groups were used for this assay.

Reagents

The following reagents were used for the collagen denaturation assay:

- Digest buffer: 1.21 g trizma base and 0.15 g calcium chloride in 100 ml distilled water. The pH was adjusted to 7.8 by adding 6 M hydrochloric acid or 6 M sodium hydroxide. The

solution was autoclaved at 121°C for 20 min and stored at room temperature for up to 1 month.

- α-chymotrypsin: α-chymotrypsin from bovine pancreas was dissolved in digestion buffer at 5 mg·ml^{-1}. The solution was used immediately.

Method

Following freeze drying (Section 2.14.1), the samples were incubated in 5 ml of α-chymotrypsin solution at 30°C for 24 h, and then centrifuged for 10 min (α-chymotrypsin only reacts with denatured collagen when the protein is not in its native folded conformation). The supernatants were then transferred to 15 cm glass test tubes with HCl (6 M, 4 ml per sample) to be acid hydrolised. Neutralisation and biochemical analysis of the samples was followed as described in Section 2.14.2.

2.14.4 Glycosaminoglycan (GAG) assay (sulphated proteoglycans)

This method was used to quantify the sulphated sugar content of the tissues.

Reagents

The following reagents were used for the GAG assay:

- Digestion buffer: 0.788 g L-cysteine and 1.8612 g sodium ethylenediaminetetraacetic acid in 1 L of PBS. The pH was adjusted to 6.0 ± 0.1 by adding 6 M hydrochloric acid or 6 M sodium hydroxide drops. The solution was stored at room temperature for up to 6 months.
- Papain digestion solution: 1250 Units of papain were dissolved in 25 ml of digestion buffer. The solution was used immediately.
- Tris solution (0.2 M) was prepared by dissolving 24.22 g of trizma base in 500 ml distilled water. The pH was adjusted to 8.0 ± 0.1 by adding 6 M hydrochloric acid. The volume was made up to 1 L using distilled water. The solution was autoclaved for up to one month at room temperature.
- Sodium di-hydrogen orthophosphate (0.1 M) prepared by dissolving 3.45 g sodium di-hydrogen orthophosphate in 250 ml distilled water. The solution was stored at room temperature for up to 3 months.

- Di-sodium hydrogen orthophosphate (0.1 M) prepared by dissolving 3.55 g di-sodium hydrogen orthophosphate in 250 ml distilled water. The solution was stored at room temperature for up to 3 months.
- Assay buffer was prepared by mixing 137 ml of 0.1 M sodium di-hydrogen orthophosphate with 63 ml 0.1 M di-sodium hydrogen orthophosphate. The pH was adjusted to 6.8 using 6 M hydrochloric acid or 6 M sodium hydroxide. The solution was stored at room temperature for up to 3 months.
- 1, 9 dimethylene blue (DMB) dye solution prepared by adding 2 g of sodium formate and 16 mg of 1,9 DMB into 5 ml of ethanol and 2 ml of formic acid using a magnetic stirrer. The volume was made up to 1 L using distilled water. The pH was adjusted to 3.0 using formic acid. The dye was stored at room temperature for up to 3 months.

Method

Papain digestion

Freeze dried tissue samples were weighed, macerated and placed in sterile universal tubes with 5 ml papain digestion solution. The samples were incubated for 36 hours with gentle agitation at 60°C.

Biochemical analysis

Standard calibrator solutions of chondroitin sulphate were prepared at 0, 3.125, 6.25, 12.5, 25, 50 and 100 $\mu g \cdot ml^{-1}$. Assay buffer was used as the blank control for the assay. Triplicates of test and standard solutions were added in a volume of 40 µl to a flat-bottomed 96 well plate. DMB dye solution (250 µl) was added to each well and the plate was gently shaken for 2 min. The optical densities were measured using a micro plate reader spectrophotometer at 525 nm. The concentration of sulphated sugars in each acid hydrolysed tissue sample was calculated by interpolation from the standard absorbance curve (Figure 2.5).

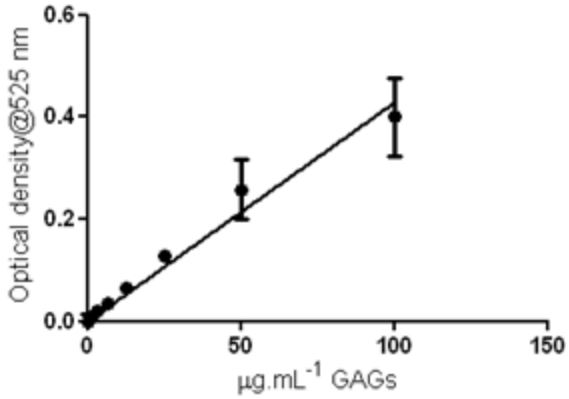

Figure 2.5: Standard curve for GAGs. Data expressed as means (n=6) ± 95% confidence limits.

2.15 MTT assay

This method was used to assess the viability of both fresh and decellularised seeded pericardial samples.

Reagents

The following reagents were used for the MTT assay:

- MTT (3-(4, 5-Dimethylthiazol-2-yl)-2,5-diphenyltetrazolium bromide) solution: 5 $mg \cdot ml^{-1}$ MTT was made in PBS pH 7.6. This solution was stored in a foil wrapped container at -20 °C, and thawed to room temperature before use.
- Dimethyl sulfoxide (DMSO).
- PBS with Ca and Mg.

Method

Tissue samples of specific weighs were macerated with a scalpel blade, placed in 1.5 ml autoclaved eppendorf tube of known weighs and then weighed aseptically. MTT solution (200 µl) and PBS with Ca and Mg (400 µl) were added to each microtube aseptically. The tubes were incubated on a blood rotator at 30 rpm for 4 h at 37°C. Following incubation, the tubes were centrifuged in a micro centrifuge at 14,000 g for 5 min, the supernatant was removed and 1 ml of DMSO was added into each tube aseptically. The tubes were further incubated on the blood rotator at 30 rpm for 17 h at 37 °C, and then centrifuged at 14,000 g for 5 min in a micro centrifuge prior to transferring aliquots of 200 µl supernatant from the micro tubes to a clear flat-bottomed 96-well plate. The absorbance was read at 570 nm with a reference filter at 630 nm. The DMSO was used as a blank.

2.15.1 MTT assay validation

The optimum amount of tissue to be used during MTT assay was validated. Three replicates out of each one of three fresh porcine pericardia were processed straight after dissection through MTT assay, at different weighs: 20, 50, 100, 150 and 200 mg. The final values of optical densities for each weigh were plotted on GraphPad Prism to get the standard absorbance curve. The optimum value of weigh of tissue to be used for future experiments was chosen to be in the linear region of the plotted standard curve. The same optimum value of weigh of fresh tissue was used for decellularised samples.

2.16 Live/dead staining of fresh and recellularised pericardial scaffolds

Fresh and decellularised seeded pericardial scaffolds were harvested for live/dead staining at different time points in order to assess the viability of the cells.

Reagents

- Live/dead staining solution was prepared using PBS at pH 7.6, supplemented with 1 µM calcein AM and 1 µM ethidium homodimer-1 (1.2 µl calcein and 5 µl of ethidium homodimer-1 in 5ml of PBS pH 7.6).
- DABCO/glycerol: 10 ml of 2.5% (w/v) DABCO into 90 ml of glycerol. Solution was stored for up to 3 months at 4°C in a foil wrapped bottle.

Method

A rectangular piece (approximately 5×6 mm^2) was cut from the central area of each sample, and placed into individual wells of a 6-well tissue culture plate, keeping the cell seeded or mesothelial surface uppermost. The samples were kept moist with complete cell culture medium during dissection. Live/dead stain solution was added into each well to completely cover the tissue. The plate was fitted with its lid and incubated at room temperature in the dark for 45 min. The samples were washed 3 times in TBS pH 7.6 for 10 min each on a plate rocker, and they were then wet mounted with DABCO/glycerol onto a microscope slide and covered with a glass coverslip. The samples were viewed using an Olympus BX51 microscope. Live cells were stained green and dead cells were stained red. The acquired pictures were then processed through Image J for live/dead cell counting.

2.16.1 Live/dead cell counting

The percentage of live and dead cells was counted using Image J. Firstly, both live and dead cells visible on the top surface of the samples were counted, followed by counting only the live cells. The percentage of live cells was then calculated. The same procedure was followed for the dead cells.

2.17 Cell culture techniques

2.17.1 Cell culture

The cells used in this study were all cultured in complete cell culture medium, (Section 2.5.4). Cell culture operations and medium changes were performed aseptically in a Class II cabinet. All culture media and reagents were allowed to equilibrate to 37°C before use. The cells were cultured at 37°C in 5 % CO_2 (v/v) in air (standard conditions).

2.17.2 Cell resurrection

The cells were removed from liquid nitrogen storage and rapidly defrosted in a 37°C water bath. The cells (1 ml) were then added to a 25 cm^2 flask with 14 ml of complete cell culture medium, (Section 2.5.4), and were cultured under standard conditions.

2.17.3 Cell passaging

Once the cells achieved confluence, the culture medium was aspirated from the culture flasks, and the cell layer was washed in PBS without calcium or magnesium for 2 min. Trypsin/EDTA (1.5 ml; Lonza) was added to the T25 culture flasks, which were then incubated under standard conditions for 5 to 10 min. Progress of cellular detachment was regularly monitored using an inverted light microscope. Gentle physical tapping of the flasks was used to help the detachment process. Culture medium (8.5 ml) was added to each flask to stop the action of the trypsin/EDTA, and the cell suspension was transferred into a universal tube and centrifuged for 10 min at 180 g. Following centrifugation, the supernatant was carefully removed and the cell pellet was re-suspended in a specific volume of complete cell culture medium, depending on the amount of cells needed for the subsequent experiments. The culture medium was changed every 2 to 3 days until the cells became confluent and ready to be passaged again.

2.17.4 Cell counting

After detachment and centrifugation (Section 2.17.3), the cell pellet was re-suspended in 1 to 2 ml of complete cell culture medium. An improved Neubauer haemacytometer (Fisher Scientific) was used to count the live cells under an inverted microscope. For this purpose, trypan blue dye (20 µl; 0.4 % w/v; Sigma) was added to 20 µl of the cell suspension, and 10 µl of the solution was added to the chamber. Non-viable cells took up the dye and appeared blue, whereas live cells appeared colourless and bright due to the fact that their cell membrane was intact, prohibiting dye intake. Viable cells were counted in 4 out of the 9 grids of the haemocytometer. The total number of viable cells per ml in the cell suspension was calculated as follows:

$$\text{Number of cell} \cdot \text{ml}^{-1} = \left(\frac{\text{number of viable cells}}{4} \right) \times 10^4 \times 2$$

Where 4 was the number of grids counted and 2 was the dilution factor required due to the dilution of the cell suspension with trypan blue.

2.17.5 Cell cryopreservation

Reagents

- Cryopreservation medium: Standard culture medium (Dulbecco's modified Eagle's medium; DMEM) supplemented with 10 % (v/v) filter-sterilised dimethyl sulfoxide (DMSO). DMSO prevented the formation of ice crystals during freezing. However, DMSO is highly toxic and, therefore, the cells were frozen immediately after aliquoting.

Method

After cell counting (Section 2.17.4), the cell suspension was diluted to 10^6 cells per ml with cryopreservation medium. The cell suspension was then aliquotted to 1 ml into cryovials and placed into a cryo-freezing pot which contained isopropanol. The pot was kept at -80 °C overnight and, subsequently, the cryovials were transferred to liquid nitrogen for long-term storage.

2.17.6 Cell characterization

Dermal fibroblasts and pSMCs were cultured for phenotyping by immunofluorescence. The markers that were used to confirm cell phenotype are summarised in Table 2.8.

Cell type	α-SMA	Calponin	Desmin	Vimentin
Fibroblast	-	Not done	-	+
SMCs	+	+	+	Not done

Table 2.8: Characterisation of SMCs and fibroblasts. Positive (+) indicates expression of the marker by the cells; negative (-) indicates that the cells did not express the marker.

2.17.6.1 Immunofluorescence labelling

The antibodies and isotype controls used in the immunofluorescence labelling are listed in Table 2.9. The protein concentration used for the isotype control was the same as used for the specific primary antibody. The secondary antibody (Alexa fluor 488, goat anti-mouse IgG) was used at a concentration of 10 $mg \cdot L^{-1}$. SMCs were used as positive control when labelling α-SMA and desmin for fibroblasts.

Antigen	Supplier	Clone	Isotype	Diluted concentration	Antibody dilution	Isotype dilution
α-SMA	Sigma A2547	1A4	Mouse IgG2a (Dako X0943)	15.25 $mg \cdot L^{-1}$	1:400	1:6
Calponin	Novocastra 26A11, NCL-CALPONIN-B	26A11	Mouse IgG2b	24 $mg \cdot L^{-1}$	1:50	1:50
Desmin	Vector VP-D502	DE-R-11	Mouse IgG1 (Dako X0931)	54 $mg \cdot L^{-1}$	1:50	1:2
Vimentin	Leica	NCL-L-VIM-V9	Mouse IgG1 (Dako X0931)	78 $mg \cdot L^{-1}$	1:50	2:3

Table 2.9: Primary antibodies, isotypes and dilutions used in immunofluorescence labelling.

Reagents

- TBS pH 7.6.
- TBS containing 0.05 % (v/v) Tween 20, pH 7.6.
- Antibody diluent: 100 ml TBS (pH 7.6) with 0.01 % (w/v) sodium azide and 0.01 % (w/v) bovine serum albumin (BSA). The pH was adjusted to 7.6, and the solution was stored at 4 °C and used within 1 month.
- PBS pH 7.2 - 7.4.

- Dye buffer: 1.211 g of trizma base, 0.3724 g of EDTA, 5.8 mg of sodium chloride in 1 L of distilled water. The solution was autoclaved at 121°C for 20 min.
- DAPI dye solution: 10 mg of DAPI in 10 ml of nuclease free water (1 mg·ml^{-1}). The solution was stored at -25°C for up to 6 months.
- Working dye solution: 2.5 µl of DAPI dye solution in 25 ml of dye buffer (0.1 mg·ml^{-1}) in a dark bottle. The pH was adjusted to 7.4 by adding 6 M hydrocholoric acid or 6 M sodium hydroxide. The solution was used immediately after preparation.

Method

Fibroblasts at passage 4 and SMCs at passage 6 were cultured on multi-spot slides for 17 hours under standard conditions. To each spot, 50 µl of cell suspension at a cell density of 2×10^3 per ml was added. Following culture, the slides were washed with 5 ml of PBS for 2 min, fixed in mixture of acetone and methanol (1:1) for 1 min, and air dried for 5 min. The slides were then rinsed in running tap water for 10 min, followed by washing in TBS for 5 min and addition of 20 µl of the appropriate primary antibody (diluted using the antibody diluent). The slides were then incubated in a moist environment for 1 hour at room temperature prior to being washed twice in TBS containing 0.05 % (w/v) Tween 20 for 10 min each, followed by 10 min wash in TBS. Subsequently, fluorochrome-labelled secondary antibody (20 µl) was added for 30 min at room temperature in the dark. The slides were then washed twice for 10 min each with TBS containing 0.05 % (w/v) Tween 20, and then rinsed once for 10 min in TBS prior to incubation in working solution for 10 min in the dark. The slides were finally rinsed in PBS three times for 10 min each in the dark before being mounted with DABCO/glycerol solution (Section 2.16).

2.18 Biomechanical testing

The biomechanical properties of the leaflets and pericardium were investigated using low strain-rate uniaxial tensile loading to failure tests according to the protocol described by Korossis *et al.* (2002). Eight groups of tissue were used for this test including PO, PP, DPP, DPO, LAC, LAR, LPC and LPR, (Table 2.5). Six samples were tested for each group.

2.18.1 Tissue sample preparation

Fresh and decellularised pericardial samples, measuring 10 mm in length by 5 mm in width, were isolated orthogonally (PO, DPO) and parallel (PP, DPP) to the direction of the collagen fibres (Fig. 2.3a, b). Fresh posterior and anterior leaflet samples, measuring 10 mm in length by 5 mm in width, were also isolated along the circumferential (LAC, LPC) and radial (LAR, LPR) directions of the mitral valve leaflets (Fig. 2.3c). The specimens were dissected using parallel razor blades fitted onto a cutting block (Figure 2.6). Prior to testing, the thickness of the sample was measured using a Mitutoyo thickness gauge (Figure 2.7) at 3 different points along its length and averaged. Subsequently, the test sample was clamped onto a titanium holder (Figure 2.8) with the aid of sandpaper and a small amount of superglue to prevent slippage.

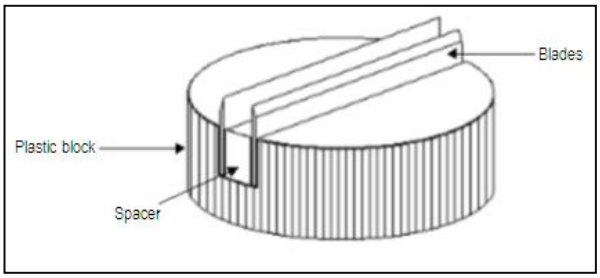

Figure 2.6: Cutting block used for the dissection of the tissue samples.

Figure 2.7: Thickness gauge used to measure the thickness of the samples.

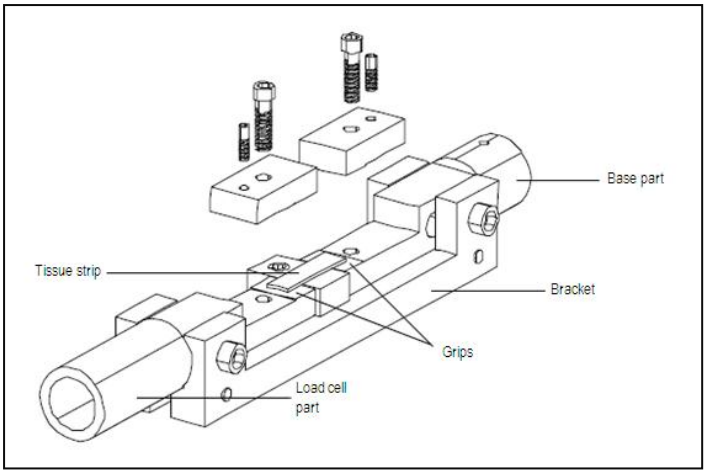

Figure 2.8: Tissue sample holder used in the tensile testing.

The holder was fitted with a removable securing bracket, which ensured that no loading was imposed to the specimen until the start of the test. The bracket was also used to set the gauge length of the specimens to 10 mm.

Once the test sample was secured to the holder, the inferior part of the holder was secured to the base of an Instron® tensile tester (model 3365) fitted with a 500 N load cell, and the crosshead was lowered at a slow speed until it locked to the superior part of the holder. Once the superior holder part was secured to the cross-head, the bracket was removed and the bath was risen up in order to accommodate testing in PBS. The solution was kept at 37°C. The experimental set up used is illustrated in Figure 2.9.

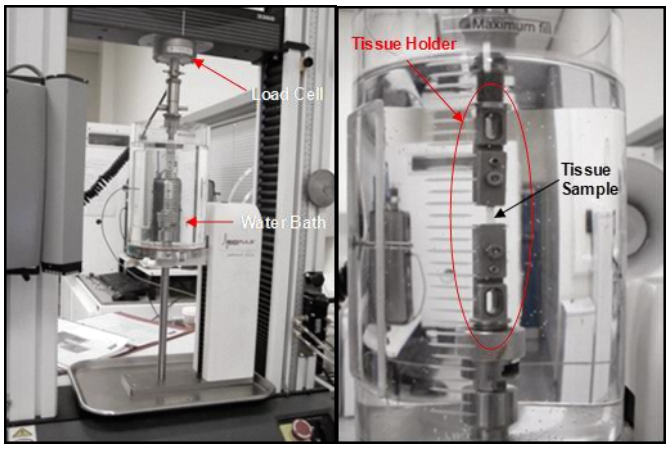

Figure 2.9: Experimental set-up used for the uniaxial tensile loading to failure in the Instron tensile tester.

2.18.2 Test procedure

Prior to testing the samples were preconditioned under cyclic loading using a double-ramp wave function at a rate of 10 mm·min^{-1} and then they were sequentially loaded to failure at the same rate. During testing, load data from the load cell and the displacement of the crosshead was recorded. Prior to the actual testing, preliminary testing was conducted in order to estimate the average transition strain (ε_t) of the different groups, which was used as the limit for the preconditioning regime. In particular, 3 additional samples from each of the 8 test groups (PP, PO, DPP, DPO, LAC, LAR, LPC, LPR), were subjected to simple uniaxial tensile loading to failure (with no preconditioning) at a rate of 10 mm·min^{-1} and their force-extension response was recorded. Subsequently, the force-extension data was converted to stress-strain (as described below) and the average (ε_t) was calculated. During the actual testing the samples of each test group were preconditioned for 50 cycles from 0% strain up to the average ε_t for the particular group, before the samples were loaded to failure. The tensile machine was set to produce a specimen preloading of 0.01 N before the operating program started to acquire any data. Thus, zero extension was recorded at the point at which a 0.01 N load was detected. The preloading allowed generation of consistent results by overcoming the problem related to the "noise" (unloaded oscillating signal) of the load cell. The preloading value was chosen in order to be just over the value of the noise of the load cell. Moreover, the tissue samples were slack when clamped into the tissue holder in order to avoid loading of the specimens during clamping and before the actual testing. Therefore, the preloading limit allowed straightening of the tissue and initiation of data recording after a load of 0.01 N was detected by the load cell. Failure was taken to occur when the first decrease in load was detected during specimen extension. The mode of failure observed was middle section necking and rupture for all of the specimens tested. During testing, load data from the load cell and specimen extension data from the stroke of the cross-head of the tensile testing machine was recorded.

2.18.3 Data processing

The recorded force-extension histories of the samples were converted to stress-strain in Microsoft Excel XP. The engineering stress (σ) was calculated from the recorded force (F) according to:

$$\sigma = \frac{F}{A}$$

where F was the acquired force in N, σ the stress in Pa, and A the original cross-sectional area (CSA) of the un-deformed specimen in mm^2. The CSA was calculated as $A = w \times t$, where w was the width of the sample (5 mm) and t its average thickness. The changes in thickness and width during preloading were considered negligible and were not taken into account. The strain (ε) was calculated from the extension data according to the formula:

$$\varepsilon = \frac{\Delta l}{l_i + \Delta l_i}$$

where Δl was the extension of the specimen (displacement of the cross head), l_i the initial gauge length of the specimen, set by the holder bracket, and Δl_i the extension produced by the preloading. Subsequently, the stress-strain behaviour of the specimens was plotted and used to obtain the elastin phase slope (El-E), collagen-phase slope (Coll-E), transition stress (σ_t) and strain (ε_t), ultimate tensile strength (σ_{uts}) and failure strain (ε_{uts}).

A typical stress-strain curve for heart valve leaflet tissue is illustrated in Figure 2.10, indicating the six parameters used in the study.

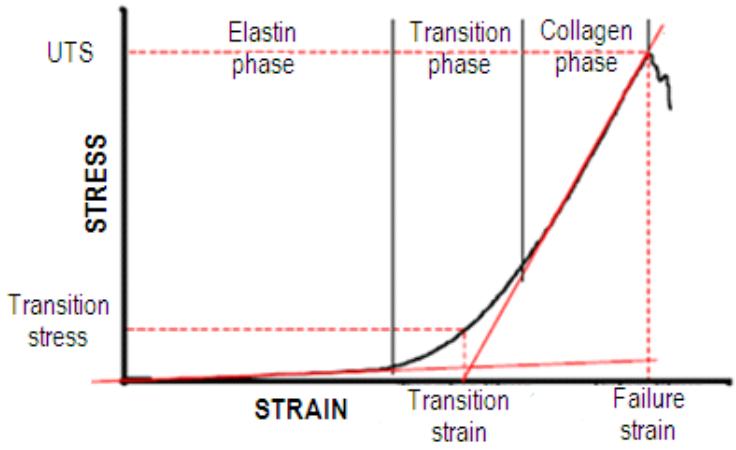

Figure 2.10: Typical stress-strain behaviour of valve leaflet tissue. UTS: ultimate tensile strength. Adapted from Fung (1984).

The files that were obtained during testing were exported from the operating program of the tensile testing machine and imported to Microsoft Excel XP as spreadsheets for further processing. In Excel, the load and extension data were manually converted to stress and strain, respectively, as described above. All the 6 mechanical parameters were determined on the basis of the stress-strain curve obtained, as illustrated in Figure 2.10. The elastin and collagen phase slope were calculated by selecting the region of the curve which better

represented the specific phase slope, and then by processing the same interval on Origin Pro 8 to calculate the slope by using the function Fit-Linear. The analysis of the results was carried out per treatment group (at least 6 replicates from 6 different pigs per group). The six parameters for each specimen were finally averaged over the number of specimens in the group, and analysed statistically.

2.19 Data analysis

Statistical analyses were carried out in Microsoft Excel (2003 or 2007) or GraphPad Prism 5, and all numerical values are presented as means ± 95 % confidence intervals (C.I.). The Student's t-test was used for comparison of groups of two means, and one-way ANOVA was applied for the comparison of data from more than two groups, followed by calculation of the minimum significant difference (MSD) by the T-method for equal sample sizes (Sokal and Rohlf, 1981). The MSD was calculated according to:

$$\mathrm{MSD} = \mathrm{Q} \times \mathrm{SE}$$

The Q-value was obtained from the table of the critical values of the studentized range with α = 0.05, whereas the standard error of the mean (SE) was calculated as:

$$\mathrm{SE} = \sqrt{\frac{\mathrm{MS}}{\mathrm{n}}}$$

where MS is the mean square (average of the variances) within groups and n the number of replicates. The MSD was compared to the differences between the means of the paired groups. Significance was accepted when the difference of the means was greater than the MSD ($p < 0.05$).

Arcsine transformation was applied to data expressed as percentages in order to fulfil the assumption of normally distributed data, required by the one-way ANOVA. The values of percentages were arcsine transformed as follows:

$$y = \frac{180°}{\pi} \times arcsin\sqrt{\frac{x}{100}}$$

where x is the data expressed as a percentage and y is the data arcsine transformed. The arcsine transformed values were then averaged and the 95 % C.I.`s were calculated. The upper and lower limits were then calculated as follows:

$$upper\ limit = mean + 95\ \%\ C.I.$$

$$lower\ limit = mean - 95\ \%\ C.I.$$

The mean, upper and lower limits values were then back transformed to report the data as percentages:

$$y = \sin\left(\frac{\pi}{180°} \times \frac{mean^2}{100}\right)$$

Finally, the upper and lower error bars were calculated as follows:

$$upper\ error\ bar = upper\ limit - mean$$

$$lower\ error\ bar = mean - lower\ limit$$

The mechanical analysis of the fresh pericardial groups (parallel and orthogonal to the collagen fibers) was performed twice, providing two different data sets for the statistical analysis presented in Chapter 3 and Chapter 4. The reason for repeating the mechanical analysis was that the use of the same data set for two different statistical analysis would increase the Type I error (which occurs when the null hypothesis is true, but is rejected).

Chapter 3

Properties of porcine pericardium and mitral valve leaflets

3.1 Introduction

In order to develop tissue-engineered substitutes for mitral valve (MV) leaflet reconstruction, it is necessary to investigate the inherent characteristics of the native MV leaflets. A deep understanding of the characteristics of the natural MV leaflets is necessary in order to develop appropriate replacement constructs with similar characteristics, structure and functional capability to the native leaflets. The work presented in this PhD thesis utilised decellularised porcine pericardium for the development of cell seeded and unseeded MV leaflet replacements. Autologous, allogeneic and chemically-treated xenogeneic (porcine) pericardium has been routinely used in the clinical setting for MV repair (Maranto and Schoen, 1988; Duran and Gometza, 1993). As such the use of decellularised porcine pericardium in MV leaflet repair represents a plausible option. Moreover, previous studies have demonstrated that the human and porcine mitral valve apparatuses share similar anatomical structure and histoarchitecture (Kunzelman *et al*., 1994). Therefore, porcine MV leaflets were used in this study for comparative purposes due to the limited availability of human tissue.

This chapter presents the biomechanical and biological properties of fresh porcine pericardium and MV leaflets. Fresh pericardium and leaflets were investigated in order to generate a benchmark and investigate (in subsequent chapters) both the effects of decellularisation on porcine pericardium and the suitability of cell-seeded and unseeded decellularised pericardium as MV leaflet replacements. The biomechanical properties were studied through low strain rate uniaxial tensile loading to failure and the biological properties were studied in terms of histoarchitecture, protein and glycosaminoglycan (GAG) content. A comparison between biomechanics and biological results was made in order to understand the relationship between structure and biomechanical properties of the tissue.

The spatial cell distribution and the distribution and organisation of the extracellular matrix (ECM) components (GAGs, collagen, and elastin) in the tissues were investigated by histological staining. GAGs are one of the main components of the ECM in heart valve leaflets

providing resistance to compression (Baeurle *et al*., 2009). Chondroitin sulphate represents one of the main acidic GAGs of the human heart valves, together with hyaluronic acid (Murata, 1981). In addition to histological staining, chondroitin sulphate distribution was investigated using immunohistochemical staining, and the amount of sulphated GAG in the tissues was quantified using the GAG biochemical assay.

Another important component of the ECM of the valve leaflets is elastin, which provides the recoiling mechanism for the large deformation of the leaflets during the cardiac cycle (Cleary and Gibson, 1996). Collagen represents the major load-bearing component of the ECM of the leaflets and its preservation following tissue decellularisation is of paramount importance for the structural integrity of the decellularised scaffold. Collagen I and III are the most abundant types in MV leaflets (Kunzelman *et al.*, 1993a), whereas collagen IV forms a two dimensional reticulum and is usually found in the basement membrane of the leaflets. The chemical composition of collagen consists of three amino acids, which include glycine, proline, and hydroxyproline (HXP), with the latter being the major component of collagen. As such, the total collagen in the tissues investigated in this study was quantified by the HXP biochemical assay. In addition, immunohistochemical staining was used to investigate collagen I, III and IV localisation and distribution in the tissues.

Immunohistochemical staining was further used to detect additional ECM proteins, including fibronectin and laminins. Fibronectin is a glycoprotein which aids cell attachment to the ECM. It has a high affinity to collagen and GAGs and a good capability of binding to cell surfaces, forming a bridge between the cell and the ECM (Ruoshlati *et al*., 1981). Laminins are major glycoproteins in the basal lamina, which is one of the layers of the basement membrane (Timpl *et al*., 1979). Laminins influence cell differentiation, migration, and adhesion, as well as phenotype and survival and they are different from fibronectin in the amino acid composition and immunological reactivity. Apart from detection of ECM proteins, immunohistochemical staining was also used to detect cytoskeletal components, namely α-smoth muscle actin (α-SMA), vimentin and Von Willebrand factor, which are indicative of particular cell types. This was necessary in order to determine the cell types and distribution present in the fresh porcine MV leaflets, with a view to guiding the selection of cells in the reseeding of the decellularised pericardial scaffolds. α-SMA is a protein typical of smooth muscle cells (SMCs) and is present in high amounts in vascular SMCs (Skalli *et al*., 1989). Vimentin is an intermediate filament protein that is expressed in mesenchymal cells (Fraga *et al*., 1998) and

it was used to stain fibroblasts in the MV leaflets. The Von Willebrand factor is a glycoprotein required to maintain normal haemostasis and it was used to detect endothelial cells (Sadler, 1998).

3.1.1 Aims and objectives

Aims:

The aim of the work presented in this chapter was to investigate the biological and biomechanical properties of fresh porcine pericardium and MV leaflets, with a view to generating a benchmark for assessing the effects of decellularisation on porcine pericardium and the suitability of cell-seeded and unseeded decellularised pericardium as MV leaflet replacements.

Objectives:

Specifically, the objectives of this chapter were to characterise:

- the presence, spatial arrangement and amount of the ECM proteins in fresh porcine pericardium and MV leaflets
- the cell types present in the MV leaflets, and
- the biomechanical properties of fresh porcine pericardium and MV leaflets.

3.2 Material and methods

The general materials and methods used for the histological, immunohistochemical, biochemical and biomechanical evaluation of the fresh porcine pericardium and MV leaflets, have been described in Chapter 2, Section 2.11, 2.12, 2.14 and 2.18, respectively. Fresh pericardial samples were dissected orthogonally (PO) and parallel (PP) to the direction of the collagen fibres, and MV leaflet samples were isolated along the circumferential (anterior: LAC; posterior: LPC) and radial (anterior: LAR; posterior: LPR) directions, for histological, immunohistochemical and biomechanical analysis, as described in Chapter 2, Section 2.9. Biochemical characterisation of fresh porcine pericardium (FP) and anterior (LA) and posterior (LP) MV leaflets with no particular fibre orientation was performed in order to quantify the amount of ECM collagen (HXP) and GAGs. A number of samples equal to 6 was used to

calculate the HXP and GAGs content; only during the validation of hydrolysis technique, a number of samples equal to 3 was used.

Various staining were used for the histological analysis of samples; haematoxylin & eosin (H&E) staining was used to investigate the general distribution of cell nuclei. Alcian blue-PAS was used to determine GAG distribution, whereas Sirius red and Miller's elastin staining was used to examine the collagen and elastin distributions in the tissues, respectively. In addition, Masson's trichrome stain was used to stain collagen, muscle, fibrin, cytoplasm and nuclei.

Immunohistochemical staining of fresh porcine pericardium and MV leaflets was performed in order to study the presence, distribution and spatial arrangement of their ECM proteins. For this purpose, tissue sections were stained with monoclonal antibodies against collagen I, III and IV, chondroitin sulphate, fibronectin and laminin. Moreover, and in order to identify the type and distribution of cells in the native MV leaflet cells, tissue sections were stained with antibodies against α-SMA, vimentin and Von Willebrand factor. All negative control sections (including isotype and omission of HRP controls) showed absence of staining.

The biomechanical behaviour of the native porcine pericardium and MV leaflets was investigated under uniaxial tensile loading to failure in order to study the directional anisotropy of the pericardium and the directional and regional (posterior vs. anterior) anisotropy of the MV leaflets (n = 6). The biomechanical parameters investigated included the overall stress-strain behaviour, elastin phase slope (El-E), collagen phase slope (Coll-E), transition stress (σ_t) and strain (ε_t), ultimate tensile strength (UTS) and failure strain (ε_{UTS}).

3.3 Results

3.3.1 Histological characterisation of porcine pericardium and mitral valve leaflets

3.3.1.1 Porcine Pericardium

Fresh pericardium showed a three-layered structure (Figure 3.1b, d, f), comprising an outer layer of cells (mesothelium), the fibrosa consisting of collagen and well organized elastin fibres, and the epipericardial layer consisting of collagen fibres and sparsely arranged elastin fibres (Figure 3.1b, d). GAGs were observed (blue; Alcian blue-PAS stain) mainly in the mesothelial layer (Fig. 3.1f, h).

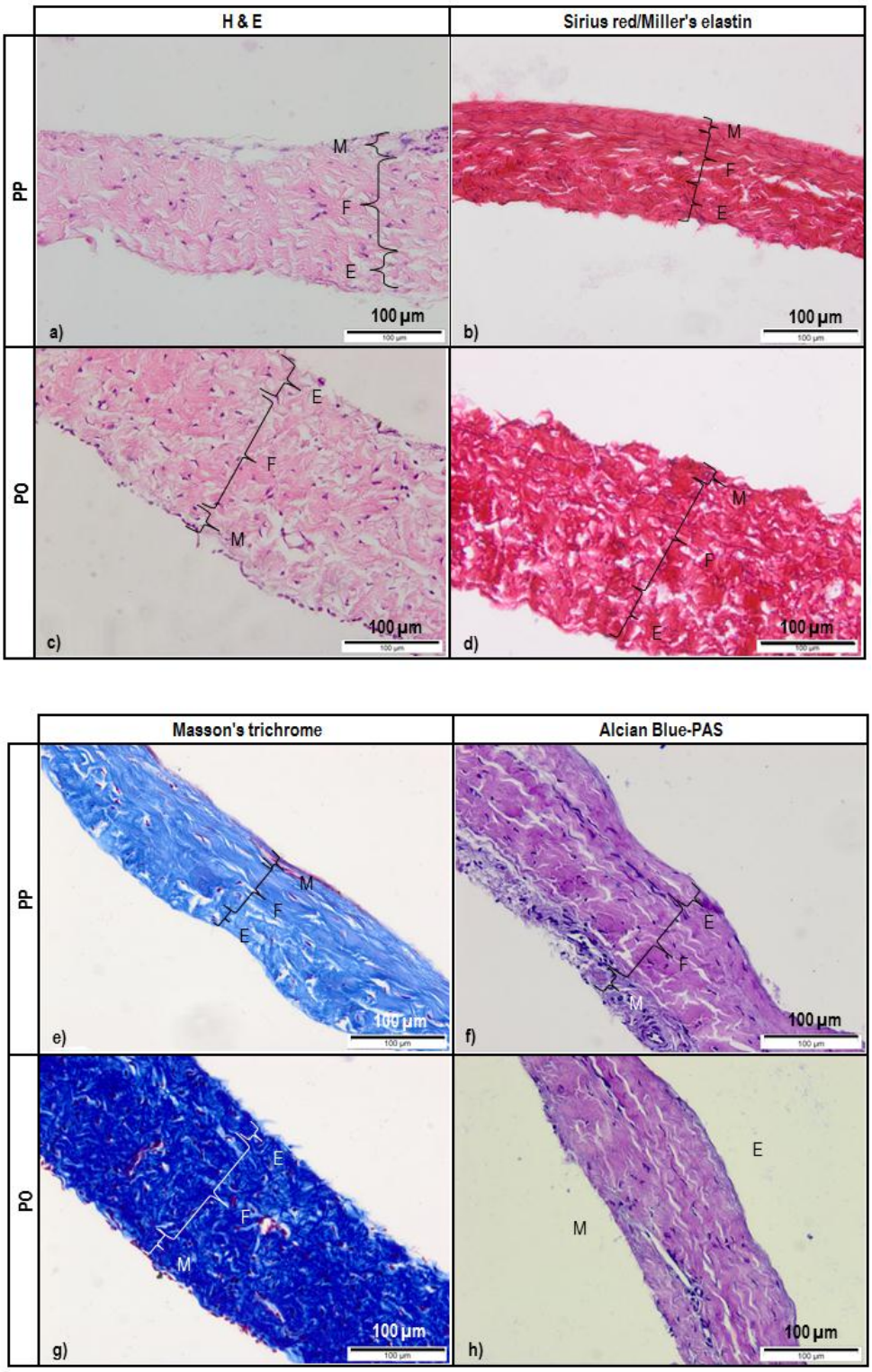

Figure 3.1: H&E, Sirius red/Miller's elastin, Masson's trichrome and Alcian blue - PAS staining of fresh pericardial samples isolated parallel (PP; a, b, e and f) and orthogonally (PO; c, d, g and h) to the direction of the collagen fibres. Sections were stained with H&E (a, c), Sirius red/Miller's elastin (b, d), Masson's trichrome (e, g) and Alcian blue - PAS (f, h). Brackets indicate the various layers. E: epipericardial layer/side; F: fibrosa; M: mesothelial layer/side. Scale bars indicate 100 µm.

H&E staining clearly demonstrated the spatial cell distribution in the pericardium (Fig. 3.1a, c), with the cell nuclei stained blue/black by haematoxylin and the cells appeared to be spread throughout the fibrosa and the epipericardial layer. Cells were also observed covering the mesothelial surface of the pericardial sections. Cell cytoplasm and most ECM fibres, such as collagen, were stained by eosin in varying shades and intensities of pink. Samples stained with Sirius red and Miller's elastin demonstrated red-stained collagen and black/purple-stained elastin fibres in the fibrosa and in the epipericardium (Fig. 3.1b, d).

Samples stained with Masson's trichrome demonstrated blue-stained collagen fibres, blue/black-stained cell nuclei, red-stained cytoplasm and deep-red-stained muscle (Fig. 3.1e, g). These samples clearly demonstrated the wavy structure of the collagen fibres. Samples stained with Alcian blue-PAS (Fig. 3.1f, h) demonstrated blue-stained GAGs, magenta-stained neutral mucins and deep-blue-stained cell nuclei. GAGs appeared to be located mainly in the mesothelial layer.

3.3.1.2 Mitral valve leaflets

The histological analysis of the MV leaflets demonstrated a characteristic quadrilaminar structure comprising the atrialis, mainly consisting of elastin fibres (Fig. 3.2b, d, f, h), the spongiosa with a high concentration of GAGs (Fig. 3.3b, d, f, h), the fibrosa consisting of collagen fibres (Fig. 3.3a, c, e, g), and the ventricularis consisting of elastin fibres (Fig. 3.2b, d, f, h). Samples stained with H&E (Fig. 3.3a, c, e, g) showed blue/black-stained cell nuclei, which were spread throughout the four layers, as well as on the surface of the leaflets forming an endothelial cell layer. Blood vessels were mainly located in the atrialis and upper fibrosa. Samples stained with Sirius red/Miller's elastin demonstrated black/purple-stained elastin fibres in both the atrialis and ventricularis, but in a higher alignment in the atrialis (Figure 3.2b, d, f, h). The quadrilaminar structure of the leaflets was particularly obvious under Masson's trichrome staining (Fig. 3.3a, c, e g). In particular, it was possible to observe the spongiosa layer consisting mainly of GAGs and pale-blue-stained loosely organised collagen fibres, and the fibrosa layer consisting of dense bands of intense-blue-stained wavy collagen. Under Masson's trichrome staining, cytoplasm and nuclei were stained red and blue/black respectively, whereas blood vessels were stained red. GAGs were visualised under Alcian blue-PAS staining, and were coloured blue when alone and blue/purple when mixed with neutral mucins (Figure 3.3b, d, f, h). No significant morphological differences in the histology between the anterior and posterior leaflets were observed.

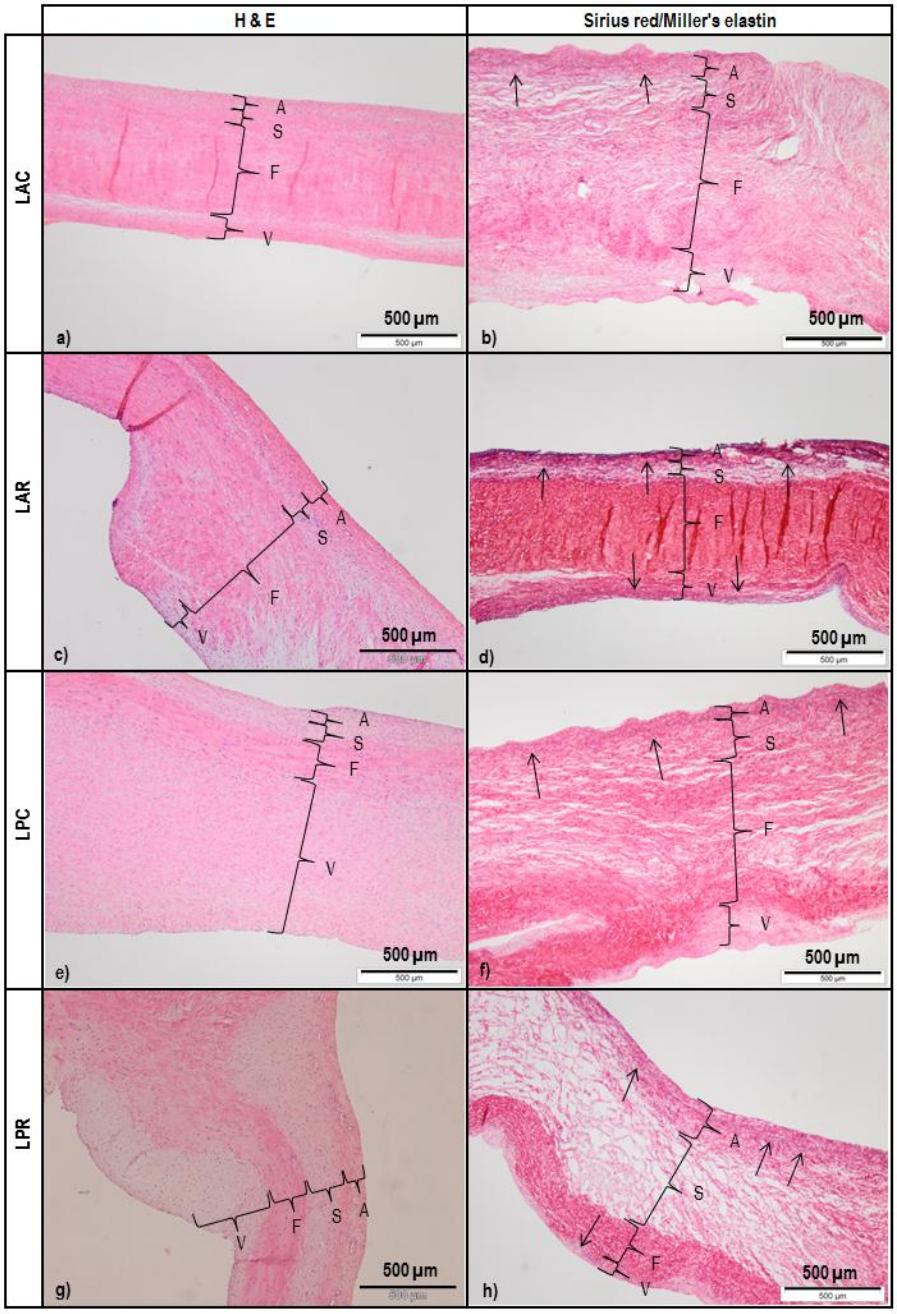

Figure 3.2: H&E and Sirius red/Miller's elastin staining of MV leaflets circumferential (LAC; a, b) and radial (LAR; c, d) anterior, circumferential (LPC; e, f) and radial (LPR; g, h) posterior. Sections were stained with H&E (a, c, e and g), Sirius red/Miller's elastin (b, d, f and h). The black arrows indicate the elastin fibres. A: atrialis layer/side; F: fibrosa; S: spongiosa; V: ventricularis layer/side. Scale indicates 500µm.

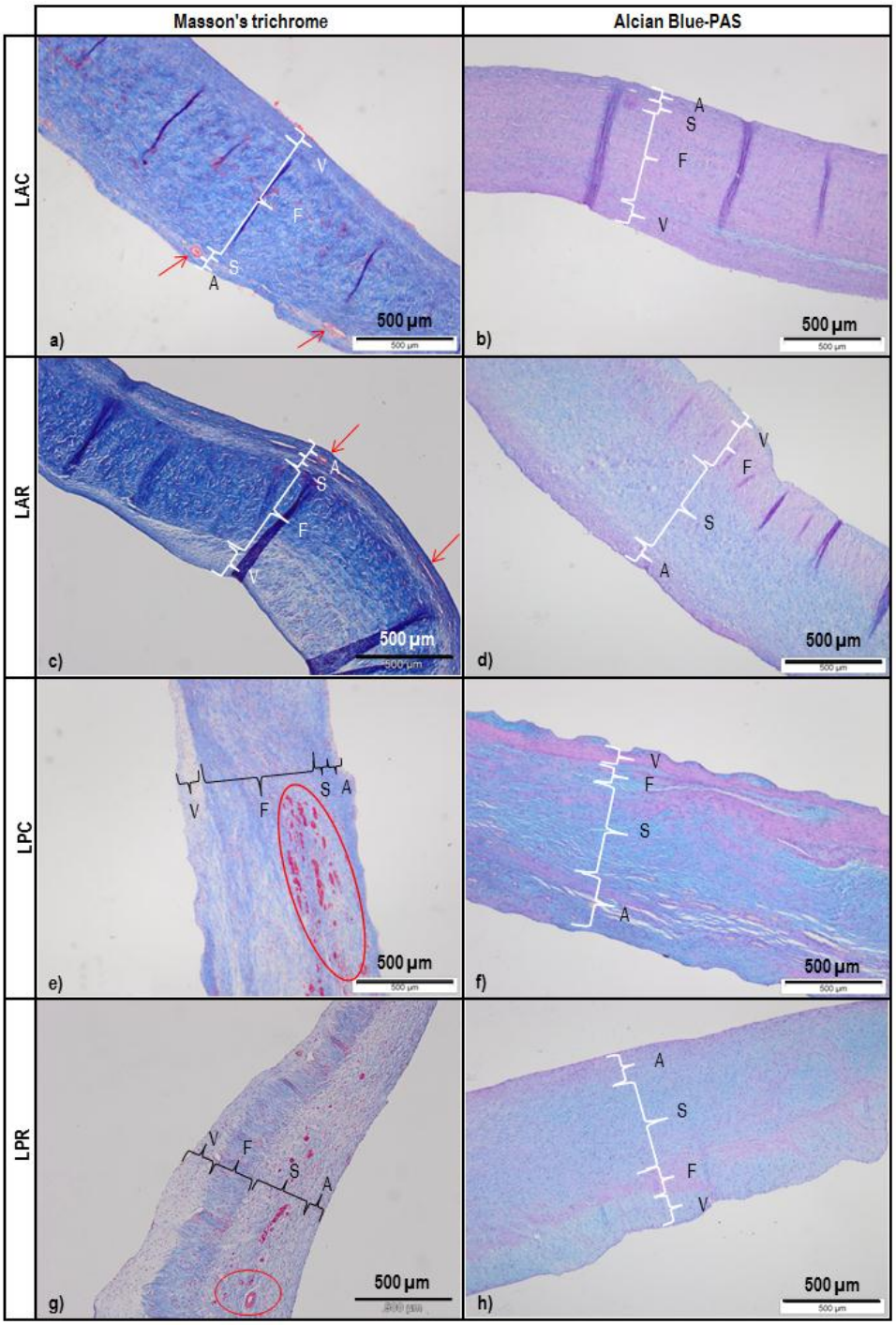

Figure 3.3: Masson's trichrome and Alcian blue – PAS staining of MV leaflets circumferential (LAC; a, b) and radial (LAR; c, d) anterior, circumferential (LPC; e, f) and radial (LPR; g, h) posterior. Sections were stained with Masson's trichrome (a, c, e and g), Alcian blue - PAS (b, d, f and h). Brackets indicate the various layers. The red arrows and circles indicate the blood vessels. A: atrialis layer; F: fibrosa; S: spongiosa; V: ventricularis layer. Scale bars indicate 500 µm.

3.3.2 Collagen and glycosaminoglycan content of porcine pericardium and mitral valve leaflets

Biochemical characterisation of fresh porcine pericardium (FP) and anterior (LA) and posterior (LP) MV leaflets was performed in order to quantify the amount of ECM collagen (HXP) and GAGs. Collagen content was assessed following acid hydrolysis and GAGs following papain digestion of a known weight of tissue. These methods have been described in Chapter 2, Section 2.14.

3.3.2.1 Collagen content

Validation of hydrolysis technique

In order to determine whether the acid hydrolysis of the tissues resulted in complete hydrolysis of the collagen it was necessary to determine the concentrations of HXP after various durations of hydrolysis. The amount of HXP ($\mu g \cdot mg^{-1}$ dry weight) determined after 2, 4, 5 and 6 h of acid hydrolysis of the pericardial and MV leaflet tissues are illustrated in Figure 3.4. The data for each tissue type was analysed by one way ANOVA. No significant difference was found in the concentration of HXP after 2, 4, 5 or 6 hours hydrolysis of the FP and LP tissues ($p = 0.148$ and $p = 0.120$, respectively). In contrast, significant differences were found in the amount of HXP released from the LA tissue between 2 h and 6 h and between the 4 h and 6 h, with the amount of HXP being higher after 6 h ($p < 0.05$; MSD = 29.013; Fig. 3.4b). There was no significant difference in the HXP released after 5 and 6 hours hydrolysis. Thus, it was decided to use the 6 h time point for the acid hydrolysis of all tissue analysed in this study.

Hydroxyproline content of tissues

The amount of HXP per mg dry weight of FP, LA and LP after 6 h of acid hydrolysis was 83.252 (±9.704) $\mu g \cdot mg^{-1}$, 99.302 (± 13.987) $\mu g \cdot mg^{-1}$ and 80.054 (± 20.433) $\mu g \cdot mg^{-1}$, respectively (Figure 3.5). The LA and LP groups were statistically compared and no significant difference was observed ($p = 0.074$). The final percentage of collagen content was 58.276% for FP, 69.511% for LA and 56.038% for LP. The final percentage of collagen was calculated as the HXP amount converted in $mg \cdot mg^{-1}$ and multiplied by 7 (as 1/7 of 1mg of collagen is HXP).

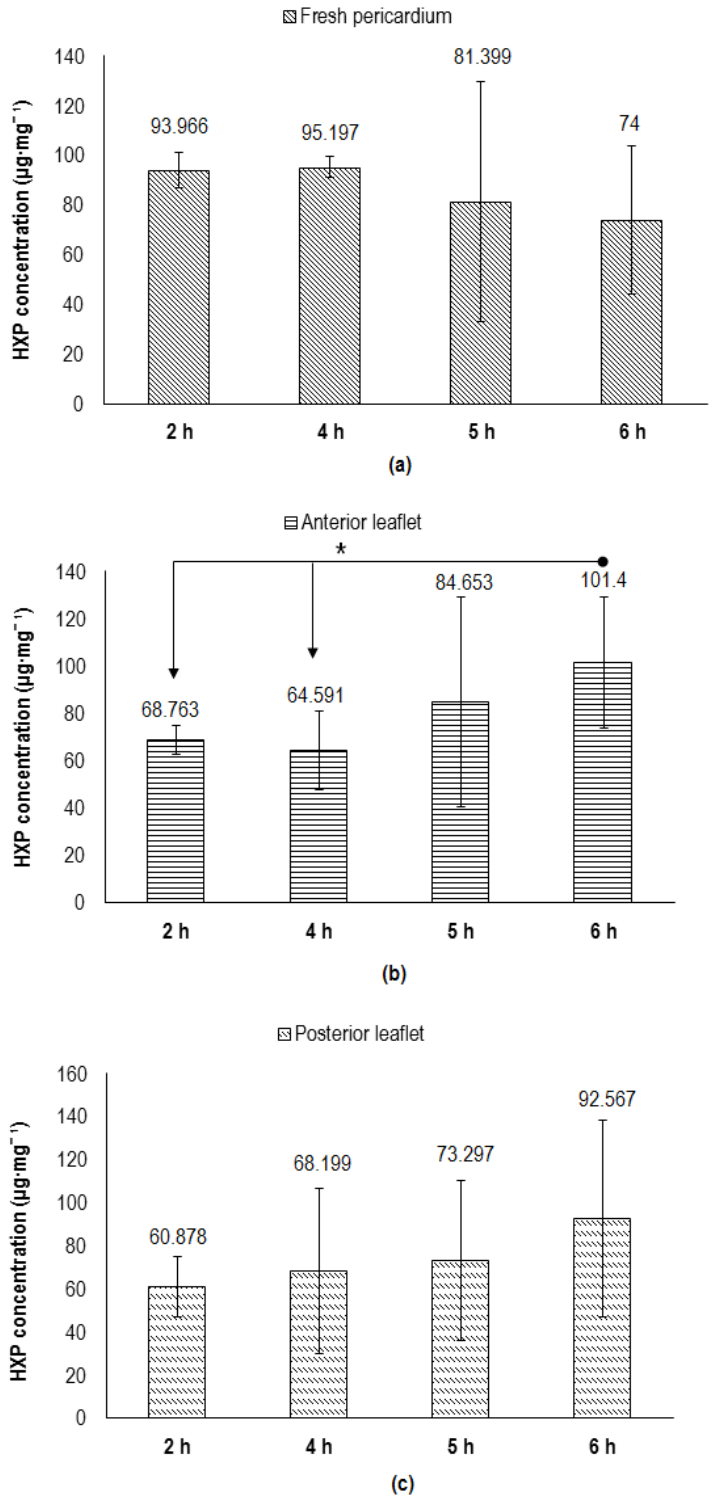

Figure 3.4: HXP content per dry weight of fresh pericardium (a), anterior (b) and posterior (c) leaflets after 2, 4, 5 and 6 h time points of acid hydrolysis. Data is presented as the mean (n=3) ±95% C.I. Asterisk and connectors indicate significant difference between originator and end-arrow column (determined by ANOVA and calculation of MSD $p < 0.05$). Significant differences were found between 2 and 6 h and between 4 and 6 h acid hydrolysis within the LA group ($p < 0.05$; MSD = 29.013). HXP: hydroxyproline.

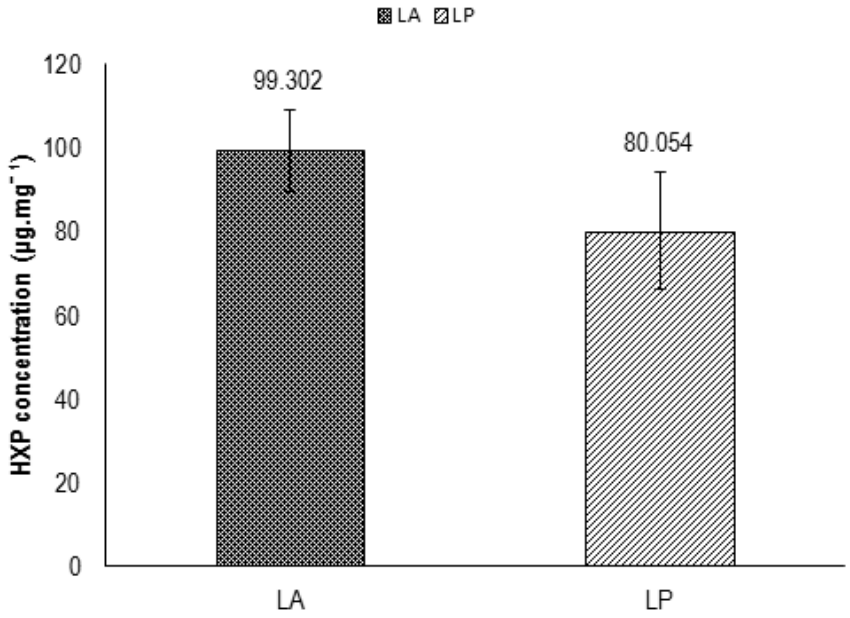

Figure 3.5: HXP content per dry weight of anterior (LA) and posterior (LP) leaflets after 6 h of acid hydrolysis. Data is presented as the mean (n=6) ± 95% C.I. Data was analysed by unpaired student`s t-test that showed no significant difference between groups (p =0.074). HXP: hydroxyproline.

3.3.2.2 GAG content of porcine pericardium and mitral valve leaflets

The amount of GAGs per dry weight of FP, LA and LP was 8.425 (±3.367) µg·mg^{-1}, 23.898 (± 8.653) µg·mg^{-1} and 24.590 (± 5.787) µg·mg^{-1}, respectively. The LA and LP groups were statistically compared and no significant difference was observed (p = 0.868; Figure 3.6).

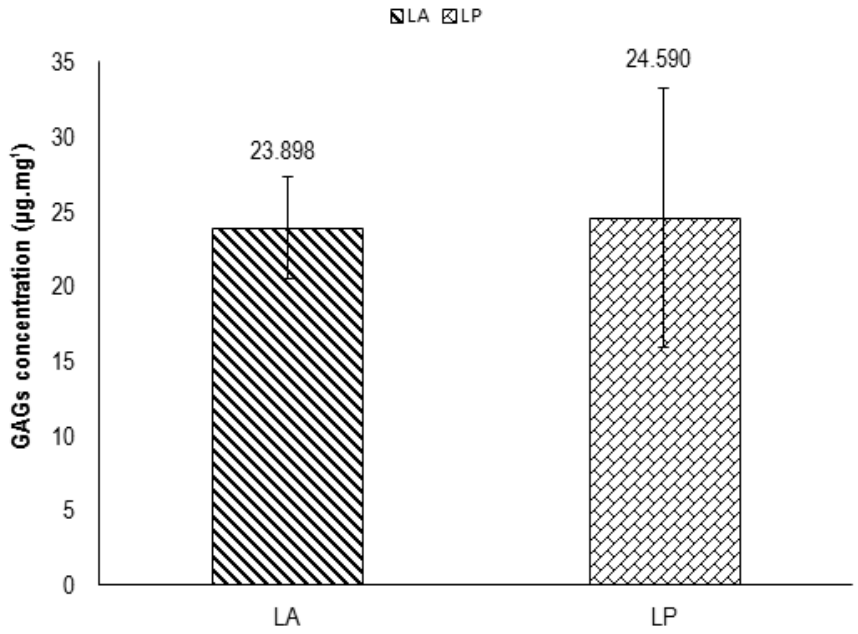

Figure 3.6: GAG content per dry weight of fresh pericardium (FP), anterior (LA) and posterior (LP) leaflets. Data is presented as the mean (n=6) ± 95%C.I. Data was analysed by unpaired student`s t-test that showed no significant difference between groups (p =0.868). GAGs: glycosaminoglycans.

3.3.3 Distribution of ECM and cellular proteins in porcine pericardium and mitral valve leaflets

3.3.3.1 Chondroitin sulphate

Images of porcine MV leaflet and pericardial sections labelled with antibody against chondroitin sulphate are shown in Figure 3.7 and 3.8, respectively. Both the anterior and posterior leaflet sections (LAR, LAC, LPR, LPC) were stained positive, indicated by a deep brown coloration, in the spongiosa layer (Fig. 3.7a - d). Positive staining was also observed in the ventricularis of the LAR section (Fig. 3.7b). Positive staining was also demonstrated in the pericardial sections, along the mesothelial layer (Fig.3.8a, b). No brown coloured staining was observed in the tissue sections stained with the isotype control (Fig. 3.7e, Fig. 3.8c).

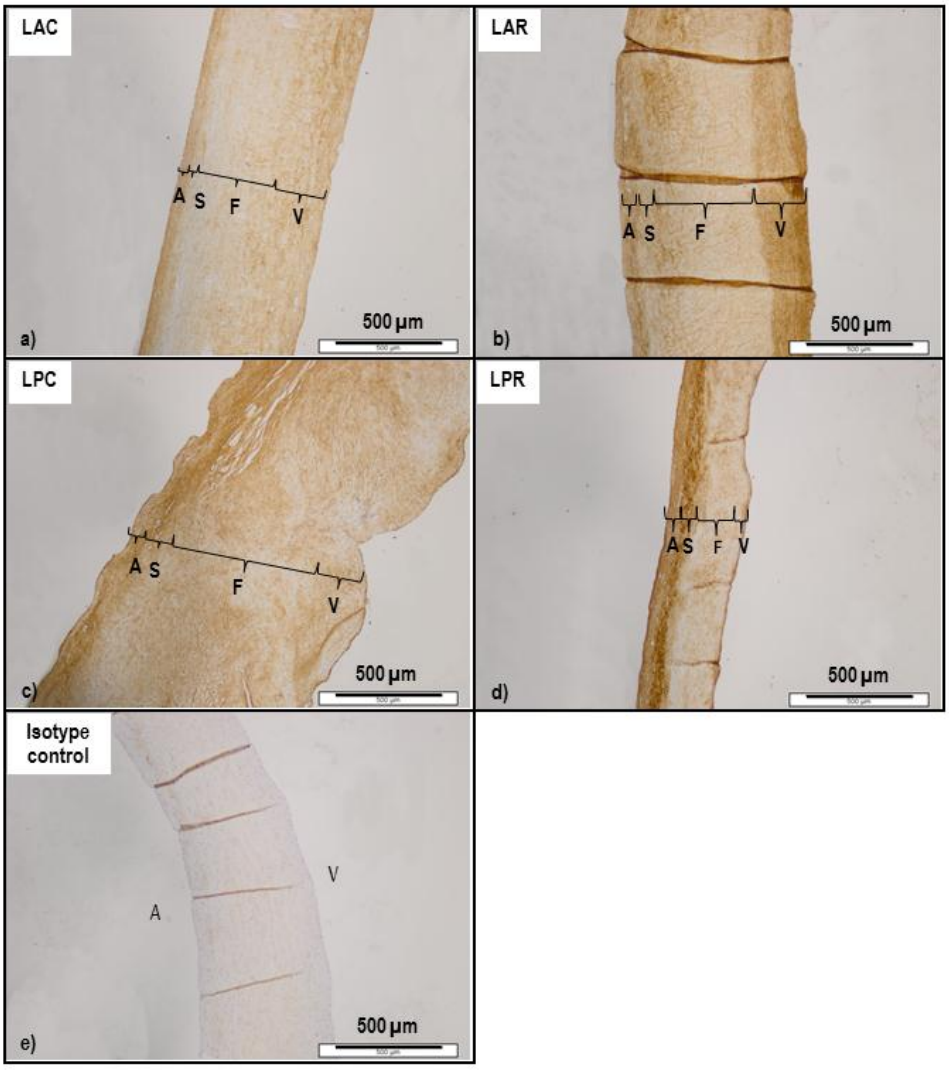

Figure 3.7: Localisation of chondroitin sulphate in MV leaflets circumferential (LAC; a) and radial (LAR; b, e) anterior, circumferential (LPC; c) and radial (LPR; d) posterior. Sections were stained with chondroitin sulphate (a - d) and isotype control (e). Portions of tissue positive for chondroitin sulphate were brown stained. No brown coloured staining was observed in the tissue section stained with the isotype control (e). Brackets indicate the various layers. A: atrialis layer/side; F: fibrosa; S: spongiosa; V: ventricularis layer/side. Scale bars indicate 500µm.

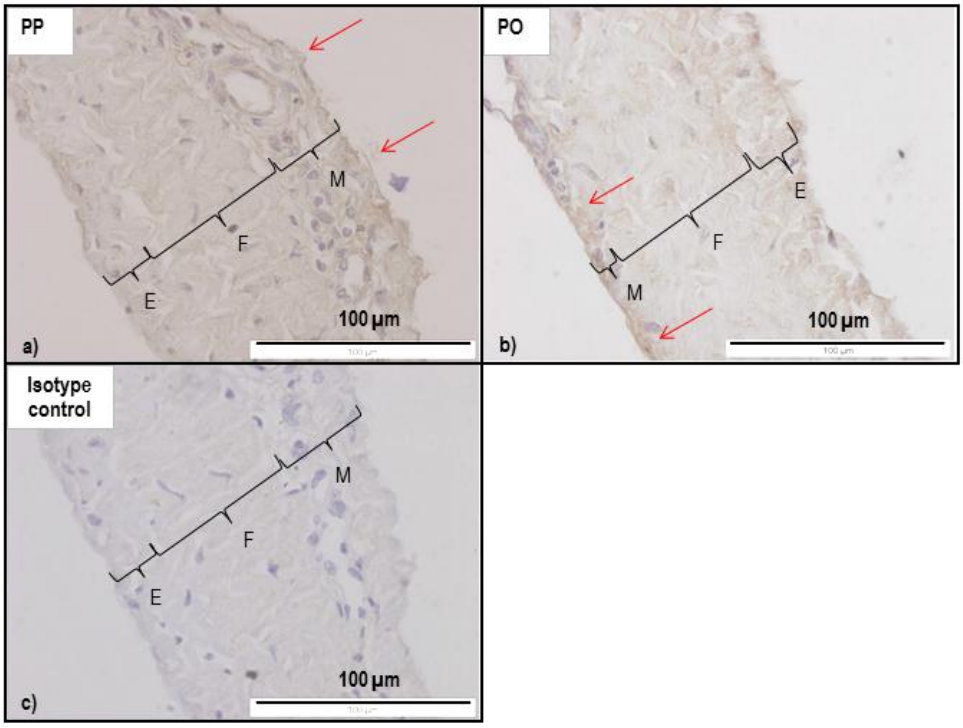

Figure 3.8: Localisation of chondroitin sulphate in fresh pericardial samples isolated parallel (PP; a, c) and orthogonally (PO; b) to the direction of the collagen fibres. Sections were stained with chondroitin sulphate (a, b) and isotype control (c). Portions of tissue positive for chondroitin sulphate were brown stained. No brown coloured staining was observed in the tissue section stained with the isotype control (c). The red arrows indicate the mesothelial layer stained brown. E: epipericardial layer/side; M: mesothelial layer/side. Scale bars indicate 100 µm.

3.3.3.2 Collagen I

The porcine MV leaflet and pericardial sections labelled with antibody against collagen I are shown in Figure 3.9 and 3.10, respectively. Positive staining, indicated by a deep brown coloration, was observed in both the anterior (LAR) and posterior (LPR) radial leaflet sections, with particular prevalence in the fibrosa. Positive staining was also observed throughout the whole thickness of the circumferential leaflet sections (Fig. 3.9a, c). In the case of the pericardial samples, collagen I was detected throughout the fibrosa and epipericardial layers of the parallel (PP) and orthogonal (PO) sections (Fig.3.10a, b). No brown staining was observed in the tissue sections stained with the isotype control (Fig. 3.9e, Fig. 3.10c).

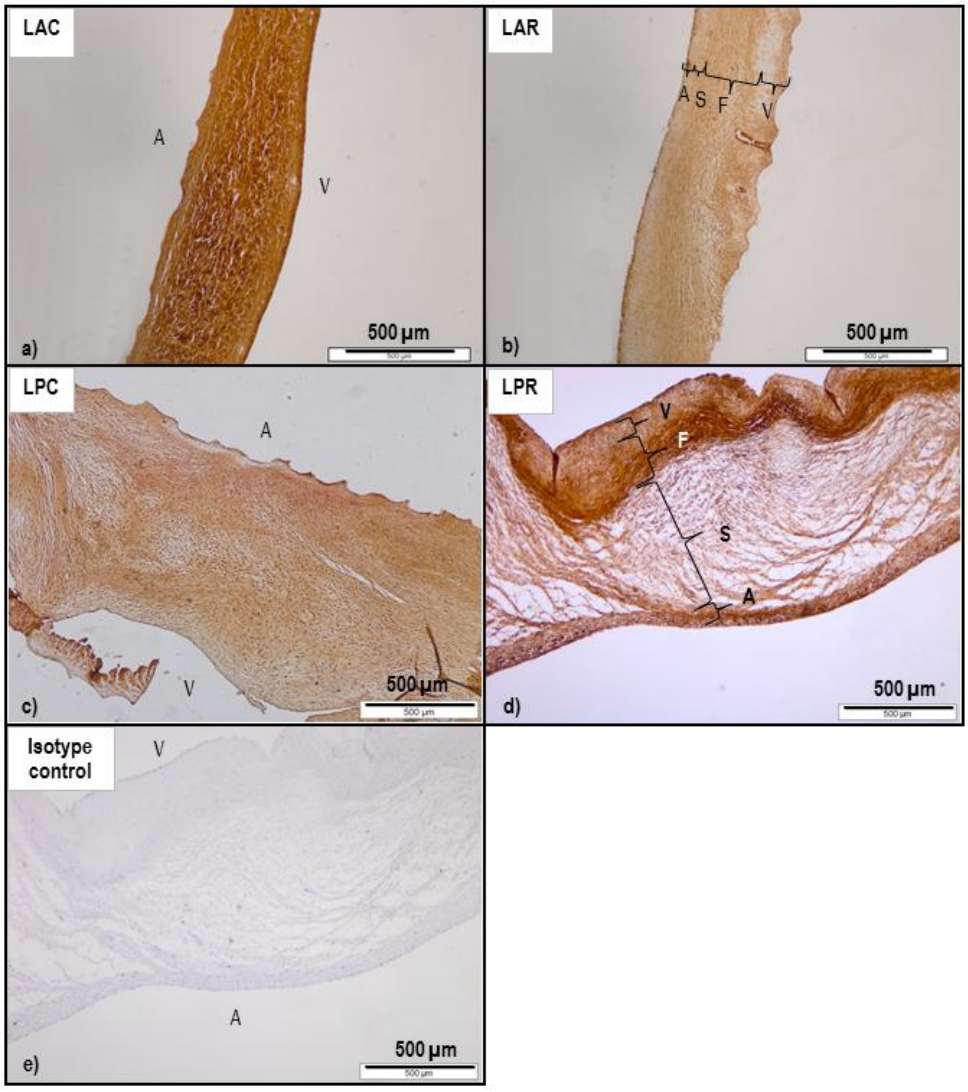

Figure 3.9: Localisation of collagen I in MV leaflets circumferential (LAC; a) and radial (LAR; b) anterior, circumferential (LPC; c) and radial (LPR; d, e) posterior. Sections were stained with collagen I (a - d) and isotype control (e). Portions of tissue positive for collagen I were stained brown. No brown staining was observed in the section stained with the isotype control (e). A: atrialis layer/side; F: fibrosa; S: spongiosa; V: ventricularis layer/side. Scale bars indicate 500 µm.

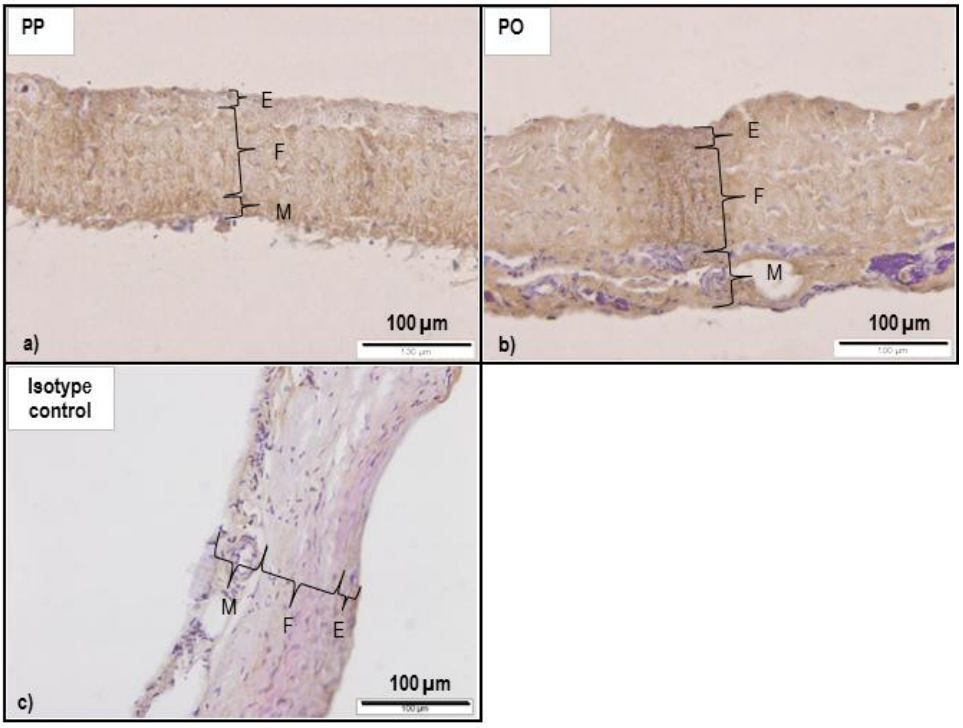

Figure 3.10: Localisation of collagen I in fresh pericardial samples isolated parallel (PP; a, c) and orthogonally (PO; b) to collagen fibre direction. Sections were stained with collagen I (a, b) and isotype control (c). Regions positive for collagen I were stained brown. No brown staining was observed in the isotype control (c). E: epipericardial layer; F: fibrosa; M: mesothelial layer. Scale bars indicate 100 µm.

3.3.3.3 Collagen III

Images of porcine MV leaflet and pericardial sections labelled with antibody against collagen III are shown in Figure 3.11 and 3.12, respectively. Positive staining (deep brown) was observed in the fibrosa of the circumferential anterior leaflet (LAC), and the circumferential (LPC) and radial (LPR) posterior leaflet sections (Fig. 3.11a, c, d). The radial anterior leaflet (LAR) section demonstrated positive staining throughout its whole thickness (Fig. 3.11b). Collagen III was also detected in the pericardial sections (PO, PP), with positive staining present throughout the fibrosa and epipericardial layers (Fig.3.12a, b). No staining was observed in the tissue sections stained with the isotype control (Fig. 3.11e, Fig. 3.12c).

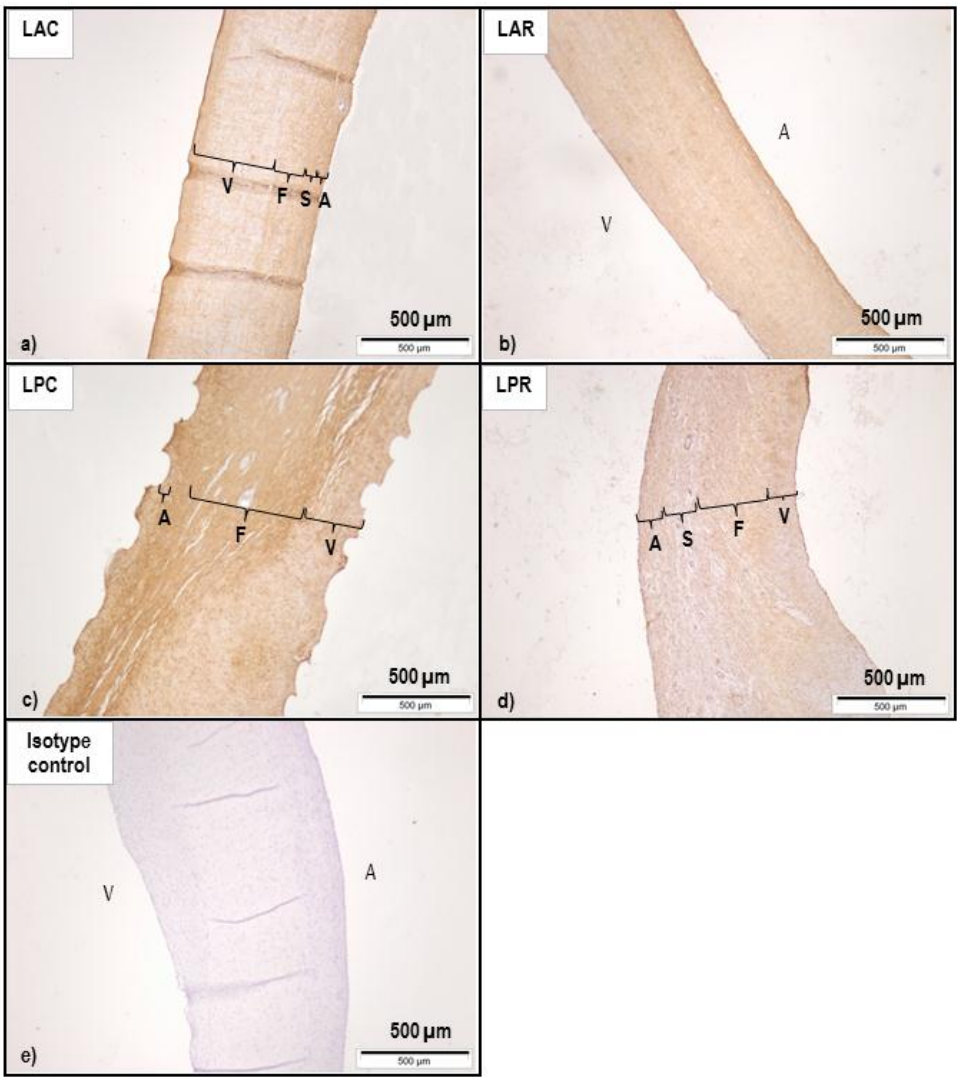

Figure 3.11: Localisation of collagen III in MV leaflets circumferential (LAC; a) and radial (LAR; b, e) anterior, circumferential (LPC; c) and radial (LPR; d) posterior. Sections were stained with collagen III (a – d) and isotype control (e). Portions of tissue positive for collagen III were brown stained. No brown coloured staining was observed in the tissue section stained with the isotype control (e). Brackets indicate the various layers. A: atrialis layer/side; F: fibrosa; S: spongiosa; V: ventricularis layer/side. Scale bars indicate 500 µm.

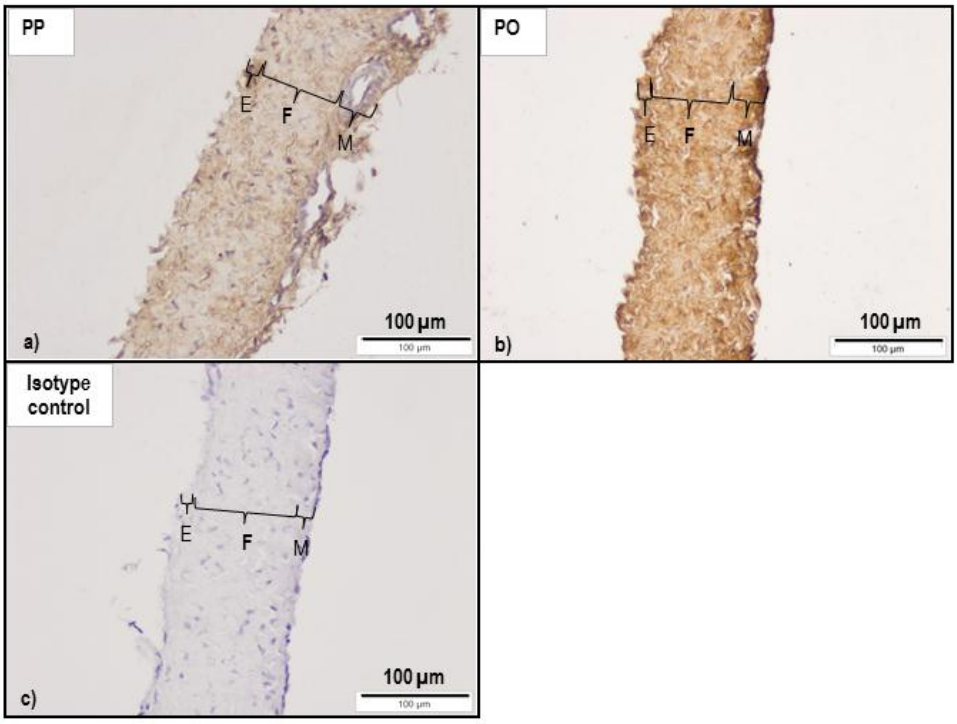

Figure 3.12: Localisation of collagen III in fresh pericardial samples isolated parallel (PP; a, c) and orthogonally (PO; b) to the direction of the collagen fibres. Sections were stained with collagen III (a, b) and isotype control (c). Portions of tissue positive for collagen III were brown stained. No brown coloured staining was observed in the tissue section stained with the isotype control (c). Brackets indicate the various layers. E: epipericardial layer; F: fibrosa; M: mesothelial layer. Scale bars indicate 100 µm.

3.3.3.4 Collagen IV

Images of porcine leaflet and pericardial sections labelled with antibody against collagen IV are shown in Figure 3.13 and 3.14, respectively. Both the anterior (LAR, LAC) and posterior (LPR, LPC) leaflet sections demonstrated positive staining (deep brown) in the sub-endothelial regions of the capillaries found within the leaflets, and the sub-endothelial regions of the atrial and ventricular surfaces of the leaflets (Fig. 3.13a - d). Positive staining for collagen IV was also observed in the mesothelial and epipericardial layers of the pericardial sections (Fig.3.14a, b). No positive staining was observed in the sections stained with the isotype control (Fig. 3.13e, Fig. 3.14c).

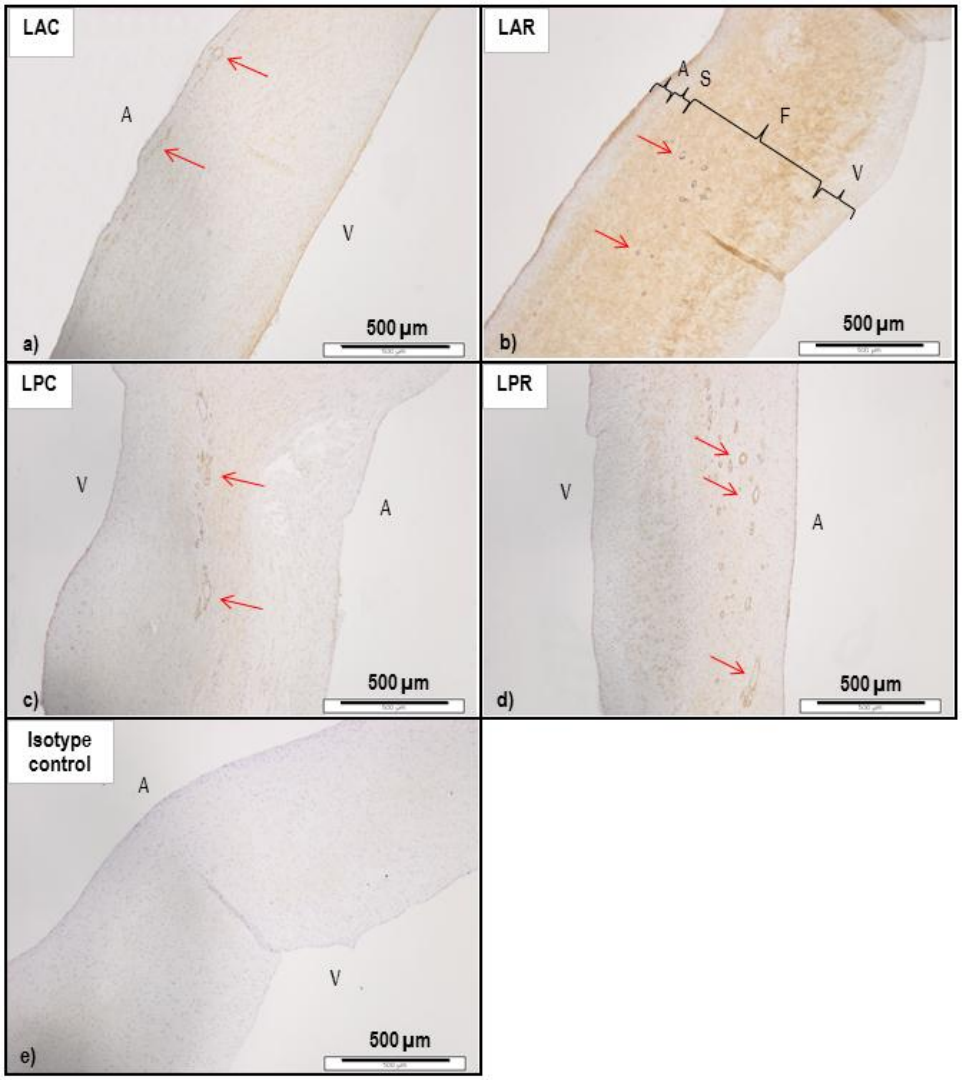

Figure 3.13: Localisation of collagen IV in MV leaflets circumferential (LAC; a) and radial (LAR; b, e) anterior, and circumferential (LPC; c) and radial (LPR; d) posterior. Sections were stained with collagen IV (a - d) and isotype control (e). Collagen IV was stained brown. No staining was observed in the isotype control (e). The red arrows indicate blood vessel stained brown. A: atrialis side; V: ventricularis side. Scale bars indicate 500 µm.

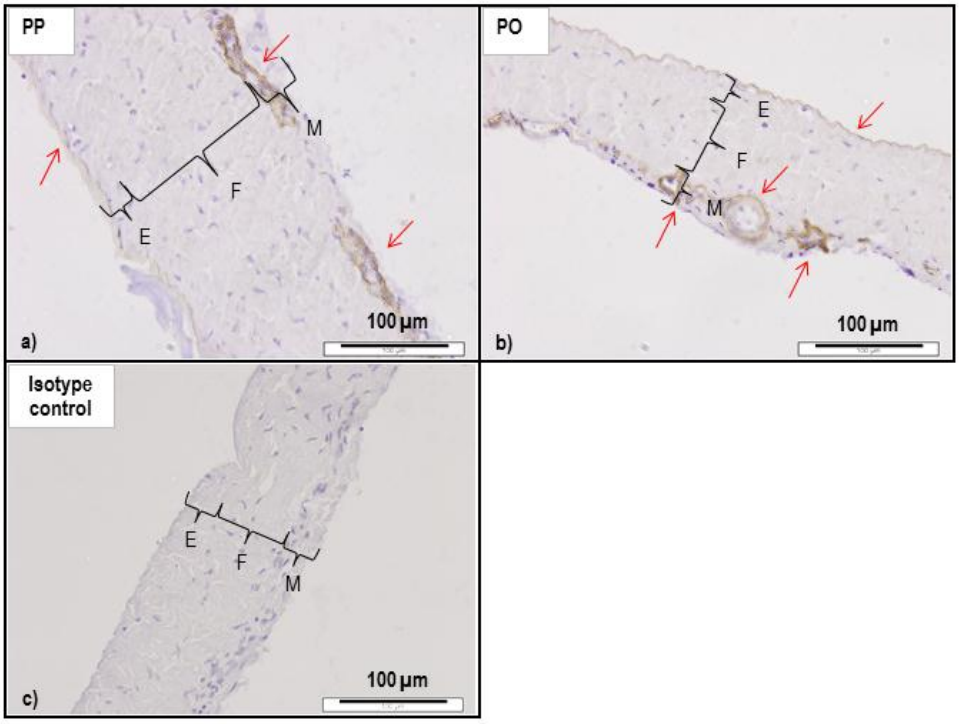

Figure 3.14: Localisation of collagen IV in fresh pericardial samples isolated parallel (PP; a, c) and orthogonally (PO; b) to the direction of the collagen fibres. Sections were stained with collagen IV (a, b) and isotype control (c). Collagen IV was stained brown. No staining was observed in isotype control (c). The red arrows indicate vessels, and the mesothelial/epipericardial layers stained brown. E: epipericardial layer; M: mesothelial layer. Scale bars indicate 100 µm.

3.3.3.5 Fibronectin

Images of porcine MV leaflet and pericardial sections labelled with antibody against fibronectin are shown in Figure 3.15 and 3.16, respectively. Positive staining (deep brown) was observed throughout the thickness of the MV leaflet sections (Fig. 3.15a - d). Fibronectin was also detected in the pericardial sections, in the region close to the mesothelium (Fig.3.16a, b). No staining was observed in the MV leaflets tissue section stained with the isotype control (Fig. 3.15e), whereas weak staining was observed in the fresh pericardial section (Fig. 3.16c).

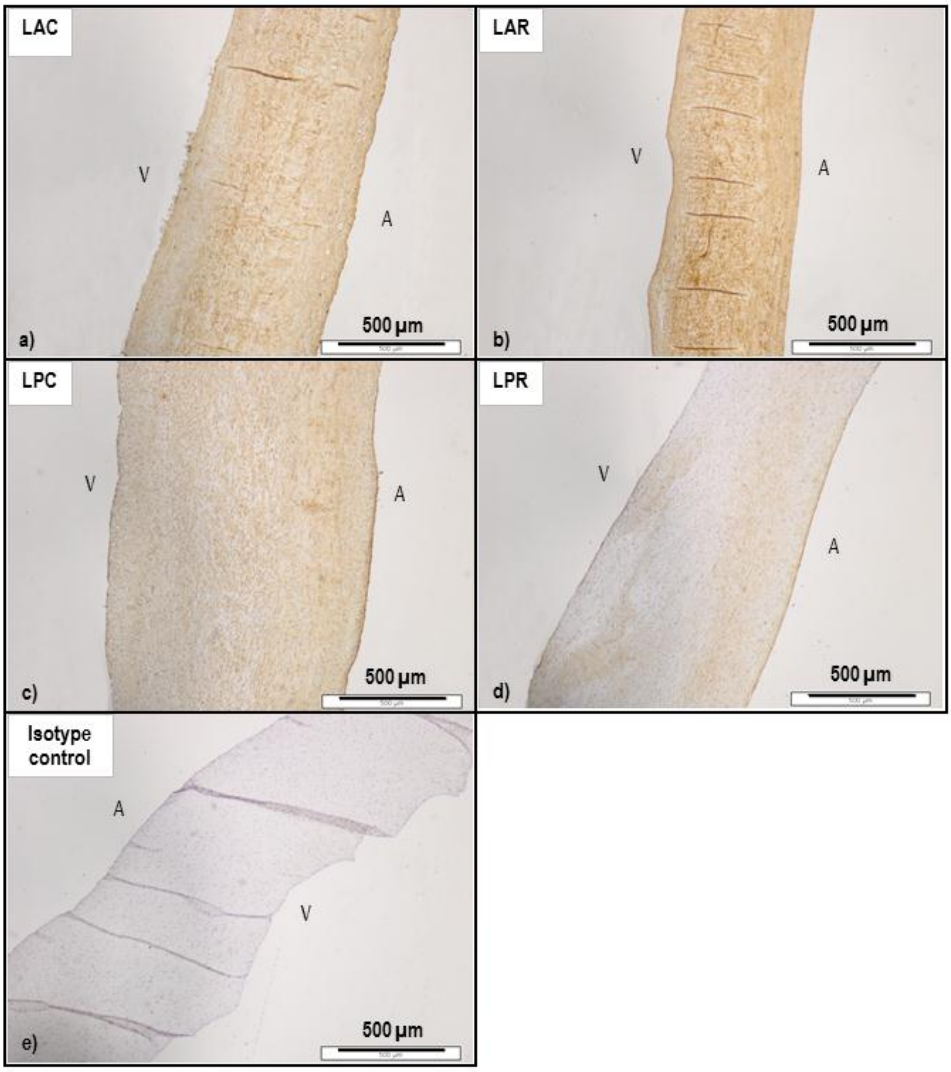

Figure 3.15: Localisation of fibronectin in MV leaflets circumferential (LAC; a) and radial (LAR; b, e) anterior, circumferential (LPC; c) and radial (LPR; d) posterior. Sections were stained with fibronectin (a – d) and isotype control (e). Portions of tissue positive for fibronectin were brown stained. No staining was observed in isotype control (e). A: atrialis side; V: ventricularis side. Scale bars indicate 500 µm.

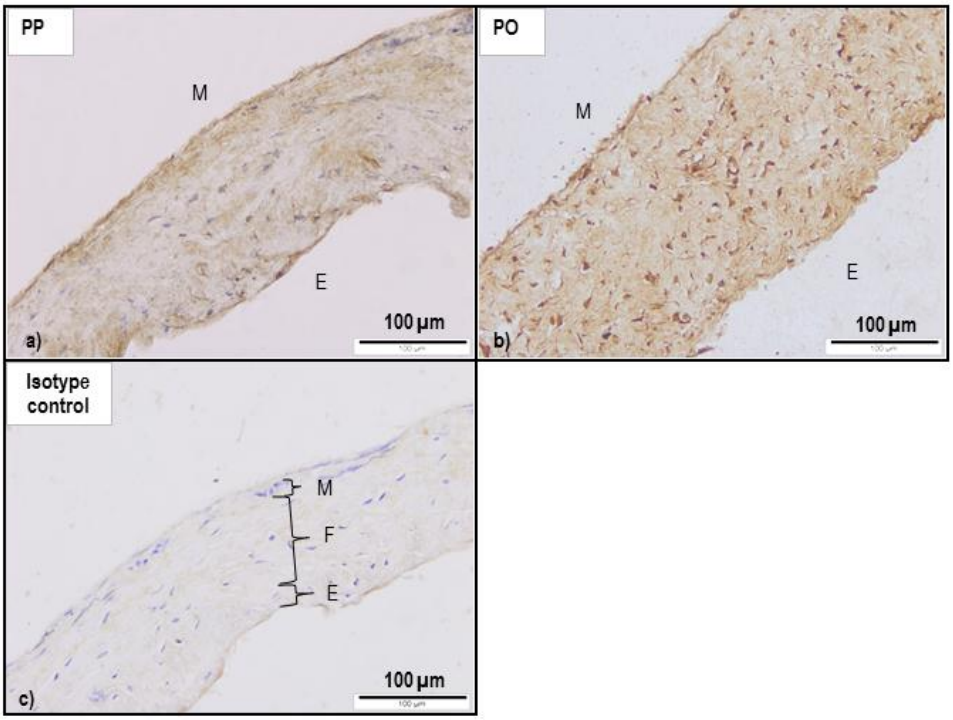

Figure 3.16: Localisation of fibronectin in fresh pericardial samples isolated parallel (PP; a, c) and orthogonally (PO; b) to the collagen fibre direction. Sections were stained with fibronectin (a, b) and isotype control (c). Regions positive for fibronectin were stained brown. Weak staining was observed in isotype control (c). E: epipericardial layer/side; M: mesothelial layer/side. Scale bars indicate 100 µm.

3.3.3.6 Laminin

Images of porcine MV leaflet and pericardial sections labelled with antibody against laminin are shown in Figure 3.17 and 3.18, respectively. Positive staining (deep-brown) was observed throughout the thickness of both the anterior and posterior leaflet sections, with particular prevalence in the sub-endothelium regions of the capillaries and the sub-endothelium regions of the atrial and ventricular surfaces of the leaflets (Fig. 3.17a - d). Positive staining was also observed throughout the thickness of the pericardial sections, with increased occurrence in the mesothelial and epipericardial layers (Fig.3.18a, b). Weak staining was observed in the MV leaflets tissue section stained with the isotype control (Fig. 3.17e), whereas no staining was observed in the fresh pericardial section (Fig. 3.18c).

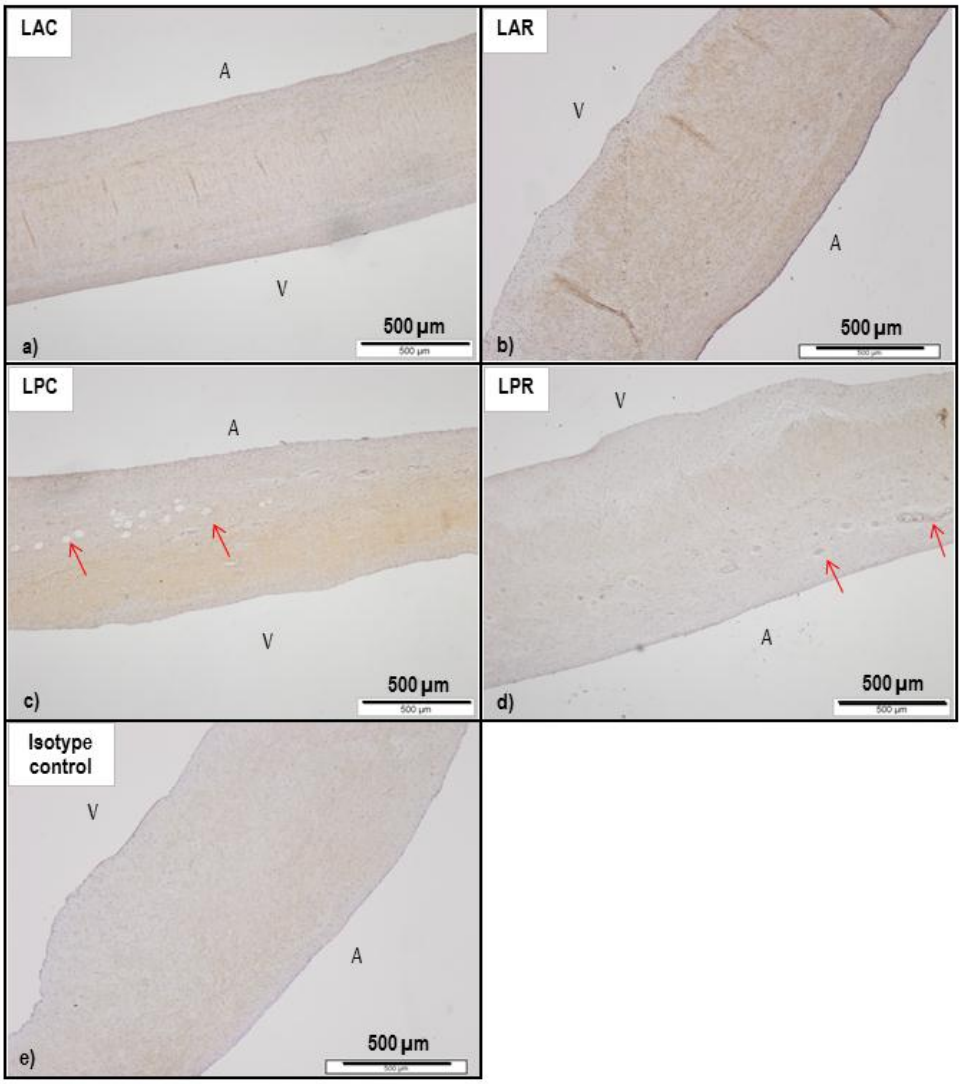

Figure 3.17: Localisation of laminin in MV leaflets circumferential (LAC; a) and radial (LAR; b, e) anterior, circumferential (LPC; c) and radial (LPR; d) posterior. Sections were stained with laminin (a – d) and isotype control (e). Regions positive for laminin were stained brown. Weak staining was observed in isotype control (e). The red arrows indicate blood vessels. A: atrialis side; V: ventricularis side. Scale bars indicate 500 µm.

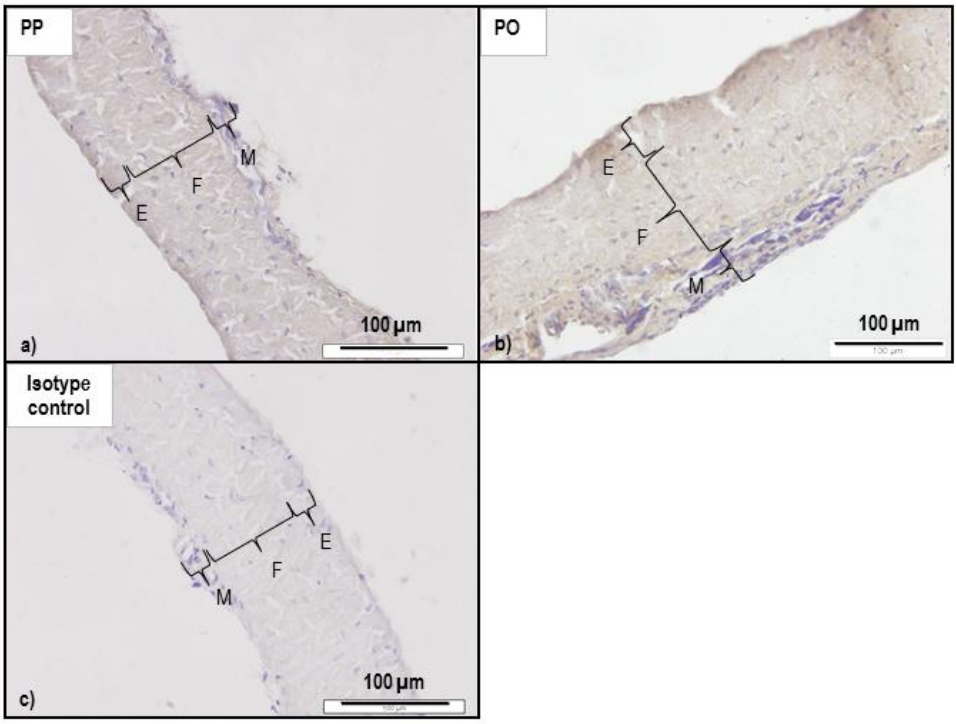

Figure 3.18: Localisation of laminin in fresh pericardial samples isolated parallel (PP; a, c) and orthogonally (PO; b) to the direction of the collagen fibres. Sections were stained with laminin (a, b) and isotype control (c). Regions positive for laminin were stained brown. No staining was observed in isotype control (c). E: epipericardial layer/side; M: mesothelial layer/side. Scale bars indicate 100 µm.

3.3.3.7 Alpha-SMA

Immunohistochemical staining of MV leaflet sections against α-SMA was performed in order to detect the presence and spatial distribution of SMCs and myofibroblasts (Figure 3.19). Positive staining (deep brown) was observed in the sub-endothelial regions of the capillaries and the atrial surface of the leaflets (Fig. 3.19a - d). Apart from these regions, positive staining was also expressed by a portion of cells throughout the leaflets, whereas the ECM was also stained with a light brown colour (Fig. 3.19a, b). No staining was observed in the tissue sections stained with the isotype control (Fig. 3.19e).

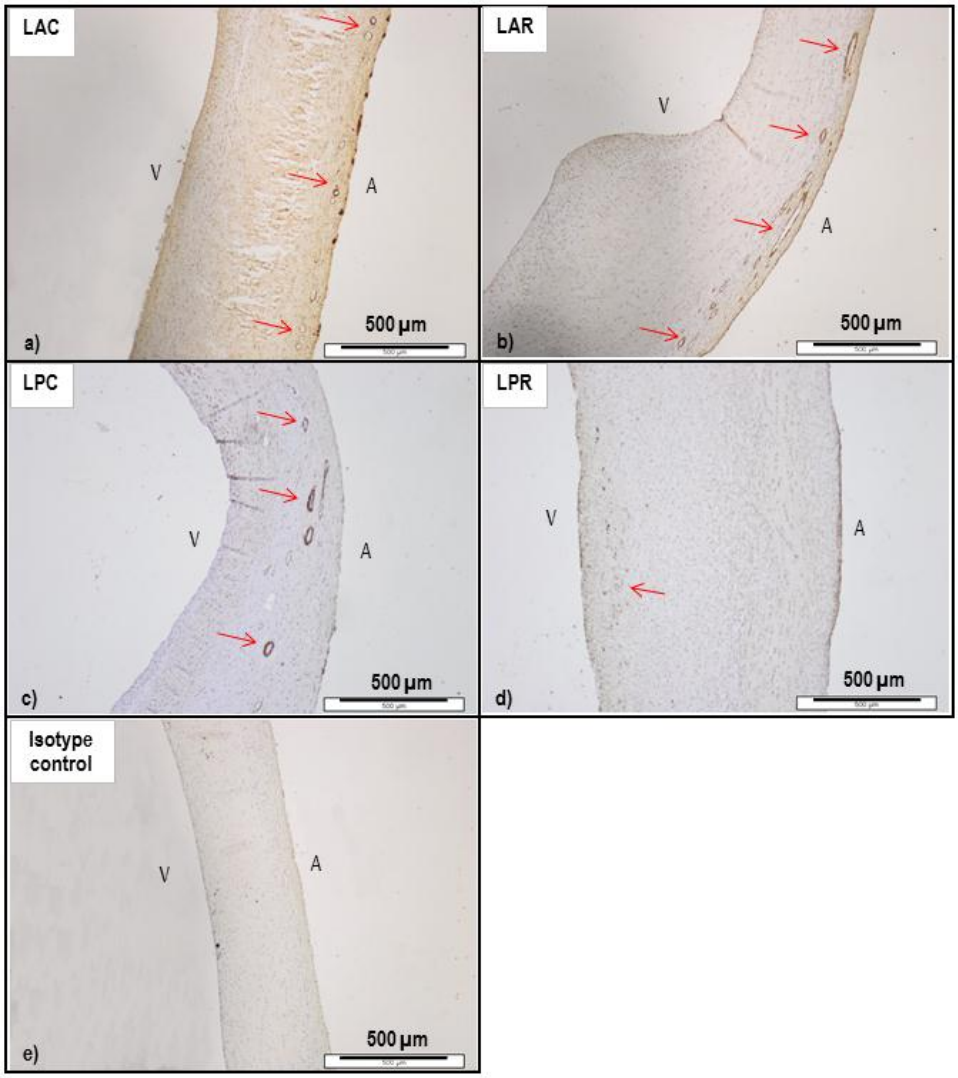

Figure 3.19: Localisation of α - SMA in MV leaflets circumferential (LAC; a) and radial (LAR; b, e) anterior, circumferential (LPC; c) and radial (LPR; d) posterior. Sections were stained with alpha – SMA (a – d) and isotype control (e). Portions of tissue positive for α - SMA were brown stained. No brown coloured staining was observed in the tissue section stained with the isotype control. The red arrows indicate the blood vessels which have been positively stained. A: atrialis side; V: ventricularis side. Scale bars indicate 500 µm.

3.3.3.8 Vimentin

Immunohistochemical staining of MV leaflets against vimentin was performed in order to detect the presence and spatial distribution of fibroblasts (Figure 3.20). Positive staining (deep-brown) was observed throughout the thickness, and around the capillaries, of both the

anterior and posterior leaflet sections (Fig. 3.20a - d). No staining was observed in the sections stained with the isotype control (Fig. 3.20e).

Figure 3.20: Localisation of vimentin in MV leaflets circumferential (LAC; a) and radial (LAR; b, e) anterior, circumferential (LPC; c) and radial (LPR; d) posterior. Sections were stained with vimentin (a – d) and isotype control (e). Regions positive for vimentin were stained brown. No staining was observed in isotype control (e). Red arrows indicate blood vessels. A: atrialis side; V: ventricularis side. Scale bars indicate 500 µm.

3.3.3.9 Von Willebrand factor

Porcine MV leaflet sections were labelled with antibody against the Von Willebrand factor in order to detect the presence and spatial distribution of endothelial cells (Figure 3.21). Positive staining (deep brown) was observed around the capillaries and on the atrial and ventricular

faces of both the anterior and posterior leaflets (Fig. 3.21a - d). No brown staining was observed in the tissue sections stained with the isotype control (Fig. 3.21e).

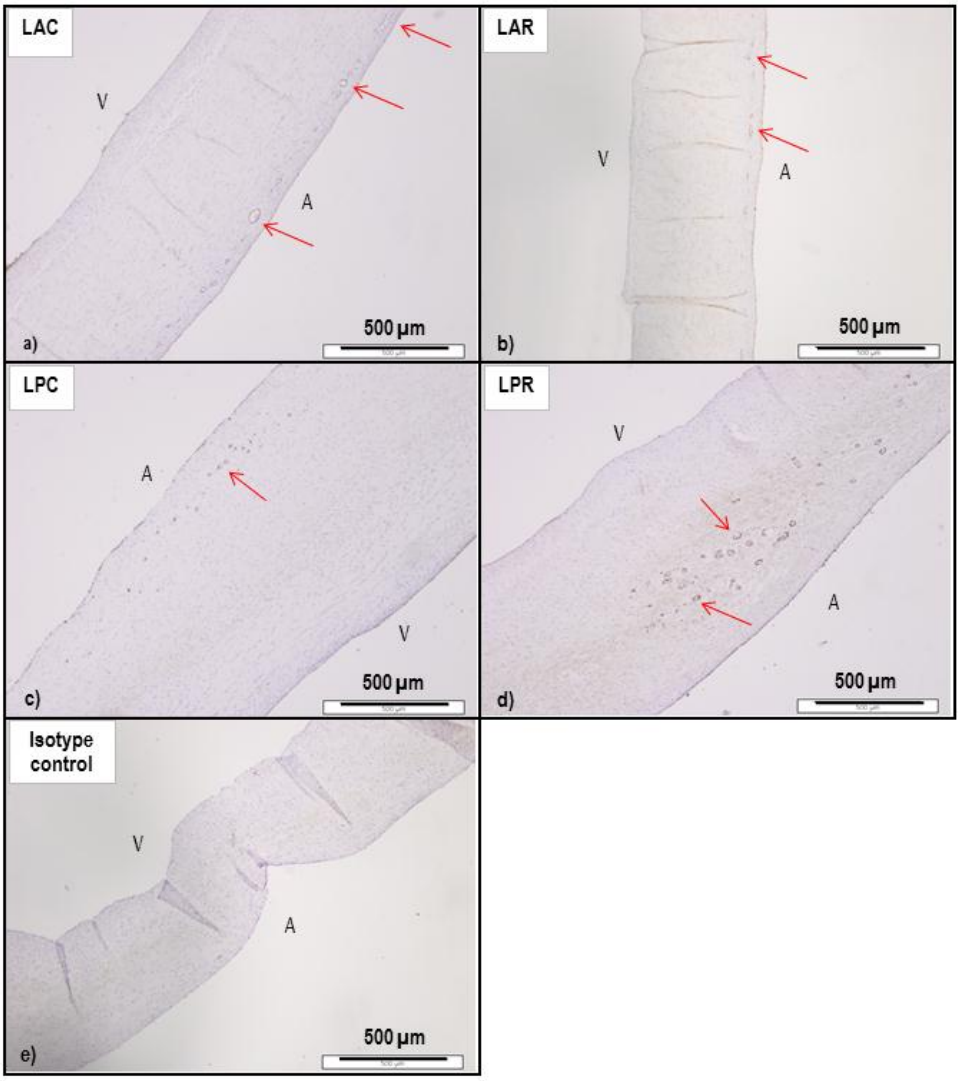

Figure 3.21: Localisation of Von Willebrand factor in MV leaflets circumferential (LAC; a) and radial (LAR; b, e) anterior, circumferential (LPC; c) and radial (LPR; d) posterior. Sections were stained with Von Willebrand factor (a – d) and isotype control (e). Regions positive for Von Willebrand factor were stained brown. No staining was observed in isotype control (e). Red arrows indicate blood vessels. A: atrialis side; V: ventricularis side. Scale bars indicate 500 µm.

3.3.4 Biomechanical properties of porcine pericardium and mitral valve leaflets

3.3.4.1 Porcine pericardium

The calculated biomechanical parameters for the fresh pericardial samples are illustrated in Figures 3.22 through to 3.28. In general, no statistically significant differences were found in

any of the biomechanical parameters studied between the two pericardial directions, indicating that pericardium is a rather isotropic tissue.

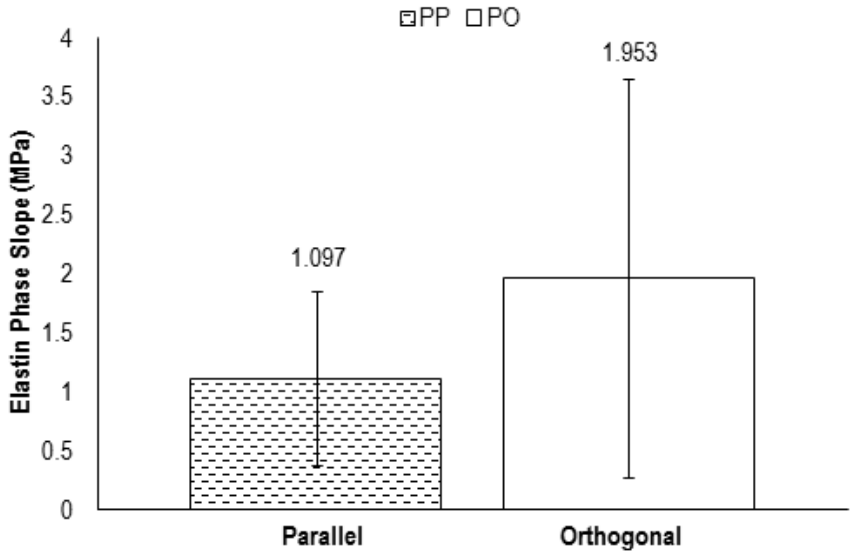

Figure 3.22: Average elastin phase slope for fresh pericardium tested along (PP) and across (PO) the collagen fibres. Data is presented as the mean (n=6) ± 95% C.I. Data was analysed by unpaired student`s t-test that showed no significant difference between groups (p =0.260).

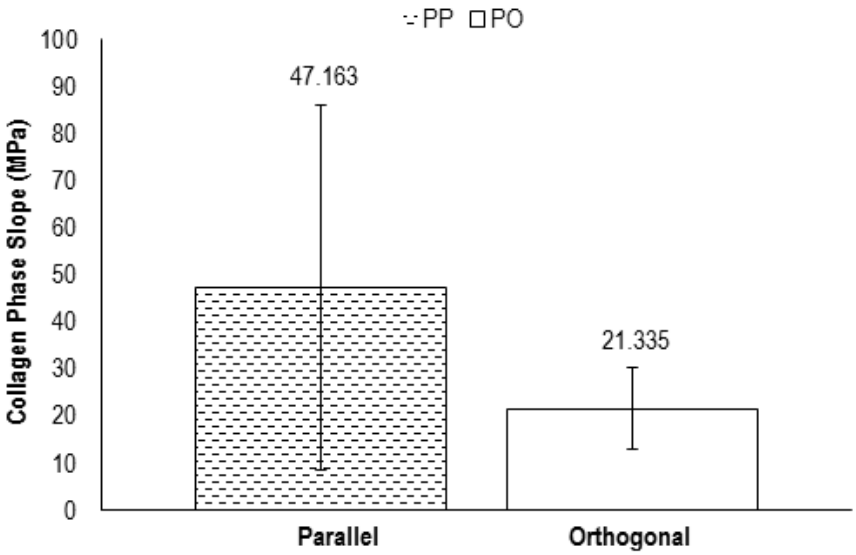

Figure 3.23: Average collagen phase slope for fresh pericardium tested along (PP) and across (PO) the collagen fibres. Data is presented as the mean (n=6) ± 95% C.I. Data was analysed by unpaired student`s t-test that showed no significant difference between groups (p =0.126).

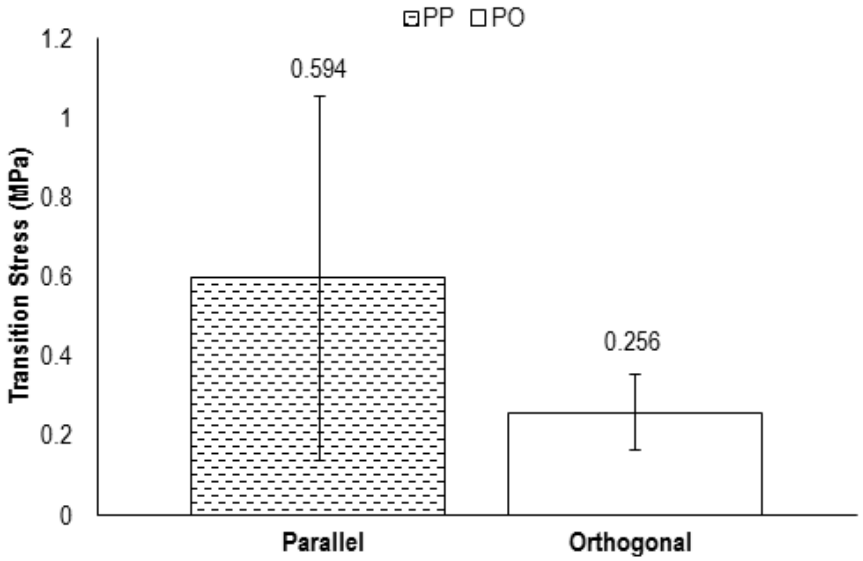

Figure 3.24: Average transition stress for fresh pericardium tested along (PP) and across (PO) the collagen fibres. Data is presented as the mean (n=6) ± 95% C.I. Data was analysed by unpaired student`s t-test that showed no significant difference between groups (p =0.093).

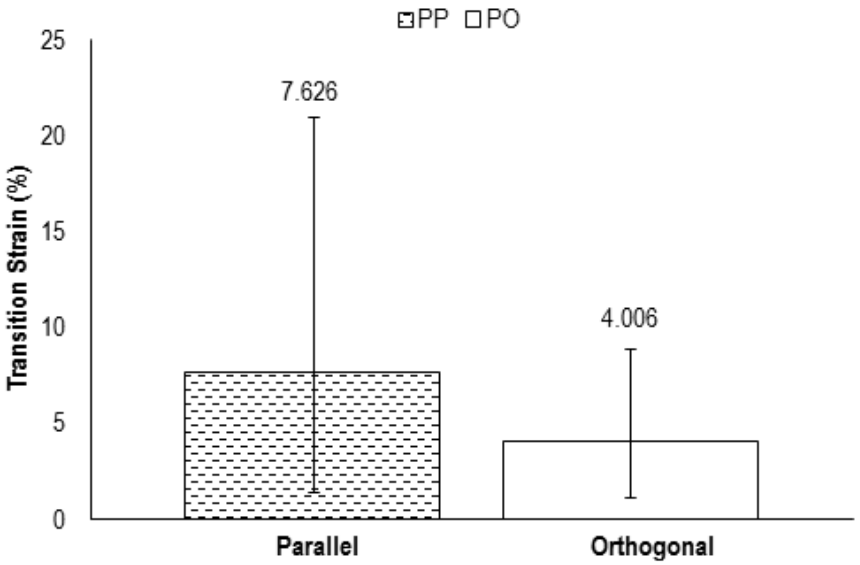

Figure 3.25: Average transition strain for fresh pericardium tested along (PP) and across (PO) the collagen fibres. Data is presented as the mean (n=6) ± 95% C.I. Data was analysed by unpaired student`s t-test that showed no significant difference between groups (p =0.240).

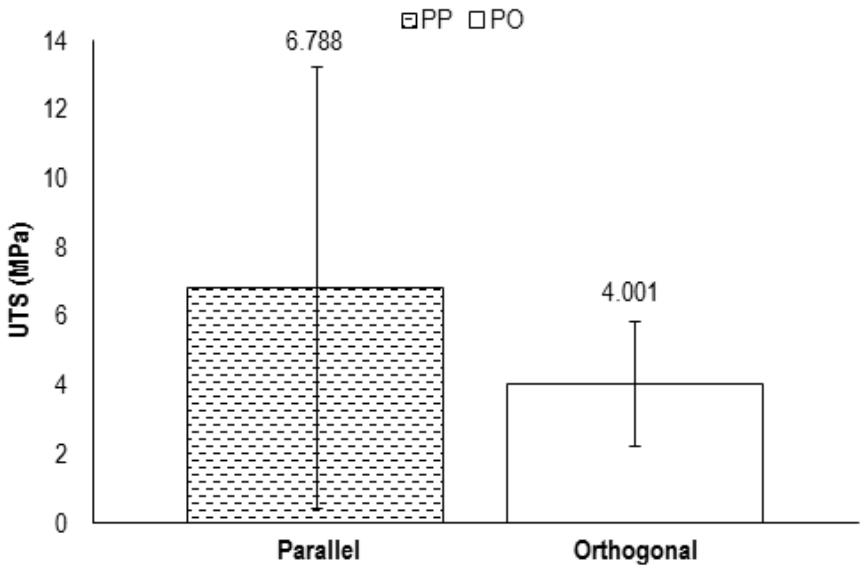

Figure 3.26: Average ultimate tensile strength for fresh pericardium tested along (PP) and across (PO) the collagen fibres. Data is presented as the mean (n=6) ± 95% C.I. Data was analysed by unpaired student`s t-test that showed no significant difference between groups (p =0.307).

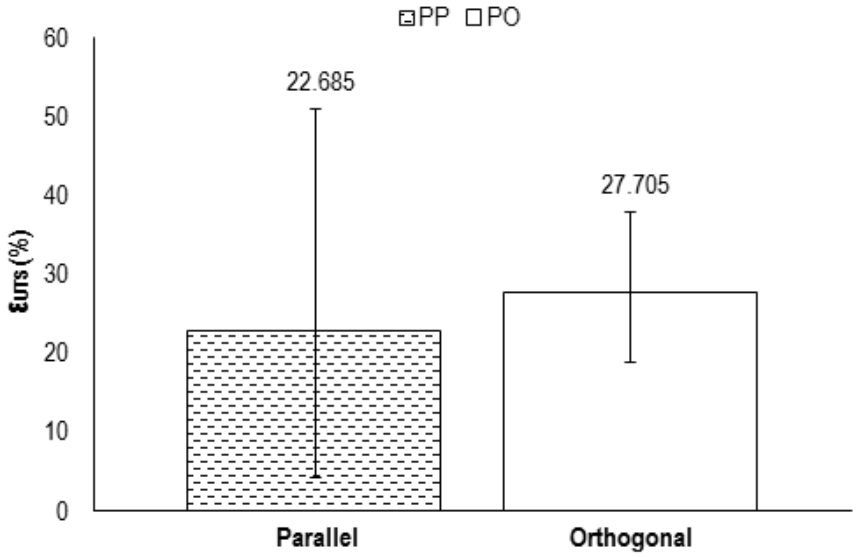

Figure 3.27: Average failure strain for fresh pericardium tested along (PP) and across (PO) the collagen fibres. Data is presented as the mean (n=6) ± 95% C.I. Data was analysed by unpaired student`s t-test that showed no significant difference between groups (p =0.192).

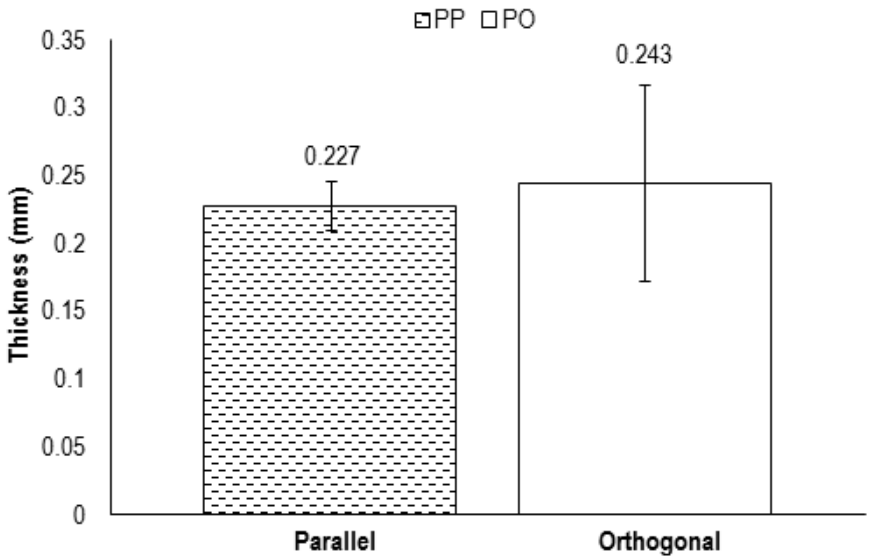

Figure 3.28: Average thickness for fresh pericardium tested along (PP) and across (PO) the collagen fibres. Data is presented as the mean (n=6) ± 95% C.I. Data was analysed by unpaired student`s t-test that showed no significant difference between groups (p =0.580).

3.3.4.2 Mitral valve leaflets

The averaged biomechanical parameters for the MV leaflet samples are illustrated in Figures 3.29 through to 3.35. The results indicated that there was no statistically significant difference between the circumferential and radial direction of the leaflets, or between the anterior and posterior leaflet groups, in the case of the transition strain (ε_t), failure strain (ε_{UTS}), and thickness ($p = 0.319$, $p = 0.180$ and $p = 0.080$, respectively; Fig. 3.32, 3.34, 3.35). However, significant differences were found in the elastin (EI-E) and collagen (Coll-E) phase slopes, transition stress (σ_t), and ultimate tensile strength (UTS) between the anterior and posterior leaflets, and between the radial and circumferential directions. Specifically, the radial anterior leaflet (LAR) group demonstrated significantly increased EI-E compared to the two posterior leaflet (LPR, LPC) groups ($p < 0.05$; MSD = 0.036, Fig. 3.29), representing a lower extensibility for the anterior leaflet along the radial direction. The anterior leaflet also demonstrated a significantly increased Coll-E along the circumferential direction (LAC) compared to both its radial direction (LAR) and the posterior leaflet (LPC, LPR) groups ($p < 0.05$; MSD = 5.444, Fig. 3.30). This indicated that at higher pressures (higher stress), the anterior leaflet extended less along its circumferential direction, in order to withstand the increased pressure, but at the same time it extended more along its radial direction in order to

close the orifice of the valve. With regards to the σ_t, the circumferential anterior leaflet (LAC) group demonstrated higher values compared to the radial posterior leaflet (LPR) group ($p < 0.05$; MSD = 0.114, Fig. 3.31). The circumferential anterior leaflet (LAC) group also showed a significantly higher UTS compared to both the radial anterior leaflet (LAR) group and the posterior leaflet (LPC, LPR) groups ($p < 0.05$; MSD = 37.245, Fig. 3.33). In general, the anterior leaflet demonstrated a significant degree of anisotropy between its radial and circumferential directions, with significant differences in the Coll-E and UTS between the two directions. On the other hand, the posterior leaflet did not demonstrate any directional anisotropy since there were no significant differences in the biomechanical parameters studied between the radial and circumferential directions of this leaflet.

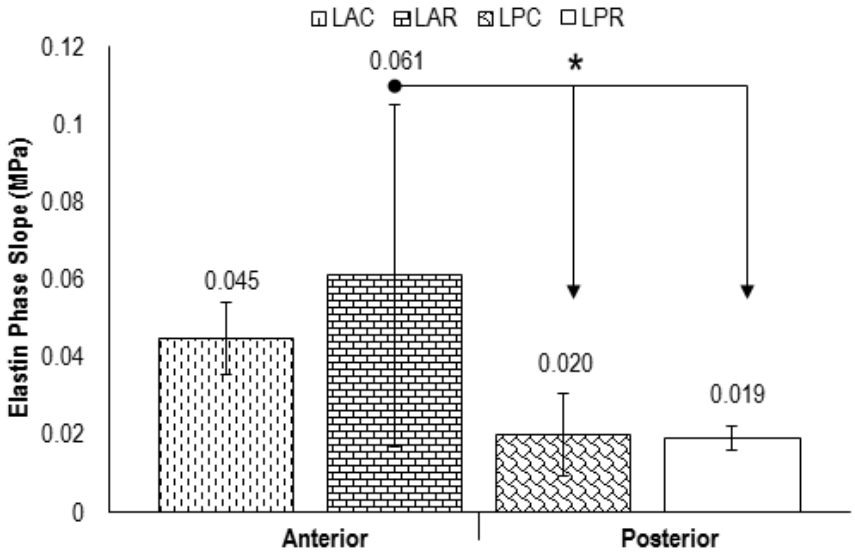

Figure 3.29: Average elastin phase slope for the anterior leaflets tested circumferentially (LAC) and radially (LAR); the posterior leaflets tested circumferentially (LPC) and radially (LPR). Data is presented as the mean (n=6) ± 95% C.I. Asterisk and connectors indicate significant difference between originator column and end arrow column, as determined by ANOVA and calculation of the MSD ($p < 0.05$; MSD = 0.036). LAC: anterior leaflet circumferential; LAR: anterior leaflet radial; LPC: posterior leaflet circumferential; LPR: posterior leaflet radial.

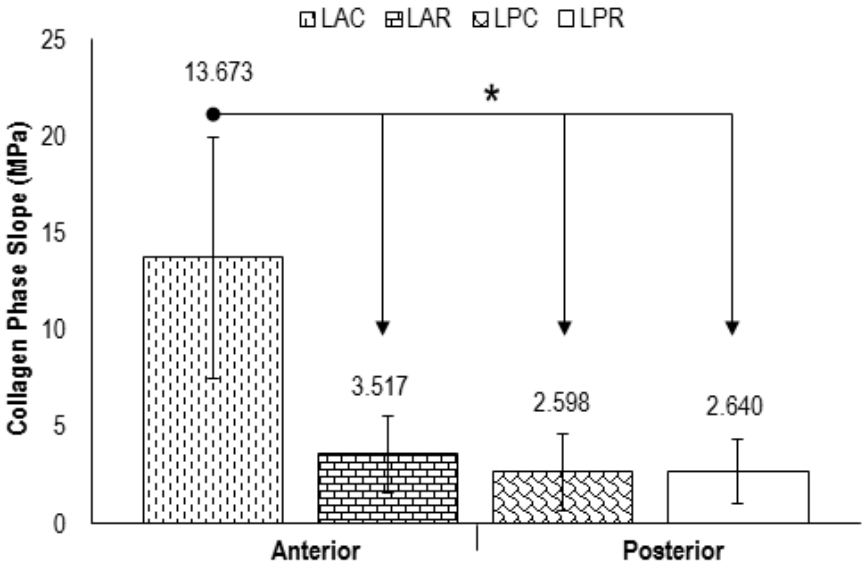

Figure 3.30: Average collagen phase slope for the anterior leaflets tested circumferentially (LAC) and radially (LAR); the posterior leaflets tested circumferentially (LPC) and radially (LPR). Data is presented as the mean (n=6) ± 95% C.I. Asterisk and connectors indicate significant difference between originator column and end arrow column, as determined by ANOVA and calculation of the MSD ($p < 0.05$; MSD = 5.444). LAC: anterior leaflet circumferential; LAR: anterior leaflet radial; LPC: posterior leaflet circumferential; LPR: posterior leaflet radial.

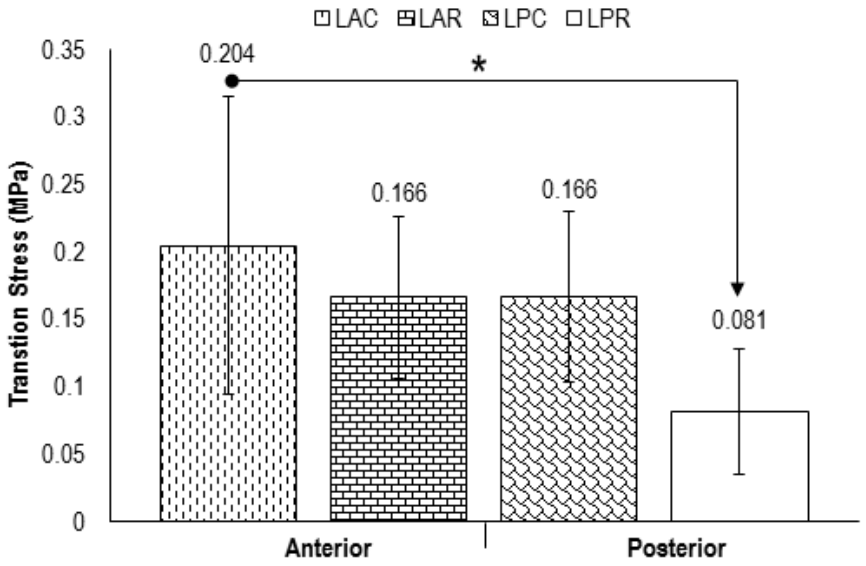

Figure 3.31: Average transition stress for the anterior leaflets tested circumferentially (LAC) and radially (LAR); the posterior leaflets tested circumferentially (LPC) and radially (LPR). Data is presented as the mean (n=6) ± 95% C.I. Asterisk and connectors indicate significant difference between originator column and end arrow column, as determined by ANOVA and calculation of the MSD ($p < 0.05$; MSD = 0.114). LAC: anterior leaflet circumferential; LAR: anterior leaflet radial; LPC: posterior leaflet circumferential; LPR: posterior leaflet radial.

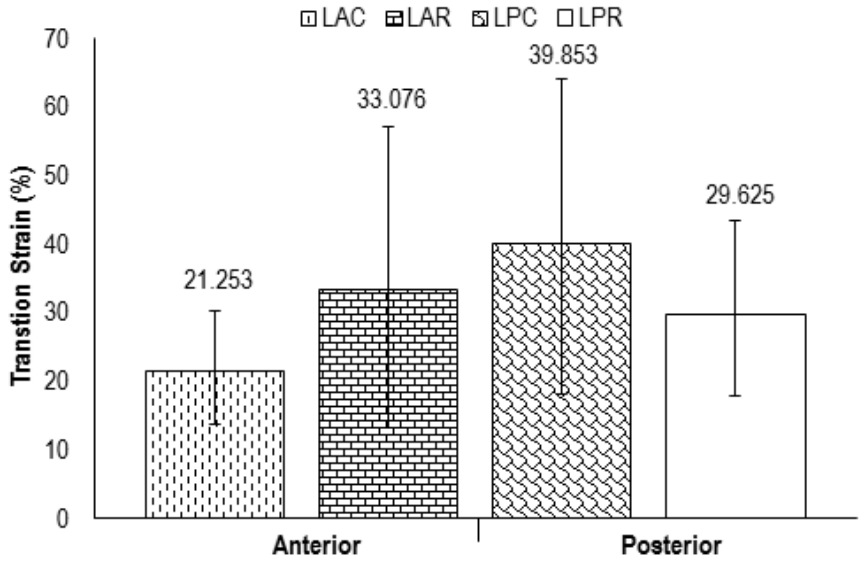

Figure 3.32: Average transition strain for the anterior leaflets tested circumferentially (LAC) and radially (LAR); the posterior leaflets tested circumferentially (LPC) and radially (LPR). Data is presented as the mean (n=6) ± 95% C.I. The data was analysed using ANOVA and calculation of the MSD which showed no significant difference between groups (p = 0.319). LAC: anterior leaflet circumferential; LAR: anterior leaflet radial; LPC: posterior leaflet circumferential; LPR: posterior leaflet radial.

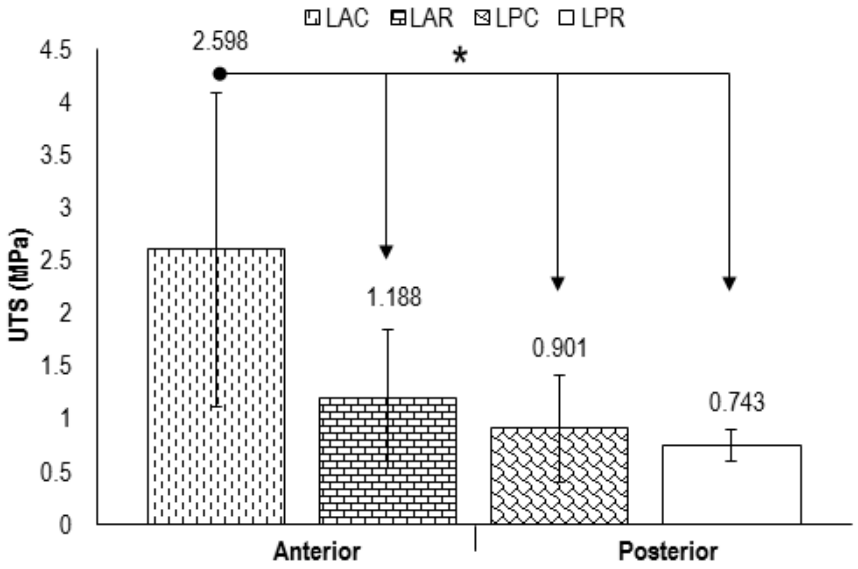

Figure 3.33: Average ultimate tensile strength for the anterior leaflets tested circumferentially (LAC) and radially (LAR); the posterior leaflets tested circumferentially (LPC) and radially (LPR). Data is presented as the mean (n=6) ± 95% C.I. Asterisk and connectors indicate significant difference between originator column and end arrow column, as determined by ANOVA and calculation of the MSD ($p < 0.05$; MSD = 37.245). LAC: anterior leaflet circumferential; LAR: anterior leaflet radial; LPC: posterior leaflet circumferential; LPR: posterior leaflet radial.

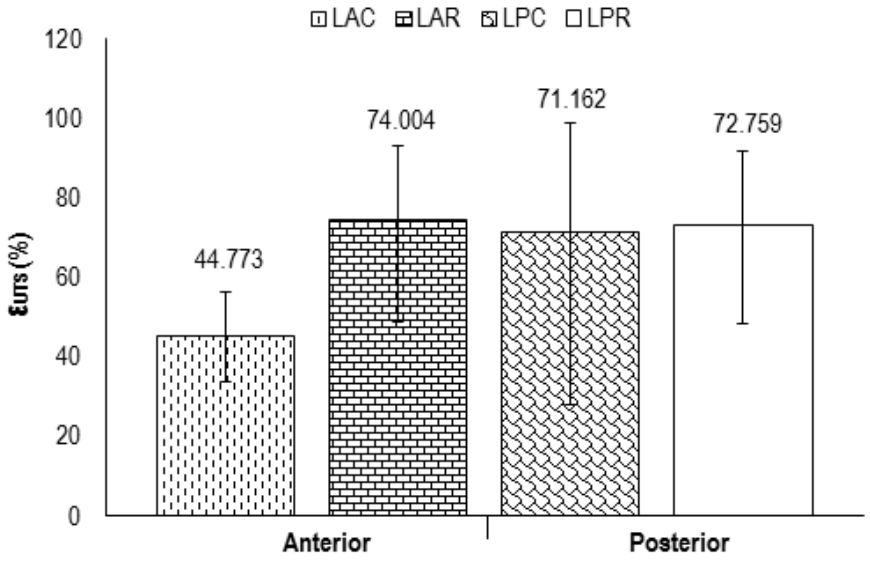

Figure 3.34: Average failure strain for the anterior leaflets tested circumferentially (LAC) and radially (LAR); the posterior leaflets tested circumferentially (LPC) and radially (LPR). Data is presented as the mean (n=6) ± 95% C.I. The data was analysed using ANOVA and calculation of the MSD which showed no significant difference between groups (p = 0.180). LAC: anterior leaflet circumferential; LAR: anterior leaflet radial; LPC: posterior leaflet circumferential; LPR: posterior leaflet radial.

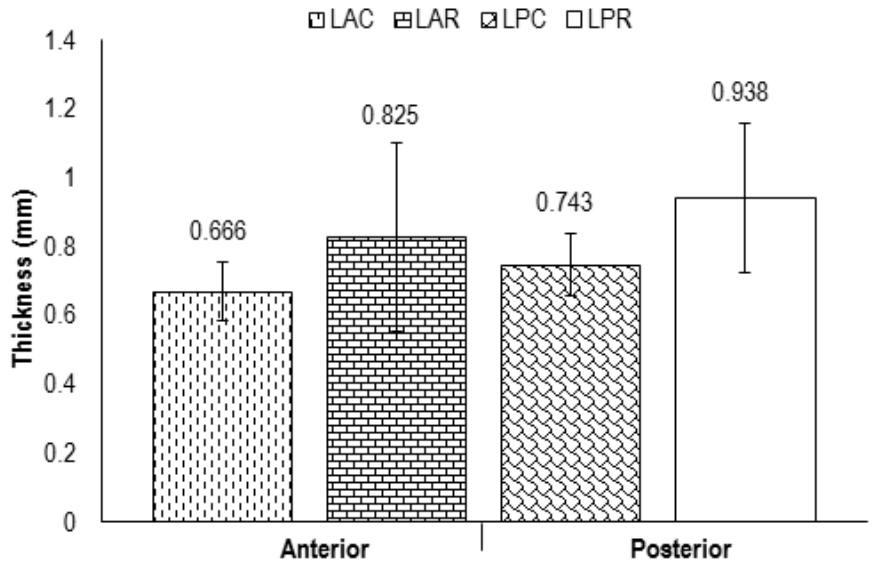

Figure 3.35: Average thickness for the anterior leaflets tested circumferentially (LAC) and radially (LAR); the posterior leaflets tested circumferentially (LPC) and radially (LPR). Data is presented as the mean (n=6) ± 95% C.I. The data was analysed using ANOVA and calculation of the MSD which showed no significant difference between groups (p = 0.080). LAC: anterior leaflet circumferential; LAR: anterior leaflet radial; LPC: posterior leaflet circumferential; LPR: posterior leaflet radial.

3.4 Discussion

This chapter presented an analysis of the biomechanical and biological properties of the native pericardium and MV leaflets. Histological examination of fresh pericardium revealed a trilaminar structure comprising the mesothelial, fibrosa and epipericardial layers, as has previously been reported in the literature (Ishihara *et al*., 1980, Bucciante, 1975). Collagen fibres appeared to be concentrated mainly in the fibrosa and epipericardial layers, as demonstrated by Masson's trichrome and Sirius red/Miller's elastin staining. Elastin was spread throughout the pericardial layers, with some fibre alignment in the fibrosa layer. Mucins and GAGs were observed through Alcian blue-PAS staining, which demonstrated neutral mucins throughout the thickness of pericardial samples, and GAGs mainly in the mesothelial layer. The biomechanical characterisation results for the pericardial specimens demonstrated an isotropic behaviour for the pericardial tissue. Similar findings have been reported for human pericardium by Lee *et al.* (1987). The values of the biomechanical parameters found in this study were comparable to those reported by Mirsadraee (2005). In particular, the values reported by Mirsadraee for the average Coll-E along and across the collagen fibre direction were 50 MPa and 35 MPa, respectively (47 MPa and 21 MPa in this study, respectively), whereas the values reported for the UTS along and across the collagen fibre direction were 9 MPa and 6 MPa, respectively (7 MPa and 4 MPa in this study, respectively). This represents a good agreement between the present and previously reported work, especially considering the fact that since the pericardium has many attachments to adjoining structures, such as the diaphragm and sternum, opening the chest could cause deformation and damage of the pericardium, modifying its biomechanical properties (Watkins and Lewinter, 1993). Braga/Vilela *et al.* (2008) have reported a collagen directionality in the pericardial sac with higher number of fibres obliquely oriented from the lower central region toward the upper left lateral region of the porcine pericardium. However, in the present study it was not possible to observe a dominant collagen directionality in the pericardial samples tested, which was also depicted on the isotropic biomechanical behaviour of the tissue. This was due to the limited size and localisation of the samples that it was possible to isolate, which were always too small to allow for a complete investigation of the whole pericardial sac.

The histological examination of the porcine MV leaflets revealed the characteristic quadrilaminar structure previously reported in the literature for both porcine and human MV leaflets (Gross and Kugel, 1931; Kunzelman *et al*., 1993a; Flanagan *et al*., 2003), comprising

the atrialis, spongiosa, fibrosa and ventricularis layers. Collagen was observed mainly in the fibrosa layer, whereas GAGs were spread particularly in the spongiosa and ventricularis. Previous studies have reported that the proteoglycan content was higher in the posterior leaflet and in the free edge of the anterior (Grande-Allen *et al.*, 2004). This particular organisation was related to the stress state of the closed valve, where the chordae and the flat region of the anterior leaflet were in tension, whereas the free edge of the anterior leaflet and most of the posterior leaflet were in appositional compression. The areas under compression require a tissue organisation able to withstand compressive forces and, therefore, the GAG content was higher in these regions since GAGs, through their hydrophilicity, are capable of withstanding compression. Elastic fibres were observed mainly in the atrialis and ventricularis. The leaflet histoarchitecture was comparable to the observed structure of the pericardium. The pericardial fibrous layer was quite comparable to the fibrosa of the leaflets, rich in densely packed collagen fibres and with sparse elastic fibres. However, the collagen fibre orientation in the pericardium was more multidirectional compared to the fibrosa of the leaflets, which was mainly aligned along the circumferential direction.

The biomechanical analysis of the porcine MV leaflets showed an anisotropic behaviour for the anterior leaflet and a rather isotropic behaviour for the posterior one. The average collagen phase slope and ultimate tensile strength of the circumferential anterior leaflet group was significantly greater than the radial anterior leaflet group and the posterior leaflet groups. Moreover, the transition stress of the circumferential anterior leaflet group was significantly higher than the radial posterior leaflet group, whereas the elastin phase slope of the radial anterior leaflet group was higher than the posterior leaflet groups. In general, the circumferential anterior leaflets group was less extensible than the other groups. The decreased extensibility of the anterior leaflet compared to the posterior one has been extensively reported in the literature. Kunzelman *et al.* (1993a) and Jensen *et al.* (2006) reported that the higher stiffness of the anterior leaflet was related to the highest stress levels during cardiac cycles. The directional anisotropy of the anterior leaflet has also been reported in the literature. May-Newman and Yin (1995) reported that the anterior leaflet was more extensible along the radial direction than along the circumferential one. Kunzelman and Cochran (1992) and Roberts (2012) observed the same directional anisotropy in the anterior leaflet.

The results reported by Roberts (2012) were similar to those reported in the present study. Specifically, the average ultimate tensile strength and failure strain values for the circumferential and radial anterior leaflet groups found in the present study were 3 MPa and 45%, and 1 MPa and 74%, respectively. These values compare well to the corresponding values of 10MPa and 50%, and 1 MPa and 60%, reported by Roberts. Similar agreement was found in the case of the ultimate tensile strength and failure strain for the posterior leaflet, with the corresponding values for the circumferential and radial groups found in the present study being 0.9 MPa and 71%, and 0.7 MPa and 73%, respectively, and the corresponding values reported by Roberts being 0.98 MPa and 77%, and 1 MPa and 40%, respectively. Several studies (Jensen, 2006; Kunzelman *et al.*, 1993a; May-Newman and Yin, 1995; Roberts, 2012) agree that the anisotropic behaviour of the anterior leaflet relates to the orientation of the collagen fibres, which are highly oriented along the circumferential direction of both MV leaflets. The histological results presented in this chapter verified this. Another reason for the biomechanical anisotropy between the radial and circumferential direction of the anterior leaflet could be related to the different thickness of the fibrosa at different regions of the anterior leaflet. Indeed, previous studies (Bucciante, 1975; Jensen *et al.*, 2006) have reported that the fibrosa (layer richest in collagen) was the thickest layer near the MV annulus, whereas the atrialis and spongiosa layers (loose connective tissue and elastin) were the thickest layer towards the free edge of the leaflets. In contrast, the histology of the posterior leaflet presented a more isotropic histoarchitecture compared to the anterior leaflet. This was also depicted in the biomechanical parameters of the posterior leaflet, which did not demonstrate any significant differences between the circumferential and radial directions. The biomechanical isotropy of the posterior leaflet found in the present study was in agreement with the results reported by Roberts (2012) and May-Newman and Yin, (1995).

In terms of the biochemical content of the tissues, no difference in the GAG and HXP content of the anterior and posterior leaflet was found. The HXP (70% for LA and 56 % for LP) and GAG (23.9 $\mu g \cdot mg^{-1}$ for LA and 24.6 $\mu g \cdot mg^{-1}$ for LP) contents of the leaflets found in the present study were similar to those reported previously for porcine and human MV leaflets (Cole *et al.*, 1984; Lis *et al.*, 1987; Grande-Allen *et al.*, 2004) (60% and 67% collagen for porcine and human, respectively; 18.9 $\mu g \cdot mg^{-1}$ GAGs). Similarly, the HXP (83.3%) and GAG (8.4 $\mu g \cdot mg^{-1}$) contents of the pericardium found in the present study were similar to those reported by Mirsadraee *et al.* (2006) for fresh human pericardium (104 $\mu g \cdot mg^{-1}$ collagen and 11 $\mu g \cdot mg^{-1}$ GAGs).

Immunohistochemical labelling was used to detect specific ECM proteins in the MV leaflets and pericardium. Positive staining for collagen I and III was shown in both the anterior and posterior leaflets, and pericardium, with particular prevalence in the fibrosa layer of the leaflets and the epipericardial layer of the pericardium. This was in agreement with previous studies, which have reported collagen III is usually co-localised with collagen I (Kuhn, 1987; Liu *et al*., 1997). The presence of the basement membrane was detected by using collagen IV and laminin staining. The basement membrane supports and facilitates the growth of epithelial cells (Brown et al., 2006). In this study, sections of anterior and posterior MV leaflets and pericardium showed specific staining for laminin and collagen IV in the atrialis and ventricularis of the leaflets, and underneath the mesothelium and in the epipericardial layer of the pericardium. Moreover, positive staining for fibronectin was observed throughout the thickness of the MV leaflet and pericardial sections, with particular prevalence in the regions close to the mesothelial layer in the pericardial samples. Chondroitin sulphate was observed in the spongiosa of both the anterior and posterior leaflets, and in the ventricularis of the radial anterior leaflet sample. Pericardial sections were stained positive for chondroitin sulphate along their mesothelial layer. Previous studies have shown the presence of chondroitin sulphate in the free edge and central region of the anterior MV leaflet providing mechanical support in these areas subjected to compression and tension (Grande-Allen *et al*., 2004).

Immunohistochemical labelling was also used to detect the type of cells and their distribution in the MV leaflets. A portion of the cells throughout the thickness of the leaflets was stained positive for α-SMA, indicating the presence of myofibroblasts or SMCs. α-SMA was also observed in the subendothelial region of the capillaries and of the atrial surface of both the anterior and posterior leaflets. The presence of SMCs in blood vessels has been previously reported in the literature (Etchevers *et al.*, 2001), whereas the presence of α-SMA in the atrialis might be related to the fact that the mechanical activity of the SMCs may offer a higher plasticity correlated to possible regulation of contraction against shear stress (Bairati and DeBiasi, 1982). Both the anterior and posterior leaflets were stained positive for vimentin throughout their thickness and around their capillaries, indicating the presence of mesenchymal cells. Positive staining for the Von Willebrand factor, which is indicative of endothelial cells (Ruggieri and Ware, 1993), was observed in both the anterior and posterior leaflets, localised in the endothelium of the capillaries and of the atrial and ventricular surfaces of the leaflets.

3.5 Conclusions

In this Chapter a detailed histological, immunohistochemical, biochemical and mechanical characterisation of porcine MV leaflets and porcine pericardium was presented. Histological examination showed the typical tri- and quadrilaminar structure of fresh pericardium and MV leaflets, respectively. The composition of the fibrosa layer was comparable between the two tissues. Immunohistochemical labelling allowed the localisation of specific proteins in the porcine MV leaflets and pericardium. Biochemical analysis showed that the MV leaflets and the fresh pericardium had HXP and GAG contents similar to those reported in the literature. Fresh pericardium demonstrated rather isotropic behaviours along the two directions studied; whereas anterior leaflet samples were more anisotropic. In particular, anterior leaflet specimens cut circumferentially were stiffer than those cut radially and the posterior leaflets.

After the characterisation of fresh pericardial tissue, decellularisation procedure was performed and assessed for effectiveness of decellularisation and maintenance of the biological and mechanical properties of tissue.

Chapter 4

Decellularisation of porcine pericardium

4.1 Introduction

This chapter describes the procedure followed for the production of the acellular porcine pericardial scaffolds, as well as their quality assessment. Decellularised porcine pericardium was used in this project for research into the development of cell-seeded and unseeded mitral valve (MV) leaflet replacements. Tissue decellularisation should not impair the integrity of the ECM proteins of the tissue and should not leave any cells or cell fragments in the scaffold that could compromise its biocompatibility. Cells and cell remnants that may still be present after decellularisation are immunologically active and might potentially carry diseases (Dohmen and Konertz, 2009). However, it has been reported that DNA remnants of less than 300 bp are acceptable since they would most likely be degraded via enzymatic breakdown after implantation (Bennett *et al*., 1985; McCoy *et al*., 2004; Gilbert *et al*., 2007; Gilbert *et al*., 2009). Xenogeneic scaffolds carry a risk of causing an immunogenic reaction, and xenogeneic disease transmission, such as the porcine endogeneous retrovirus (PERV) (Weiss, 1998; Wilson et al., 1998). However, previous studies have shown that with a maximum 2% residual DNA still present in the scaffold there was no risk of PERV transmission to another species (Leyh *et al*., 2003). In addition, xenogeneic scaffolds are readily available and this makes them more attractive than allogeneic scaffolds.

In humans, the immunogenic reaction upon implantation of xenogeneic tissues is initiated by the galalpha1-3Galbeta1-(3)4GlcNAc-R (α–gal) epitope. α–gal has been reported to cause a hyper-acute immune reaction, which is mediated by pre-formed anti-α–gal antibodies. The pericardial scaffolds researched in the present study were decellularised according to an in-house patented protocol. This protocol has been used to develop a vascular patch, which is now marketed in Europe (Tissue Regenix Group plc). As such, the particular protocol has previously undergone extensive assessment, and it has been shown to effectively remove the α-gal epitope from porcine tissues (Stapleton *et al*., 2008), as well as retaining ECM proteins which play an important role in cell attachment, such as fibronectin and laminins, despite causing a loss of collagen IV (Mirsadraee *et al*., 2007). Hence, α-gal detection as well as

immunohistochemical staining of ECM proteins was not repeated in the present study for the assessment of the pericardial scaffolds. Another important issue with decellularised scaffolds is their potential cytotoxicity, which can be caused by residuals of the reagents used in the decellularisation, and can generate adverse effects after implantation.

The decellularisation protocol used in the present study for the decellularisation of pericardium utilised sodium-dodecyl-sulphate (SDS) at a concentration of 0.1 % w/v in the presence of proteinase inhibitors. SDS is an ionic detergent, which has been shown to effectively remove the cellular components from human pericardium, porcine heart valves, human amniotic membrane and tendons (Booth *et al*., 2002; Grauss *et al*., 2005; Wilcox *et al*., 2005; Mirsadraee *et al*., 2006; Wilshaw *et al*., 2006). However, it has also been associated with loss of GAGs and growth factors (Courtman *et al*., 1994; Kasimir *et al*., 2003; Reing *et al*., 2010), as well as with protein denaturation, by disrupting protein-protein interactions, when used at high concentrations (Gilbert *et al*., 2006). The protocol also employed nucleases (RNAse, DNAse). Endonucleases catalyse the hydrolysis of the interior bonds of the ribonucleotide and deoxyribonucleotide chains, whereas exonucleases catalyse the hydrolysis of the terminal bonds of deoxyribonucleotide and ribonucleotide chains, leading to the degradation of RNA or DNA (Freyman, 2005). EDTA was included in the initial wash buffers. EDTA is a chelating agent, which can bind the bivalent cations Ca^{2+} and Mg^{2+}, necessary for cell attachment, and as such it facilitates in the removal of the cellular material from the tissue (Klebe, 1974; Klebe, 1975; Gailit and Ruoslahti, 1988; Moore *et al*., 1994). It is also an inhibitor of metalloproteinases.

Cell lysis in the decellularisation protocol used in the present study, was facilitated through treatment with a hypotonic solution, which lysed the cells through osmotic shock (Martins-Green and Bissell, 1995; Vyavahare *et al*., 1997; Goissis *et al*., 2000; Dahl *et al*., 2003; Woods and Gratzer, 2005). However, the hypotonic solution alone was not sufficient to remove the cellular debris, this was facilitated by additional nuclease and chemical treatments (Dahl *et al*., 2003). During cell lysis, various proteases are released from the disrupted cells, which have the potential to cause ECM damage. This can be avoided by protease inhibitors, such as aprotinin or leupeptin. In addition, many proteases can be inhibited by controlling the temperature and pH of, and the exposure time of the tissues to the solutions used during decellularisation. The decellularisation protocol used in this study, utilised aprotinin and EDTA at pH 7-8 in order to avoid the proteolysis of the ECM proteins (Gilbert *et al*., 2006). Moreover,

the present study utilised peracetic acid (PAA) to sterilise the pericardial scaffolds. Previous studies have reported the use of peracetic acid (PAA) to both remove cellular fragments and provide sterilisation and disinfection. It has also been reported that following treatment with PAA, several types of collagen (I, III, IV, V, VI, and VII) were still identified within porcine tissue, such as small intestinal submucosa and urinary bladder (Badylak *et al*., 1995; Brown *et al*., 2006). In addition, many of the ECM GAGs (hyaluronic acid, heparin, heparin sulphate, chondroitin sulphate A, dermatan sulphate), as well as laminin and fibronectin were also retained following PAA treatment (Hodde *et al*., 1996, 2002; Brown *et al*., 2006). PAA has also been shown not to have any adverse effect on the mechanical behaviour of decellularised scaffolds (Freytes *et al*., 2004).

4.1.1 Aims and objectives

Aims:

The aim of the work present in this chapter was to adapt the in-house protocol to effectively decellularise porcine pericardium, and to assess the decellularised scaffolds.

Objectives:

- To produce batches of decellularised porcine pericardium using an established method
- To determine the extent of decellularisation using histology and DNA assays
- To determine the effects of the decellularisation on:
    - Histoarchitecture of the scaffold
    - Biocompatibility of the scaffold
    - Total collagen and glycosaminoglycan content
    - Biomechanical properties

4.2 Materials and methods

4.2.1 Decellularisation

This method was developed by Fisher *et al.* (2008).

4.2.1.1 Solutions used in the decellularisation protocol

Wash buffer I with EDTA (2.7 mM; 0.1%) and aprotinin (10 KIU·ml^{-1})

EDTA (1 g) was added to 1 L of PBS. The pH was adjusted to 7.2-7.4 by adding 6 M hydrochloric acid or 6 M sodium hydroxide while stirring. The solution was autoclaved at 121°C for 20 min and stored at room temperature for up to one month. Aprotinin (1 ml, 10,000 KIU·ml^{-1}) was added aseptically to the solution just before use. The solution with added aprotinin was then stored at 4-5°C for up to 1 week.

Wash buffer II with aprotinin (10 KIU·ml^{-1})

Aprotinin (1 ml, 10,000 KIU·ml^{-1}) was added aseptically to 1 L of PBS just before use; solution with added aprotinin was stored at 4 - 5°C for up to 1 week.

Disinfection solution

Disinfection solution was made up by supplementing 100 ml of PBS with 0.5 mg·ml^{-1} of gentamicin, 0.2 mg·ml^{-1} of polymyxin B and 0.5 mg·ml^{-1} of vancomycin hydrochloride. The pH was adjusted to 7.2 - 7.4, and the solution was sterilised by filtration using a 0.2 µm pore size filter into a sterile container. The volume was finally made up to 500 ml with sterile PBS.

Hypotonic buffer plus EDTA (2.7 mM) and aprotinin (10 KIU·ml^{-1})

Trizma base (1.21 g) and EDTA (1 g) were dissolved in 900 ml of distilled water. The pH was adjusted to 8.0 – 8.2 and the volume made up to 1 L. The solution was autoclaved at 121°C for 20 min and stored at room temperature for up to one month. Aprotinin (1 ml, 10,000 KIU·ml^{-1}) was added aseptically just before use.

SDS (0.1% w/v) in hypotonic buffer

SDS (0.1% w/v) stock solution was prepared by adding 10 g of SDS to 100 ml distilled water. The solution was sterilised by filtration and stored for up to one month at room temperature. SDS stock solution (5 ml) was then added aseptically to 495 ml of autoclaved hypotonic buffer. The solution was stored for up to one week at 4 - 5°C.

Nuclease solution with DNAse (50 U·ml^{-1}) and RNAse (1 U·ml^{-1})

Deoxyribonuclease I (DNAse) was rehydrated to a final concentration of 10,000 U·ml^{-1} (according to the manufacturer's instructions) using DNAse reconstitution buffer. Ribonuclease I (RNAse) was rehydrated to a final concentration of 100 U·ml^{-1} (according to

the manufacturer's instructions) using distilled water. Both the DNAse and RNAse solutions were filter sterilised. Aliquots (5 ml) were made in bijous and stored at -20°C for up to three months.

Trizma base (6.1 g) and magnesium chloride (2.0 g) were dissolved in 80 ml of distilled water. The pH was adjusted to 7.5 - 7.7 and the volume was made up to 990 ml with distilled water. The solution was autoclaved at 121°C for 20 min and stored at room temperature for up to one month. On the day of use, 10 ml of RNAse stock and 5 ml of DNAse stock were added to the solution, which was then used within 10 min.

Hypertonic buffer with Tris (50 mM) and sodium chloride (1.5 M)

Sodium chloride (87.66 g) and Tris (6.06 g) were added to 900 ml of distilled water. The pH was adjusted to 7.5 - 7.7. The volume was then made up to 1000 ml with distilled water. The solution was autoclaved at 121°C for 20 min and stored at room temperature for up to one month.

Peracetic acid solution (0.1 % v/v)

Peracetic acid (1.57 ml) was added to a 500 ml of autoclaved PBS. The pH was adjusted to 7.3 and the solution was used within one hour of preparation.

4.2.1.2 Procedure

Fresh porcine pericardia were dissected, as described in Chapter 2, Section 2.8, and a sample measuring 9 cm × 6 cm was isolated from each pericardium. The sample size was sufficient to carry out all necessary post-decellularisation assessment. Each sample was cut crosswise at one of the edges, as shown in Figure 4.1, to identify the mesothelial and epipericardial surfaces. Following isolation, the samples were stored in moist filter paper at -20C° for subsequent use.

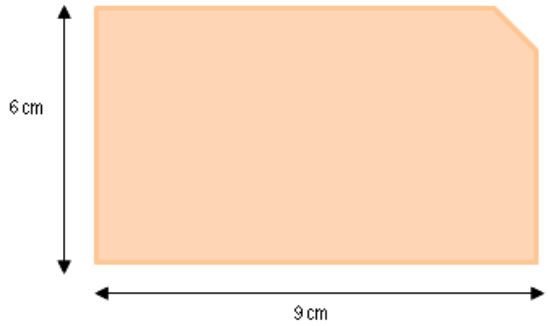

Figure 4.1: Size and shape of the decellularised pericardial sample showing the mesothelial surface.

Prior to decellularisation, the frozen pericardial samples were placed in a pot, with enough wash buffer II to cover the whole surface of the sample, and thawed for 15 to 30 min at 37°C in an incubator. The samples were then cleaned with forceps to remove as much of the fat as possible. After cleaning, the samples were incubated in disinfection solution (1 ml·cm^{-2}) with agitation at 100 rpm (Grant bio shaker) for 30 min at 37°C. They were then washed in wash buffer I (4 ml·cm^{-2}) for 3 periods of 30 min each with agitation at 100 rpm on a plate shaker, at room temperature. Subsequently, the samples were incubated overnight at 4 - 5°C in hypotonic buffer (2 ml·cm^{-2}) with agitation at 100 rpm, before they were incubated in SDS in hypotonic buffer (2 ml·cm^{-2}) at room temperature for 24 h with agitation at 100 rpm. The samples were then washed in wash buffer II (4 ml·cm^{-2}) for 3 periods of 30 min each with agitation at 100 rpm on a plate shaker and at room temperature. The samples were then incubated in nuclease solution (2 ml·cm^{-2}) for 3 h at 37°C with agitation at 50 rpm. Following this, the samples were washed in wash buffer I (4ml·cm^{-2}) for 3 periods of 30 min each with agitation at 100 rpm on a plate shaker, and at room temperature. They were then incubated in hypertonic buffer (2 ml·cm^{-2}) overnight at 37°C with agitation at 100 rpm. The samples were then washed in wash buffer II (4 ml·cm^{-2}) for 3 periods of 30 min each with agitation at 100 rpm on a plate shaker, and at room temperature. Tissues were then incubated in peracetic acid solution (2 ml·cm^{-2}) for 3 h at room temperature with agitation at 150 rpm. Finally, the samples were washed in wash buffer II (4 ml·cm^{-2}) for 3 periods of 30 min each with agitation at 100rpm on a plate shaker, and at room temperature prior of being stored in wash buffer II (2 ml·cm^{-2}) at 4°C for up to 3 months. The process is summarised in Figure 4.2.

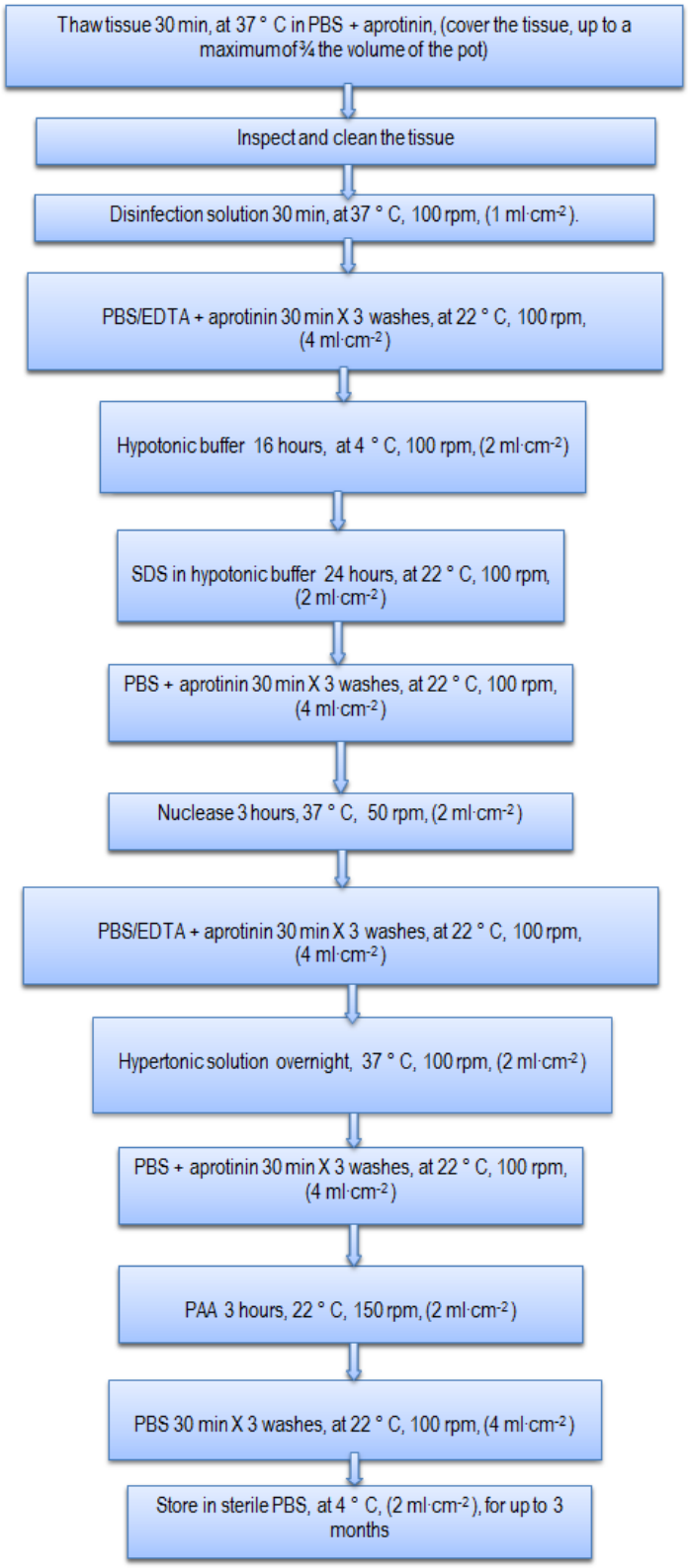

Figure 4.2: Process flow diagram of decellularisation method.

4.2.2 Characterisation of decellularised pericardium

The materials and methods used for the histological, biochemical, microscopical (SEM and ESEM) and biomechanical evaluation of the decellularised pericardia have been described in Chapter 2. The biocompatibility of the scaffolds was evaluated through contact and extract cytotoxicity assays, and their sterility using both nutrient broths and agar plates. The effectiveness of decellularisation was determined in terms of DNA removal through DNA assay. A sample size of n= 6 was used for the biochemical, biomechanical, cytotoxicity and assessment of the DNA content of the scaffolds.

4.2.2.1 Contact cytotoxicity assay

Decellularised pericardial samples (n = 6) of a 5 mm^2 area were attached to a 6-well culture plate using 10 µl collagen solution prepared from rat tails by Dr Andrew Aldridge, neutralised and gelled with 5 µl sodium hydroxide (0.1 M) in a 2:1 ratio. Collagen solution (20 µl), neutralised and gelled with 10 µl of sodium hydroxide, was placed into one of the wells as a negative control, whereas a drop of cyanoacrylate contact adhesive was placed into the centre of a second well as a positive control. Prior to cell seeding, all wells were washed three times with PBS for 10 min each. Cell suspension (2 ml) of porcine dermal fibroblasts at passage 5 (P5, cultured as described in Chapter 2, Section 2.17), was added into each well at a concentration of 3×10^5 cells·ml^{-1} of complete cell culture medium (Chapter 2, Section 2.5.4). The seeded samples were cultured for 48 hours at 37 °C in 5 % (v/v) CO_2 in air and then observed and photographed under phase contrast light microscopy. The medium was then aspirated and the wells were washed gently using PBS containing Ca^{+2} and Mg^{+2}. The cells were then fixed using 10 % (w/v) NBF for 10 min. Subsequently, the NBF was aspirated and the cells were stained using Giemsa solution for 5 min. The wells were rinsed with tap water until the water run clear and the plate was allowed to air dry. Finally, the samples were photographed again under light microscopy. The assay was repeated with pMSCs at P5 (cultured as described in Chapter 2, Section 2.17).

4.2.2.2 Extract cytotoxicity assay

Reagents

Culture medium containing double strength FBS: DMEM supplemented with 20% (v/v) FBS, 200 U·ml^{-1} penicillin, 200 U·ml^{-1} streptomycin, and 4 mM L-glutamine. The medium was stored for up to 2 weeks at 4°C.

Method

Soluble extracts were prepared using decellularised pericardial samples (n = 6). DMEM with 80% (v/v) DMSO was used as positive (cytotoxic) control and cell culture medium (Section 2.5.4) was used as negative control. The samples were finely minced with a scalpel and incubated in DMEM (1 ml per 100 mg tissue weight) for 72 h at 37°C with agitation. The samples were then centrifuged at 19,000 g for 15 min and the supernatants were collected, checked for sterility by plating 100 µl onto agar plates (nutrient agar, fresh blood agar and Sabouraud), and stored at -20°C for up to one month until required. Porcine dermal fibroblasts at P6 (cultured as described in Chapter 2, Section 2.17) were seeded at a density of 1×10^4 cells per well of a 96 wells plate and cultured for 24 h at 37 °C in 5 % (v/v) CO_2 in air in order to achieve 80 % confluence after 48 hours. The previously produced extracts were thawed at 37°C and centrifuged at 19,000 g for 15 min. The culture medium was then aspirated and replaced with 100 µl of culture medium containing double strength FBS. The tissue extracts, and the positive and negative controls, were added in replicates of 6 to wells of the 96-well plate with the fibroblasts, and the cells were cultured for a further 48 h under standard conditions. Subsequently, the adenosine triphosphate (ATP) content of the cells was determined using the ATPLite-M assay (Perkin Elmer) following the manufacturer's instructions. Prior to carrying out the ATPLite-M assay, the reagents were equilibrated to room temperature after incubation and the vial of lyophilised substrate solution was reconstituted by adding 25 ml of substrate buffer. The original cell culture medium was then aspirated from each well and 50 µl of culture medium was added. Mammalian cell lysis solution (50 µl) was added to each well and shaken at 500 rpm for 5 min. Following this, 50 µl of substrate solution was added to each well and shaken at 500 rpm for 5 min. The luminescence was measured using a Top Count NXT; data were recorded in counts per second and plotted using Microsoft Excel or GraphPad Prism.

4.2.2.3 DNA quantification

The DNA content of fresh (n = 6) and decellularised (n = 6) pericardial samples (25 mg and 250 mg of wet tissue, respectively) was isolated using the DNeasy kit (Qiagen, DNeasy Blood & Tissue Kit), according to the manufacturer's instructions. Each sample was macerated using a scalpel blade and placed in a sterile 1.5 ml microcentrifuge tube. Buffer ATL (180 µl for fresh and 360 µl for decellularised pericardium) and proteinase K (20 µl for fresh and 40 µl for decellularised pericardium) was added to the macerated tissue, mixed by vortexing, and

incubated at 56°C for 3 h or until the tissue was completely digested. During the 3 h incubation, the samples were vortexed every 30 min to enhance dispersion. Following this, each sample was vortexed again for 15 s. Buffer AL (200 µl for fresh and 400 µl for decellularised pericardium) was added to each sample, and mixed thoroughly by vortexing; then ethanol (100 %, v/v) was added (200 µl for fresh and 400 µl for decellularised pericardium), and mixed thoroughly by vortexing.

Each sample was then transferred to a separate DNeasy Mini spin column in a 2 ml collection tube, and centrifuged at 6,000 g for 1 min. The flow-through was discarded together with the collection tube. The DNeasy Mini spin column was placed in a new 2 ml collection tube and 500 µl Buffer AW1 was added, and centrifuged for 1 min at 16,000 g. The flow-through was discarded together with the collection tube. The DNeasy Mini spin column was placed in a new 2 ml collection tube. Buffer AW2 was added (500 µl) and centrifuged for 3 min at 20,000 g to dry the DNeasy membrane. Drying the membrane of the DNeasy Mini spin column was important, since residual ethanol might interfere with subsequent reactions. The flow-through was discarded again together with the collection tube. The DNeasy Mini spin column was then placed in a clean 1.5 ml or 2 ml microcentrifuge tube, and 200 µl Buffer AE was pipetted directly onto the DNeasy membrane. The samples were then incubated at room temperature for 1 min, and then centrifuged for 1 min at 6000 g to elute the DNA. The elution process was repeated twice for maximum DNA yield. The extracted DNA was either subjected to quantification immediately, or stored at –20 °C until required. The final concentration of DNA was quantified using a Nanodrop spectrophotometer (ND-1000 V3.71). Buffer AE (2 µl) was used as a blank. The extracted DNA sample (2 µl) was loaded onto the Nanodrop and the absorbance was determined at 260 nm. Three readings were taken for each sample, and the mean was considered as the sample absorbance. The DNA concentration ($ng \cdot \mu l^{-1}$) in the sample was used to calculate the DNA weight/tissue weight ($\mu g \cdot mg^{-1}$) according to:

$$\text{DNA weight/tissue weight } (\text{ng} \cdot mg^{-1}) = \frac{\text{DNAc} \times 400}{\text{w}}$$

where DNAc represented the DNA concentration in the Buffer AE ($ng \cdot \mu l^{-1}$) and w the total weight of the sample. The volume of the Buffer AE containing extracted DNA was 400 µl (twice elution). The total weight for each sample was 25 mg for fresh and 250 mg for decellularised pericardium. The mean ± 95 % C.I. of the DNA weight/tissue weight ($ng \cdot mg^{-1}$) for each of the fresh and decellularised groups was calculated.

4.2.2.4 Sterility assessment

Reagents

The reagents used in the sterility assessment included:

- Nutrient broth, which was used to detect aerobic bacterial contamination.
- Thioglycolate broth: 29 g of thioglycolate broth was dissolved in 1 L of distilled water, which was then aliquotted in glass universals (10 ml each). The solution was autoclaved at 121°C for 20 min prior to use. The thioglycolate broth is an enriched isolation mediuim used primarily to differentiate various organisms in terms of oxygen requirements. The oxygen level throughout the broth was reduced via reaction with sodium thioglycolate. This broth was used for the detection of anaerobic bacterial contamination.
- Agar plates, inlcuding nutrient agar (NA), fresh blood agar (FBA) and Sabouraud agar (SAB). These were used for the detection of aerobic bacterial contamination.

Method

A 5 mm^2 sample was dissected from each one of the 6 decellularised pericardial patches. The samples were minced and put separately in nutrient broths and kept at 37°C for up to 21 days to assess aerobic bacteria growth. The nutrient broth was used for the cultivation of less fastidious microorganisms. The sterility was checked after 2, 7 and 21 days.

A sample from each one of the 6 decellularised pericardial patches was minced and put separately in thioglycolate broth, and kept at 37°C for 72 h. After incubation, the solution of each sample was spread aseptically onto an individual fresh blood agar plate and left in an anaerobic incubator (AnaeroGenTM, OXOID, 3.5 l) at 37°C for up to 15 days.

The sterility of the liquid in which the tissues were stored was also tested using different agar plates. A volume of 100 µl was plated on the agar plates. Specifically, NA was used for the detection of non-fastidious micro-organisms, FBA was used for the detection of fastidious micro-organisms, and SAB was used for the detection of fungal growth, since it has had a low pH that inhibited the growth of most bacteria. The plates were kept for up to 21 days at 37°C, with the exception of the SAB plates, which were kept at 30°C. Sterility was checked after 2, 7 and 21 days.

4.3 Results

4.3.1 Histioarchitecture of decellularised pericardium

Following decellularisation, pericardial scaffold sections were cut parallel and orthogonally to the collagen fibre alignment, and stained with H & E, Sirius red/Miller's elastin, Masson trichrome and Alcian blue-PAS. Histological analysis of the sample sections did not reveal any remaining cells (Fig. 4.3a, c, e - h). Following decellularisation, the pericardium appeared swollen and there were gaps in the ECM at the locations where cells used to reside; this was obvious in all the images. The histoarchitecture of the collagen and elastin fibres was preserved (Fig. 4.3b, d, e and g), and a weak GAG presence could still be observed in the outer layers of the decellularised pericardium, on the mesothelial surface (Fig. 4.3f).

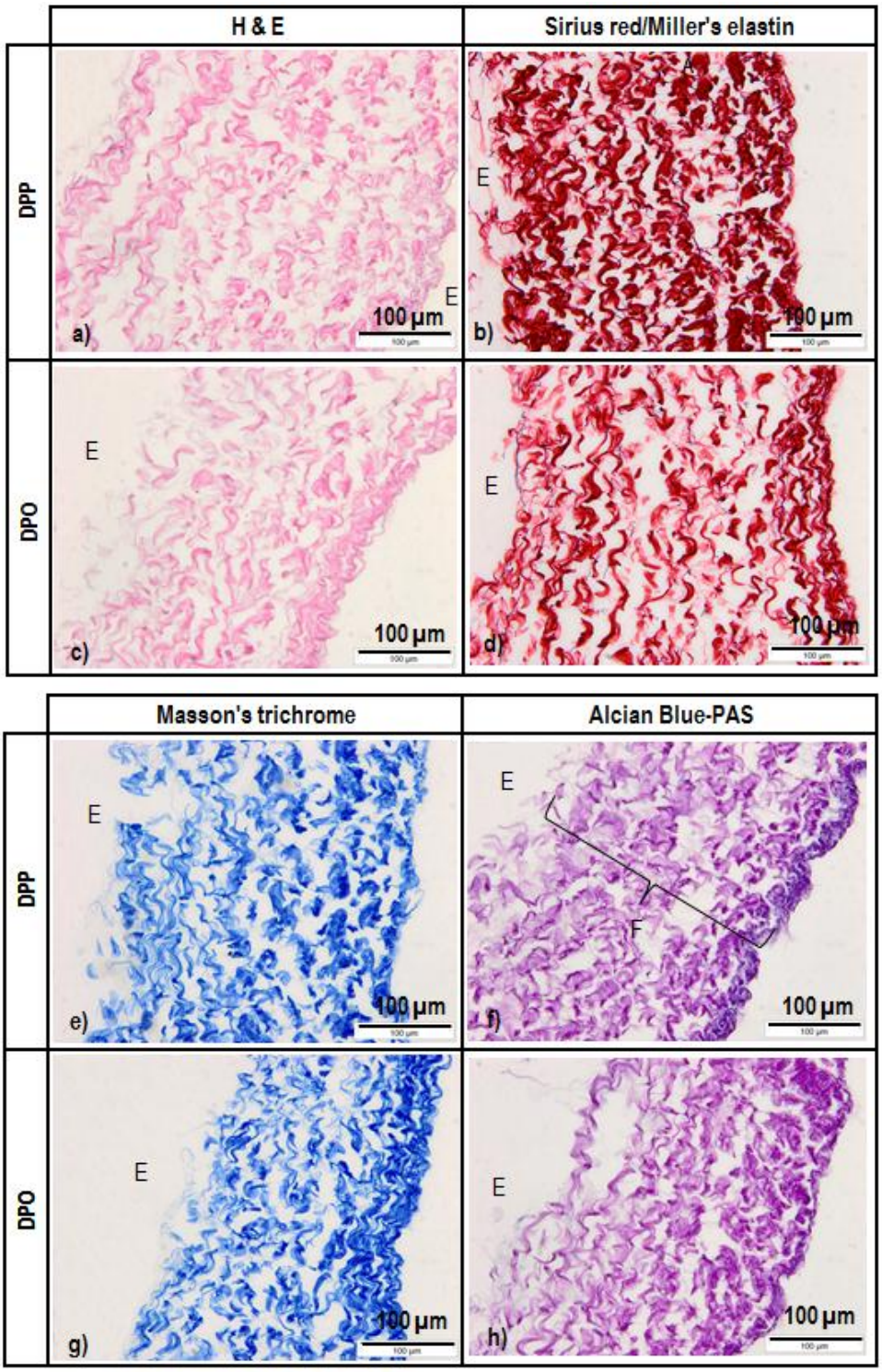

Figure 4.3: Histology of decellularised pericardial scaffolds isolated parallel (DPP) and orthogonally (DPO). Sections were stained with H&E (a, c), Sirius red/Miller's elastin (b, d), Masson's trichrome (e, g) and Alcian blue-PAS (f, h). E: epipericardial surface; F: fibrosa layer. Scale bars indicate 100 µm.

4.3.2 Collagen, denatured collagen and GAG content of native and decellularised pericardium

The results presented in Chapter 3 with regards to the validation of the hydrolysis technique, demonstrated that there was a statistically significant difference in the hydroxyproline (HXP) amount between 2 h and 6 h and between 4 h and 6 h hydrolysis within the anterior leaflet group. Thus, the 6 h time point was used in the present study for the hydrolysis of all tissues.

The HXP content per dry weight of decellularised pericardium (115.954 ± 18.3 μg·mg^{-1}) was significantly higher compared to the HXP content per dry weight of fresh pericardium (83.252 ± 7.4 μg·mg^{-1}) ($p = 0.009$; Figure 4.4). The HXP content of denatured collagen per dry weight of fresh and decellularised pericardium was 2.845 ± 1.4 μg·mg^{-1} and 1.531 ± 1.7 μg·mg^{-1}, respectively. There was no significant difference in the denatured HXP content between fresh and decellularised pericardium ($p = 0.262$; Figure 4.4). The GAG content per dry weight of fresh pericardium (8.425 ± 2.6 μg·mg^{-1}) was significantly higher than that of the decellularised pericardium (0.134 ± 0.07 μg·mg^{-1}) ($p = 0.000$; Figure 4.4).

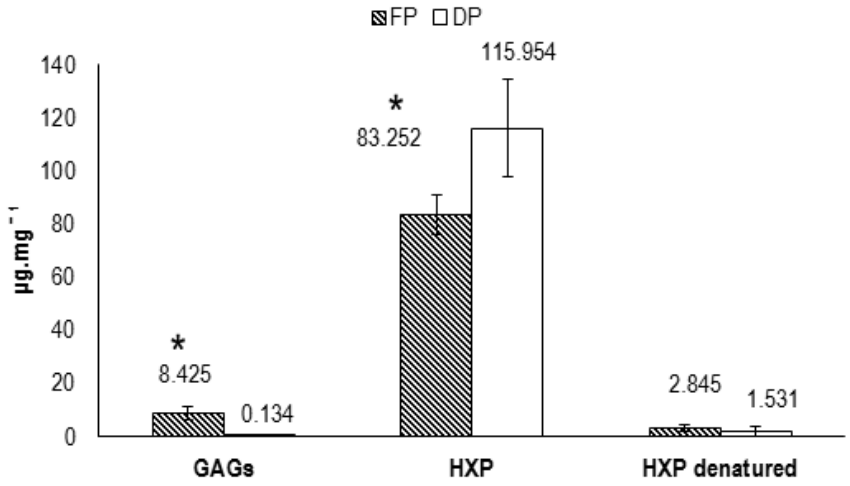

Figure 4.4: HXP, HXP of denatured collagen (HXP denatured) and GAG content per dry weight of fresh (FP) and decellularised (DP) pericardium. Data is presented as the mean (n=6) ± 95% C.I. The final percentage of collagen content was 58.3% for FP and 81.3% for DP. The final percentage of collagen was calculated as the HXP amount converted in mg·mg^{-1} and multiplied by 7 (as 1/7 of 1mg of collagen is HXP). Asterisks indicate significant difference, as determined by unpaired student`s t-test ($p = 0.009$ for HXP; $p = 0.262$ for HXP denatured and $p = 0.000$ for GAGs).

4.3.3 Biomechanical properties of native and decellularised pericardium

The calculated biomechanical parameters for the fresh and decellularised pericardial groups are illustrated in Figures 4.5 through to 4.11. In general, no significant differences were found in any of the biomechanical parameters studied ($p > 0.05$), except in the case of the transition stress and strain, and thickness ($p < 0.05$; Fig. 4.5 - 4.11).

The results demonstrated that decellularisation had an effect on the transition stress ($p < 0.05$; MSD = 0.399, Fig. 4.7), with the orthogonal decellularised pericardial group demonstrating a significantly higher transition stress compared to the parallel and orthogonal fresh pericardial groups. Further significant differences were found in the average transition strain, with the orthogonal fresh pericardial group achieving significantly lower values than the parallel decellularised group ($p < 0.05$; MSD = 21.954; Fig. 4.8). The average thickness of the orthogonal fresh pericardial group was significantly higher than that of the parallel fresh and orthogonal decellularised pericardial groups ($p < 0.05$; MSD = 0.021; Fig. 4.11).

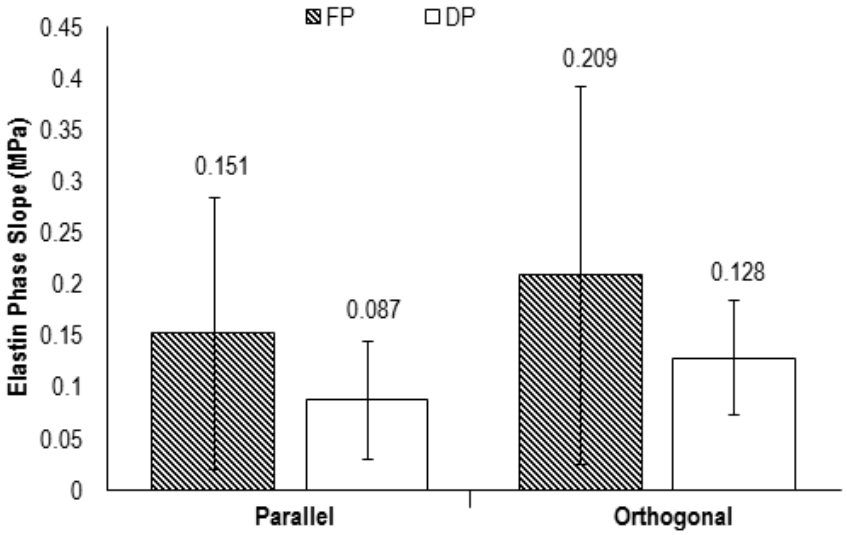

Figure 4.5: Average elastin phase slope for fresh (FP) and decellularised (DP) pericardium tested parallel and orthogonally to the collagen fibre direction (n = 6). Error bars indicate 95% C.I. The data was analysed using ANOVA which showed no significant variation in the data ($p = 0.3417$).

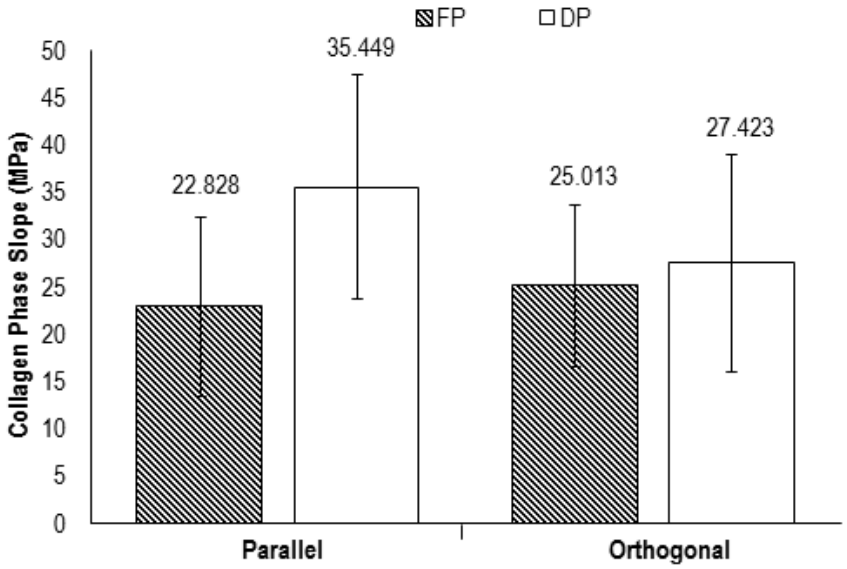

Figure 4.6: Average collagen phase slope for fresh (FP) and decellularised (DP) pericardium tested parallel and orthogonally to the collagen fibre direction (n = 6). Error bars indicate 95% C.I. The data was analysed using ANOVA, which showed no significant variation in the data ($p = 0.1725$).

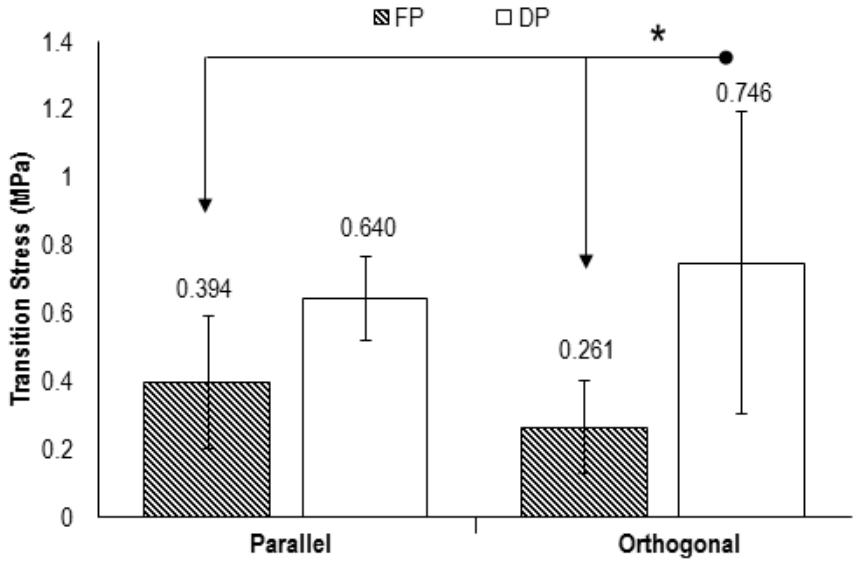

Figure 4.7: Average transition stress for fresh (FP) and decellularised (DP) pericardium tested parallel and orthogonally to the collagen fibre direction (n = 6). Error bars indicate 95% C.I. Asterisk and connectors indicate significant difference between originator and end arrow column, determined by ANOVA and MSD. Significant difference was observed between the orthogonal DP and both the parallel and orthogonal FP groups ($p < 0.05$; MSD = 0.399).

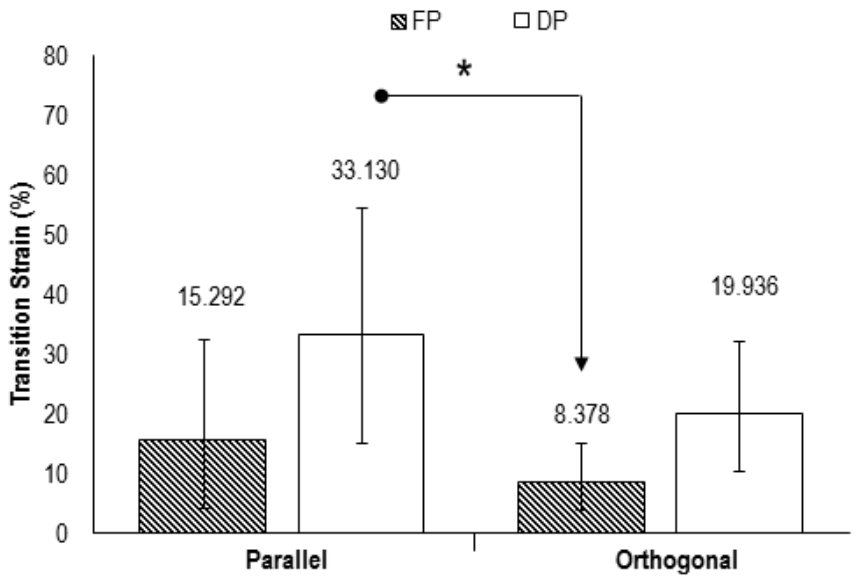

Figure 4.8: Average transition strain for fresh (FP) and decellularised (DP) pericardium tested parallel and orthogonally to the collagen fibre direction (n = 6). Error bars indicate 95% C.I. Asterisk and connectors indicate significant difference between originator and end arrow column, determined by ANOVA and MSD. Difference was observed between the parallel DP and orthogonal FP group ($p < 0.05$; MSD = 21.954).

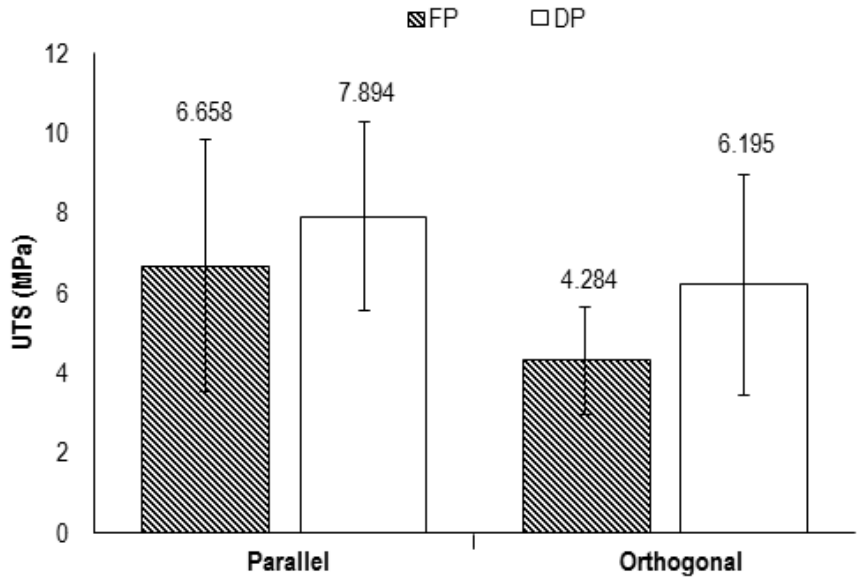

Figure 4.9: Average ultimate tensile strength (UTS) for fresh (FP) and decellularised (DP) pericardium tested parallel and orthogonally to the collagen fibre direction (n = 6). Error bars indicate 95% C.I. Data was analysed using ANOVA which showed no significant variation in the data ($p = 0.0997$).

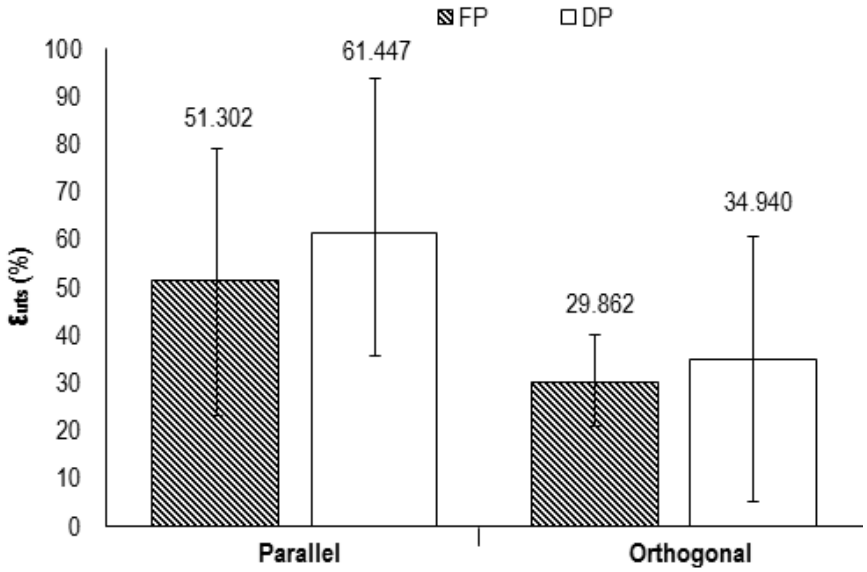

Figure 4.10: Average failure strain (ε_{uts}) for fresh (FP) and decellularised (DP) pericardium tested parallel and orthogonally to the collagen fibre direction (n = 6). Error bars indicate 95% C.I. The data was analysed using ANOVA, which showed no significant variation in the data ($p = 0.1268$).

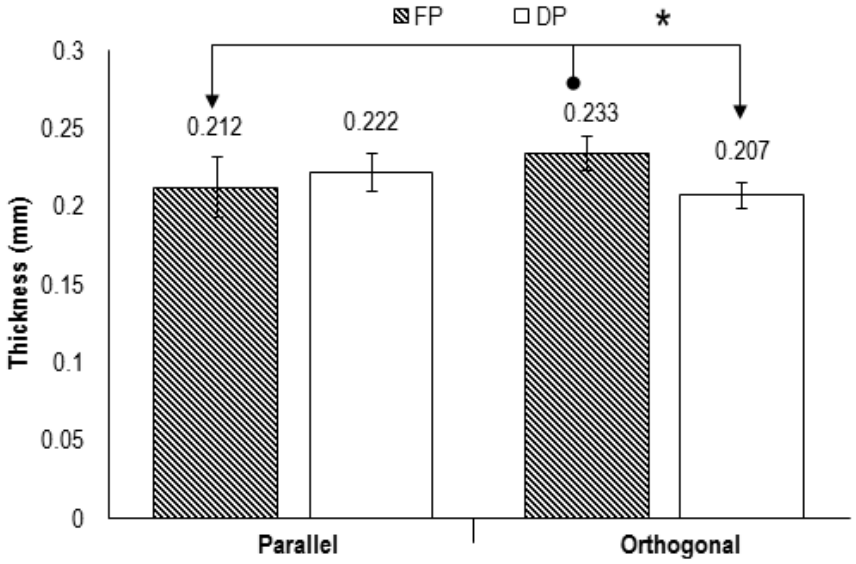

Figure 4.11: Average thickness for fresh (FP) and decellularised (DP) pericardium tested parallel and orthogonally to the collagen fibre direction (n = 6). Error bars indicate 95% C.I. Asterisk and connectors indicate significant difference between originator and end arrow column, determined by ANOVA and MSD. Significant difference was observed between the orthogonal FP and both the orthogonal DP and parallel FP groups ($p < 0.05$; MSD = 0.021).

4.3.4 Contact biocompatibility of decellularised pericardium

Microscopic analysis of the contact cytotoxicity plates showed that both the porcine fibroblasts and MSCs attached and grew well into contact with the decellularised pericardium, with no evidence of contact inhibition (Fig. 4.12a, d; Fig. 4.13a, d). No changes in cell morphology were observed next to the decellularised pericardium or the collagen gel (negative control) (Fig. 4.12a, b, d and e; Fig. 4.13a, b, d and e). This provided evidence that the decellularised pericardial scaffold was not cytotoxic, whereas the cyanoacrylate glue (positive control) was clearly cytotoxic (Fig. 4.12c, f; Fig. 4.13c, f).

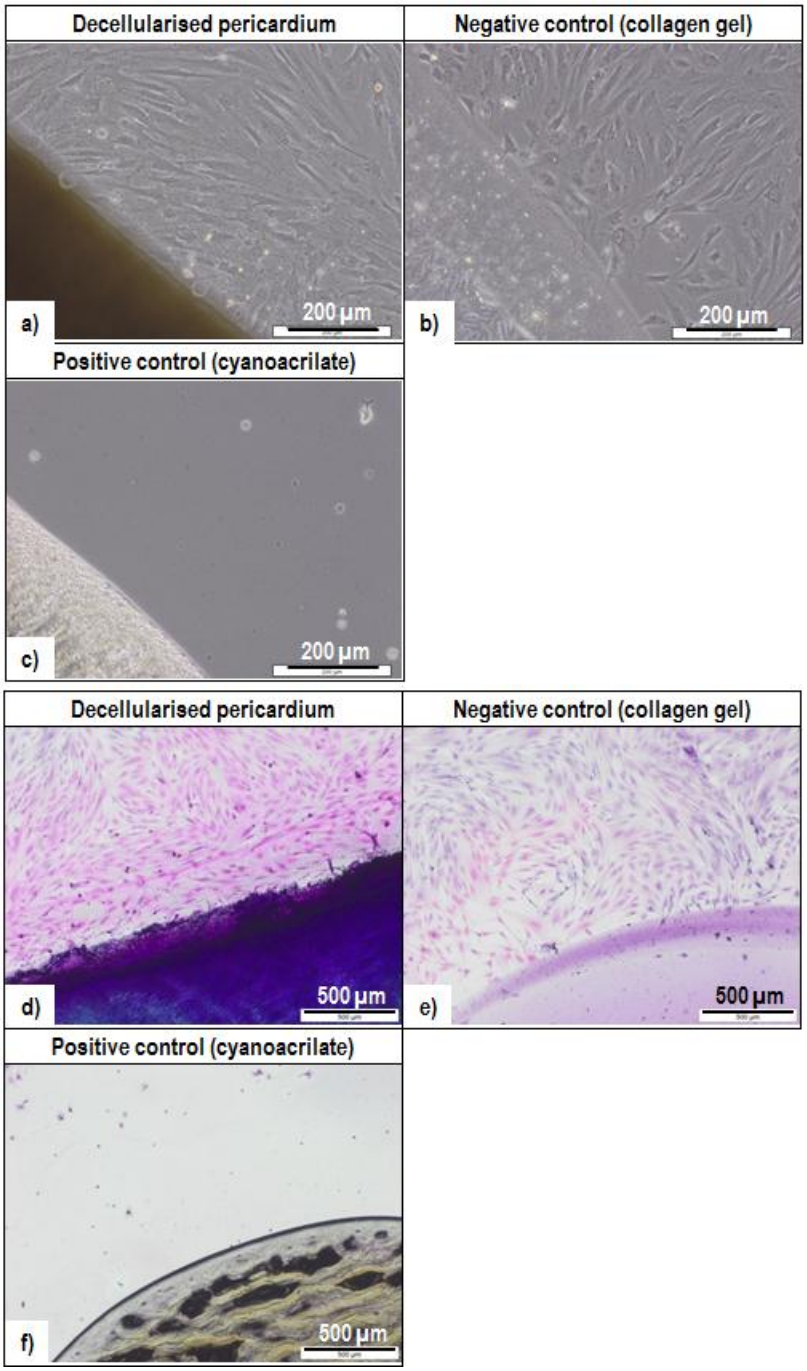

Figure 4.12: Contact cytotoxicity of decellularised porcine pericardium cultured with porcine skin fibroblasts at P5. The figure shows phase contrast (a, b, c) and Giemsa staining (d, e, f) pictures. a, d) decellularised pericardium; b, e) collagen gel (negative control); c, f) cyanoacrilate glue (positive control). Scale bars indicate 200 (a, b and c) and 500 (d, e and f) µm.

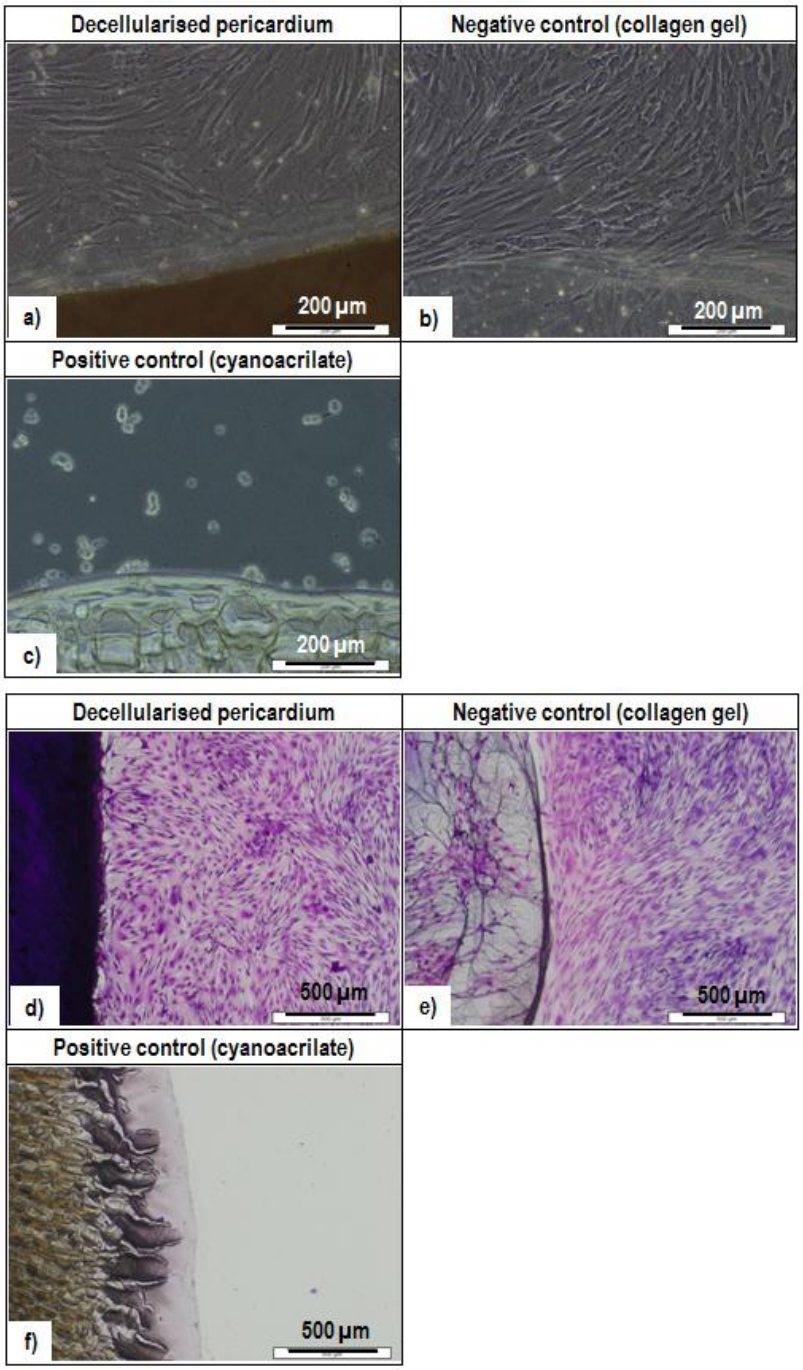

Figure 4.13: Contact cytotoxicity of decellularised porcine pericardium cultured with pMSCs at P5. The figure shows phase contrast (a, b, c) and Giemsa staining (d, e, f) pictures. a, d) decellularised pericardium; b, e) collagen gel (negative control); c, f) cyanoacrilate glue (positive control). Scale bars indicate 200 (a, b and c) and 500 (d, e and f) µm.

4.3.5 Extract biocompatibility of decellularised pericardium

The extract cytotoxicity results are illustrated in Figure 4.14. In general, there was no significant change in the cellular ATP content (measure of cell viability) of the porcine skin fibroblasts incubated with any of the 6 decellularised pericardium extracts compared to the DMEM only group (negative control), except in the case of sample 3, which showed a higher ATP content compared to the negative control (Fig.4.14). The ATP content in all 6 decellularised pericardium extracts and the negative control, were significantly higher compared to the DMSO group (positive control) ($p < 0.05$; MSD = 1.9E+6; Fig. 4.14).

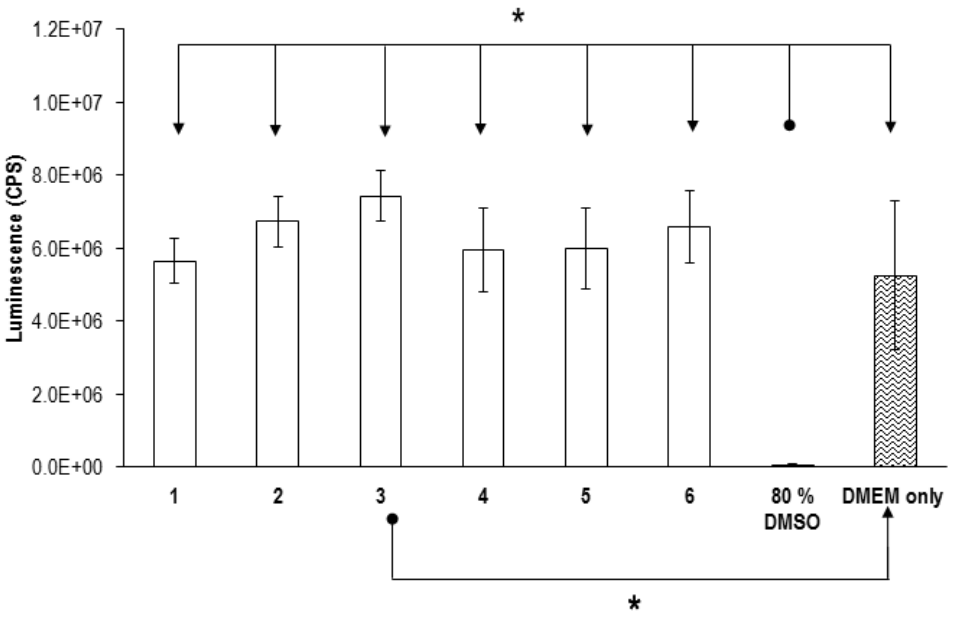

Figure 4.14: ATP content of porcine skin fibroblasts incubated with decellularised pericardium extracts, DMEM alone (negative control) and 80% (v/v) DMSO (positive control). The results represent the means ± 95% C.I. (n = 6). CPS indicates counts per second. Asterisk and connector indicate significant difference between originator and end arrow column, determined by ANOVA and calculation of the MSD. Significant difference was found between sample 3 and the DMEM only group and between all groups and the 80% DMSO group ($p < 0.05$; MSD = 1868259).

4.3.6 DNA content of fresh and decellularised pericardium

The DNA amount per wet weight of fresh and decellularised pericardium was 417.69 ± 143.60 $ng \cdot mg^{-1}$ and 3.23 ± 0.79 $ng \cdot mg^{-1}$, respectively (Figure 4.15). This represented approximately 99% reduction in the DNA content following decellularisation ($p < 0.05$).

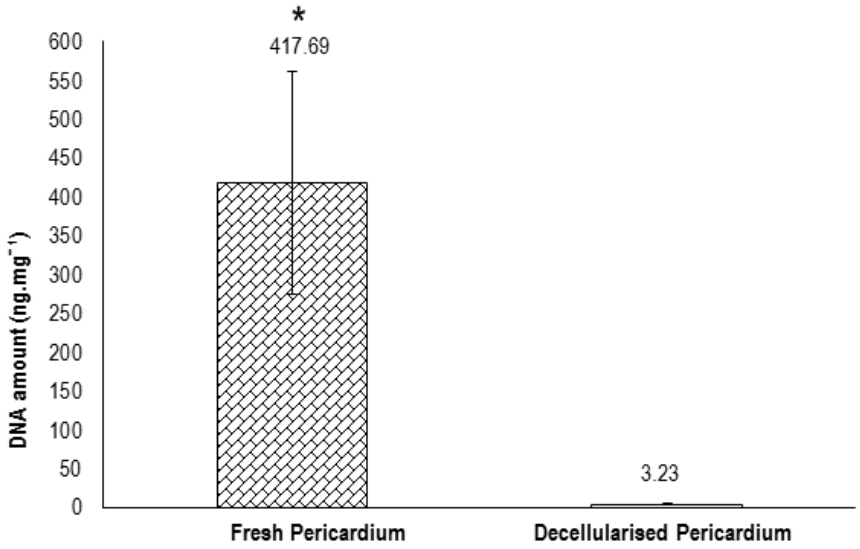

Figure 4.15: DNA content of fresh and decellularised pericardium determined by Nanodrop spectrophotometer at 260 nm. The results represent the means ± 95% C.I. (n = 6). The data was analysed using unpaired student`s t-test, which showed significant difference between groups (p = 0.000). The asterisk indicates significant difference.

4.3.7 Ultrastructure of native and decellularised pericardium

The ultrastructure of fresh and decellularised pericardium was evaluated using SEM and ESEM and images are shown in Figure 4.16 and 4.17, respectively. The complex network of wavy fibres (collagen and elastin) in the fibrosa layer of the fresh and decellularised pericardium is illustrated in Fig. 4.16b and d, respectively. Cell presence was observed on the surface of fresh pericardium in contrast to decellularised pericardium (Fig. 4.16a and d). The ESEM surface images showed similar histoarchitectures between the fresh and decellularised pericardium (Fig. 4.17a and b).

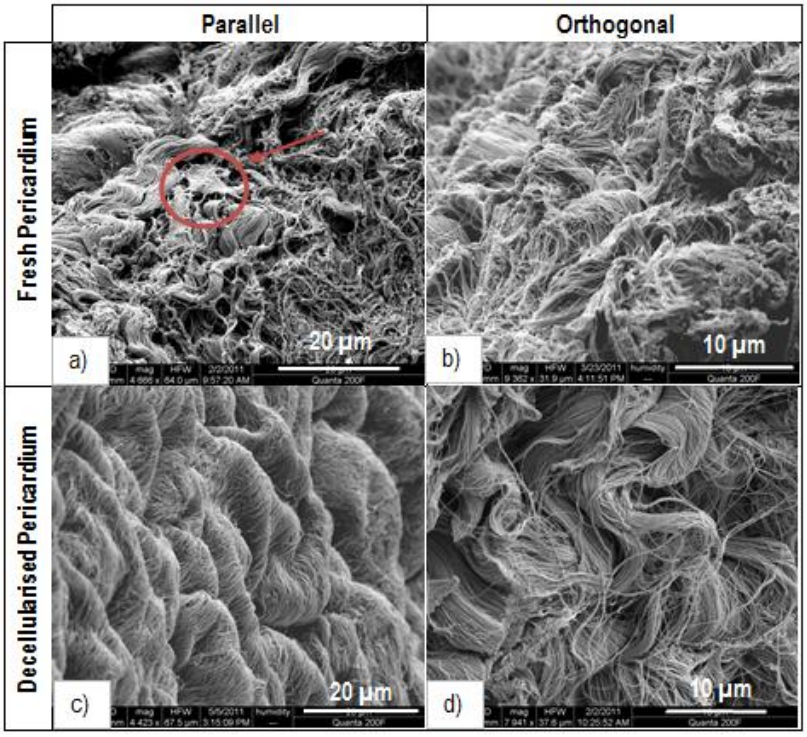

Figure 4.16: SEM images of fresh (a, b) and decellularised (c, d) pericardium. a, c) surface; b ,d) cross section. The red arrow and circle indicate cell presence.

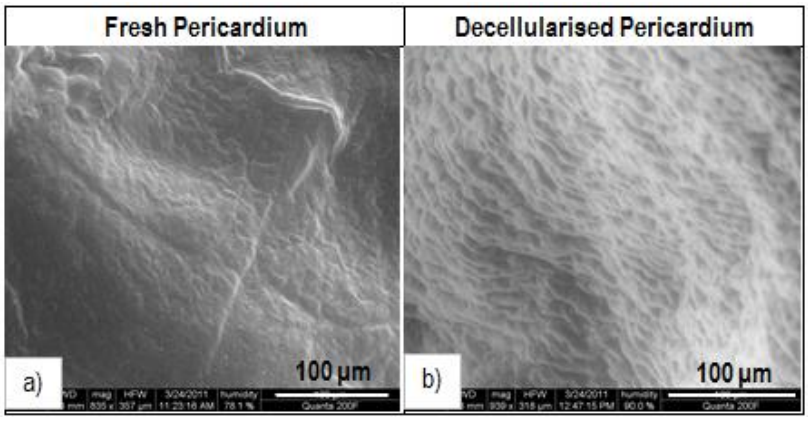

Figure 4.17: ESEM images of fresh (a) and decellularised (b) pericardium.

4.3.8 Assessment of the sterility of the decellularised pericardium

No bacterial growth was observed in the nutrient and thioglycolate broths. A few colonies were visible on one of the NA and one of the FBA plates, but they were not on the streaks and they seemed to be growing within the agar (probably due to batch contamination).

4.4 Discussion

This chapter presented the assessment of the biological and biomechanical properties of decellularised porcine pericardial scaffolds, and compared them to the properties of fresh porcine pericardium. SEM, ESEM and histological examination revealed that following decellularisation the native histoarchitecture of pericardial tissue was well maintained. The fibrosa and epipericardial layers were still present after decellularisation, whereas the cell-rich mesothelial layer was removed. The fibrosa layer of the fresh and decellularised pericardium was comparable to that of the MV leaflets shown in Chapter 3, despite the different alignment of the collagen fibres. The histoarchitecture of the collagen and elastin fibres of the decellularised pericardium was well preserved, as demonstrated by Sirius red/Miller's elastin and Masson's trichrome staining. Nevertheless a high loss of GAGs was observed along the mesothelial side, which was also confirmed by the biochemical analysis. Specifically, the GAG content of the fresh pericardium was significantly higher compared to the GAG content of the decellularised pericardium. In addition, both fresh and decellularised pericardium showed an average lower GAG content compared to both the anterior and posterior leaflet (Table 4.1). The higher GAG content of the MV leaflets can be attributed to the high compressive stresses experienced by the MV leaflets during the cardiac cycle, which are counteracted by the GAGs acting as shock absorbers.

Group	HXP ($\mu g \cdot mg^{-1}$)	GAGs ($\mu g \cdot mg^{-1}$)
LA	99.30 ± 13.99	23.90 ± 8.65
LP	80.05 ± 20.43	24.59 ± 5.79
FP	83.25 ± 7.40	8.43 ± 2.60
DP	115.95 ± 18.30	0.13 ± 0.07

Table 4.1: Mean HXP and GAG content for the anterior (LA) and posterior (LP) leaflet group and the fresh (FP) and decellularised (DP) pericardial group. Data is presented as the mean (n=6) ± 95% C.I.

Moreover, the decellularised pericardium showed significantly higher HXP content compared to the fresh. This increase was most likely due to the relative increase in the ratio of these molecules to the total dry weight, due to the loss of soluble proteins and cell components following decellularisation (Mirsadraee *et al*., 2006). The HXP contents of the fresh and decellularised porcine pericardium were similar to the corresponding contents for human

pericardium reported by Mirsadraee *et al.* (2006) (104 μg·mg^{-1} for fresh and 118 μg·mg^{-1} for decellularised human pericardium). Moreover, the HXP content of decellularised pericardium was higher compared to that of both the anterior and posterior leaflets (Table 4.1). No significant difference was observed in the denatured HXP content between fresh and decellularised pericardium, indicating that the decellularisation protocol did not cause the denaturation of the collagen.

Decellularisation treatments should not leave any cells or cell fragments in the scaffold, since they have been associated with inflammation and calcification, which may impair the longevity of the scaffold *in vivo* (Oswal *et al*., 2007). The results from the present study indicated a 99% reduction in the DNA content of the pericardium following decellularisation. Moreover, the contact and extract cytotoxicity assays verified the adequate removal of SDS from the pericardial scaffolds, which allowed fibroblasts and pMSCs to grow well in contact with the scaffold and with scaffold extracts. One sample of the decellularised scaffold extracts showed higher cellular ATP content compared to the negative control. This was probably due to the soluble proteins released by the decellularised tissue which might have improved cell growth. In addition, the biocompatibility test results showed that disinfection with PAA did not affect scaffold biocompatibility. Similar results were obtained by Booth *et al.* (2002), who reported successful decellularisation of porcine aortic valves, without compromising the ECM, using the same concentration of SDS in hypotonic buffer. Mirsadraee *et al.* (2006) reported similar biocompatibility results with human pericardium, which was decellularised using the same concentration of SDS in hypotonic buffer.

In terms of the biomechanics, both fresh and decellularised pericardium demonstrated rather isotropic behaviours, with similar mechanical properties along and across the collagen fibre directions. In addition, most of the biomechanical parameters studied did not demonstrate any statistically significant differences between the fresh and decellularised pericardium. However, significant differences were observed in the transition stress, transition strain, and thickness between fresh and decellularised pericardium. Specifically, the transition stress and strain of the decellularised pericardium were higher than that of the fresh tissue. This has also been reported by Korossis *et al.* (2002).

Compared to the biomechanics of the MV leaflets presented in Chapter 3, both fresh and decellularised pericardium demonstrated higher average collagen phase slope, UTS and transition stress (Table 4.2). Moreover, the average transition strain of both fresh pericardium

groups (orthogonal and parallel), and the orthogonal decellularised pericardium group, were lower compared to both the anterior and posterior leaflet groups. The fresh and decellularised orthogonal pericardium groups also demonstrated lower average failure strains compared to both the anterior and posterior leaflet groups. The lower transition and failure strains suggested a reduced extensibility for the fresh and decellularised pericardium compared to the MV leaflets. The fresh and decellularised pericardium also demonstrated lower average thicknesses compared to the leaflets, but similar to those for human and bovine pericardium, commonly used for mitral valve repair (Mirsadraee *et al*., 2006; Oswal *et al*., 2007).

Group	El-E (MPa)	Coll-E (MPa)	σ_t (MPa)	ε_t (%)	UTS (MPa)	ε_{UTS} (%)	Thickness (mm)
LAC	0.05 ± 0.01	13.67 ± 6.25	0.20 ± 0.11	21.25 +8.90 -7.70	2.60 ± 1.49	44.77 +11.39 -11.11	0.67 ± 0.08
LAR	0.06 ± 0.04	3.52 ± 2.01	0.17 ± 0.06	33.08 +23.85 -19.96	1.19 ± 0.66	74.00 +18.83 -25.37	0.83 ± 0.27
LPC	0.02 ± 0.01	2.60 ± 2.01	0.17 ± 0.06	39.85 +24.20 -21.82	0.90 ± 0.51	71.16 +27.44 -43.33	0.74 ± 0.09
LPR	0.02 ± 0.00	2.64 ± 1.67	0.08 ± 0.05	29.63 +13.63 -11.99	0.74 ± 0.15	72.76 +18.78 -24.53	0.94 ± 0.22
PP	0.15 ± 0.13	22.83 ± 9.49	0.39 ± 0.20	15.29 +16.98 -11.37	6.66 ± 3.16	51.30 +27.80 -28.24	0.21 ± 0.02
PO	0.21 ± 0.18	25.01 ± 8.54	0.26 ± 0.14	8.38 +6.48 -4.75	4.28 ± 1.33	29.86 +10.15 -9.23	0.23 ± 0.01
DPP	0.09 ± 0.06	35.45 ± 11.83	0.64 ± 0.12	33.13 +21.24 -18.14	7.89 ± 2.36	61.45 +32.27 -25.99	0.22 ± 0.01
DPO	0.13 ± 0.06	27.42 ± 11.54	0.75 ± 0.45	19.94 +12.07 -9.78	6.20 ± 2.75	34.94 +25.73 -29.82	0.21 ± 0.01

Table 4.2: Mean biomechanical parameters for the anterior leaflet circumferential (LAC) and radial (LAR); the posterior leaflet circumferential (LPC) and radial (LPR); the fresh pericardium parallel (PP) and orthogonal (PO); the decellularised pericardium parallel (DPP) and orthogonal (DPO). Data is presented as the mean (n=6) ± 95% C.I.; El-E: Elastin phase slope; Coll-E: collagen phase slope; σ_t: transition stess; ε_t: transition strain; UTS: ultimate tensile strength; ε_{UTS}: failure strain.

Despite these differences between decellularised pericardium and MV leaflets highlighted above, decellularised pericardial scaffolds could potentially represent a valuable choice for

MV leaflet repair both in terms of *in vivo* and *in vitro* regeneration. This is especially the case when decellularised pericardium is compared to chemically-treated autologous, allogeneic and bovine pericardia, which have been reported to have much higher stiffness and lower extensibility compared to both decellularised pericardium and MV leaflets (Oswal et al., 2007), and not to be able to regenerate and remodel in the patient.

Chapter 5

Cell phenotyping and static cell seeding of decellularised pericardium

5.1 Introduction

This chapter describes the characterisation of the different cell types that were used in experiments to investigate the re-population of decellularised pericardial scaffolds, and the investigation of the optimum cell density and time for the cell-seeding of the scaffolds. Identification of the optimum seeding density and static seeding time was necessary in order for the cells to firmly adhere on the surface of the scaffold prior to dynamic culture in the bioreactor. The cells chosen for the repopulation experiments were those that expressed a phenotype similar to mitral valve (MV) interstitial cells (VICs). VICs are present throughout the MV leaflet tissue and comprise different cell populations concerned with the regulation of ECM remodelling and repair (Rabkin-Aikawa *et al.*, 2005). There are three different phenotypes of VICs, namely fibroblasts, smooth muscle cells (SMCs) and myofibroblasts, which have characteristics of both fibroblasts and SMCs (Taylor *et al*., 2003; Sacks and Yoganathan, 2007). Porcine skin fibroblasts and vascular SMCs were used in the cell seeding experiments.

Differentiated cells such as fibroblasts and SMCs become senescent after prolonged culturing *in vitro* (Hayflick, 1965) due to the fact that they are already aged prior to isolation and, therefore, it may be difficult to generate sufficient numbers of cells for scaffold seeding. The potential senescence of differentiated cells could also limit their capacity for the repopulation and regeneration of the scaffold. In addition, in the clinical setting, it may be difficult to isolate fibroblasts and SMCs from the intended recipient of the implant. Due to the limitations associated with the use of differentiated cells, porcine bone-marrow-derived mesenchymal stem cells (MSCs) were also used in the experiments with the pericardial scaffolds. In the clinical setting, MSCs can be easily isolated from bone marrow biopsies and expanded to large numbers without loss of their proliferative capacity (Till and McCulloch, 1961). Once sufficient cell numbers are available, differentiation into the appropriate lineage(s) could then be induced by mechanical stimulation in a bioreactor (Banes *et al.*, 1995; Sato *et al.*, 1996;

Butt and Bishop, 1997; Hishikawa and Lüscher, 1997; Eastwood *et al.*, 1998; Sirois *et al.*, 1998; Breen, 2000; Grinell, 2000; Altman *et al.*, 2002; Väänänen, 2005; Ku *et al*., 2006).

5.1.1 Aims and objectives

Aims:

The aim of the work presented in this chapter was to investigate the optimum cell density and culture time point for seeding the decellularised pericardium prior to dynamic seeding in a bioreactor.

Objectives:

- To characterise, through immunofluorescence, the phenotype of the cells used for seeding experiments
- To investigate, through SEM, histology and a cell viability assay, the optimum cell density and static seeding time required to form a monolayer of cells on the pericardial scaffold prior to loading in a bioreactor.

5.2 Materials

5.2.1 Equipment

The equipment used for the static cell seeding experiments is summarised in Table 5.1:

Equipment	Supplier	Function
Cylindrical cutting tool	Bespoke design; manufactured in-house	Dissection of pericardial scaffold discs (40 mm diameter)
Tissue holder	Bespoke design; manufactured in-house	Clamping of pericardial scaffold discs for static culture
Culture tub with filter	Nalgene	Culture of the cell-seeded pericardial disc clamped in the tissue holder

Table 5.1: Equipment used for the static cell seeding of the decellularised pericardial scaffolds.

The cutting tool and tissue holders were made of 316L stainless steel. The culture system comprising the tissue holder and culture tub are illustrated in Figure 5.1, the cutting tool was

used to obtain a scaffold patch of 4.6 cm in diameter, which was clamped between the top and bottom part of the tissue holder. The patch was clamped in between the two parts of the holder, which were held together by six screws (Figure 5.1b).

Following clamping, the exposed portion of the scaffold patch was a 3 cm diameter disc. The bottom part of the tissue holder was a mesh (Figure 5.1a) to allow the cell culture medium to permeate the inferior surface of the-cell seeded scaffold. The size of the mesh holes (1.5 mm) was small enough to avoid any deformation of the pericardial scaffold disc, but large enough to ensure a supply of medium to most of the surface. The holder with the secured pericardial patch was placed in the culture tub (Figure 5.1c) by lifting it by the middle screws (Figure 5.1b).

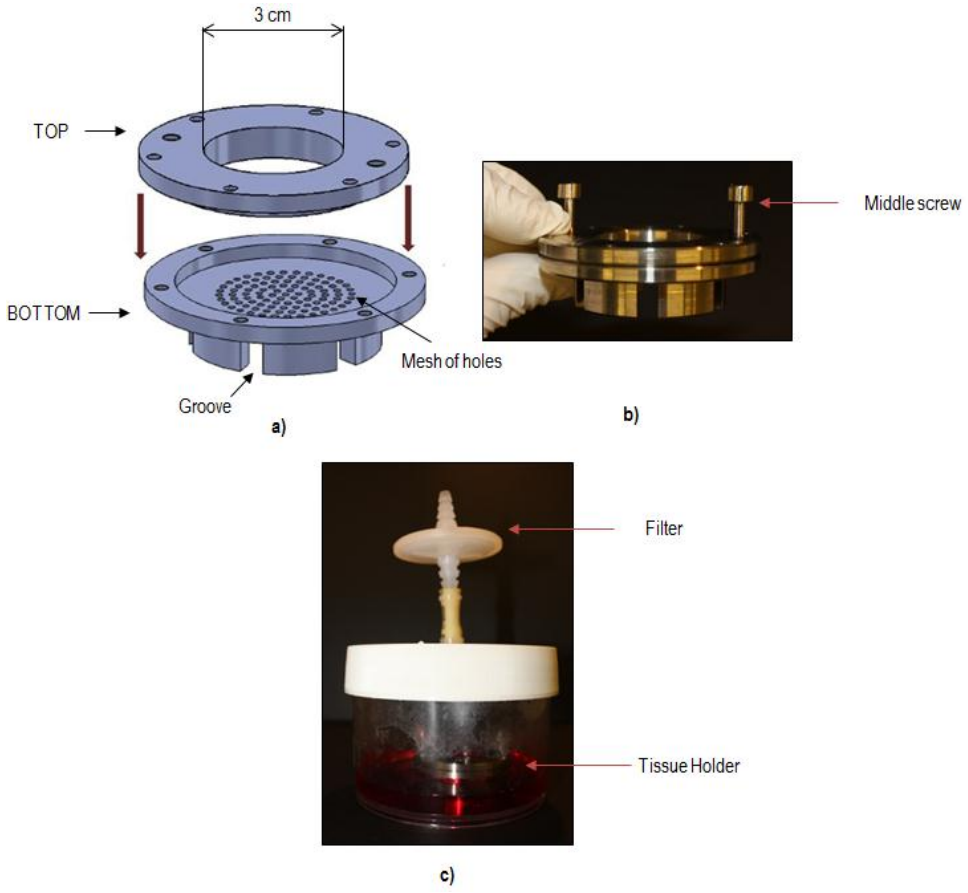

Figure 5.1: Tissue holder (a, b) and culture tub (c) used in the static cell-seeding experiments.

During the seeding experiments, culture medium was added (up to the mesh of the bottom part of the tissue holder) in the culture tub, which was fitted with a filter to allow oxygen exchange. A simple experiment was carried out to determine the optimum volume of culture medium to be added to the surface of the pericardial scaffold patch (in the well formed by the

tissue holder). A 4.6 cm diameter patch of native pericardium was loaded on the tissue holder, which was then positioned in the culture tub. The culture tub was filled with 105 ml of cell culture medium (Chapter 2, Section 2.5.4), up to the mesh of the lower part of the tissue holder, such that the medium contacted the inferior surface of the pericardial patch. Cell culture medium (2 ml) was added to the upper surface of the patch, in the well formed by the top part of the tissue holder. The tissue holder was incubated (37°C in 5% v/v CO_2 in air) overnight to observe the level of evaporation of the culture medium. The head volume of 2 ml was chosen in order to cover the top surface of the patch, to allow passive diffusion of oxygen, and to allow for potential evaporation of the culture medium without drying of the tissue patch. The head volume (V) corresponded to a culture medium height (h) in the well, which was calculated as follows:

V= patch area × medium height in well = $\pi \times r^2 \times h = \pi \times 1.5^2 \times h = 2$ ml $\rightarrow$ h = 2.8 mm

where r was the radius of the sample. This height was similar to the height of the volume of cell culture medium in the flasks, used in cell culture.

Following overnight incubation, there was some evaporation of the culture medium, but there was still enough culture medium in the well to cover the pericardial patch.

5.2.2 Pericardial scaffolds

Fresh pericardium was isolated and decellularised as described in Chapter 4, Section 4.2.1.

5.2.3 Cells

Porcine MSCs, dermal fibroblasts and SMCs were cultured on the mesothelial surface of decellularised pericardial scaffolds. Cells were cultured as described in Chapter 2, Section 2.17.

5.3 Methods

5.3.1 Static seeding of decellularised pericardial scaffolds

5.3.1.1 Sterilisation of tissue holders and culture tubs

Prior to conducting the seeding experiments, all the equipment was sterilised. The upper and lower parts of the tissue holders were placed in a metal container, together with the allen keys and the cutting tool, and sterilised by dry heat sterilisation. A metal tray, which was also used

in the experiments as a working surface, was covered with tin foil and sterilised by dry heat. The air filters of the culture tubs were covered with tin foil and fixed with autoclave tape. The tubs was then closed loosely and sterilised by autoclaving. After autoclaving, the tubs were left to dry in a 45 °C drying room for 2 - 3 days prior to use.

5.3.1.2 Scaffold mounting on tissue holders and cell seeding

Porcine MSCs, dermal fibroblasts and SMCs were cultured on the mesothelial surface of pericardial scaffolds in order to determine the optimal cell density and static seeding time required to form a cell monolayer on the scaffold surface prior to dynamic conditioning in the bioreactor. Previous studies (Mirsadraee, 2005) have reported that cells, particularly fibroblasts, showed a better attachment on the mesothelial surface of decellularised pericardium compared to the epipericardial surface. Hence the mesothelial surface was chosen as the cell seeding surface.

All work was carried out aseptically in a class II safety cabinet. Decellularised porcine pericardia were prepared as described in Chapter 4, Section 4.2.1 and 27 (one sample per cell density per cell type per time point) 46 mm in diameter circular patches were dissected aseptically using the cylindrical cutting tool. The lower part of each tissue holder was positioned on top of a sterile square petri dish, which was placed on a sterile metal tray. A scaffold patch was placed onto the lower part of each tissue holder, and the upper part screwed in place. The whole unit was then placed in a culture tub. A volume of cell culture medium equal to 105 ml was added to the culture tub, as described in Section 5.2.1. The various cell types were used at different passage numbers depending on the duration of culture on the pericardial scaffold: MSCs at passage 2 (24 h) and at passage 6 (3 days and 1 week); porcine dermal fibroblasts at passage 4 (24 h), passage 5 (3 days) and passage 3 (1 week); SMCs at passage 4 (24 h) and passage 5 (3 days and 1 week). Following resurrection, each cell type was cultured to the specific passage number, re-suspended and counted. The cell suspensions were then adjusted to the 3 required cell seeding densities, and 2 ml of each suspension was pipetted on 3 (for time point analysis) of the samples (in the well formed by each tissue holder). The seeding densities used for the three different cell types are summarised in Table 5.2. The cell densities were chosen on the basis of previous work on MSCs, fibroblasts (Mizrachi, 2009; Thomas *et al.*, 2009) and Sinha (personal communication) for SMCs. The cell densities that were seeded on each sample were calculated as follows:

$$\text{Cell density (cells/cm}^2\text{)} \times \text{Sample area (cm}^2\text{)} = \text{Number of cells}$$

The sample area was calculated from:

$$\text{Sample area} = \pi \times r^2$$

where r is the radius of the circular patch equal to 15 mm (since the effective diameter of the patch was 30 mm).

Cell type	Cell densities (cells·cm^{-2})	Cells per sample (in 2 ml cell suspension)	Time points	Type of assessment
MSCs	2×10^4	1.413×10^5	24 hours	SEM
			3 days	H & E
			1 week	H&E and live/dead
	1×10^5	7.065×10^5	24 hours	SEM
			3 days	H & E
			1 week	H&E and live/dead
	2×10^5	1.413×10^6	24 hours	SEM
			3 days	H & E
			1 week	H&E and live/dead
Skin fibroblasts	2×10^4	1.413×10^5	24 hours	SEM
			3 days	H & E
			1 week	H&E and live/dead
	1×10^5	7.065×10^5	24 hours	SEM
			3 days	H & E
			1 week	H&E and live/dead
	2×10^5	1.413×10^6	24 hours	SEM
			3 days	H & E
			1 week	H&E and live/dead
SMCs	2.5×10^4	1.766×10^5	24 hours	SEM
			3 days	H & E
			1 week	H&E and live/dead
	5×10^4	3.532×10^5	24 hours	SEM
			3 days	H & E
			1 week	H&E and live/dead
	1×10^5	7.065×10^5	24 hours	SEM
			3 days	H & E
			1 week	H&E and live/dead

Table 5.2: Parameters used in the static seeding experiments with the decellularised pericardial scaffolds. One sample was used for each seeding density of each cell type at each time point (n = 27).

The seeded scaffolds were incubated for either 24 hours, 3 days or 1 week under standard conditions. After 24 hours, 9 seeded scaffolds, corresponding to each cell density and cell type, were harvested and assessed for cell attachment by scanning electron microscopy (SEM). Nine more scaffolds, again corresponding to each cell density and cell type, were harvested after 3 days and assessed for cell penetration using histology and H&E staining. The final 9 samples were harvested after 1 week and assessed for cell penetration and amount of live/dead cells using histology (H&E) and live/dead staining, respectively (Table 5.1). Cell culture medium (2 ml) was added to the top surface of the seeded scaffold every 2 days during the 1-week incubations.

5.3.2 SEM of cell seeded pericardial scaffolds

The attachment of the different cell types to the pericardial scaffolds was assessed after 24 hours using SEM. A rectangular piece was cut from the central area of each seeded scaffold, and processed for SEM as described in Chapter 2, Section 2.13.

5.3.3 Histological analysis of recellularised pericardial scaffolds

Cell seeded scaffolds were harvested for histological analysis after 3 days and 1 week to investigate the capacity of the cells to both form a monolayer on the surface of the scaffold and to penetrate its thickness. A rectangular piece was cut from the central area of each seeded scaffold, processed, and stained with H&E as described in Chapter 2, Section 2.11.1.

5.4 Results

5.4.1 Characterisation of porcine fibroblasts & SMCs

Immunofluorescence labelling of porcine dermal fibroblasts and SMCs was performed using antibodies to α-SMA, calponin (SMCs only), desmin and vimentin (fibroblasts only). The dermal fibroblasts isolated through collagenase digestion only expressed vimentin, whereas the SMCs explanted from porcine aorta were positive for calponin and desmin, and strongly positive for α-SMA (Figure 5.2).

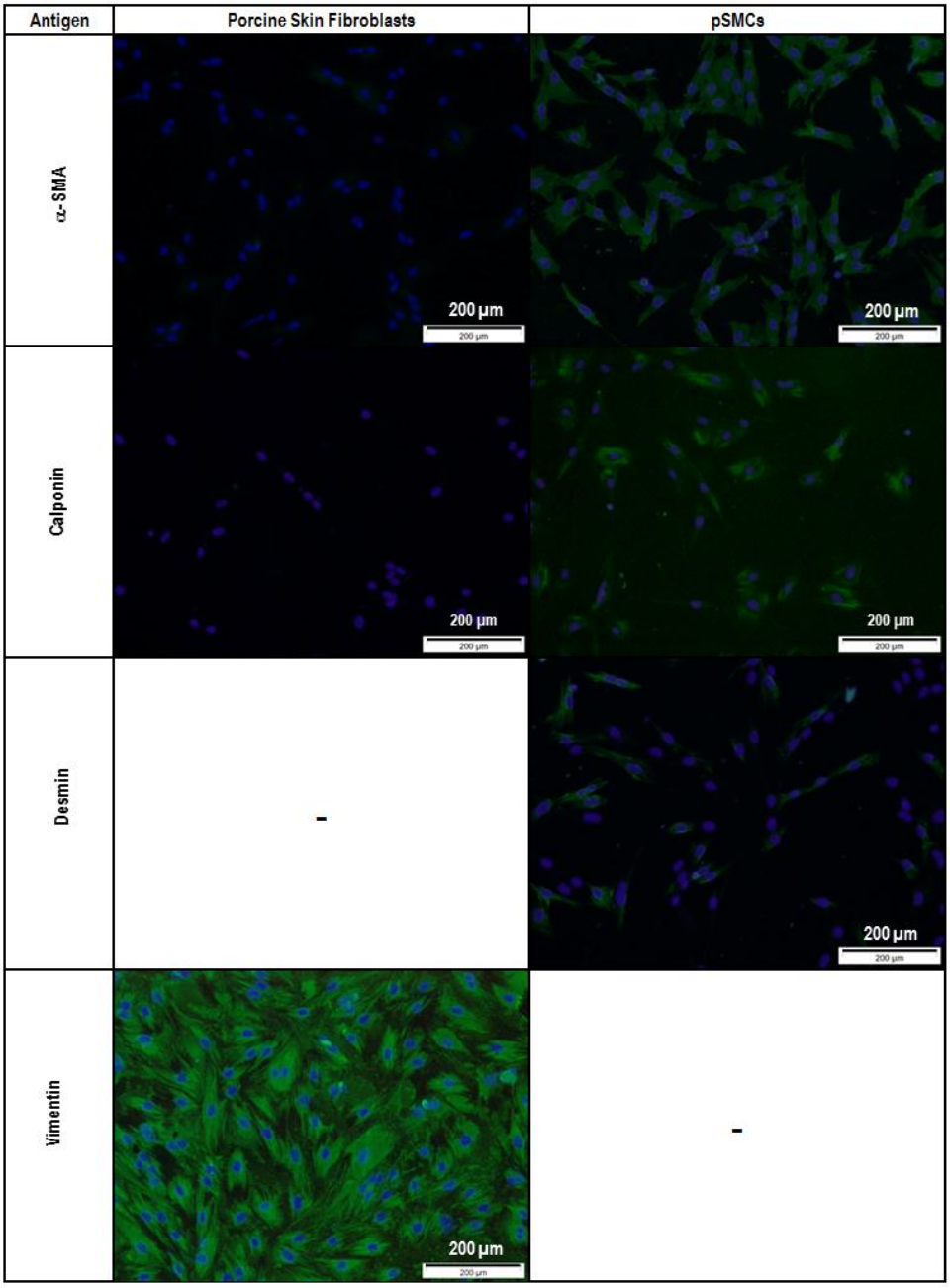

Figure 5.2: Immunofluorescence labelling of porcine fibroblasts and SMCs. Fibroblasts expressed vimentin only. SMCs expressed α-SMA, calponin and desmin. The blank boxes indicate that cells were not phenotyped for that specific marker. Scale bars indicate 200 µm. pSMCs: porcine SMCs.

5.4.2 Optimisation of cell seeding density

Porcine MSCs, fibroblasts and SMCs were cultured on the mesothelial surface of pericardial scaffold samples to determine the optimal cell density and seeding time required to form a

monolayer of cells on the surface of tissue prior to dynamic conditioning of the scaffolds in the bioreactor. The samples were analysed by SEM after 1 day, H&E staining after 3 days and 1 week, and by live/dead staining after 1 week.

5.4.2.1 Cell attachment after 24 hours culture visualised by SEM

After 24 hours static culture, the fibroblasts and SMCs readily attached to the scaffold at all seeding densities. The SMCs and fibroblasts looked sparsely distributed at the lowest densities (2×10^4 cells·cm^{-2} and 2.5×10^4 cells·cm^{-2}, respectively), with small cell patches observed on the surface of the scaffolds (Figure 5.3a, g). At the intermediate cell densities (1×10^5 cells·cm^{-2} for fibroblasts and 5×10^4 cells·cm^{-2} for SMCs), the cells started forming a monolayer (Figure 5.3b, h). At the high cell densities (2×10^5 cells·cm^{-2} for fibroblasts and 1×10^5 cells·cm^{-2} for SMCs), the cells formed monolayers (Figure 5.3c, i). The MSCs attached well onto the scaffold at both the intermediate and high densities (1×10^5 cells·cm^{-2} and 2×10^5 cells·cm^{-2}, Figure 5.3e, f). At the low density (2×10^4 cells·cm^{-2}) only a few MSCs were observed, most of them round in shape, suggesting that the cells did not attach to the scaffold (Figure 5.3d). Generally, the attached cells demonstrated a characteristic spread morphology suggesting good attachment to the scaffolds (Figure 5.4a - f).

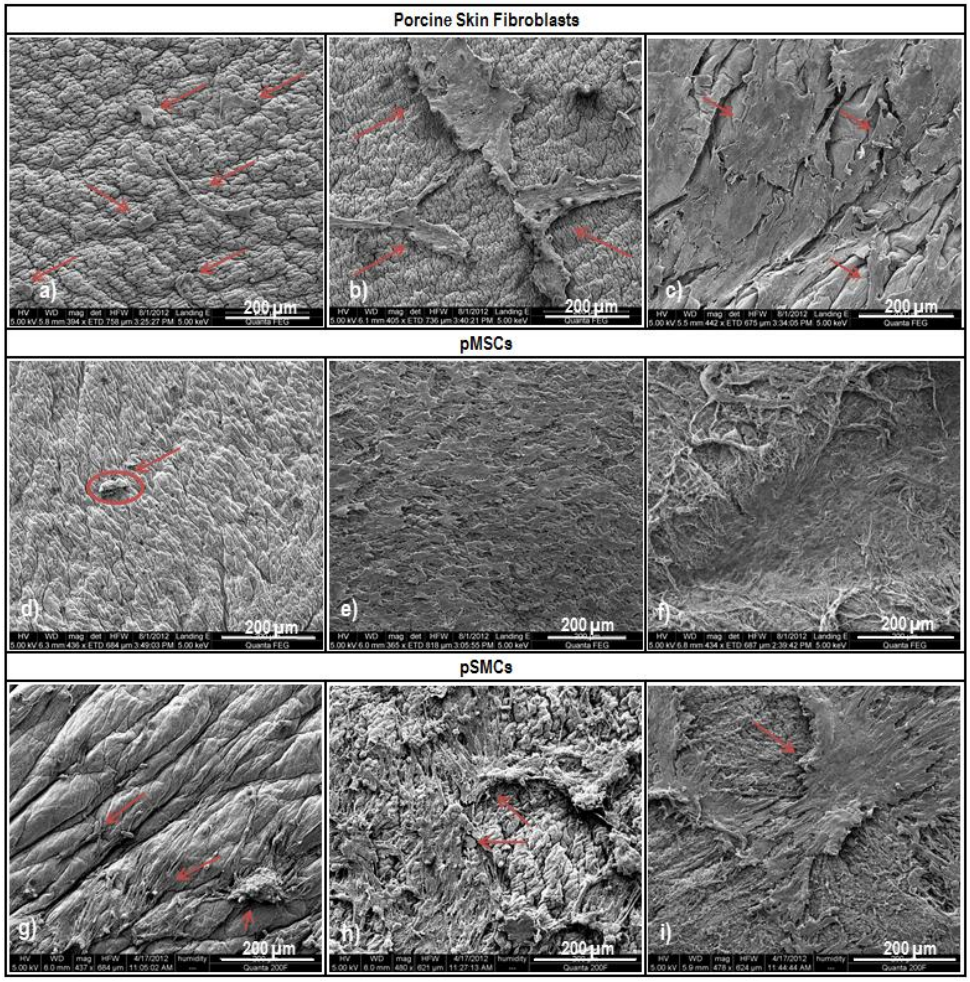

Figure 5.3: SEM of porcine fibroblasts, pMSCs and pSMCs seeded on porcine pericardial scaffolds after 24 hours culture. (a, d) 2×10^4 cells·cm^{-2}; (b, e), 1×10^5 cells·cm^{-2}; (c, f) 2×10^5 cells·cm^{-2}cm^2; (g) 2.5×10^4 cells·cm^{-2}; (h) 5×10^4 cells·cm^{-2}; (i) 1×10^5 cells·cm^{-2} . The red arrows and circles indicate cells. Scale bars indicate 200 µm. pMSCs: porcine MSCs; pSMCs: porcine SMCs.

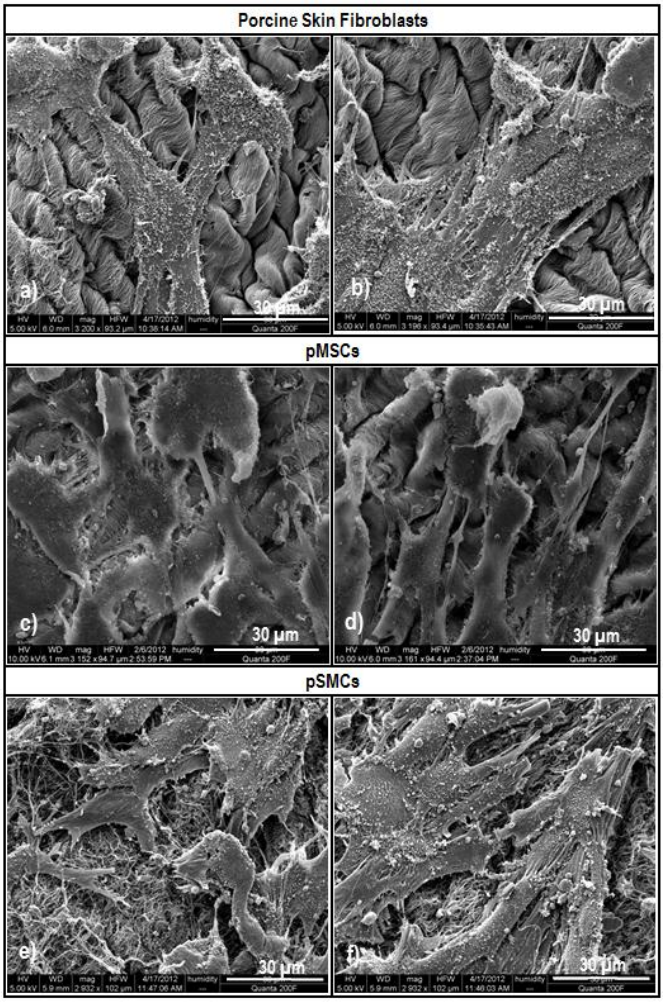

Figure 5.4: SEM of porcine fibroblasts, pMSCs and pSMCs showing cell attachment onto porcine pericardial scaffolds after 24 hours culture. Fibroblasts and MSCs at 2×10^5 cells·cm^{-2} (a, b, c and d); SMCs at 1×10^5 cells·cm^{-2} (e, f). Scale bars indicate 30 µm. pMSCs: porcine MSCs; pSMCs: porcine SMCs.

5.4.2.2 Cell attachment and, penetration and viability after 3 days and 1 week culture visualised by histology and live/ dead staining

The histology images (3 days and 1 week) and live/dead (1 week only) staining results of the 3 cell types seeded on the pericardial scaffolds are illustrated in Figures 5.5, 5.6 and 5.7. After 3 days of static seeding, no fibroblasts or SMCs were observed through histology and H&E staining of sections on the mesothelial surface of scaffolds at the lowest and intermediate densities (2×10^4 and 1×10^5 cells·cm^{-2} for fibroblasts; 2.5×10^4 and 5×10^4 cells·cm^{-2} for SMCs), as shown in Figure 5.5a, b and 5.7a, b. Sparsely arranged cells were observed at the highest densities (2×10^5 cells·cm^{-2} for fibroblasts and 1×10^5 cells·cm^{-2} for SMCs), as shown in

Figure 5.5c and 5.7c. In contrast , after 3 days of culture MSCs were observed as an early monolayer when seeded at the intermediate and highest densities (1×10^5 and 2×10^5 cells·cm^{-2}; Figure 5.6b and 5.6c, respectively), and they were seen to have penetrated into the scaffold, especially at the highest density. The penetration and migration of the MSCs into the scaffold was more apparent after 1 week of static seeding at both the intermediate and high seeding densities, whereas only sparsely arranged cells were observed on the scaffolds seeded at the low cell density.

Following 1 week culture, the fibroblasts and SMCs became more confluent on the scaffold surface, especially when seeded at the intermediate and high cell densities, (Figures 5.5e, f and 5.7e, f), forming a continuous (fibroblasts) or almost continuous (pSMCs) monolayer at the highest cell seeding density (Figures 5.5f and 5.7f). In contrast to the fibroblasts and MSCs, the SMCs were not observed within the scaffolds after 1 week of culture, demonstrating a tendency to form agglomerates on the scaffold surface. The most favourable seeding densities for fibroblasts and MSCs were 2×10^5 cells·cm^{-2} and 1×10^5 cells·cm^{-2}, respectively, representing the lowest densities at which the cells were found to populate the surface of the scaffold. Based on the same criterion, the most favourable static culture duration was 1 week for fibroblasts and 3 days for MSCs.

The results for the live/dead staining (Chapter 2, Section 2.16) after 1 week static culture of the 3 cell types are shown in Figure 5.5g - i, 5.6g - i and 5.7g - i. All 3 cell types were mostly stained green when seeded on the pericardial scaffolds at all cell densities investigated, with the exception of MSCs at the lowest cell density, which were mostly stained red (Figure 5.6g). Counting of the live (green) and dead (red) cells (Chapter 2, Section 2.16.1) indicated that 68% and 78% of fibroblasts and SMCs, respectively, were alive when seeded at the lowest cell density, whereas only 25% of MSCs were alive when seeded at the lowest cell density. Moreover, 91%, 81% and 74% of fibroblasts, pMSCs and SMCs, respectively, were alive after 1 week following seeding onto the pericardial scaffolds at the intermediate cell density and 89%, 74% and 77% viable when seeded at the high cell densities.

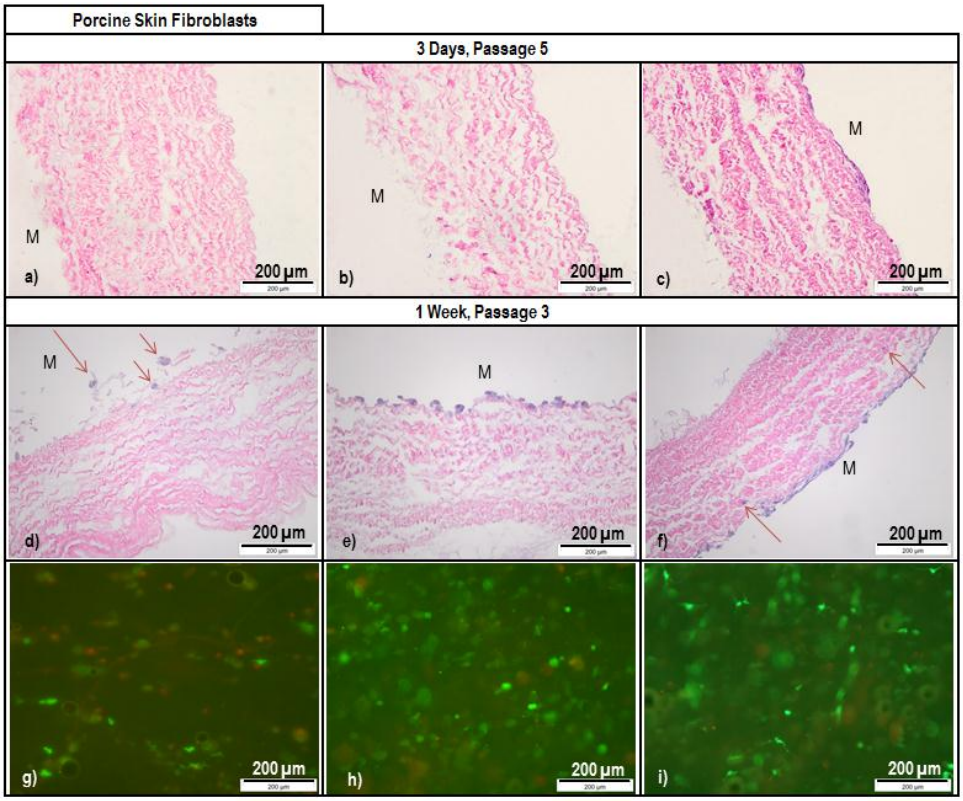

Figure 5.5: H&E stained sections (a - f) and live/dead (g - i) stained samples of decellularised pericardial scaffolds seeded with porcine fibroblasts at different cell densities at 3 days (a - c) and 1 week (d - i). (a, d, g) 2×10^4 cells·cm^{-2}; (b, e, h) 1×10^5 cells·cm^{-2}; (c, f, i) 2×10^5 cells·cm^{-2}. At 3 days, the fibroblasts appeared as a discontinuous monolayer when seeded at the high cell density (c). At 1 week, the cells were observed to form a continuous monolayer at the high cell seeding density, and were present through the thickness of the scaffold (f). Most of the cells that had been seeded at the intermediate (h) and high (i) cell densities were stained green, in contrast to the cells seeded at the low cell density (g). Arrows indicate cells. M: mesothelial surface. Scale bars indicate 200 µm.

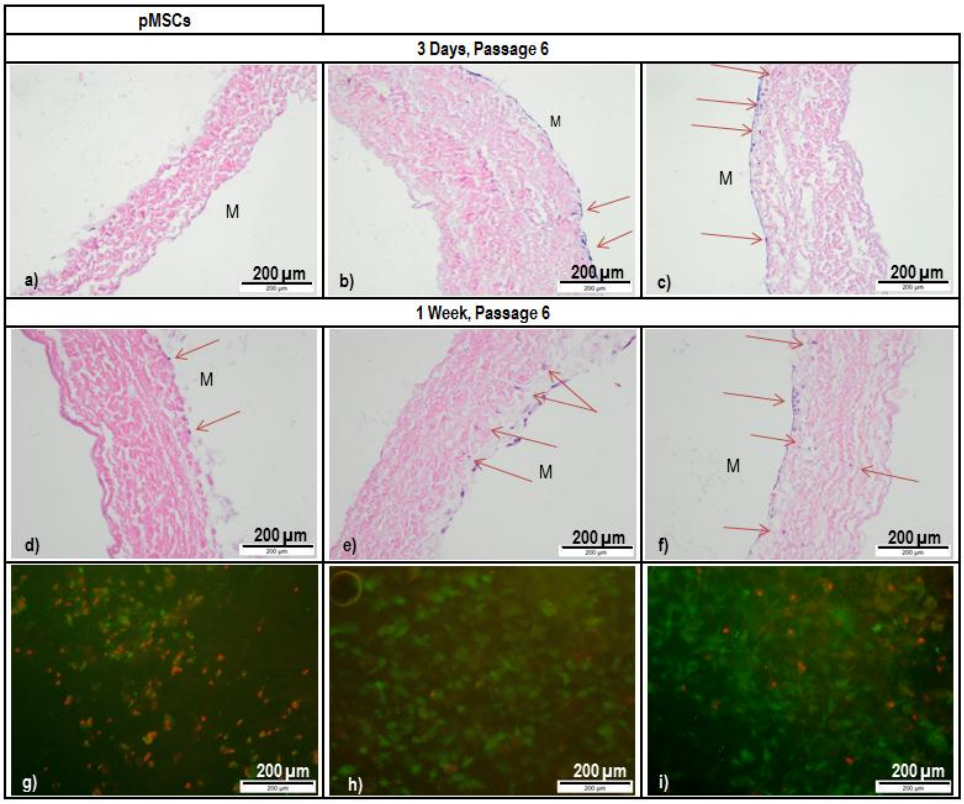

Figure 5.6: H&E stained sections (a - f) and live/dead (g - i) stained samples of decellularised pericardial scaffolds seeded with porcine MSCs at different cell densities at 3 days (a - c) and 1 week (d - i). (a, d, g) 2×10^4 cells·cm^{-2}; (b, e, h) 1×10^5 cells·cm^{-2}; (c, f, i) 2×10^5 cells·cm^{-2}. Following 3 days and 1 week, the MSCs attached well to the scaffold forming continuous monolayers at the middle and high densities (b, c, e, f). At the high density, the cells started infiltrating the scaffold after 3 days (c), whereas after 1 week they started migrating further into the scaffold. Most of the cells at the middle (h) and high (i) densities were stained green, in contrast to the low density (g) at which most of the cells were stained red. Arrows indicate cells. M: mesothelial surface. Scale bars indicate 200 µm. pMSCs: porcine MSCs.

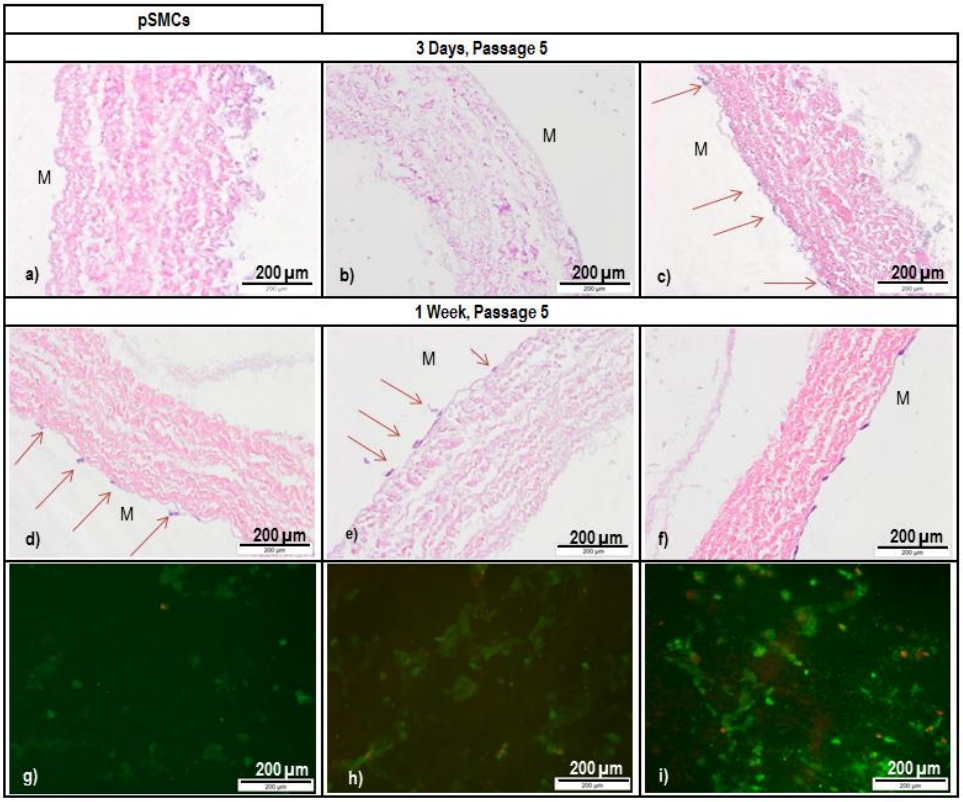

Figure 5.7: H&E stained sections (a - f) and live/dead (g - i) stained samples of decellularised pericardial scaffolds seeded with porcine SMCs at different cell densities at 3 days (a - c) and 1 week (d - i). (a, d, g) 2.5×10^4 cells·cm^{-2}; (b, e, h) 5×10^4 cells·cm^{-2}; (c, f, i) 1×10^5 cells·cm^{-2}. Following 3 days a low amount of cells was observed on the scaffold at the high density (c). After 1 week, the SMCs were observed to form a discontinuous layer at the middle density (e) and an almost continuous layer at the high density (f). Most of the cells at the low (g), middle (h) and high (i) densities were stained green. Arrows indicate cells. M: mesothelial surface. Scale bars indicate 200 µm. pSMCs; porcine SMCs.

5.5 Discussion

The studies described in this chapter aimed at verifying the phenotype of porcine fibroblasts and SMCs that were subsequently used in the seeding of decellularised pericardial scaffolds, and at investigating the cell density and static culture duration for the cell seeding of decellularised pericardial scaffolds prior to their dynamic conditioning under mitral-valve-relevant mechanical stimulation in a bioreactor. The results from the immunofluorescence staining confirmed the phenotype of fibroblasts and SMCs. Fibroblasts were strongly positive for vimentin and negative for α–SMA and desmin, in accordance to the literature (Rensen *et*

al., 2007; Wilcox *et al*., 2005). In addition, α-SMA, calponin and desmin are among the markers most commonly used to confirm SMC phenotype (Wilcox *et al*., 2005). The SMCs investigated in this study were all strongly positive for α-SMA and most of them were positive for calponin and desmin. Rensen *et al*. (2007) reported that the expression levels of the contractile marker proteins, such as α–SMA, calponin and desmin, gradually decrease when SMCs are cultured *in vitro*. This could explain the weak level of expression of calponin and desmin by the SMCs used in this study.

Identification of an acceptable cell seeding density and time is essential for the effective cellularisation of scaffolds. The seeding density has an effect on cell proliferation rates (Fossett and Khan, 2012); both too high and too low seeding densities might lead to cell senescence, affecting the proliferation and differentiation capabilities of cells (Hayflick, 1965). High cell density may also cause contact inhibition which can lead to lower growth rates (Mochizuki *et al.*, 2006), whereas low seeding densities may allow for a higher availability of nutrients per cell, improving cell growth (Both *et al.,* 2007; Lode *et al*., 2008). However, if the cell density is too low, it could take longer for the cells to populate the scaffold, and a high number of cell doubling times will be required, potentially leading to cell senescence. Van den Bos *et al*. (1998) reported that human MSCs undergo programmed cell death at low seeding densities. This could explain the high number of dead MSCs observed when seeded onto the pericardial scaffold at the low cell density in this study. MSCs isolated from porcine bone marrow have been used in previous studies for the population of decellularised porcine pericardial scaffolds under static conditions. Thomas *et al.* (2009) investigated the use of different MSCs densities, ranging from 1×10^4, 1×10^5 and 2×10^5 cells·cm^{-2}, at different time points to populate pericardial scaffolds produced by the same method as in the present study. Their findings showed that a cell density of 1×10^5 cells·cm^{-2} was the most favourable seeding density. This was in accordance to the results reported here, representing the lowest density at which the cells were capable of populating the scaffold and migrating through its thickness.

Bone marrow derived MSCs have been used in several studies for the production of tissue engineered constructs, including bone, cartilage, vascular grafts and heart valves (Ponticiello *et al.* 2000; Meinel *et al*. 2004; Wang *et al*. 2005; Vincentelli *et al.,* 2007). The affinity of bone marrow derived MSCs towards an osteogenic lineage might represent an issue when using these cells for cardiac tissue engineering. Yoon *et al.* (2004) reported that homologous MSCs, derived from the bone marrow of rats, caused myocardial calcification two weeks after

injection in rats with myocardial infarction. They reported that this was due to the high plasticity of bone marrow MSCs and the possible predilection for calcification in infarcted myocardium. The authors also suggested that during the isolation of the MSCs some bone precursor cells might have been isolated, since they used unselected MSCs. MSCs differentiation can be influenced by cell density which affects cell shape and cytoskeletal tension, guiding biochemical signalling (Mc Beath *et al.*, 2004). The optimum density of porcine bone marrow MSCs found in the present study (1×10^5 cells·cm^{-2}, corresponding to 3.533×10^5 cells·ml^{-1}) was lower compared to previous reports by Engelmayr *et al*. (2006), Hoerstrup *et al.* (2002) and Sutherland *et al*. (2005) for heart valve regeneration (8×10^6 cells·ml^{-1}, 4.5 to 5.5×10^6 cells·cm^{-2}; 4×10^7 cells·ml^{-1}, respectively).

Following 1 week in static culture, the SMCs showed a tendency to agglomerate on the surface of the scaffold rather than penetrating through its thickness. This result indicated the possible need for prolonged culture times, and the possible technical error in mixing and separating the cell suspension before seeding. Co-workers at iMBE have previously investigated the seeding density and culture time for porcine vascular SMCs and skin fibroblasts on pericardial scaffolds, and reported that SMCs seeded at a density of 5×10^4 cells·cm^{-2} required 2 weeks to fully populate the surface of the scaffold, whereas after 3 weeks the number of cells in the scaffold had decreased. Remuzzi *et al.* (2004) also observed a decrease in SMCs numbers over time in cellularising polymeric scaffolds at cell densities higher than those described in this study (3.75×10^5 and 3×10^6 cells·cm^{-2} and 2.5×10^4, 5×10^4 and 1×10^5 cells·cm^{-2}, respectively). The authors hypothesized that the loss of cells was the consequence of an increasing number of cells undergoing apoptosis. The SMC viability could potentially be improved by dynamic conditioning, as described by Jeong *et al.* (2004), who reported that shear stress could enhance tissue development and retention of contractile cell phenotypes.

Dermal fibroblasts have been used in various tissue engineered products for skin regeneration, such as Dermagraft (Advanced BioHealing, La Jolla, CA, U.S.A.) and Apligraf (Novartis, Basel, Switzerland) for the treatment of burns, chronic venous ulcers and several other clinical applications in dermatology and plastic surgery (Wong *et al*., 2007), and cells have been reported to enhance ECM deposition and wound healing. With regards to the fibroblasts used in the present study, coverage of the scaffold surface and initiation of cell infiltration was achieved after 1 week at a density of 2×10^5 cells·cm^{-2}. On the other hand,

MSCs reached confluence and initial infiltration after only 3 days and at a density of 1×10^5 cells·cm^{-2}. The longer time and higher cell density required for populating the scaffold with both fibroblasts and SMCs might have been related to the nature of the differentiated cells, which might have already been aged. Co-workers at iMBE have previously reported that at least 3 weeks were needed in order to fully populate decellularised porcine pericardial scaffolds with porcine dermal fibroblasts at a density of 5×10^4 cells·cm^{-2}. Previous studies by Masoumi *et al.* (2013b) and Weber *et al.* (2012) have reported higher dermal fibroblast densities (10×10^6 and 1.5×10^6 cells·cm^{-2}, respectively) for heart valve tissue engineering compared to the seeding density found in the present study (2×10^5 cells·cm^{-2}).

Chapter 6

Biaxial bioreactor description & calibration

6.1 Introduction

This chapter describes the procedure followed for the calibration and commissioning of the biaxial bioreactor, which was used for the dynamic conditioning of the cell-seeded pericardial scaffolds. Bioreactors represent one of the main components in the development of tissue-engineered heart valves *in vitro*. Heart valve bioreactors facilitate the dynamic conditioning of cell seeded scaffolds under valve-relevant mechanical stimulation, with a view to guiding the regeneration of tissue-engineered valves *in vitro*. The bioreactor system used in the present study for the engineering of mitral valve (MV)-leaflet-equivalents was able to simulate the mechanical environment that the native MV leaflets experience *in vivo*. In particular, the native MV apparatus is subjected to cyclic loading *in vivo*, which is characterised mainly by the inflation and deflation of the leaflets during the cardiac cycle (Nolan *et al.,* 1969).

The cyclic loading of heart valve leaflets, in general, can be decomposed into components of circumferential and radial stretch, compression, shear stress, and flexure (Berry *et al*., 2010). Several studies have investigated the influence of these loading components on cell seeded scaffolds (Jockenhoevel *et al*., 2002; Butcher *et al*., 2004, 2006; Englemayr *et al*., 2005, 2006, 2008; Ku *et al*., 2006; Merryman *et al*., 2007; Balachandran *et al*., 2009). Accordingly, several bioreactors have been reported in the literature, which have been designed to simulate one or more of the loading components experienced by heart valves *in vivo* (Zeltinger *et al*., 2001; Weston and Yoganathan, 2001; Dumont *et al*., 2002; Hildebrand *et al*., 2004; Mol *et al*., 2005; Lichtenberg *et al*., 2006; Karim *et al*., 2006; Syedain and Tranquillo, 2009). The majority of bioreactors reported in the literature have the capacity to simulate either one of the loading components experienced by the heart valve apparatus, or the whole haemodynamic environment of the heart valve, as in the case of the aortic valve. The complex geometry and, indeed, the complex haemodynamics of the MV apparatus, make it difficult to simulate the local haemodynamic environment of the MV apparatus for tissue engineering purposes. This is especially the case, when engineering a construct for replacing/repairing an individual component of the MV apparatus, such as the MV leaflets.

The present study employed a bioreactor that was able to exert variable biaxial strain and flexure on cultured constructs, representative of the cyclic inflation-deflation experienced by the native MV leaflets *in vivo.* Moreover, the present study employed physiological levels of strain for the conditioning of the cell-seeded pericardial scaffolds. Specifically, the cell-seeded scaffolds were conditioned under the maximum strain experienced by the native anterior MV leaflets during the cardiac cycle *in vivo*, which was obtained through finite element (FE) computational models of the whole MV apparatus, using a physiological MV geometry and input pressures (Roberts, 2012). In addition to relevant and highly controllable mechanical stimulation, the bioreactor system used also provided control over a number of additional parameters, including culture medium temperature, pH and oxygen tension, which are fundamental for the appropriate function of the cells seeded onto the scaffold.

6.1.1 Aims and objectives

Aims:

The aims of the work presented in this chapter were to calibrate and commission the biaxial bioreactor, which was subsequently used for the dynamic conditioning of cell-seeded pericardial scaffolds.

Objectives:

- To set up the bioreactor in order to exert MV-leaflet-relevant biaxial strain fields to the conditioned constructs under cyclic conditions
- To calibrate the main components of the bioreactor system
- To develop the general methodology for conditioning and culturing the cell-seeded scaffolds in the bioreactor under aseptic conditions.

6.2 Description of the biaxial bioreactor system

The bioreactor system used for the dynamic culture of cell-seeded pericardial scaffolds was designed and constructed in iMBE by Dr Sotirios Korossis and Mr Lee Wetherill, respectively. The system was designed to mimic the biaxial loading that the native MV leaflets experienced *in vivo*. The bioreactor comprised four main parts, including: i) a linear actuator, which provided the mechanical stimulation exerted to the construct; ii) four construct stations, which

housed the cell-seeded scaffolds; iii) a chemostat system, which conditioned the culture medium in terms of temperature, pH and oxygen partial pressure (pO_2).

The electric linear actuator (Industrial Devices Ltd, UK; model N2-T31-10-05B-4-MF3-FT1M-2PSR) was connected to a programmable single-axis digital stepper controller (Industrial Devices Ltd, UK; model SmartStep23), through which the desired cycling rate, stroke volume and waveform of the actuator could be set. A schematic of the linear actuator connected to the bioreactor chamber is shown in Figure 6.1. A piston, which was connected to the linear actuator, pushed the water inside the bioreactor chamber (Figure 6.1), generating a cyclic volume displacement within the bioreactor chamber. This volume displacement caused, in turn, the cyclic inflation/deflation of the silicone rubber diaphragms mounted at the bottom of each of the four bioreactor stations (Figure 6.1) which also acted as an impermeable barrier to maintain sterility of the culture medium in the chambers. The cyclic inflation/deflation of the silicone rubber diaphragms caused, in turn, the generation of a volume displacement of the culture medium in the lower part of the bioreactor stations and a synchronous inflation/deflation of the pericardial scaffolds mounted between the lower and upper parts of the stations (Figure 6.3). The stations were positioned symmetrically on top of the bioreactor chamber and, therefore, the volume displacement produced by the actuator was divided equally between the four stations. In order to generate the necessary volume displacement of water in the bioreactor chamber to accommodate the four bioreactor stations, an increased diameter piston head was used, the frictionless motion of which was supported by a rolling diaphragm inflated by pressurised air. The deformation of the scaffolds in the bioreactor stations duplicated the deformation of the MV leaflets *in vivo*, characterised by inflation during systole and deflation during diastole. The deformation of the MV leaflets during the cardiac cycle is shown in Figure 6.2. Although the actuator controller was able to generate a range of different waveforms, a simple (non-physiological) sinusoidal waveforms, with a frequency of 1Hz, was chosen for the operation of the bioreactor in order to simplify the experiments and to limit the study to the effect of the physiological strain magnitude on the cell seeded scaffolds.

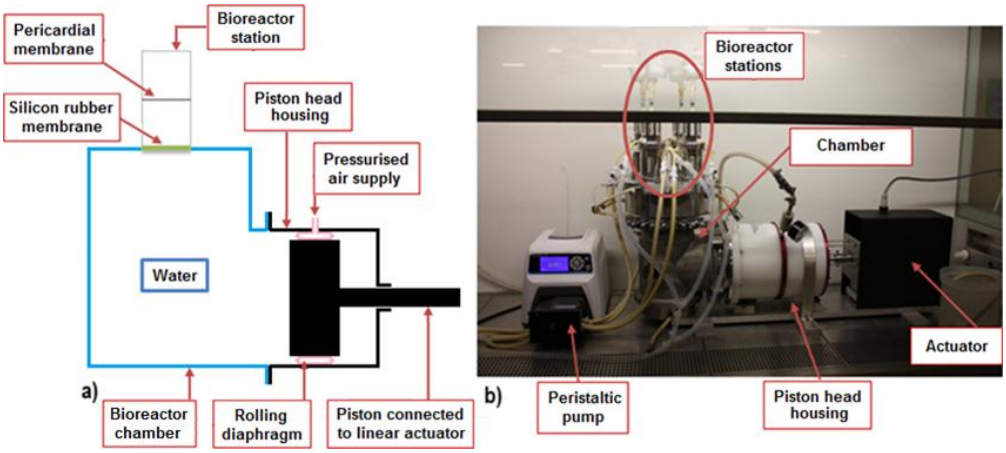

Figure 6.1: Schematic (a) and photograph (b) of the actuator connected to the bioreactor chamber.

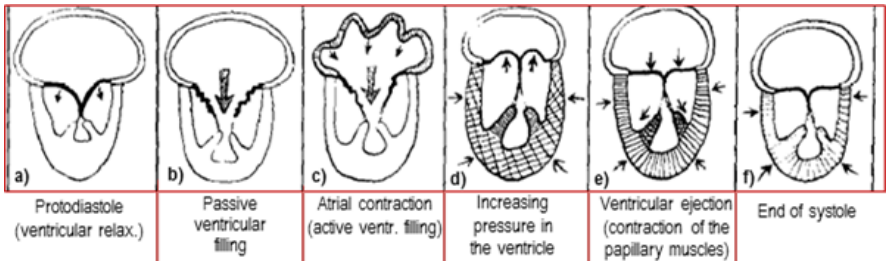

Figure 6.2: Schematic of the deformation of the MV leaflets *in vivo*. Adapted from Nolan *et al*. (1969).

The bioreactor was able to accommodate four cell-seeded scaffolds at the same time; one in each station. Each station comprised an upper and lower part and a central disk onto which the pericardial membrane was loaded. The set-up of the bioreactor stations is illustrated in Figure 6.3. The parts of each station were interconnected via silicone tubing (Figure 6.3b), and also featured viewing ports for inspection of the culture medium and cell-seeded scaffolds during culture. Following preliminary trials, the initial design of the bioreactor stations was improved by adding a stopcock and a tube open to the atmosphere, in order to control the direction of the flow of the culture medium and to allow for better aeration during medium filling. The diameter of the circular sample loaded on the central disk of each station was 4.6 cm, however the effective diameter of the scaffold (following mounting) that was mechanically stimulated was 3 cm (Figure 6.3d).

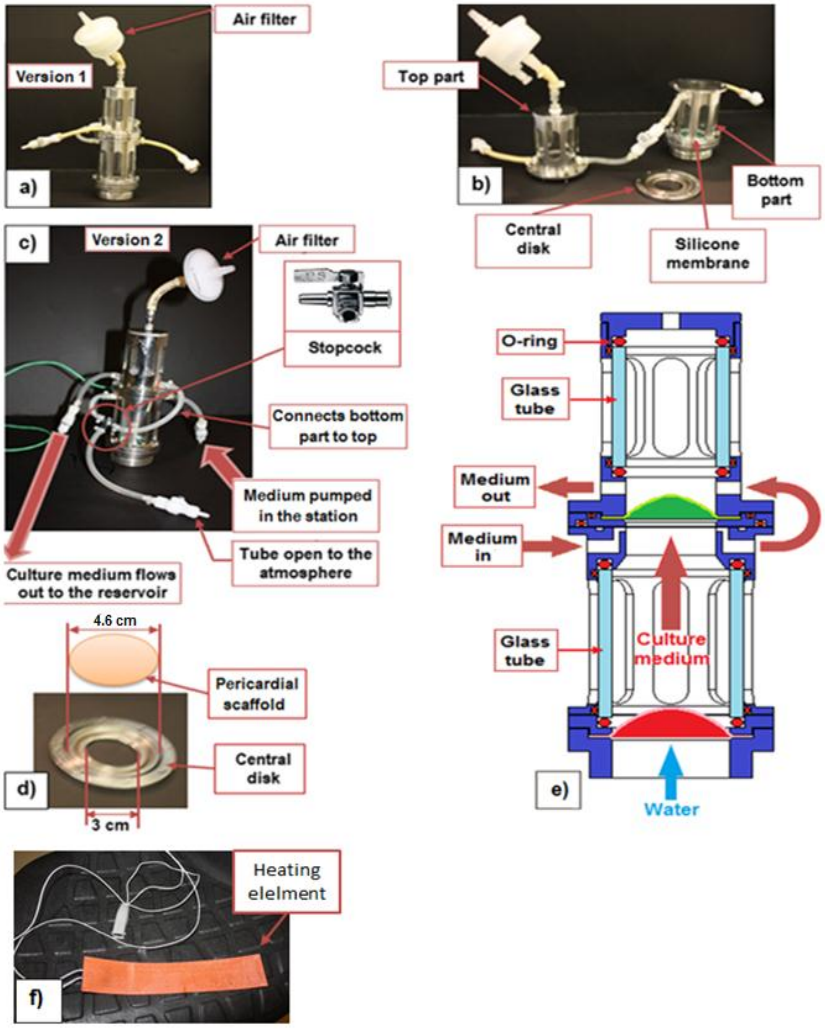

Figure 6.3: Setup of the bioreactor stations. The first version of the stations (a, b) was improved by adding a tube open to the atmosphere together with a stopcock in order to allow for a better release of the air trapped in the station (c). The scaffold was loaded on the central disk, which was then clamped between the upper (top) and lower (bottom) parts. The medium was pumped into the lower part of the station and overflowed into the upper part. It then flowed out of the station into a collection reservoir (c). (e) Station cross-section showing the scaffold stimulation principle (green: scaffold; red: silicone rubber membrane). (f) Image of the silicone rubber heating element which was wrapped around each bioreactor station.

The circulation of the culture medium in the bioreactor system is illustrated in Figure 6.4. The culture medium was conditioned in a 2 L autoclavable chemostat vessel (Applikon Biotechnology, UK), attached to an ADI 1010 Bio Controller and ADI 1025 Bio Console (Applikon Biotechnology, UK). In the chemostat the medium was maintained at pH 7.2 - 7.4, and pO_2 21%. A heating element, wrapped around the chemostat vessel, and controlled by

the Bio Controller, was used for temperature control. A stirrer attached to the vessel, provided continuously stirring of the medium at 100 rpm. Following mounting the cell-seeded scaffolds into the bioreactor stations, culture medium was pumped from the chemostat into the lower parts of the bioreactor stations using a four-channel peristaltic pump (Multichannel pump 7536-04, Cole parmer). Culture medium was pumped into the stations until it completely filled the lower parts of the stations and overflowed into the upper parts through side ports (Figure 6.3c). From there, the medium was allowed to freely flow out of the upper parts of the stations, through a side port, into a collection reservoir, assisted by gravity (as shown by the thick red arrows in Figure 6.3c). From the collection reservoir, the culture medium was pumped back into the chemostat vessel using a single-channel peristaltic pump (Easy load II77200-50, Cole parmer). The culture medium perfusion rate between the chemostat and the stations was balanced so that a constant culture medium level was maintained in both the chemostat vessel and the bioreactors stations. The temperature in the chemostat was maintained at 42ºC, as described in Section 6.5.

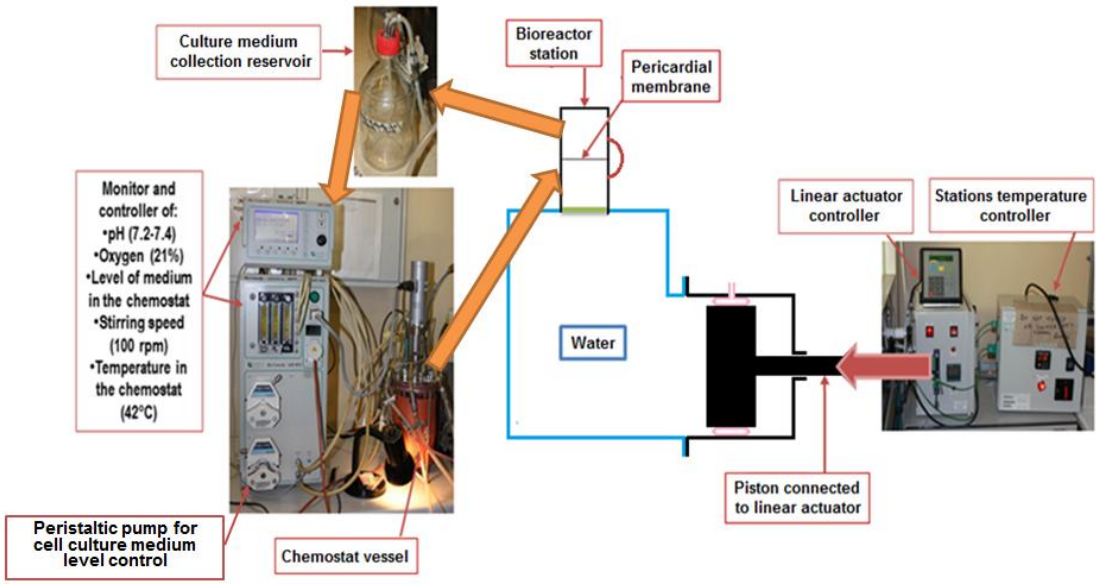

Figure 6.4: Schematic of the culture medium circulation in the bioreactor system. The culture medium was pumped from the chemostat vessel to the lower part of each bioreactor station using a four-channel peristaltic pump. Once the lower part of the stations was full, the medium flowed over to the upper part of the stations, before it was allowed to overflow out of the upper parts and into the collection reservoir, assisted by gravity. From the collection reservoir, the medium was driven back to the chemostat vessel using a single-channel peristaltic pump.

The temperature of the culture medium in the bioreactor stations was controlled by using a thermocouple attached to one of the bioreactor stations and 4 silicone rubber heating elements (Fig. 6.3f) wrapped around the four bioreactor stations (one for each station). The silicone-rubber heaters and thermocouple were connected to a temperature controller (Eurotherm, UK; Model 3216). The autoclavable thermocouple was fitted into the lower part of one of the stations and was in direct contact with the culture medium. The culture medium temperature in the other three stations was assumed to be equal to the temperature of the station fitted with the thermocouple (see Section 6.5). During the experiments, the temperature controller was set to maintain a culture medium temperature of 37ºC in all stations.

6.3 Correlation of bioreactor actuator stroke to scaffold strain

Prior to conditioning of the cell-seeded scaffolds, the bioreactor actuator required calibration in terms of the strain it exerted on the scaffolds. Specifically, the stroke (piston displacement) of the actuator required correlation to the volume displacement of water in the bioreactor chamber and this, in turn, to the strain experienced by the scaffolds in the bioreactor stations. Previous FE simulations of the whole MV apparatus, which were based on the physiological geometry and pressure conditions of the MV apparatus, predicted that the central regions of the anterior MV leaflets experienced a maximum tensile strain magnitude of around 10% (Roberts, 2012). Thus, the value of 10% tensile strain was chosen for the conditioning of the cell-seeded pericardial scaffolds.

In order to obtain the relationship between the stroke of the actuator and the strain imposed onto the pericardial scaffolds, the deformed shape of the scaffolds was assumed to approximate a spherical cap (Figure 6.5). Since the deformation of the scaffolds was caused

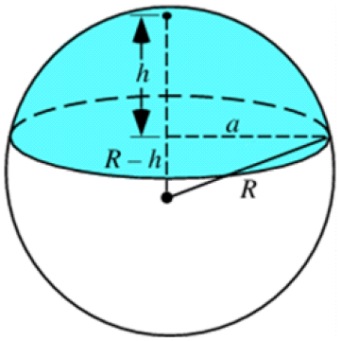

Figure 6.5: Deformed shape of the pericardial scaffold under the assumption of approximating a spherical cap. The blue coloured volume represents the stroke volume per bioreactor station (v_{cap}).

by the volume displacement (stroke volume) of the actuator, the volume enclosed by the spherical cap (V_{cap}) of each deformed scaffold mounted in each of the four bioreactor stations, corresponded to the volume per station displaced by the actuator. Therefore, the strain imposed onto the scaffolds was a function of the actuator stroke volume. The volume of the spherical cap (V_{cap}) was calculated according to:

$$V_{cap} = \frac{1}{6}\pi \times h \times (3\alpha^2 + h^2)$$

where α was the base radius (equal to 15 mm) and h the height of the spherical cap (Figure 6.5). The actuator stroke necessary to exert the required stroke volume (V_{cap}) at all four stations was calculated according to:

$$\text{Stroke} = \frac{V_{cap} \times \text{No of stations}}{\text{Piston head area}}$$

where *Piston head area* was the area of the piston head of the actuator equal to 167.44 cm^2, and *No of stations* the number of bioreactor stations in the system equal to 4. The relation between α, h and R (radius of the sphere) was obtained by the Pythagorean Theorem:

$$(R - h)^2 + \alpha^2 = R^2 \rightarrow R = \frac{(h^2 + \alpha^2)}{2h}$$

Considering the 2D representation illustrated in Figure 6.5, the length of the arc AB represents the deformed (stretched) length of the scaffold. The length of the arc AB was calculated according to:

$$\text{Arc length AB} = R \times 2\theta$$

the angle θ was calculated according to:

$$\sin\theta = \frac{\alpha}{R} \rightarrow \theta \equiv \sin^{-1}\frac{\alpha}{R} \quad (\theta \text{ in radians})$$

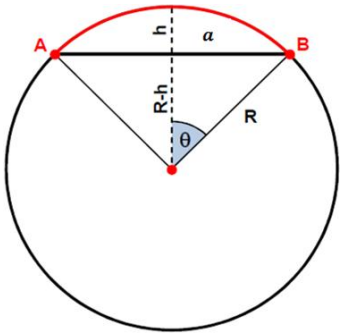

Figure 6.6: Arc length (AB) of the deformed pericardial membrane.

Therefore, the approximated engineering tensile strain in the pericardial scaffold was calculated according to:

$$\varepsilon = \frac{\text{Deformed length - Original length}}{\text{Original length}} = \frac{\text{Arc length AB - } 2\alpha}{2\alpha} \times 100\%$$

Based on the above formulation, the engineering tensile strain, stroke volume per station (V_{cap}), and actuator stroke were calculated for different values of h. These results are illustrated in Table 6.1. The table highlights the stroke volume per station and actuator stroke required to produce 10% strain in the cell-seeded scaffolds. The volume per station required to produce 10% strain was calculated to be 2.19 ml, and the corresponding actuator stroke was 0.52 mm.

h (mm)	R (mm)	θ (radians)	Arc length (mm)	Strain (%)	Stroke Volume (ml)	Stroke (mm)
5.00	25.00	0.64	32.18	7.25	1.83	0.44
5.10	24.61	0.66	32.26	7.54	1.87	0.45
5.20	24.23	0.67	32.35	7.83	1.91	0.46
5.30	23.88	0.68	32.44	8.13	1.95	0.47
5.40	23.53	0.69	32.53	8.43	1.99	0.48
5.50	23.20	0.70	32.62	8.73	2.03	0.49
5.60	22.89	0.71	32.71	9.05	2.07	0.49
5.70	22.59	0.73	32.81	9.36	2.11	0.50
5.80	22.30	0.74	32.91	9.69	2.15	0.51
5.90	**22.02**	**0.75**	**33.00**	**10.01**	**2.19**	**0.52**
6.00	21.75	0.76	33.10	10.35	2.23	0.53

Table 6.1: Numerical correlation between h, R, θ, ε, stroke volume per station and stroke.

6.4 Calibration of the linear actuator

Prior to operation, the linear actuator was calibrated in terms of correlating the actuator controller setting to the actual displacement (stroke) of the actuator piston. For this purpose,

the actuator connected to the piston head (Figure 6.1) was detached from the bioreactor system. During calibration, the actuator controller was set to produce a cycling rate of 1 Hz and a speed of 1 mm·s^{-1} of the actuator piston, as well as five different actuator stroke settings ranging from 0.5 to 1.5 at 0.25 intervals. At each setting, the displacement (stroke) of the actuator was measured three times using callipers and averaged. These results are presented in Table 6.2. The plot showing the linear relationship between the controller setting and the measured actuator stroke is illustrated in Figure 6.7.

Controller setting	Stroke (mm)
0.50	0.11
0.75	0.37
1.00	0.63
1.25	0.90
1.50	1.15

Table 6.2: Calibration of the actuator controller setting with respect to the actual actuator stroke amplitude.

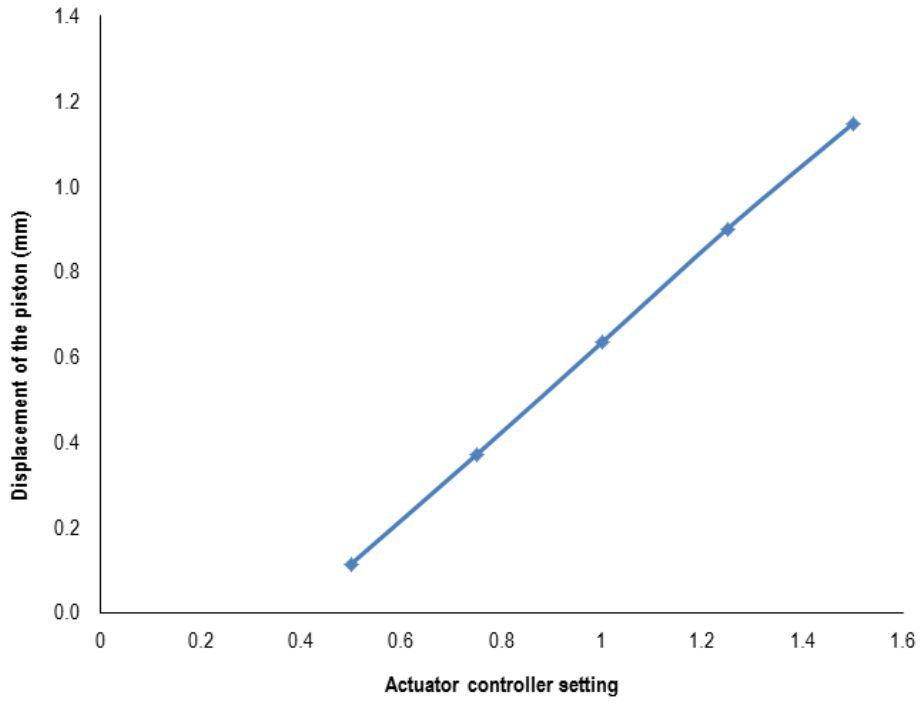

Figure 6.7: Calibration plot of the measured actuator stroke against the controller setting.

Having obtained the calibration plot that correlated the controller setting to the actual stroke produced by the actuator, the controller setting that corresponded to the actuator stroke of 0.52 mm (as calculated in Section 6.3), required to produce a strain of 10% in the cell-seeded scaffolds was calculated. For this purpose, linear regression was performed to the controller

setting against the actuator stroke data (Table 6.2, Figure 6.7), with a view to obtaining the mathematical relationship between the two parameters. The linear regression returned an equation of the form:

$$y = mx + q \rightarrow \text{Stroke} = 1.04 \times \text{Controller setting} - 0.41$$

with a regression correlation coefficient $R^2 = 0.9999$. Using the above equation, the controller setting for a stroke of 0.52 mm was calculated as:

$$\text{Controller setting} = \frac{\text{Stroke} + 0.41}{1.04} = \frac{0.52 + 0.41}{1.04} = 0.89$$

Therefore, using a controller setting of 0.89 for the actuator stroke, which corresponded to an actuator stroke amplitude of 0.52 mm, and a frequency of 1 Hz, the actuator was set to produce the following stroke waveform:

$$\text{Stroke}(t) = \frac{\text{Stroke}_{\text{amplitude}}}{2} \times \left[1 - \sin\left(2\pi t + \frac{\pi}{2}\right)\right]$$

The graphical representation of the actuator stroke over time is illustrated in Figure 6.8.

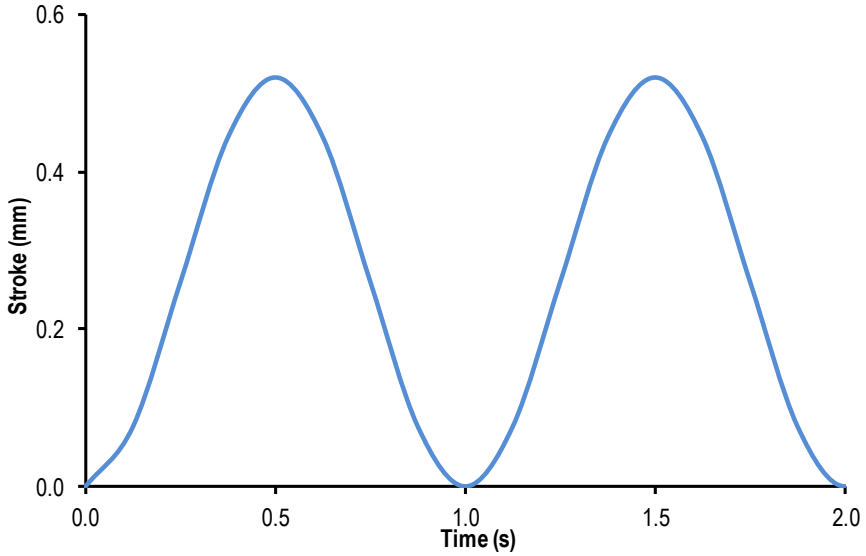

Figure 6.8: Actuator stroke waveform used for the conditioning of the cell-seeded pericardial scaffolds (two cycles).

6.5 Calibration of the heating system and peristaltic pump

During both static and dynamic culture experiments, the culture medium temperature within the bioreactor stations was maintained at 37ºC. In order to achieve this, the heating system of

the bioreactor was calibrated. For this purpose, the chemostat vessel was filled with distilled water and connected to the bioreactor station which was fitted with the thermocouple. The station was not fitted with its heating wrap. The chemostat vessel was wrapped with its silicone heater and the temperature was raised to 42°C. Temperature-conditioned water was then perfused from the chemostat vessel to the bioreactor station using one of the channels of the four -channel peristaltic pump at a rate of 10 ml·min^{-1}. During the perfusion of water, the temperature in the bioreactor station was monitored. The water temperature in the station stabilised at 26.4°C, indicating a temperature drop of 15.6 °C between the chemostat and the station, probably due to the length of the tubing, which was not insulated. Subsequently, the station was wrapped with its heating element, and the heating controller was set to 37°C. The temperature of the chemostat vessel remained set at 42°C, to ensure that the medium in the stations would stabilised at 37°C relatively quickly. Using the selected perfusion rate of 10 ml·min^{-1}, the water temperature in the station stabilised at 37°C after 5 to 10 min. The additional three stations were then mounted in the bioreactor and wrapped with their heating elements, which were also connected to the heating controller. The three stations were also connected to the chemostat vessel and water was perfused to all four stations using the four-channel peristaltic pump at a rate of 10 ml·min^{-1}. After the water was perfused for 10 min, the water temperature in the stations was measured manually using a thermometer. All stations reached a temperature of 37°C ± 0.3°C.

In order to ensure that the four-channel peristaltic pump was running at an actual perfusion of 10 ml·min^{-1}, an empty universal was weighed (14.5 g) and then filled with water, which was pumped at a set rate of 10 ml·min^{-1} for 1 min, using the same silicone tubing (Masterflex) as in the experiments. After 1 min the peristaltic pump was stopped and the universal was weighed again (24.14 g). The volume of water collected after 1 min was equal to 9.63 ml. A second pump was used to return the culture medium from the medium collection reservoir to the chemostat vessel. During the bioreactor cultures, this pump was controlled by the chemostat controller and the level probe fitted in the chemostat vessel, which was maintaining a constant culture medium level in the chemostat vessel.

6.6 Chemostat sterilisation, set-up, calibration and culture medium loading

Prior to operation, the bioreactor stations and the chemostat vessel (Figure 6.9) including all the culture-medium-contacting components (pO_2 probe, pH probe, stirrer propeller) and

ventilation filters, together with the silicone tubing, were sterilised by autoclaving at 121°C and 15 lb. sq. in.

Bioreactor stations sterilisation

Prior to autoclaving, the bioreactor stations, upper and lower parts, central disk and tubes, were washed with 1% (v/v) Trigene (Figure 6.3a, b and c). All of the air filters were taken off the system during washes. The various parts of the bioreactor stations were then rinsed with running tap water until clear. The parts were then air-dried on the bench, and the air filters were assembled back in their correct position. Following air drying, the upper part of each station was screwed to the central disk and the lower part. All the ends of the quick connectors were covered with double layers of tin foil and fixed with autoclave tape, including the air filters and the lower part of each station which were covered with only one layer of tin foil and fixed with autoclave tape. Each station was finally put in an autoclave bag which was folded twice and fixed with autoclave tape. The bioreactor stations were left to completely dry in a 45°C drying room for 1 week after autoclaving.

Chemostat vessel sterilisation and calibration

The pH probe of the chemostat vessel was calibrated before autoclaving using pH standard solutions at pH 4 and 7. The values were taken when the reading reached a steady state. The values of pH were related to specific values of voltage. Prior to autoclaving, the chemostat vessel connected to the reservoir and the tubes and bottles used for the cell culture medium loading procedure, were washed with 1% (v/v) Trigene. The various parts of the system were then rinsed with two washes of distilled water. A few millilitres of distilled water were left at the bottom of the chemostat to help the steam penetrate throughout all the tubes and bottles connected to the chemostat during the autoclaving process and to avoid drying of the pH probe. All the ends of the quick connectors were covered with double layers of tin foil and fixed with autoclave tape, including the air filters, which were covered with only one layer of tin foil. The chemostat vessel together with the various tubes and bottles was autoclaved once. Following autoclaving, the equipment was stored at room temperature for 1 week to dry, prior to loading the culture medium and calibrating the pO_2 probe. After the drying period, the pO_2 and pH probes, attached to the chemostat vessel, were connected to the chemostat controller, and the gas inlet of the chemostat vessel was connected to the gas supply via a filter. In addition, the water inlet and outlet of the condenser, attached to the headplate of the

chemostat vessel, were also connected to the water supply and drainage, respectively, of the chemostat control unit (Figure 6.9). The chemostat vessel was then filled with 2.5 L of culture medium using a peristaltic pump, and wrapped with its silicone-rubber heater, which was connected to the chemostat controller. The thermocouple (PT100) monitoring the temperature in the vessel was also connected to the controller and then inserted inside a closed-end stainless steel sleeve, which was immersed in the chemostat vessel and its outer surface was in contact with the culture medium. Finally, the motor of the stirrer was attached to the chemostat vessel headplate and the stirrer was set running at 100 rpm.

For all bioreactor studies involving cell-seeded scaffolds, the cell culture medium (Chapter 2, Section 2.5.4) was supplemented with 10 $ml \cdot L^{-1}$ of antifungal (amphotericin B). Initially, the cell culture medium was left in the chemostat vessel at 37°C for 3 days prior to the commencement of an experiment and its sterility was assessed by visual inspection of its transparency. If the culture medium in the chemostat was still transparent, the FBS was added to the medium on the day of the experiment.

On the day of the commencement of the bioreactor experiments, the temperature in the chemostat vessel was raised to 42°C and the pO_2 was calibrated. Prior to calibration, the pO_2 probe was left to equilibrate in the culture medium for at least 12 hours. The calibration was performed between 0% and 21% pO_2. The 0% pO_2 was set by pumping 100% N_2 into the chemostat vessel through the sparger fitted at the bottom of chemosat vessel, and the 21% pO_2 which was also used during the bioreactor cultures, was set by pumping 5% CO_2 in air. During the experiments in the bioreactor, the level probe was switched on, and 5% (v/v) CO_2 in air was continuously pumped through the system at a flow rate of 0.1 $L \cdot min^{-1}$, to maintain a pH value of 7.4 and a pO_2 level of 21%.

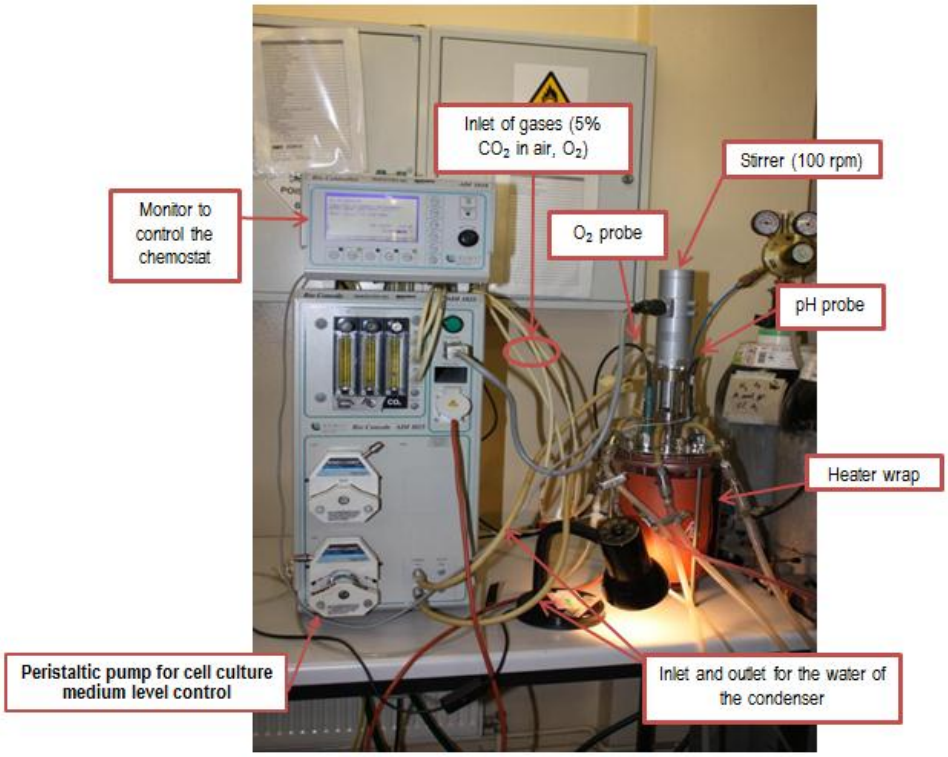

Figure 6.9: The chemostat system with its vessel loaded with culture medium.

6.7 Discussion

This chapter described the design, set up and calibration of the biaxial strain bioreactor used in this project for the conditioning of cell seeded pericardial scaffolds. The bioreactor was calibrated in order to exert a tensile strain value of 10% at a frequency of 1 Hz to the cultured tissues under a mode of cyclic inflation/deflation. The tensile strain of 10% was chosen as being representative of the maximum physiological strain experienced by the MV leaflets during the cardiac cycle, obtained through computational modelling of the MV apparatus (Roberts, 2012). Dynamic flexure induced by cyclic inflation/deflation has been reported as being the major mode of deformation of heart valve leaflets (Vesely *et al.*, 1989).

Several studies have focused on the use of cyclic flexure for the development of tissue engineered heart valves. Engelmayr *et al.* (2003) developed a bioreactor to study the effects of uniaxial cyclic flexure on the stiffness of non-cell-seeded polyglycolic acid (PGA) scaffolds. This bioreactor used a linear actuator to exert dynamic flexural deformation on the samples at 1 Hz in order to emulate the cardiac cycle. Their finding indicated that dynamically flexed scaffolds were 72% (after three weeks) and 76% (after five weeks) less stiff than static controls and that they developed directional anisotropy after 3 weeks of conditioning. These

results suggested that dynamic flexure can produce significant changes in the mechanical properties of scaffolds. The same system was used by the same group in an additional study with ovine SMCs seeded on PGA and poly-L-lactic acid (PLLA) scaffolds (Engelmayr *et al*., 2005). Seeded and unseeded scaffolds were subjected to cyclic uniaxial three-point flexure at 1 Hz and amplitude of 6.35 mm for up to 3 weeks. They reported that cyclic flexure increased stiffness, collagen production, and transmural cell distribution compared to static controls.

In another study, Engelmayr *et al.* (2006) investigated the effects of cyclic flexure and laminar flow on PGA and PLLA scaffolds seeded with ovine MSCs and conditioned in a flex-stretch-flow bioreactor for 1 and 3 weeks. The laminar flow was provided by culture medium recirculation within the bioreactor, whereas cyclic flexure was applied at 1 Hz and a curvature of 0.554 mm^{-1}. This value of curvature was obtained from a previous study on the opening and closing of trileaflet heart valves *in vitro* (Iyengar *et al*., 2001). The results from this study suggested that cyclic flexure and laminar flow could accelerate tissue formation within the cell seeded scaffolds. Merryman *et al.* (2007) investigated the influence of both biomechanical (cyclic tension) and biochemical factors on the phenotype and collagen biosynthesis of aortic valve interstitial cells by applying cyclic tension (15%) and transforming growth factor beta-1 (TGF-β1). The choice of the tension magnitude was based on a previous study by Billiar and Sacks, (2000), which measured the physiological range of tension in aortic valve cusps. The study suggested that the presence of TGF- β1 and cyclic mechanical stimuli *in vivo* might lead to altered ECM architecture, compromised valve function, and ultimately degenerative valvular disease.

Other studies have reported the use of similar strain values to the one used in the present study (10%). Balachandran *et al.* (2009) used the same bioreactor described by Engelmayr *et al.* (2003) to stimulate rectangular samples of porcine aortic cusps under cyclic tensile stretch at three levels of strain, including 10% (physiological; Thubrikar *et al*., 1980), 15% (pathological/hypertensive), and 20% (hyperpathological/severely hypertensive) at 1.167 Hz (70 beats/min), for 24 and 48h. The study investigated whether the elevated cyclic stretch could cause increased expression and activity of proteolytic enzymes in the valve cusp. The results indicated an altered cell turnover and increased expression of metalloproteinase and cathepsin, potentially leading to valve degeneration. In another study, Gupta *et al.* (2008) seeded collagen gels with MV interstitial cells or chordal cells and subjected them to 10% strain at 1.167 Hz for 24 h, followed by a static phase (relaxation) for 24 h. The results

showed that GAG secretion was significantly upregulated during cyclic stretch and downregulated during relaxation.

Chapter 7

Bioreactor cultures

7.1 Introduction

Prior to the dynamic conditioning of the decellularised cell-seeded pericardial scaffolds in the biaxial strain bioreactor, it was necessary to optimise the culture conditions in terms of oxygen supply, pH and temperature maintenance, tissue sterility and cell viability. This chapter describes the series of experiments performed during the optimisation of the static cultures, as well as the results from short-term (1 day) dynamic conditioning of decellularised pericardial scaffolds seeded with porcine mesenchymal stem cells (pMSCs). Initially, fresh porcine pericardia were cultured under static conditions in the bioreactor stations and in separate tissue holders, in order to optimise the static culture in terms of pO_2, pH and temperature. Subsequently, decellularised pericardia were seeded with pMSCs and cultured in the bioreactor under static and then 10% dynamic strain with a view to investigating the effect of this strain on the cell viability in the construct. Pericardial scaffolds seeded with pMSCs were also maintained in static culture, in both the bioreactor and in separate tissues holders, and used as controls.

7.1.1 Aims and objectives

Aims:

The aim of the work presented in this chapter was to investigate the static and dynamic culture of decellularised pericardial scaffolds seeded with pMSCs, and to investigate the effect of 10% cyclic biaxial strain on the viability of the pMSCs.

Objectives:

The specific objectives were to:

- Investigate the disinfection of fresh porcine pericardium using Cambridge antibiotic solution
- Investigate the static culture of fresh pericardium under sterile conditions

- Investigate the static and dynamic culture of cell-seeded pericardial scaffolds in the biaxial bioreactor under sterile conditions
- Investigate the effect of 10% dynamic strain on pMSC-seeded decellularised pericardial scaffolds.

7.2 Disinfection of fresh pericardium

Studies of the static culture conditions were firstly carried out using fresh pericardium. Therefore, it was necessary to ensure that the fresh pericardium was not contaminated with microbes that might affect the cell viability of the fresh tissue obtained from the abattoir. Cambridge antibiotic disinfection solution was used since it is the one most frequently used in tissue banks in the UK. The cell viability of the tissue treated with this solution was determined by the MTT assay (Chapter 2, Section 2.15).

7.2.1 Materials and methods

7.2.1.1 MTT assay validation

The MTT assay was performed and validated as described in Chapter 2, Section 2.15 and 2.15.1, respectively. The amount of tissue to be used was chosen on the basis of the standard absorbance curve (Section 7.2.2.1).

7.2.1.2 Cambridge antibiotic treatment

Fresh porcine pericardia were treated in Cambridge antibiotics for 3 different durations (30 min, 1 and 2 h) to investigate the optimal time for effectively disinfecting the tissue without affecting its cell viability. The Cambridge antibiotics solution was supplied by the NHS Blood & Transplant Tissue Bank, Speke, Liverpool, UK. This antibiotic solution comprised of i) medium 199 ii) HEPES (14.7 $g \cdot L^{-1}$; Sigma M2520), iii) vancomycin HCl USP (0.2 $g \cdot L^{-1}$; Sigma V8138), iv) polymyxin B sulphate (0.2 $g \cdot L^{-1}$; Sigma P0972), v) nystatin (2.5 million units $\cdot L^{-1}$; irradiated), vi) imipenem/cilastatin sodium (0.25 $g \cdot L^{-1}$), vii) gentamicin sulphate (4 $g \cdot L^{-1}$).

7.2.1.3 Tissue disinfection

Thirty-six fresh porcine pericardial tissue samples with a size of 9 x 6 cm^2 were dissected, (Chapter 2, Section 2.8), providing 12 samples for each duration of antibiotic treatment (30

min, 1 and 2 h). For each time, 3 samples were treated at 37° C in 60 ml each of Cambridge antibiotics; 3 were processed for MTT assay immediately after dissection (positive control at 0 min treatment); 3 were kept in 60 ml each of cell culture medium at 37°C (positive control) and 3 in 60 ml each of 10% (v/v) NBF (negative control) at 37°C. Triplicates of tissue weighing 50 mg (wet weight) were used for each pericardium of each group for MTT assay. In addition, one piece of tissue (5 mm^2) of each of the pericardial samples treated in Cambridge antibiotics was cut prior and after treatment and processed for sterility assessment, as described in Chapter 4, Section 4.2.2.4.

7.2.2 Results

7.2.2.1 MTT assay validation

Following the MTT assay, the absorbance was read at 570 nm with a reference filter at 630 nm and plotted against the corresponding weights of fresh pericardial samples (Figure 7.1). For weights above 100 mg, the optical density decreased. Thus, it was decided to perform a dilution of 1 in 2 in order to investigate whether the decrease was related to a high signal from the samples weighing more than 100 mg. The results after the dilution showed that the values of optical density above 100 mg still decreased; there was a plateau between 100 and 150 mg and then the optical density decreased (Figure 7.2). The decrease in absorbance for samples weighing above 100 mg was probably related to the large amount of tissue, which did not allow for adequate permeation of the MTT solution throughout the inner mass of tissue. Thus, only the optical densities corresponding to sample weights between 0 and 100 mg were included in the final standard absorbance curve (Figure 7.3). A tissue weight of 50 mg was chosen for subsequent experiments.

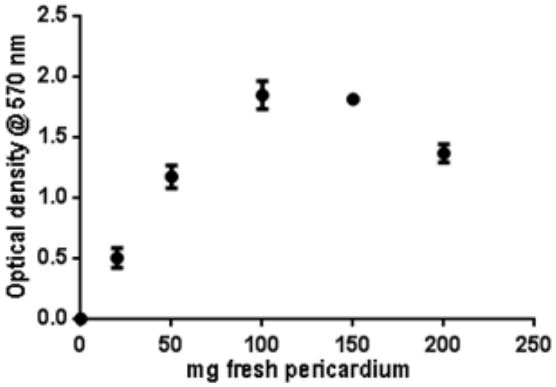

Figure 7.1: Optical density against wet weight (mg) of fresh pericardial samples following MTT assay. Data expressed as means (n=3) ± 95% C.I.

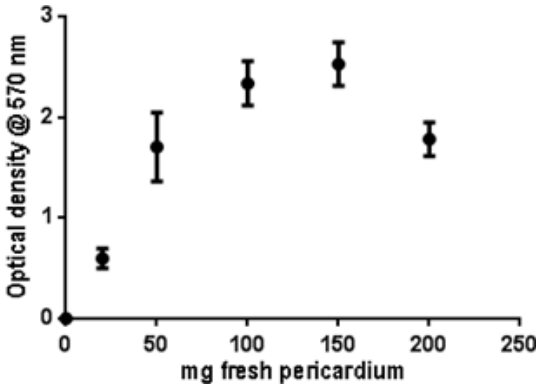

Figure 7.2: Optical density after 1 in 2 dilution against wet weight (mg) of fresh pericardial samples following MTT assay. Data expressed as means (n=3) ± 95% C.I.

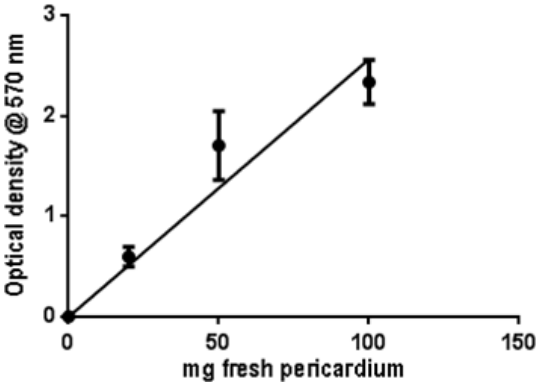

Figure 7.3: Standard curve of optical density vs wet weight of tissue for the MTT assay. Data expressed as means (n=3) ± 95% C.I.

7.2.2.2 Tissue disinfection

Following treatment with the Cambridge antibiotics solution for different durations (30 min, 1 h and 2 h), the fresh pericardial samples were assayed for cell viability using the MTT assay and the absorbance was read at 570 nm with a reference filter at 630 nm. The optical density values of the test and control groups are illustrated in Figure 7.4, 7.5 and 7.6.

After 30 min treatment in Cambridge antibiotics, fresh pericardial tissue were sterile; no significant difference was observed between the levels of MTT conversion by the fresh pericardium treated in Cambridge and both fresh pericardium treated in cell culture medium (positive control) and fresh pericardium processed immediately after dissection (positive control at 0 min treatment), as shown in Figure 7.4. Fresh pericardium treated in 10% (v/v) NBF (negative control) showed significantly lower levels of MTT conversion compared to all the other groups ($p < 0.05$; MSD = 0.005).

Similar observations were apparent following 1 h treatment of the pericardium ($p < 0.05$; MSD = 0.002), as shown in Figure 7.5. However, the samples treated in Cambridge antibiotics for 1 hour, showed significantly lower levels of MTT conversion compared to those in culture medium (positive control).

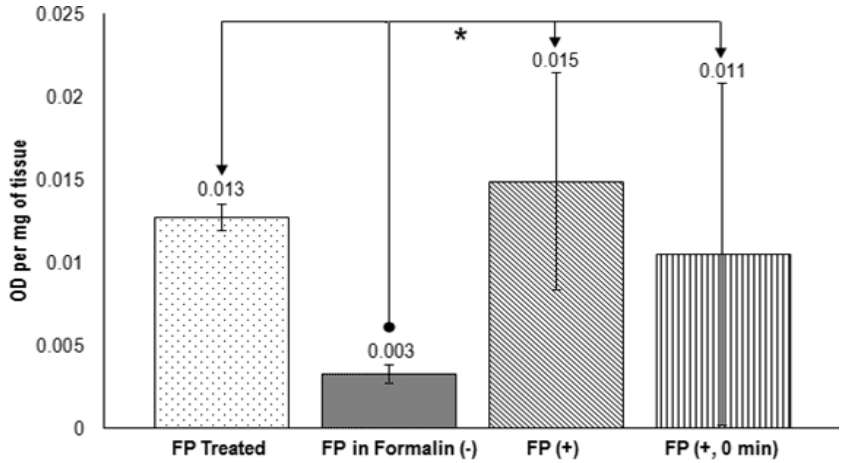

Figure 7.4: Cell viability of fresh pericardium treated in Cambridge antibiotics for 30 min (FP treated). Data expressed as means (n=3) ± 95% C.I. Asterisk and connectors indicate significant difference between originator and end-arrow column, as determined by ANOVA and calculation of MSD ($p < 0.05$; MSD = 0.005). FP in Formalin (-): fresh pericardium treated in 10% NBF (-ve control); FP (+): fresh pericardium treated in culture medium (+ve control); FP (+, 0min): fresh pericardium processed straight after dissection (+ve control at t = 0 min).

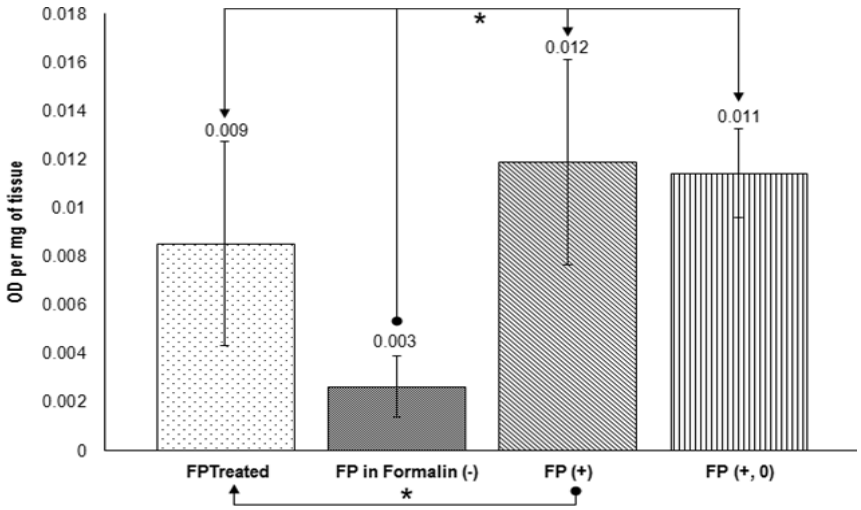

Figure 7.5: Cell viability of fresh pericardium treated in Cambridge antibiotics for 1 h (FP treated). Data expressed as means (n=3) ± 95% C.I. Asterisk and connectors indicate significant difference between originator and end-arrow column, as determined by ANOVA and calculation of MSD ($p < 0.05$; MSD = 0.002). FP in Formalin (-): fresh pericardium treated in 10% NBF (-ve control); FP (+): fresh pericardium treated in culture medium (+ve control); FP (+, 0min): fresh pericardium processed straight after dissection (+ve control at t = 0 min).

After the 2 h treatment with Cambridge antibiotics, the samples were also sterile, and the levels of MTT conversion by the samples treated in 10% (v/v) NBF were significantly lower compared to the other groups (Figure 7.6; $p < 0.05$, MSD = 0.004). The level of MTT conversion by the samples treated in culture medium (positive control) were significantly higher compared to both the samples processed immediately after dissection (positive control at t = 0 min) and the samples treated in Cambridge antibiotics. Therefore, the optimum time point for the disinfection of fresh pericardium was 30 min, which represented the shortest duration for disinfecting the tissue without affecting its viability.

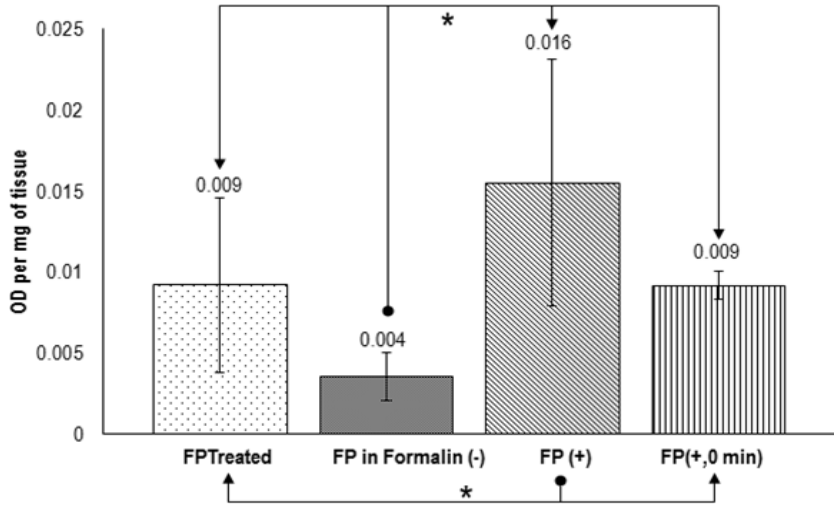

Figure 7.6: Cell viability of fresh pericardium treated in Cambridge antibiotics for 2 h (FP treated). Data expressed as means (n=3) ± 95% C.I. Asterisk and connectors indicate significant difference between originator and end-arrow column, as determined by ANOVA and calculation of MSD ($p < 0.05$; MSD = 0.004). FP in Formalin (-): fresh pericardium treated in 10% NBF (-ve control); FP (+): fresh pericardium treated in culture medium (+ve control); FP (+, 0min): fresh pericardium processed straight after dissection (+ve control at t = 0 min).

7.3 Static culture of fresh pericardium

7.3.1 Overview

Fresh pericardial samples were cultured statically in the bioreactor stations and in separate tissue holders, in order to validate the bioreactor system in terms of sterility and culture medium perfusion. The bioreactor was originally designed to operate with two dynamically-conditioned samples and two statically-maintained samples as controls. In order to increase the number of dynamically-conditioned samples per experiment to four, this series of experiments was carried out to investigate whether there was a difference between samples maintained statically in the bioreactor stations and static controls maintained in separate tissue holders. The experiments were designed to investigate the sterility, viability and histoarchitecture of samples maintained in static cultures for 1 day. The 1 day experiments were repeated three times (method 1, 2 & 3) to optimise the system in terms of both tissue viability and maintenance of sterility. Fresh pericardial samples were cultured in tissue holders, which were housed in culture tubs and placed in an incubator, and in bioreactor stations for 1 day. The stations were mounted to the bioreactor and wrapped with their heating element to maintain a temperature of 37°C.

7.3.2 Materials and methods

7.3.2.1 Sterilisation and calibration of equipment

Prior to each experiment, the tissue holders and bioreactor stations were sterilised as described in Chapters 5 Section 5.3.1.1 and Chapter 6, Section 6.6, respectively.

7.3.2.2 Pericardium dissection and disinfection

For each experiment, 12 fresh pericardial samples were dissected, as described in Chapter 2, Section 2.8, from 12 different pericardia (Figure 7.7). Four of the samples were loaded to the bioreactor stations, 4 to the tissue holders (positive control for MTT assay, live/dead staining, and histology) and 4 were treated in 10% (v/v) NBF (negative control for MTT assay). The positive control and the samples loaded on the bioreactor stations were cut in a rectangular shape, (9 x 6 cm^2 in size), and crosswise at one of the edges to identify the mesothelial surface; they were then treated in 60 ml of Cambridge antibiotics for 30 min at 37°C and cut to size for loading on either the tissue holders or the bioreactor stations. The tissue remaining after the cutting of each pericardial sample (tissue remnant) before treatment in antibiotic solution, was used as the positive control at t = 0 for (i) MTT assay (50 mg) (ii), histological analysis (iii), live/dead staining (with the exception of the samples for method 1) and (iv) sterility assessment, (Chapter 2 Section 2.15, 2.11.1, 2.16, and Chapter 4, Section 4.2.2.4, respectively) (Figure 7.7).

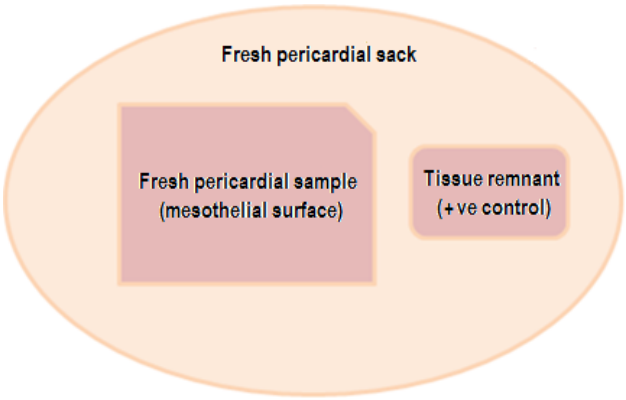

Figure 7.7: Isolation of fresh porcine pericardial samples. The samples (9 × 6 cm^2) were cut crosswise at one of their edges to identify the mesothelial surface. The remaining tissue (tissue remnant), was used as a positive control for MTT assay, H&E and live/dead staining (with the exception of the samples for method 1 which were not processed for live/dead staining).

7.3.2.3 Loading of bioreactor stations and tissue holders

Unless otherwise stated, all work was carried out in class II laminar flow cabinet. Following disinfection, the bioreactor station and tissue holder samples were transferred aseptically into individual sterile pots filled with 60 ml culture medium, and then loaded onto the bioreactor stations and tissue holders. The samples were loaded on the tissue holders and then placed in culture tubs, as described in Chapter 5, Section 5.2.1. Prior to loading on the bioreactor station, tissue was cut to size with the sterile cutting guide. The procedure for loading samples on the bioreactor stations is illustrated in Figure 7.8c: the upper station part was separated from the bottom and placed on the sterile loading guide (Figure 7.8a, b and d). The upper part was then separated from the central disk (Figure 7.8e) and the sample was placed onto the central disk. The upper station part was then placed back onto the central disk and screwed to it (Figure 7.8f). The upper part of the station was then screwed back to the lower part. The procedure of loading the culture medium in the stations varied at each experiment, due to continuous optimisation of the system.

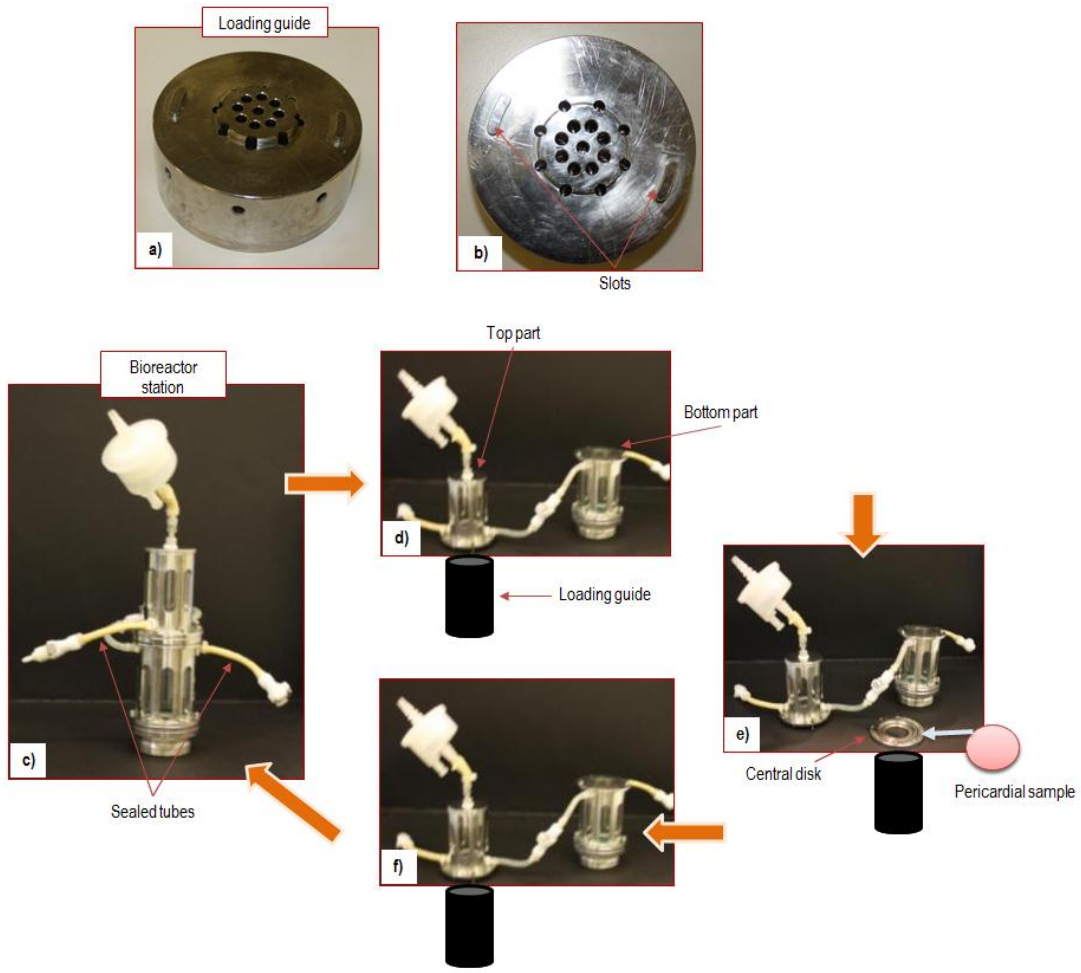

Figure 7.8: Loading tissue and cell culture medium on the bioreactor stations. The loading guide and the various components of the bioreactor station are illustrated in the Figure (a, b and c, d, e).

7.3.2.4 One day static culture (method 1)

Fresh pericardial samples were dissected**,** disinfected and loaded to the bioreactor stations and holders as described in Sections 7.3.2.2 and 7.3.2.3. The bioreactor stations were then filled with culture medium using a peristaltic pump, in order to facilitate the escape of the air trapped in the lower part of the station. Prior to loading the medium, the external port of the upper part of the station was sealed off. Culture medium was then pumped into the lower part of the station until it filled the interconnected upper part up to height of approximately 3 mm (Figure 7.9). The tube connected to the bottom part of the station was sealed off. Each of the stations were then mounted to the main bioreactor and wrapped with their heating element in order to maintain the temperature at 37°C.

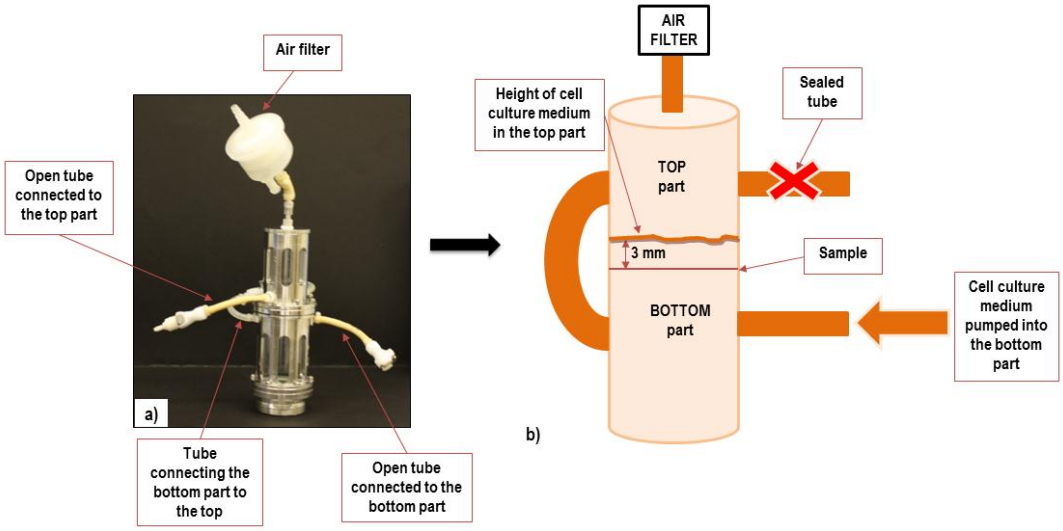

Figure 7.9: Filling of the bioreactor stations with culture medium (method 1). Photograph (a) and schematic (b) of the bioreactor station. During filling, the top tube was sealed off (b) and the culture medium was pumped into the lower part until the level in the top part was 3 mm above the samples.

After 1 day of static culture, the bioreactor station (Bior. Stations group) and tissue holder (T. Holders group) samples were harvested aseptically and assessed for their viability (MTT assay), sterility, and histoarchitecture (H&E). In addition, samples from the remnants of the pericardia used to isolate the station (Bior. Remn. Group; positive control) and holder (T. H. Remn. group; positive control) samples, together with samples treated in 10% (v/v) NBF (Tissue in formalin group; negative control), were also assessed for their viability, sterility and histoarchitecture.

7.3.2.5 One day static culture (method 2)

The 1 day static culture experiment was repeated due to issues with air entrapment in the stations, underneath the tissue, using method 1 (Section 7.3.2.4) for the culture medium loading procedure. For this reason, the design of the station was slightly changed by adding a stopcock and a tube open to the atmosphere, (Figure 7.10). Fresh pericardial samples were isolated, disinfected and loaded to the bioreactor stations and tissue holders as described in Sections 7.3.2.2 and 7.3.2.3. The cell culture medium was bubbled with 5% (v/v) CO_2 in air for 10 min, and then it was loaded in a sterile bottle fitted with a filter and a tube, used for subsequent filling of the station. The tube of the sterile bottle was then attached to a peristaltic pump and primed to remove the air in it; then it was connected to the bioreactor station. During filling, the station was kept horizontally, with the stopcock opened to the atmosphere

(Figure 7.10) and medium was pumped in the station through the port of the bottom part. When medium started leaking, the stopcock was turned to seal the port from the atmosphere (the tube itself was also sealed off by clamping) and direct the flow towards the upper part of the station. The medium was then allowed to flow in the upper part until a head of 3 mm was developed above the samples. Following filling, the stations were mounted to the main bioreactor and wrapped with their heating element in order to maintain the temperature at 37°C during the culture.

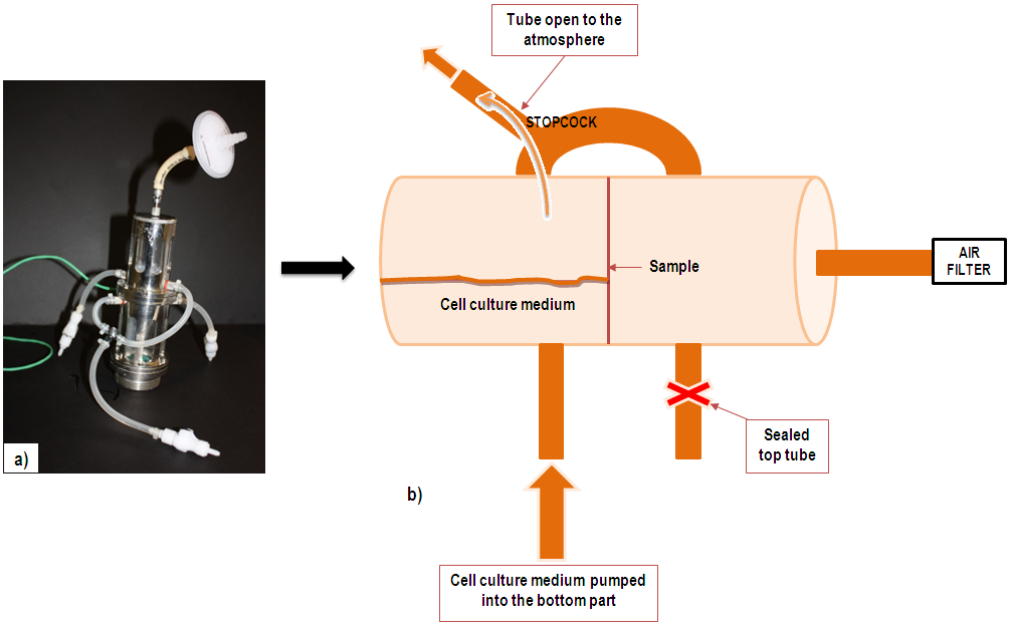

Figure 7.10: Filling of the bioreactor stations with culture medium (method 2). Photograph (a) and schematic (b) of the bioreactor station. During filling, the port of the upper part was sealed off (b), and the stopcock was opened to the atmosphere. Culture medium was pumped into the lower part, which was kept horizontally. When medium started leaking, the stopcock was turned to seal the port from the atmosphere and direct the flow towards the upper part.

After 1 day of static culture, the bioreactor station (Bior. Stations group) and tissue holder (T. Holders group) samples were harvested and assessed for viability (MTT assay and live/dead staining), sterility and histoarchitecture (H&E). In addition, samples from the remnants of the pericardia used to isolate the station (Bior.Remn. group; positive control) and holder (T.H.Remn. group; positive control) samples, together with samples treated in 10% (v/v) NBF (Tissue in formalin group; negative control), were assessed for their viability, sterility and histoarchitecture.

7.3.2.6 One day static culture (method 3)

The 1 day time point for static culture was repeated in order to improve the maintenance of the viability of samples in the stations with a better control of pO_2 and pH. Fresh pericardial samples were isolated, disinfected and loaded to the bioreactor stations and tissue holders as described in Sections 7.3.2.2 and 7.3.2.3. The number of replicates for the tissue remnants groups (Bior.Remn. group and T.H.Remn. group; positive controls) was increased in order to decrease the high level of variability previously observed within each positive control group, so to improve the accuracy of measurements for the MTT assay. Four pieces of tissue were cut out of each pericardium and then averaged to obtain one positive control for each pericardial sample (Figure 7.11).

HEPES (hydroxyethyl-piperazineethane-sulfonic acid buffer from Lonza; 25ml·L^{-1}) was added to the cell culture medium to improve the maintenance of the pH at 7.2 during the 1 day static culture; then, it was bubbled with 5% (v/v) CO_2 in air for 10 min, and finally loaded in the lower stations, as described in Section 7.3.2.5. After loading the bottom station, cell culture medium was added to the top station by using a different procedure so to improve the passive diffusion of the oxygen. The air filter at the top of the stations was then temporarily removed and 2 ml of culture medium was added in the upper top part with a syringe through the filter port. This ensured a head volume of culture medium of 2.8 mm above the samples, which allowed passive oxygen diffusion (Chapter 5, Section 5.2.1).

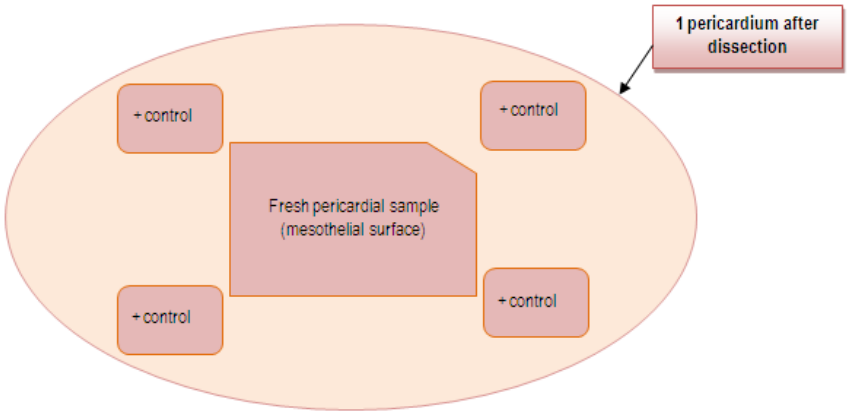

Figure 7.11: Isolation of fresh porcine pericardial samples. The samples (9 × 6 cm^2) were cut crosswise at one of their edges to identify the mesothelial surface. In the last 1 day static culture experiment (method 3), 4 pieces of tissue were taken from different regions of the same pericardium and used as the +ve control (tissue remnant) for MTT assay.

After 1 day of static culture, the bioreactor station (Bior. Stations group) and tissue holder (T. Holders group) samples were harvested and assessed for viability (MTT assay and live/dead staining), sterility and histoarchitecture (H&E). In addition, samples from the remnants of the pericardia used to isolate the station (Bior.Remn. group; positive control) and holder (T.H.Remn. group; positive control) samples, together with samples treated in 10% (v/v) NBF (Tissue in formalin group; negative control), and were assessed for their viability, sterility and histoarchitecture.

7.3.3 Results

7.3.3.1 One day static culture (method 1)

Sterility assessment

Following treatment in Cambridge antibiotics, the fresh pericardial samples used in the experiment were sterile. The sterility of the samples was maintained during the 1 day time static culture in the bioreactor stations and tissue holders, despite a leakage that was developed in one of the bioreactor stations. The leakage was developed at one of the polyvinylidene fluoride (PDVF) luer fittings used to connect the silicone tubing. These fittings could get damaged quite easily when they were screwed in the stations made of stainless steel. These fittings were replaced with stainless steel fittings in subsequent experiments.

Cell viability- MTT assay

The measured cell viability of the groups used in this experiment was averaged over the number of samples in each group (n = 4). The results are illustrated in Figure 7.12. The Tissue in Formalin group (negative control) demonstrated significantly lower cell viability compared to all the other groups, with the exception of the Bior.Stations group ($p < 0.05$; MSD = 0.009). The Bior.Stations group showed significantly lower viability compared to the T.H.Remn. group (positive control). The reduced viability of the Bior.Stations group was related to air entrapped underneath the samples in the bioreactor stations. Indeed, in spite of filling the stations with culture medium by employing a peristaltic pump, the samples were doming during the filling process, which was evidence of air entrapment. This caused inadequate supply of medium to both the top and bottom surfaces of the samples.

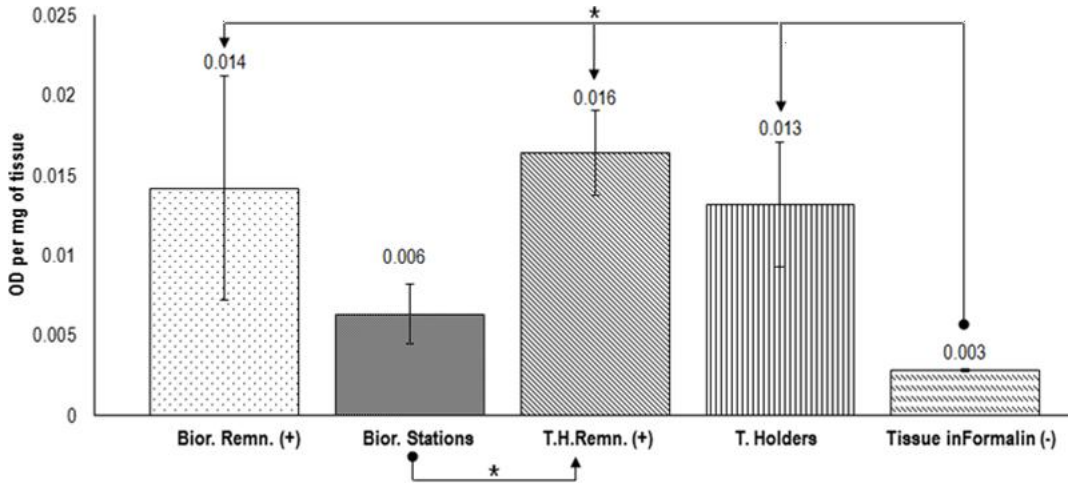

Figure 7.12: Cell viability (MTT assay) after 1 day static culture of fresh pericardium in bioreactor stations (Bior. Stations) and tissue holders (T. Holders) (method 1). The data also shows the viability of the remnants of the pericardia used to isolate the station (Bior.Remn.; +ve control) and holder (T.H.Remn.; +ve control) samples, together with the group treated in 10% (v/v) NBF (Tissue in formalin; -ve control). Data expressed as means (n=4) ± 95% C.I. Asterisk/connectors indicate significant difference between originator and end-arrow column (ANOVA and calculation of MSD) ($p < 0.05$; MSD = 0.009).

Histological analysis

The general histoarchitecture of the fresh pericardial samples cultured in both the bioreactor stations and the tissue holders appeared to be intact (Figure 7.13). The mesothelial cell layer was partially intact in most of the bioreactor station samples (Figure 7.13b, l, p). One of the station samples showed a complete loss of mesothelium, and the same was observed for its correspondent positive control (Figure 7.13f and e, respectively). A high loss of the mesothelium was observed in 3 of the tissue holder samples. However, this was also apparent in their positive controls (Figure 7.13h, n, r and g, m, q respectively).

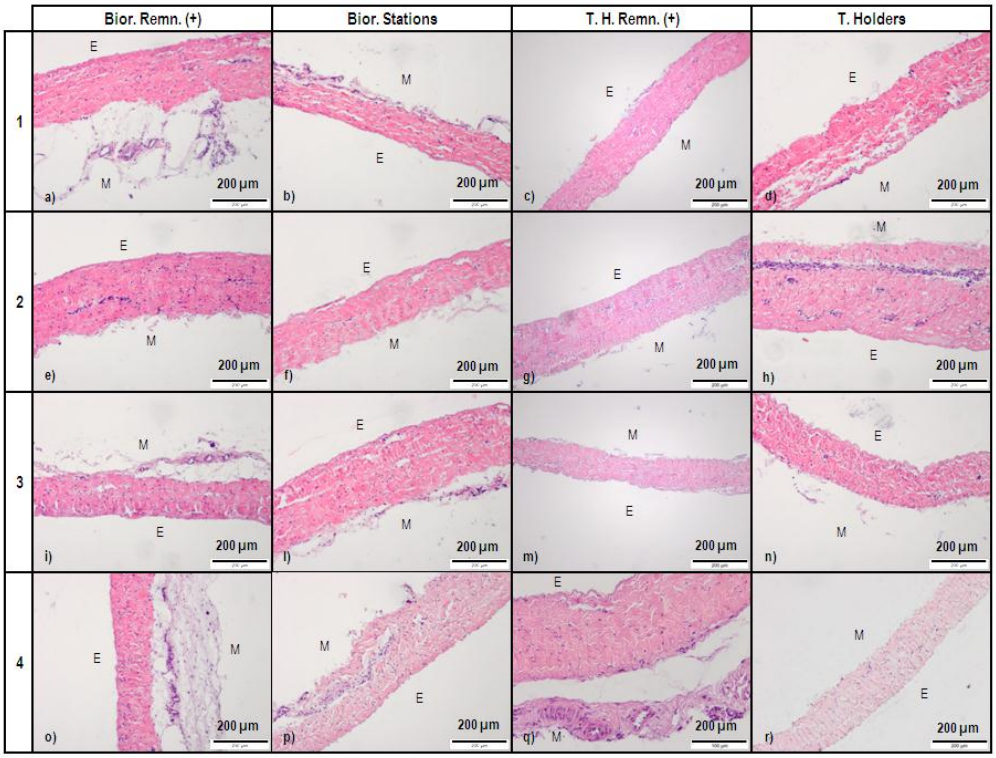

Figure 7.13: H&E stained sections of pericardial samples (n = 4) after 1 day static culture in the bioreactor stations (Bior. Stations; b, f, l and p) and tissue holders (T. Holder; d, h, n and r) (method 1). The figure also includes H&E-stained sections of the remnants of the pericardia used to isolate the station (Bior.Remn. (+); a, e, i and o) and holder (T.H.Remn. (+); c, g, m and q) samples. E: epipericardial surface; M: mesothelial surface. Scale bar indicates 200 µm.

7.3.3.2 One day static culture (method 2)

Sterility assessment

Following treatment in Cambridge antibiotics, the pericardial samples used in the experiment were sterile. The sterility of the samples was maintained during the 1 day static culture.

Cell viability - MTT assay

The averaged viability of the samples cultured statically for 1 day according to method 2, together with their controls, is shown in Figure 7.14. The viability of the Tissue in Formalin group was significantly reduced compared to the Bior.Remn and T.H.Remn groups, but not compared to the Bior.Stations and T.Holders ones ($p < 0.05$; MSD = 0.006). The Bior.Stations group showed significantly lower viability compared to the T.H.Remn. group. The cause for

the drop in viability of the Bior.Stations group was related to a not appropriate oxygen and pH control. Also, a high variability in the viability values of samples was observed.

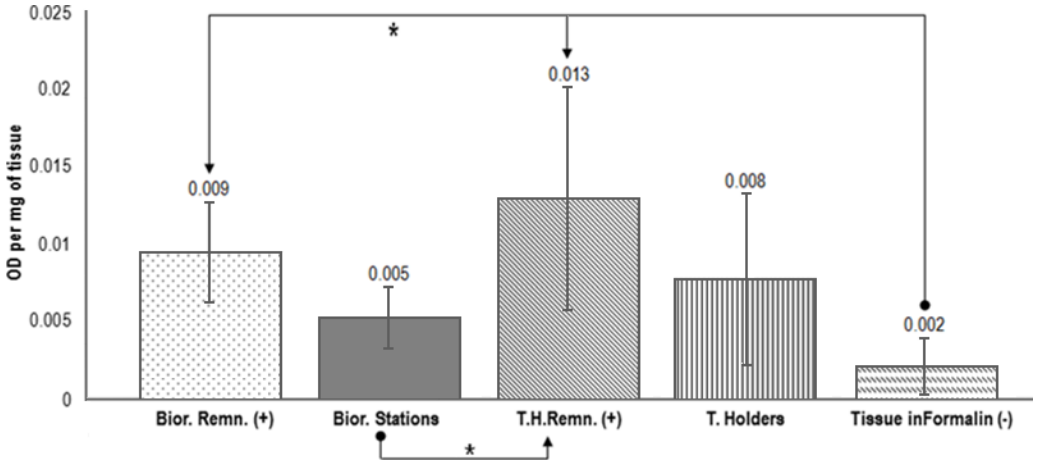

Figure 7.14: Cell viability (MTT assay) after 1 day static culture of fresh pericardium in bioreactor stations (Bior. Stations) and tissue holders (T. Holders) (method 2). The data also shows the viability of the remnants of the pericardia used to isolate the station (Bior.Remn.; +ve control) and holder (T.H.Remn.; +ve control) samples, together with the group treated in 10% (v/v) NBF (Tissue in formalin; -ve control). Data expressed as means (n=4) ± 95% C.I. Asterisk/connectors indicate significant difference between originator and end-arrow column (ANOVA and calculation of MSD) ($p < 0.05$; MSD = 0.006).

Histological analysis

Following the 1 day culture, the general histoarchitecture of the bioreactor station and tissue holder samples appeared to be intact, (Figure 7.15). Absence of mesothelium was observed in 2 of the station samples (Figure 7.15b, f). However, the positive controls for these samples (Figure 7.15a, e) were also absent of mesothelium. Mesothelium presence was observed in all 4 positive controls of the tissue holder samples (Figure 7.15c, g, m q). However, only 2 of the tissue holder samples (Figure 7.15h, n) maintained their mesothelium after 1 day static culture.

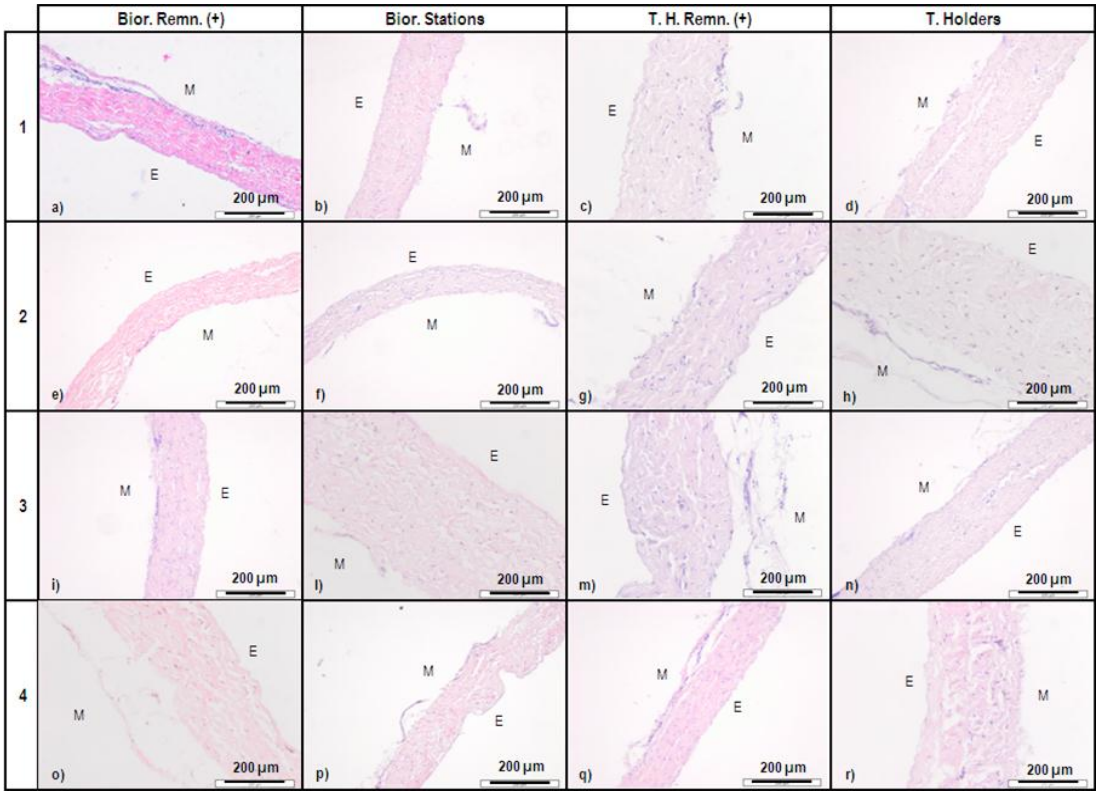

Figure 7.15: H&E stained sections of pericardial samples (n = 4) after 1 day static culture in the bioreactor stations (Bior. Stations; b, f, l and p) and tissue holders (T. Holder; d, h, n and r) (method 3). The figure also includes H&E-stained sections of the remnants of the pericardia used to isolate the station (Bior.Remn. (+); a, e, i and o) and holder (T.H.Remn. (+); c, g, m and q) samples. E: epipericardial surface; M: mesothelial surface. Scale bar indicates 200 µm.

Cell viability - Live/dead staining

The live/dead staining of the samples cultured in the stations and holders according to Method 3, together with their controls, is shown in Figure 7.16. Most cells were stained red (dead) on the mesothelial surface, which also demonstrated a high level of green autofluorescence.

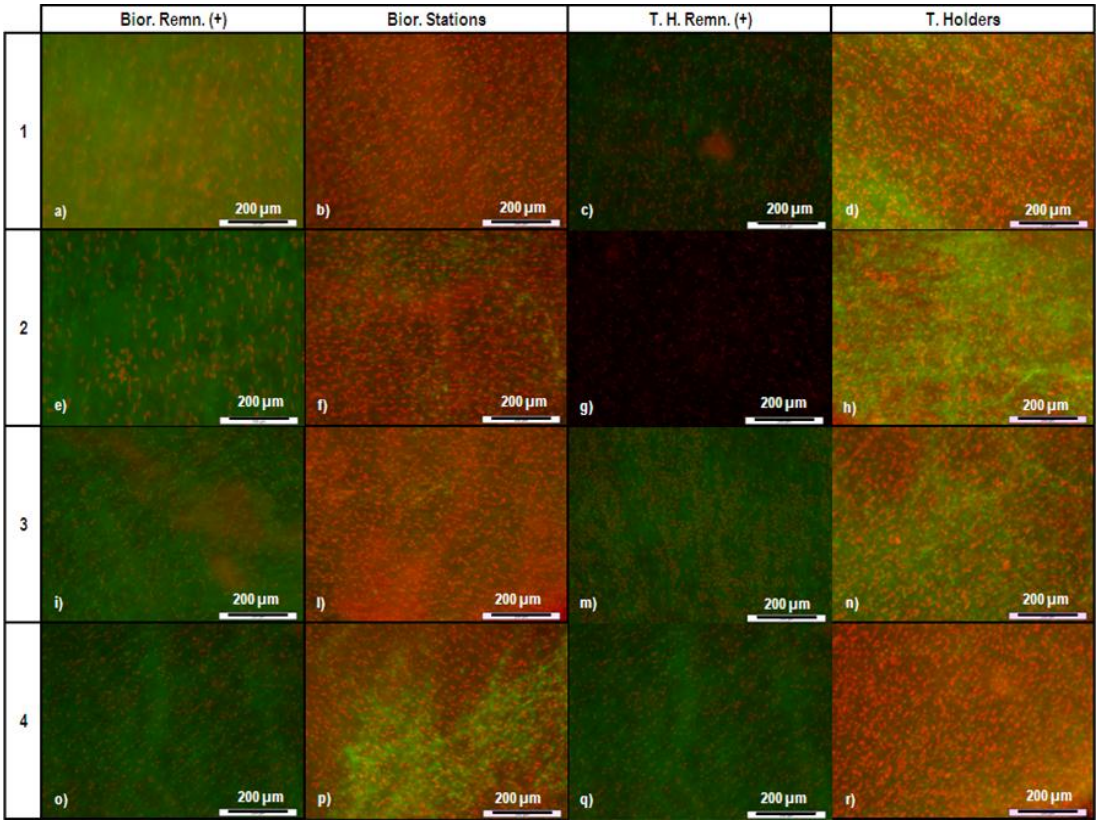

Figure 7.16: Live/dead stained pericardial samples (n = 4) after 1 day static culture in bioreactor stations (Bior. Stations; b, f, l and p) and tissue holders (T. Holder; d, h, n and r) (method 2). The figure also shows the live/dead stained remnants of the pericardia used to isolate the station (Bior.Remn. (+); a, e, i and o) and (T.H.Remn. (+); c, g, m and q) samples. Dead cells were stained red and live cells green. Scale bars indicate 200 µm.

7.3.3.3 One day static culture (method 3)

Sterility assessment

Following treatment in Cambridge antibiotics, the pericardial samples used in the experiment were sterile. The sterility of the samples was maintained during the 1 day static culture.

Cell viability - MTT assay

The averaged viability of the bioreactor station and tissue holder groups cultured statically for 1 day according to Method 3, together with their controls, is shown in Figure 7.17. All groups, except the Bior.Stations. group, demonstrated significantly higher viabilities compared to the Tissue in Formalin group (negative control) ($p < 0.05$; MSD = 0.005). In spite of using control samples from 4 different regions of each pericardium used to isolate each of the bioreactor station and tissue holder samples (Figure 7.17), there was still a high variability in the

Bior.Remn and T.H.Remn. groups. Indeed, a high level of variability was observed in the cell viability values of the 4 different portions of tissue cut out of the same pericardium, suggesting that, depending on the area considered of the same pericardium, there were different levels of viability. Also, within the T.Holders group, some of the samples showed low values of viability, similar to those obtained for the bioreactor stations group.

This suggested uneven cell viability/cell distribution across the fresh pericardia used in the study, and indicated the use of a tissue in which the cell viability was better controlled. It was decided that a cell-seeded decellularised pericardial scaffold might offer better control over cell number/viability.

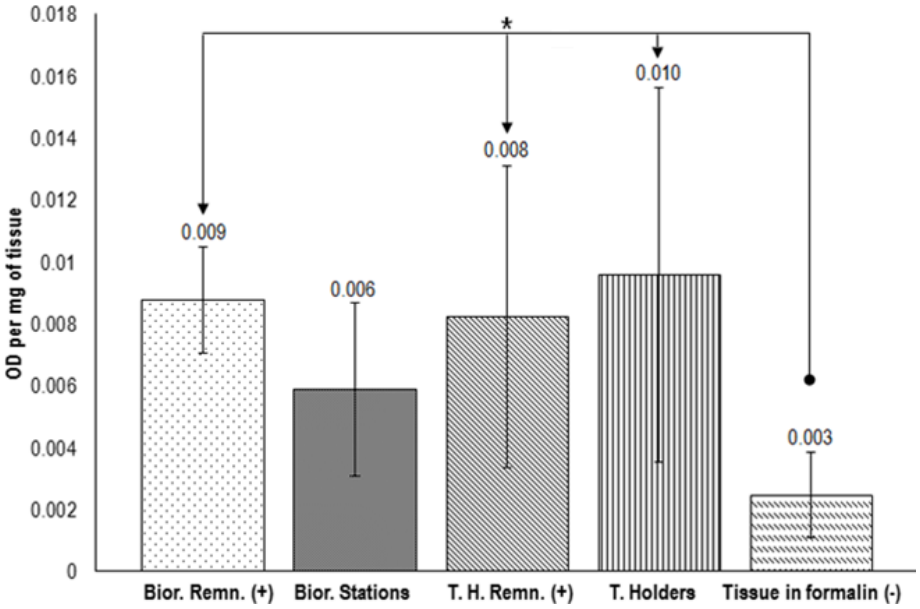

Figure 7.17: Cell viability (MTT assay) after 1 day static culture of fresh pericardium in bioreactor stations (Bior. Stations) and tissue holders (T. Holders) (method 3). The data also shows the viability of the remnants of the pericardia used to isolate the station (Bior.Remn.; +ve control) and holder (T.H.Remn.; +ve control) samples, together with the group treated in 10% (v/v) NBF (Tissue in formalin; -ve control). Data expressed as means (n=4) ± 95% C.I. Asterisk/connectors indicate significant difference between originator and end-arrow column (ANOVA and calculation of MSD) ($p < 0.05$; MSD = 0.005).

Histological analysis

In general, the histoarchitecture and mesothelium of the test and control samples appeared to be intact (Figure 7.18). However, sample 1 of the Bior.Stations group (Figure 7. 18b) and

sample 3 of the T.Holders group (Figure 7.18n) were void of a mesothelium, in contrast to their control.

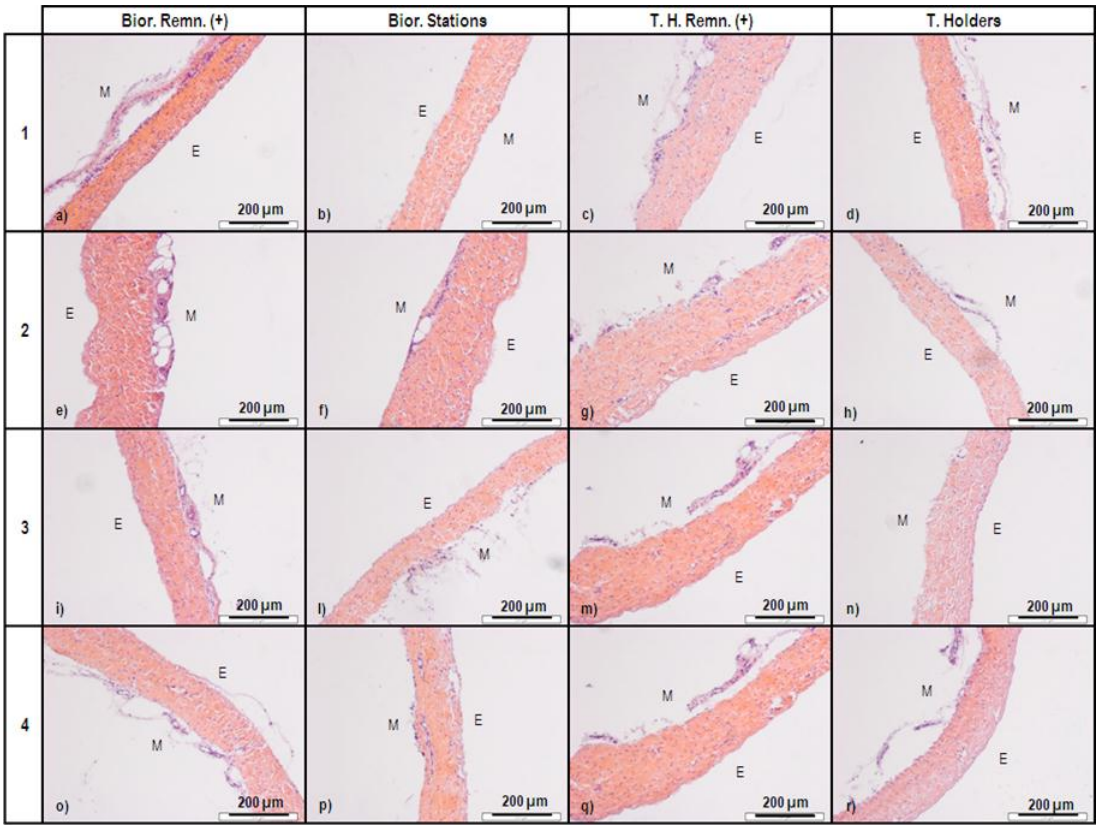

Figure 7.18: H&E stained sections of pericardial samples (n = 4) after 1 day static culture in the bioreactor stations (Bior. Stations; b, f, l and p) and tissue holders (T. Holder; d, h, n and r) (method 3). The figure also includes H&E-stained sections of the remnants of the pericardia used to isolate the station (Bior.Remn. (+); a, e, i and o) and holder (T.H.Remn. (+); c, g, m and q) samples. E: epipericardial surface; M: mesothelial surface. Scale bar indicates 200 µm.

Cell viability - Live/dead staining

The live/dead staining of the samples cultured in the stations and holders according to Method 3, together with their controls is shown in Figure 7.19. Most cells were stained red (dead) on the mesothelial surface, which also demonstrated a high level of green autofluorescence.

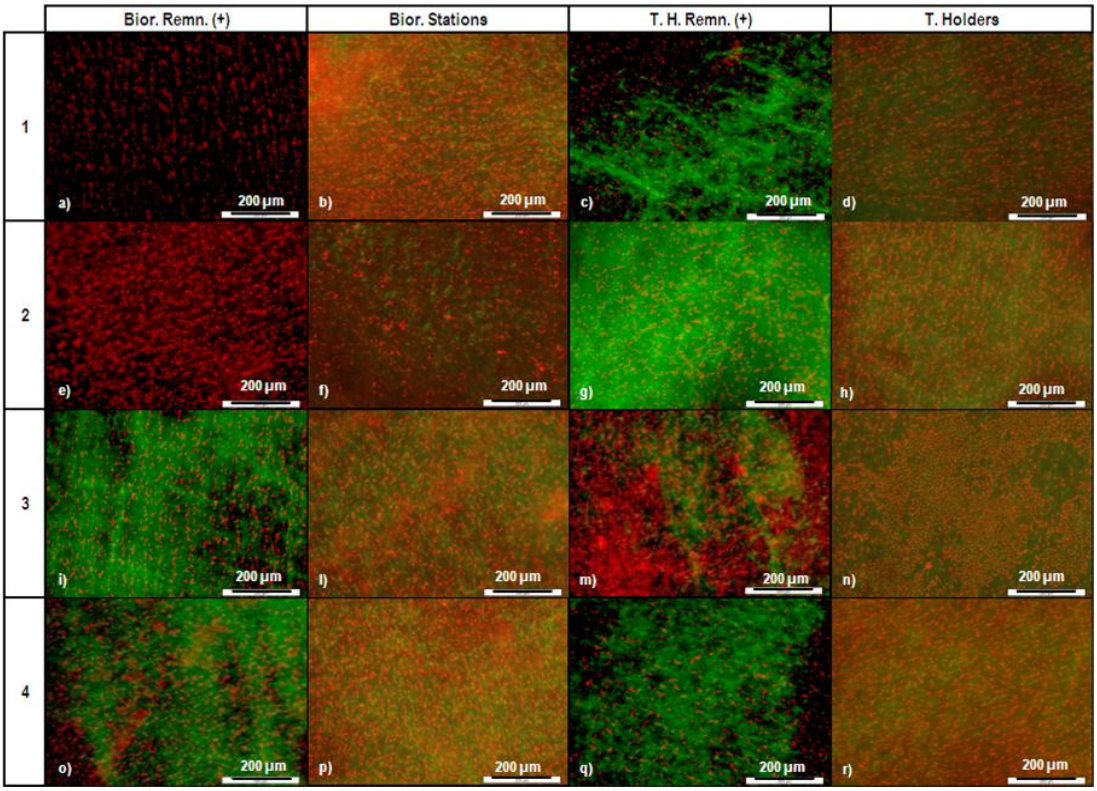

Figure 7.19: Live/dead staining of pericardial samples (n = 4) after 1 day static culture in bioreactor stations (Bior. Stations; b, f, l and p) and tissue holders (T. Holder; d, h, n and r) (method 3). The figure also shows the live/dead stained remnants of the pericardia used to isolate the station (Bior.Remn. (+); a, e, i and o) and holder (T.H.Remn. (+); c, g, m and q) samples. Dead cells were stained red and live cells green. Scale bars indicate 200 µm.

7.4 Static and dynamic bioreactor cultures of cell-seeded scaffolds

7.4.1 Overview

The purpose of this part of the study was to investigate the cell viability and histoarchitecture of pMSC-seeded decellularised porcine pericardial scaffolds, cultured either dynamically in the bioreactor or statically in tissue holders for 1 day. Dynamic experiments with fresh pericardium to optimise the dynamic cultures could not be performed due to the high variability in the cell viability of the available tissue. The culture medium loading technique, and pO_2 and pH control, developed during the static cultures with fresh pericardium were used during the experiments with the seeded scaffolds. The experiments were designed to investigate the sterility, viability and histoarchitecture of the seeded pericardial scaffolds maintained in static and dynamic cultures. The experiments that were performed are summarised below:

A. One day static culture: Decellularised pericardial samples were seeded with pMSCs and cultured statically in either bioreactor stations or tissue holders to investigate any potential differences in the viability between samples cultured in bioreactor stations and in tissue holders. This was necessary in order to assess whether samples cultured in the tissue holders could be used as static controls.
B. One day dynamic cultures (methods 1 & 2): Decellularised pericardial samples were seeded with pMSCs and cultured either in the bioreactor dynamically, or in tissue holders statically to investigate the effect of dynamic culture on pMSCs viability and alignment, and scaffold histoarchitecture.

7.4.2 Materials and methods

7.4.2.1 Sterilisation and calibration of the equipment

Prior to each experiment, the tissue holders and bioreactor stations were sterilised as described in Chapters 5, Section 5.3.1.1 and Chapter 6, Section 6.6, respectively. The chemostat was sterilised and calibrated as described in Chapter 6. The chemostat was used only during the dynamic experiments, in order to avoid the waste of a large amount of medium in case of contamination or failure of the static experiment. The culture medium (2.5 L) added to the chemostat was prepared as described in Chapter 6, Section 6.6.

7.4.2.2 Decellularisation and seeding of pericardium

Unless otherwise stated, all work was carried out in class II laminar flow cabinet. For each experiment, 8 fresh pericardial samples were decellularised as described in Chapter 4, Section 4.2.1.2, then cut into size and mounted to tissue holders, as described in Chapter 5, Section 5.3.1.2. The holders were then placed in culture tubs, filled with 105 ml of medium and the scaffolds were seeded with pMSCs at P5 and at a density of 1×10^5 cells·cm^{-2} (Chapter 5, Section 5.3.1.2), and cultured statically for 3 days at 37°C in an incubator with an atmosphere of 5% (v/v) CO_2 in air. The remaining decellularised tissue was used as negative control for the MTT assay.

7.4.2.3 Loading of bioreactor stations and tissue holders

All work was carried out in class II laminar flow cabinet. Following the 3 days of static culture in the tissue holders, half of the samples (n = 4 for each experiment) were aseptically

unloaded from the tissue holders and transferred to the bioreactor stations as described in Section 7.3.2.3, and cultured statically or dynamically for 1 day. The other 4 samples were maintained in the tissue holders in the incubator (positive control). The bioreactor stations were filled with culture medium as described in Section 7.3.2.6 for both static and dynamic studies, but only during dynamic studies the stations were filled directly from the chemostat, and HEPES and 5% (v/v) CO_2 in air were not added to the cell culture medium.

7.4.2.4 One day static culture

Following the 3-day static seeding of the pericardial scaffolds (Section 7.4.2.2), 4 out of the 8 samples were maintained in static culture in the tissue holders in the incubator (T.Holders group), and the other 4 were transferred to stand-alone bioreactor stations (Bior.Stations), as described in Section 7.4.2.3. Subsequently, the stations were filled as described in Section 7.3.2.6, and mounted on the main bioreactor, and then they were wrapped with their heaters to maintain 37°C. After 1 day of static culture, the samples from both groups were harvested and assessed for their sterility, cell viability (MTT assay and live/dead assay), and histoarchitecture (H&E).

7.4.2.5 One day dynamic culture (method 1)

The chemostat vessel was filled with 2.5 L of culture medium, which was prepared and calibrated as described in Chapter 6, Section 6.6, with the addition of antifoam (0.05% v/v; Sigma). Following the 3-day static seeding of the pericardial scaffolds (Section 7.4.2.2), 4 out of the 8 samples were maintained in static culture in the tissue holders in the incubator (T.Holders group), and the other 4 were transferred to stand-alone bioreactor stations (Bior.Stations), as described in Section 7.4.2.3. The stations were then filled directly from the chemostat using the 4-channel peristaltic pump. Four tubes were loaded on the peristaltic pump, one per each station; one tube only was used for filling all the 4 stations while the others were sealed off. The technique used for filling the station was similar to that described in Section 7.3.2.6. The upper station was filled by pumping the medium to just above the height of the inlet port of the tube connecting the upper and lower station, to avoid air entrapment during dynamic motion of the medium. After filling, each station was mounted to the main bioreactor and connected to the inlet tube from the chemostat and to the outlet tube to the reservoir. The stations were then wrapped with their heaters to maintain a temperature of 37°C. Subsequently, the bioreactor actuator was set to produce 10% dynamic strain, and

the samples were dynamically conditioned for 1 day. During the experiment, medium from the chemostat was continuously perfused to the stations using the 4-channel peristaltic pump. After 1 day, the statically-maintained and dynamically-conditioned samples were harvested and assessed for their sterility, cell viability (MTT assay and live/dead assay), and histoarchitecture (H&E).

7.4.2.6 One day dynamic culture (method 2)

Due to persisting issues with air entrapment in both the bioreactor stations and the bioreactor chamber (Figure 6.1), which was filled with water and transferred the volume displacement generated by the actuator to the bioreactor chambers, the dynamic experiment (Section 7.4.2.5) was repeated. The method of filling the stations was performed with the outmost care to remove the air entrapped underneath the seeded pericardial membrane. The height of the medium above the pericardial membrane was also monitored during mechanical conditioning of the samples; if the height reduced the medium pump speed was increased to avoid air escaping from the upper to the lower station. The medium flow rate was finally set at 10 $ml \cdot min^{-1}$. The presence of air in the bioreactor chamber, underneath the bottom silicone membrane of some stations, caused an unequal volume displacement between the 4 stations and, therefore, slightly different strain levels between the samples. During this experiment, outmost care was taken to avoid air trapped within the bioreactor chamber. This was achieved by pumping some additional water in the bioreactor chamber, after mounting the stations, until all the air trapped underneath the silicone membranes of the 4 stations was removed.

7.4.3. Results

7.4.3.1 One day static culture

Sterility assessment

The pMSC-seeded scaffolds in both the tissue holders and bioreactor stations were sterile after 1 day of culture.

Cell viability - MTT assay

The calculated cell viability values of the test and control groups had to be discarded due to a technical fault with the Micro plate spectrophotometer used for measuring the optical densities of the samples.

Histological analysis

After 1 day of culture, the histoarchitecture of the pMSC-seeded scaffolds maintained statically in both the bioreactor stations and tissue holders was intact (Figure 7.20 and 7.21, respectively). All samples of both the Bior.Stations and T.Holders groups demonstrated an almost continuous layer of pMSCs on the mesothelial surface (seeding surface). In addition, there was evidence of cells penetrating the thickness of the scaffold.

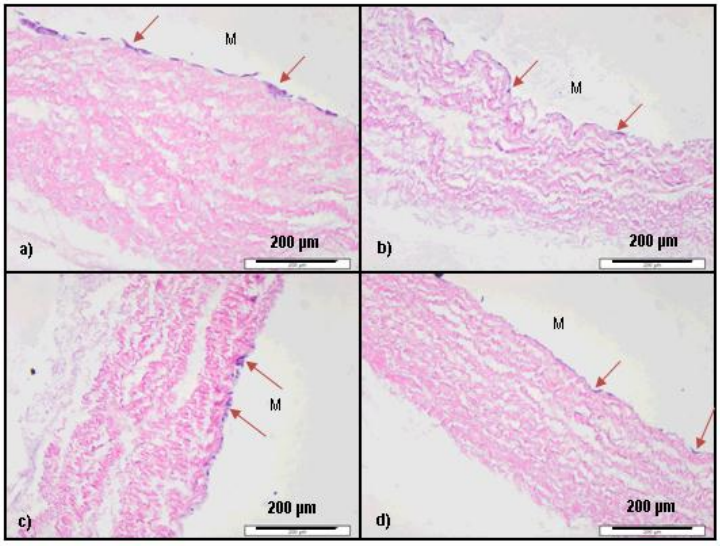

Figure 7.20: H&E stained sections of pMSC-seeded scaffolds (n = 4) after 1 day static culture in the bioreactor stations (Bior.Stations; a - d). Cells started penetrating through the thickness of the scaffold, as indicated by the red arrows. M: mesothelial surface. Scale bar indicates 200 µm.

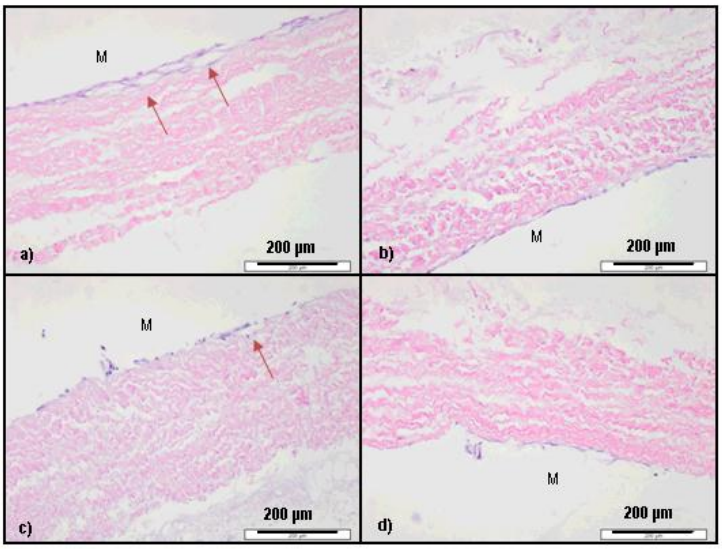

Figure 7.21: H&E stained sections of pMSC-seeded scaffolds (n = 4) after 1 day static culture in the tissue holders (T.Holders; a - d). Cells started penetrating through the thickness of the scaffold, as indicated by the red arrows. M: mesothelial surface. Scale bar indicates 200 µm.

Cell viability - Live/dead staining

The pMSCs in both the bioreactor station and tissue holder samples appeared to be stained green (live) after 1 day of static culture (Figure 7.22 and 7.23), with the exception of one of the tissue holder samples, which showed a high amount of dead red cells (Figure 7.23a). The high amount of dead cells in this sample might have been related to cell senescence or inadequate cell attachment to the scaffold. Cells counting revealed similar numbers of live cells in the two groups, with the Bior.Stations group scoring 80-94 % live cells, and the T.Holders group 81-88 %. The tissue holder sample that demonstrated the high amount of red-stained cells, scored only 20% live cells. These results suggested that there was no difference in terms of viability between the constructs cultured statically in the tissue holders and bioreactor stations. Thus, the tissue holders could be used as static controls during the dynamic experiments.

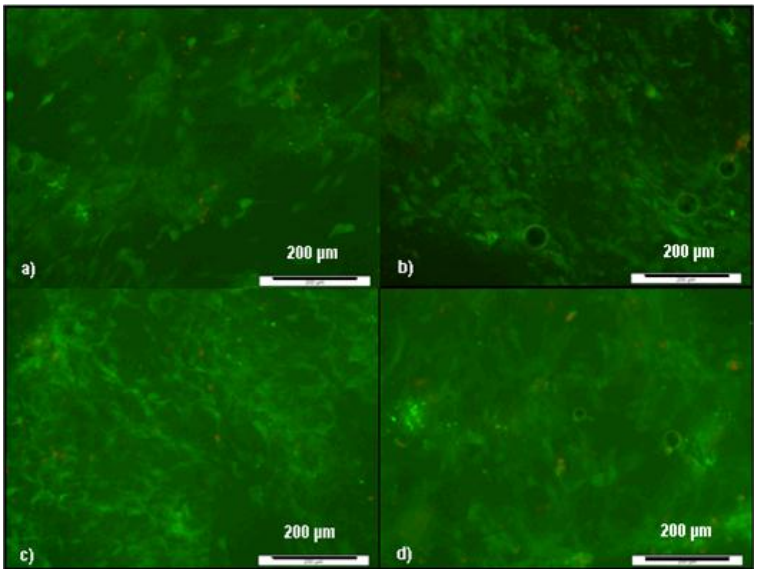

Figure 7.22: Live/dead stained pMSC-seeded scaffolds (n = 4) after 1 day of static culture in the bioreactor stations (Bior.Stations; a - d). Dead cells were stained red and live cells green. Scale bars indicate 200 µm.

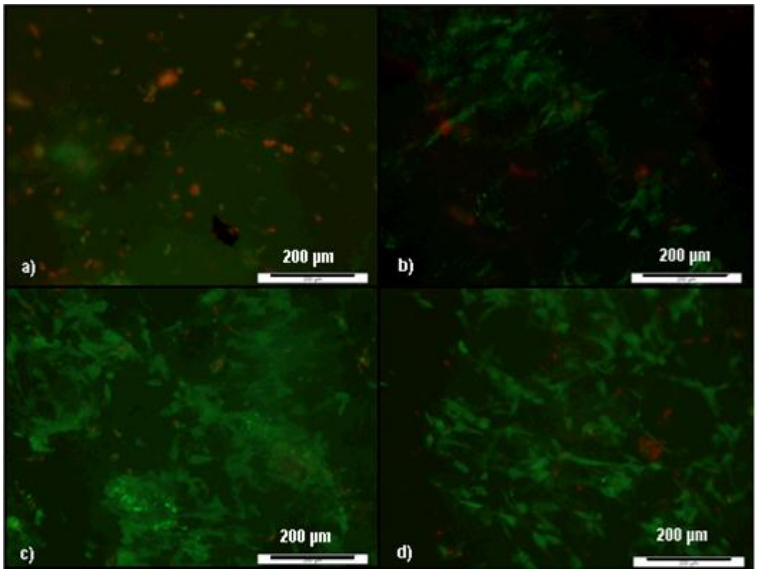

Figure 7.23: Live/dead stained pMSC-seeded scaffolds (n = 4) after 1 day of static culture in tissue holders (T.Holders; a - d). Dead cells were stained red and live cells green. Scale bar indicates 200 µm

7.4.3.2 One day dynamic culture (method 1)

Sterility assessment

After 1 day of culture, both the statically-maintained and dynamically-conditioned pMSC-seeded scaffolds were sterile.

Cell viability - MTT assay

The averaged viability of the dynamically-conditioned (Bior.Stations; Method 1) and statically-maintained (T.Holders) pMSC-seeded constructs after 1 day of culture, together with the negative control (decellularised pericardium), is shown in Figure 7.24. The T.Holder constructs demonstrated significantly increased viability compared to both the Bior.Station constructs and negative control ($p < 0.05$; MSD = 0.005). No significant difference was found between the Bior.Station constructs and negative control. This result was due to the high variability in the Bior.Station constructs viability values. Indeed, 2 samples showed very low viabilities, which were close to the mean of the negative control, whereas the other 2 showed viabilities similar to the T.Holder group. The decreased viability of the 2 dynamically-conditioned samples was most likely due to the fact that during conditioning, the level of the culture medium in the bottom part of the stations hosting these two constructs dropped, probably due to air trapped in the bioreactor stations. This resulted to the bottom surface of the constructs not being in contact with the culture medium, and being deprived of nutrients during the dynamic culture.

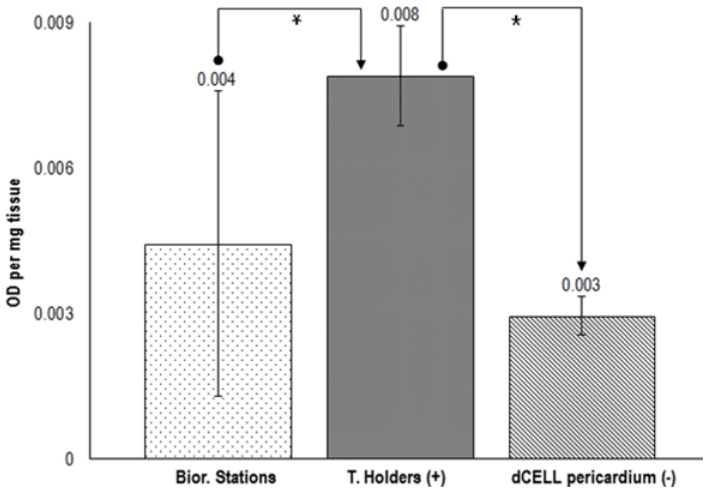

Figure 7.24: Cell viability (MTT assay) of pMSC-seeded pericardial scaffolds after 1 day dynamic culture in bioreactor stations (Bior. Stations), and 1 day static culture in tissue holders (T.Holders) (method 1). The data also shows the viability of decellularised pericardium (dCELL pericardium; -ve control). Data expressed as means (n=4) ± 95% C.I. Asterisk/connectors indicate significant difference between originator and end-arrow column (ANOVA and calculation of MSD) ($p < 0.05$; MSD = 0.003).

Histological analysis

The histoarchitecture of both the statically-maintained and dynamically-conditioned pMSC-seeded scaffolds was intact (Figure 7.25 and 7.26) after 1 day of culture. All samples of both groups demonstrated an almost continuous layer of pMSCs on the mesothelial surface (seeding surface). In addition, there was evidence of cells started penetrating the thickness of the scaffold, especially in the case of the T.Holders group.

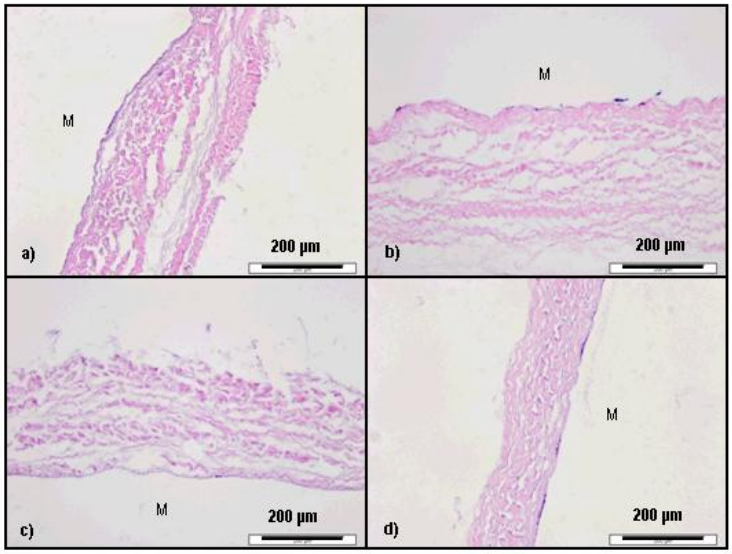

Figure 7.25: H&E stained sections of pMSC-seeded scaffolds (n = 4) after 1 day of dynamic culture in the bioreactor stations (Bior.Stations; a - d) (method 1). Cells started penetrating through the thickness of the scaffold. M: mesothelial surface. Scale bars indicate 200 µm.

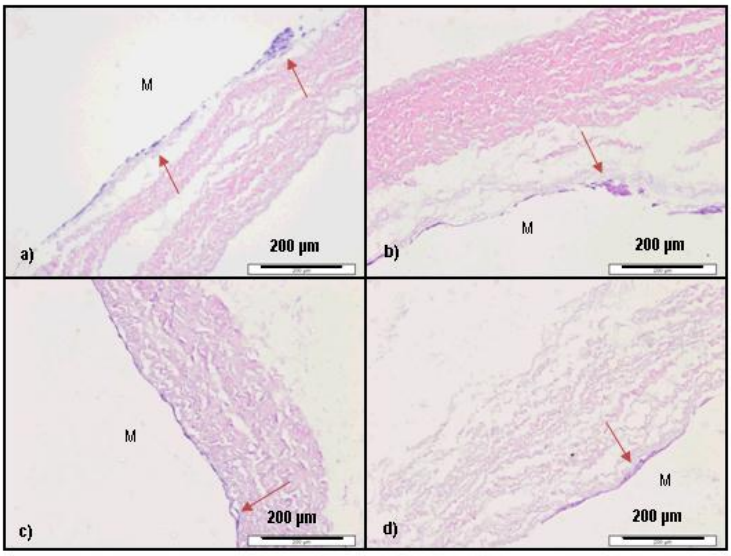

Figure 7.26: H&E stained sections of pMSC-seeded scaffolds (n = 4) after 1 day of static culture in the tissue holders (T.Holders; a - d) (method 1). Cells started penetrating through the thickness of the scaffold, as indicated by the red arrows. M: mesothelial surface. Scale bars indicate 200 µm.

Cell viability - Live/dead staining

Two of the pMSC-seeded scaffolds, which were dynamically conditioned in the bioreactor, appeared to be stained heavily green, with a percentage of viable cells between 57 – 76% (Figure 7.27a, b). In these two samples, the cells appeared to be aligned along specific

directions. The other two dynamically-conditioned samples demonstrated only 4% - 21% viable cells (Figure 7.27c, d). The high amount of dead cells in these two samples was in accordance with the MTT assay results. In contrast to the bioreactor station samples, all tissue holder samples demonstrated a higher amount of live cells, with percentages between 86 - 98% (Figure 7.28).

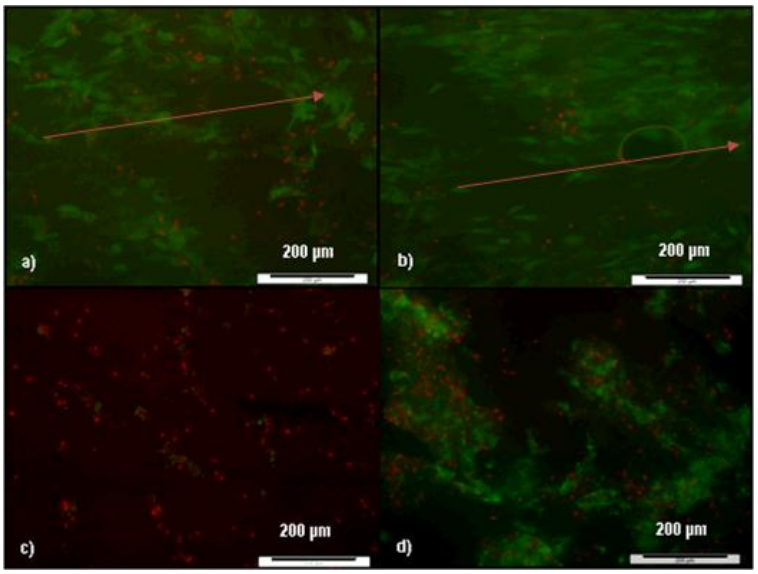

Figure 7.27: Live/dead stained pMSC-seeded scaffolds (n = 4) after 1 day of dynamic culture in the bioreactor stations (Bior.Stations; a - d) (method 1). Dead cells were stained red and live cells green. Red arrows indicate cells aligned along specific directions. Scale bar indicates 200 µm.

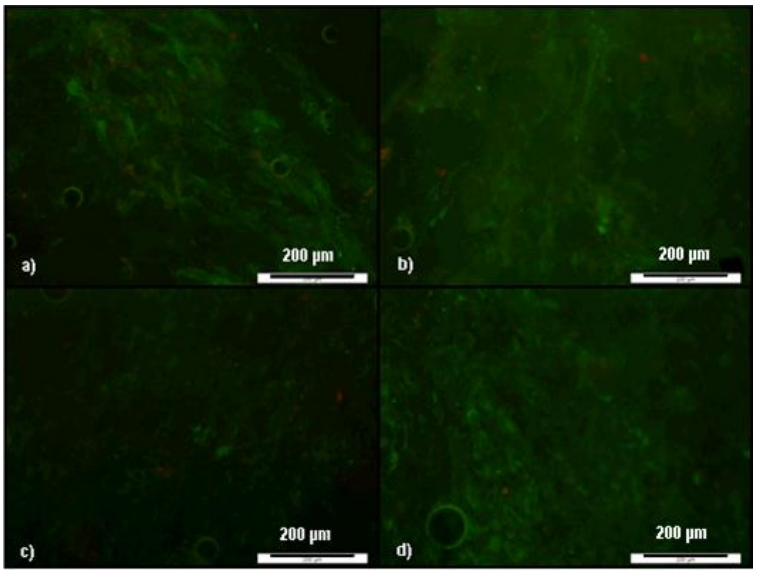

Figure 7.28: Live/dead stained pMSC-seeded scaffolds (n = 4) after 1 day of static culture in tissue holders (T.Holders; a - d) (method 1). Dead cells were stained red and live cells green. Scale bars indicate 200 µm.

7.4.3.3 One day dynamic culture (method 2)

Sterility assessment

After 1 day of culture, both the statically-maintained and dynamically-conditioned pMSC-seeded scaffolds were sterile.

Cell viability - MTT assay

The averaged viability of the dynamically-conditioned (Bior.Stations; Method 2) and statically-maintained (T.Holders) pMSC-seeded constructs after 1 day of culture, together with the negative control (decellularised pericardium), is shown in Figure 7.29. The T.Holders group demonstrated high variability due to 2 samples registering significantly lower viability values compared to the other 2 (almost half). This was in disagreement with the live/dead staining that showed all four T.Holder constructs expressing mostly viable cells (Figure 7.33). The probable cause of this discrepancy was the time taken to process these 2 samples. Indeed, these 2 samples were the first to be cut and put in the eppendorf with PBS only, waiting for the other samples to be harvested and cut before addition of the MTT solution. Thus, these 2 samples were excluded from the analysis. Both the Bior.Stations and T.Holder groups demonstrated significantly increased viabilities compared to negative control ($p < 0.05$; MSD = 0.002). No significant difference was found between the Bior.Stations and T.Holder groups.

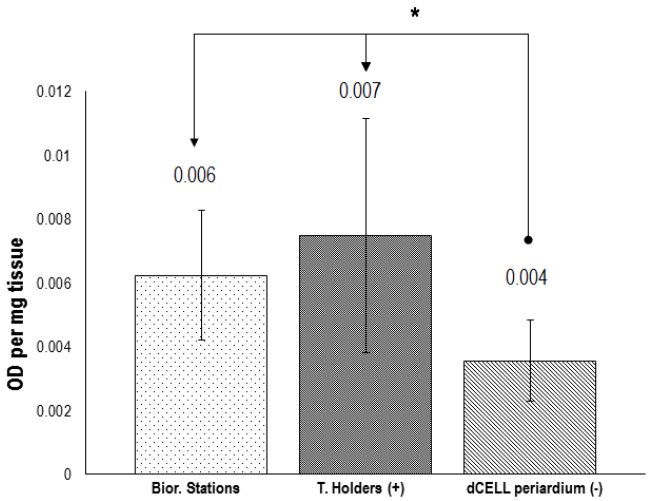

Figure 7.29: Cell viability (MTT assay) of pMSC-seeded pericardial scaffolds after 1 day dynamic culture in bioreactor stations (Bior. Stations; n = 4), and 1 day static culture in tissue holders (T. Holders; n = 2) (method 2). The data also shows the viability of decellularised pericardium (dCELL pericardium; -ve control; n = 4). Data expressed as means ± 95% C.I. Asterisk/connectors indicate significant difference between originator and end-arrow column (ANOVA and calculation of MSD) ($p < 0.05$; MSD = 0.003).

Histological analysis

The histoarchitecture of both the dynamically-conditioned and statically-maintained pMSC-seeded scaffolds was intact (Figure 7.30 and 7.31) after 1 day of culture. All samples of both groups demonstrated a layer of pMSCs on the mesothelial surface (seeding surface). In addition, there was evidence of cells penetrating the thickness of the scaffold.

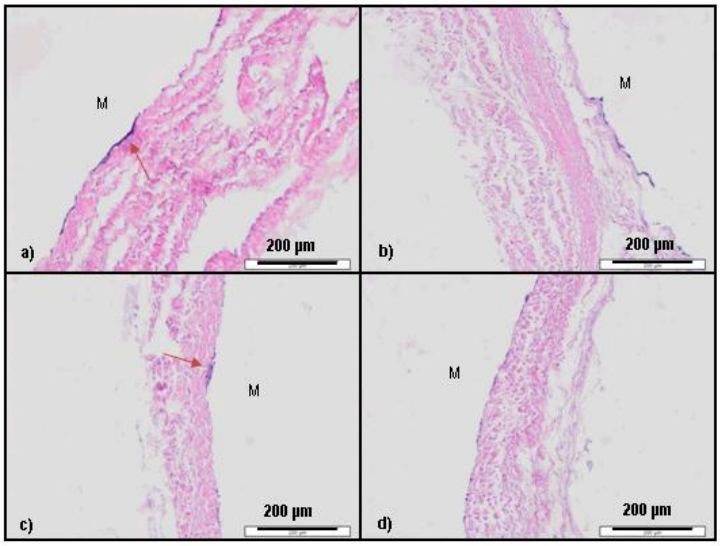

Figure 7.30: H&E stained sections of pMSC-seeded scaffolds (n = 4) after 1 day of dynamic culture in the bioreactor stations (Bior.Stations; a - d) (method 2). Cells started penetrating through the thickness of the scaffold, as indicated by the arrows. M: mesothelial surface. Scale bar indicates 200 µm.

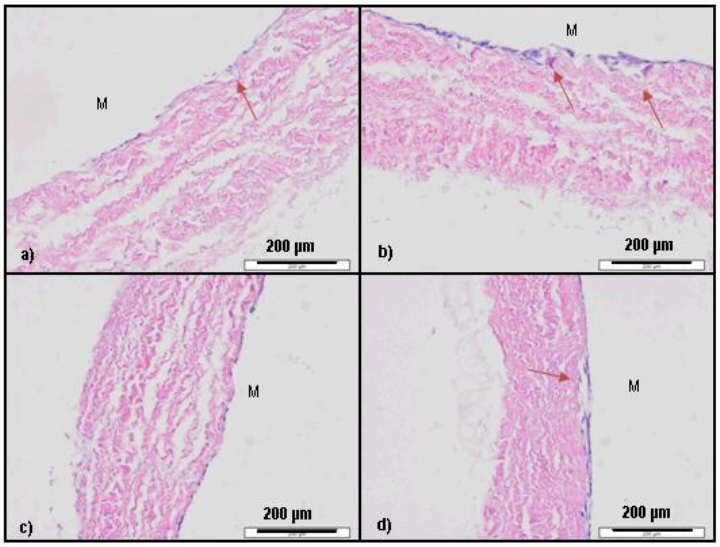

Figure 7.31: H&E stained sections of pMSC-seeded scaffolds (n = 4) after 1 day of static culture in the tissue holders (T.Holders; a - d) (method 2). Cells started penetrating through the thickness of the scaffold, as indicated by the arrows. M: mesothelial surface. Scale bar indicates 200 µm.

Cell viability - Live/dead staining

Most of the pMSCs in both the dynamically-conditioned (Figure 7.32) and statically-maintained (tissue holders) constructs (Figure 7.33) appeared to be stained green (live) after 1 day of culture. The cell counting revealed 69 - 84% live cells for the dynamically-conditioned constructs and 96 - 97% live cells for the statically maintained constructs. Under the mechanical stimulation, the constructs in the bioreactor stations demonstrated significant cell alignment along specific directions (Figure 7.32a, c).

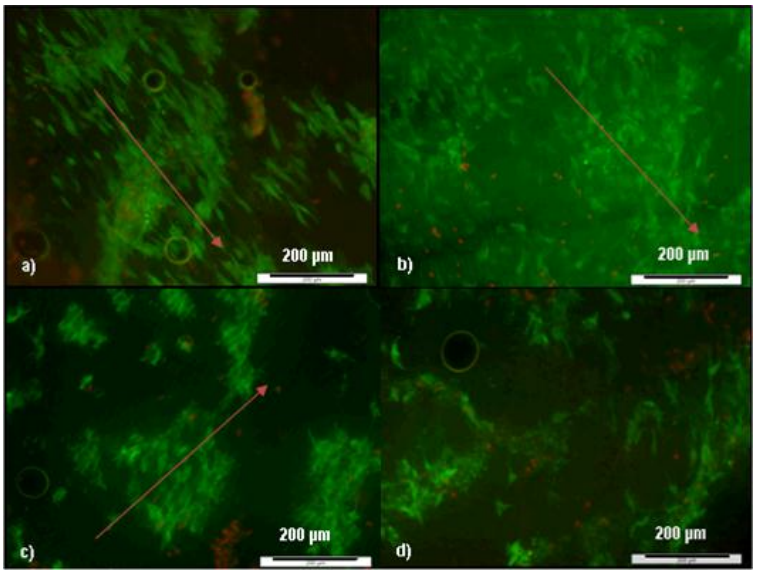

Figure 7.32: Live/dead stained pMSC-seeded scaffolds (n = 4) after 1 day of dynamic culture in the bioreactor stations (Bior.Stations; a - d) (method 2). Dead cells were stained red and live cells green. Red arrows indicate cells aligned along specific directions. Scale bars indicate 200 µm.

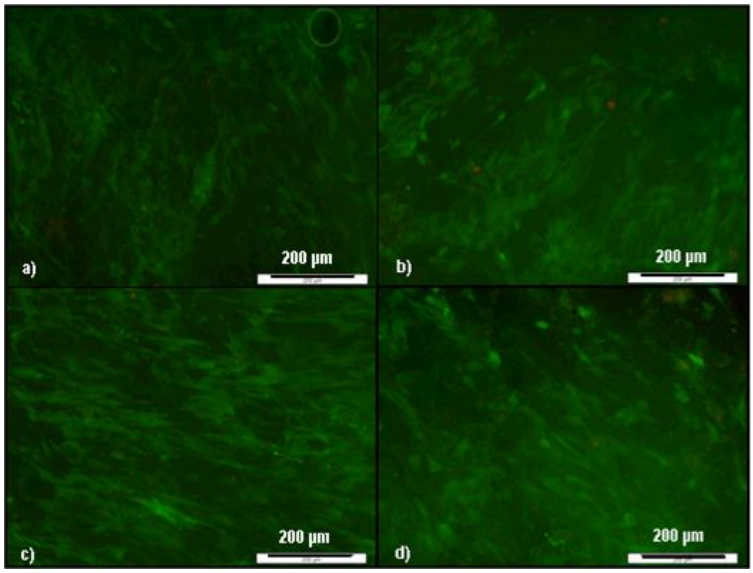

Figure 7.33: Live/dead stained pMSC-seeded scaffolds (n = 4) after 1 day of static culture in tissue holders (T.Holders; a - d) (method 2). Dead cells were stained red and live cells green. Scale bars indicate 200 µm.

7.5 Discussion

This chapter described the culture of fresh and pMSC-seeded decellularised pericardium under static and dynamic conditions in tissue holders and bioreactor stations, with a view to developing the use of the bioreactor system and investigating the effect of MV-leaflet relevant mechanical stimulation on the cell-seeded scaffolds. This investigation was based on assessing the sterility and histoarchitecture of the cultured samples, as well as on the qualitative and quantitative assessment of their cell viability using live/dead staining and the MTT assay, respectively. The MTT assay is an enzyme-based assay and it depends on the mitochondrial activity and not cell viability *per se*, (Mosmann, 1983; Twentyman and Luscombe, 1987). Therefore, and since the MTT assay results might be misleading, live/dead staining was used in conjunction with the MTT assay.

Prior to the tissue cultures, it was necessary to ensure sterility of the fresh pericardium in order to be used in the cultures. The Cambridge antibiotics solution, which included a cocktail of different antibiotics, was used for disinfection of the fresh pericardium, since it is the most commonly used disinfection solution employed by the NHS Tissue Bank. Fresh pericardium treated in Cambridge antibiotics was sterile at every time point considered (30mins, 1h and 2h); all the groups had significantly higher viability compared to the negative control at each

time point, thus, the lowest time point (30 min) was chosen as the optimum to be used for future experiments. The viability of the positive control stored in cell culture medium was higher than that of tissue treated in Cambridge after 1 and 2 hours, as well as of the tissue remnants, after 2 hours; these results were probably affected by the use of cell culture medium which improved the viability of tissue. The high variability in terms of viability observed in each group was most likely affected by the different time of death of the various pigs from which the hearts were dissected.

In preliminary studies the bioreactor stations were filled with cell culture medium without using a peristaltic pump; results showed a high decrease in cell viability compared to the positive control. This was attributed to the entrapment of air, which was observed underneath most of the samples in the bioreactor stations, probably due to the procedure followed for filling the stations with medium. In the first 1 day static culture experiment (method 1) a peristaltic pump was used to fill the bioreactor stations with culture medium, with a view to avoiding the air entrapment underneath the tissue. Sterility was maintained after 1 day of static culture in the stations mounted in the main bioreactor, despite a small leakage that was developed. However, the viability of the tissue in the bioreactor stations was significantly reduced due to the persisting air entrapment underneath the tissue.

The 1 day static culture experiment was repeated (method 2) again by changing the set-up of the bioreactor stations, and by introducing a new technique for filling the stations with culture medium. The new culture medium filling technique helped to avoid air entrapment in the stations. However, the fresh pericardial samples in the bioreactor stations again demonstrated low viability, which was not significantly different to the negative control. This drop in cell viability was attributed to inadequate oxygen and pH control. Previous studies have shown that, if the oxygen supply is inadequate, the mitochondria are unable to effectively synthesise ATP, leading to increased glycolysis, and subsequent increased production of pyruvate. The pyruvate is then converted to lactate, which can cause pH drop, inhibiting cell growth (Hochachka and Mommsen, 1983) and potentially leading to cell swelling and death (Staub *et al*., 1990). The 1 day static culture experiment with fresh pericardium was repeated once more (method 3), by introducing a pH-stabilising buffer (HEPES), and a better control of the head volume of culture medium on top of the samples in the bioreactor stations. In addition, the number of replicates for the positive control for the MTT assay was increased to improve the accuracy of the results. In spite of these changes, a high variability was still observed in the

cell viability results. This was probably due to the quality of the fresh tissue. It has been reported that some cellular organelles start deteriorating shortly after death, affecting and decreasing the cell viability of the tissues (Alessandrini *et al*., 1994). Owing to this, it was decided to use a tissue whose cell viability was more controllable, such as the pMSC-seeded pericardial scaffolds, in the subsequent dynamic cultures.

Porcine MSC-seeded pericardial scaffolds were cultured statically in both bioreactor stations and tissue holders to investigate any potential differences in the viability and histoarchitecture maintenance between samples cultured in stations and in tissue holders. This investigation was performed to assess whether samples cultured in the tissue holders could be used as static controls. The protocol previously optimised for the static culture of fresh pericardia in the bioreactor stations (method 3) was used during static culture in the stations of the pMSC-seeded pericardial scaffolds. Results after 1 day static culture showed that the histoarchitecture was intact for both tissue holders and bioreactor stations group, and all samples demonstrated an almost continuous layer of pMSCs on the mesothelial surface (seeding surface). Samples cultured in the stations showed viability similar to most of the samples of the tissue holders group; only one sample of the tissue holders group showed a high number of dead cells probably due to cell senescence or inadequate cell attachment to the scaffold. In conclusion, the tissue holders could be used as positive control during dynamic experiments.

Porcine MSC-seeded pericardial scaffolds were then cultured dynamically (method 1) in the bioreactor stations and statically in the tissue holders for up to 1 day to investigate the effects of dynamic culture on cell viability, directionality and sample histoarchitecture. The results of the MTT assay after 1 day dynamic conditioning showed that 2 out of 4 samples of the bioreactor stations group had low values of viability, close to the values of the negative control. This was related to air entrapment issues; indeed, the level of medium underneath the 2 samples was not into contact with the tissue after 1 day dynamic stimulation, probably due to some air trapped in the system during the dynamic motion of the cell culture medium. Nevertheless, the histoarchitecture of samples was intact and pMSCs formed an almost continuous monolayer of cells on the seeding surface and started penetrating the matrix. Also, cell alignment was observed in the bioreactor stations samples. Unfortunately, it was not possible to define along which direction cells were aligning (circumferential or radial).

Finally, the 1 day dynamic culture was repeated (method 2) again to overcome the issues in terms of air entrapment in some of the bioreactor stations and the bioreactor chamber, the latter to have a more homogeneous strain level distribution on the sample. The bioreactor stations samples showed viability similar to the tissue holders and significantly higher than the negative controls. The histoarchitecture of samples was intact, and pMSCs started forming an almost continuous monolayer of cells on the seeded surface, as well as started penetrating through the thickness of samples. The alignment of cells along specific directions was obvious again in the samples cultured dynamically in the bioreactor stations. Cell alignment can guide the deposition of ECM proteins, such as collagen and elastin, along specific directions, guiding the formation of specific histoarchitecture, as reported in previous studies (Kim *et al.,* 1999; Altman *et al.*, 2002; Mol *et al.*, 2003). It has been described that the realignment of the ECM is driven by the cytoskeleton of cells, to which the ECM is connected via protein complexes; cells probably align the ECM proteins by pulling the collagen fibers and aligning them in a direction parallel to their bodies (Grenier *et al.*, 2005).

Chapter 8

Discussion, conclusions & future work

Valvular heart disease represents a major cause of mortality worldwide. In the USA alone there are approximately 100,000 valve replacement or repair operations and 20,000 associated deaths per year (Otto and Bonow, 2009). Mitral valve (MV) dysfunction, manifested by valve regurgitation and/or stenosis, represents the second major valvular disorder in the Western world, after aortic valve dysfunction (Chockalingam *et al*., 2004). Current strategies for MV dysfunction are mainly focused on the repair of the diseased valve or its replacement with a mechanical, bioprosthetic, homograft (semilunar or MV) or autograft (pulmonary) valve (Moon *et al*., 2001). However, both strategies only deliver biocompatible solutions that cannot regenerate or grow with the patient, causing serious disadvantages especially for young patients (Chauvaud *et al*., 2003; Dumont *et al*., 2007). Tissue engineering approaches have the potential to deliver solutions to the problems associated with conventional MV repair and replacement through the development of tailor-made MV replacements or reconstruction materials. In addition, particularly for the pediatric population, tissue-engineered heart valves could represent the optimal solution for valve reconstruction due to their potential for growth, repair and remodelling (Sapirsten and Smith, 2001; Booth, *et al*., 2002; Vesely, 2005).

The overall aim of this study was to investigate the functional tissue engineering of MV leaflets. The approach adopted was to utilise decellularised porcine pericardium seeded with porcine cells. The long term strategy was envisaged as the production of decellularised xenogeneic donor pericardial scaffolds seeded with the patient's own MSCs, isolated from the bone marrow, and mechanically conditioned in a bioreactor, to allow for the remodelling of the scaffold in order to obtain a MV-leaflet-equivalent tissue prior to implantation. Human cells were not used in this study due to the limited availability of human tissue.

During the course of this study, the biomechanical and biological properties of porcine MV leaflets were studied with a view to understanding the histoarchitectural, biomechanical and functional requirements of the tissue engineered (TE) constructs. The properties of native and decellularised porcine pericardium were also studied to assess the effects of decellularisation

on the histoarchitecture, biomechanics and function of the pericardium, as well as to assess the suitability of pericardium for MV leaflet repair. The biocompatibility and DNA content of pericardium after decellularisation were investigated.

The decellularised pericardia were then seeded with different cells types (porcine smooth muscle cells (pSMCs), porcine skin fibroblasts and porcine mesenchymal stem cells (pMSCs)) to investigate the seeding density and time point to culture the samples statically, prior to loading on the bioreactor for dynamic stimulation. A novel bioreactor system was described, calibrated and optimised for static and dynamic experiments with both fresh and cell-seeded decellularised porcine pericardium. In particular, fresh pericardium was used to validate the system, in terms of oxygen and pH control, during static culture; subsequently, 1 day static and dynamic (at 10% strain) experiments were performed in the bioreactor using decellularised pericardium seeded with pMSCs.

Porcine MV leaflets were used in this study for comparative purposes due to the limited availability of human tissue. Previous studies have demonstrated that the anatomic structure of human and porcine MV apparatus is similar (Kunzelman *et al*., 1994). Decellularised pericardium was chosen as the natural scaffold for the regeneration of MV leaflets; the reason for the choice of this specific tissue was that pericardium has been commonly used in the clinic for the repair of MV leaflets (Maranto and Schoen, 1988; Chauvad *et al*., 1991; Duran and Gometza, 1993; Muhercke *et al*., 1997; Chauvad *et al*., 2001; Dillon *et al*., 2013). In addition to this, a natural scaffold was chosen over a synthetic alternative due to its inherent properties; natural scaffolds present natural histoarchitecture and biochemical cues, which can potentially favour cell adhesion, migration and proliferation (Mendelson and Schoen, 2006). Synthetic materials have limitations in terms of their mechanical properties, which are usually poor and make them unlikely candidates for implantation to the demanding valvular environment in the body (Rabkin and Schoen, 2002).

Another option amongst the natural scaffolds was a reconstituted extracellular matrix (ECM) protein-based scaffold; in particular, a recombinant human collagen scaffold might represent a good alternative to a decellularised biological scaffold for MV leaflet reconstruction. Indeed, collagen is the major component of the ECM and it provides mechanical strength to tissues; recombinant human collagen has the same amino acid sequence as human tissue-derived collagen and can be produced with a similar degree of stability as natural collagen (Yang *et al*., 2004). Recombinant human collagens types I and III have been used as corneal

substitutes for implantation in *in vivo* studies (Merret *et al*., 2008). This approach for the production of collagen has some advantages in comparison to collagen derived from an animal, such as better quality and purity as well as no risk of transmission of infectious agents. Nevertheless, collagen constructs, as well as reconstituted protein scaffolds in general, have limitations in terms of both excessive shrinkage of the construct after cell seeding and insufficient mechanical properties (Shi and Vesely, 2004; Mendelson and Schoen, 2006). The dynamic conditioning of collagen constructs seeded with cells might help to overcome problems of shrinkage of the scaffold; the mechanical stimuli could potentially withstand the contractile forces developed by the cells.

The histological examination of fresh pericardium revealed its characteristic trilaminar structure. The histoarchitecture was maintained after decellularisation; nevertheless, a high loss of glycosaminoglycans (GAGs), mainly concentrated in the mesothelial region, was observed. Histological analysis of MV leaflets showed the collagen fibre alignment along the circumferential direction and revealed their characteristic quadrilaminar structure. The conclusions from the histological analysis were that the fibrous layer of fresh and decellularised pericardium was quite comparable to the fibrosa of the MV leaflets, rich in densely packed collagen fibres and with small and few elastic fibres, however, the collagen fibre orientation in the pericardium was more multidirectional compared to that in the fibrosa of the leaflets which was mainly aligned along the circumferential direction.

The biochemical analysis of the tissues showed that both fresh and decellularised pericardium had a lower GAG content compared to both the anterior and posterior MV leaflet, and the hydroxyproline (HXP) content of decellularised pericardium was higher compared to that of both the anterior and posterior leaflets.

The biomechanical characterisation of the porcine MV leaflet specimens showed the characteristic anisotropic behaviour of the anterior and the rather isotropic behaviour of the posterior leaflets. The anterior leaflets demonstrated a higher collagen phase slope and ultimate tensile strength (indicative of a stiffer tissue) in the circumferential direction compared to the radial direction, as well as compared to the circumferential and radial directions of the posterior leaflets. This behaviour of the anterior leaflet is related to its distinct histoarchitecture that features circumferentially-aligned collagen fibres, and compensates for the significantly higher stress that the anterior leaflet experiences during the cardiac cycle (Jensen, 2006; Kunzelman *et al*., 1993a; May-Newman and Yin, 1995; Roberts, 2012). Both fresh and

decellularised pericardium demonstrated rather isotropic mechanical behaviours, in contrast to the anisotropic properties observed for the MV anterior leaflets. In addition, both fresh and decellularised pericardium were less compliant and stiffer compared to the leaflets.

These findings showed that MV leaflets and porcine pericardium presented different biological and mechanical properties. Despite these limitations, decellularised porcine pericardium was still considered a good choice for this project.

This was because mechanical stimulation of cell-seeded decellularised pericardium *in vitro* in a bioreactor, could potentially guide the histoarchitectural, biochemical and biomechanical remodelling of the scaffold towards a more leaflet-like histoarchitecture, biochemistry and biomechanics.

In addition to histochemical and mechanical analysis, the DNA content and biocompatibility of decellularised pericardium were determined. A reduction in the DNA content of 99% was observed following decellularisation and the cytotoxicity assays showed that porcine fibroblasts and pMSCs grew well in contact with the scaffold and with scaffold extracts, demonstrating adequate removal of the chemicals used during the decellularisation process.

Prior to static and dynamic experiments with the bioreactor, the potential of decellularised pericardial samples to support cell attachment was investigated. Cells needed to attach to and form a continuous monolayer on the surface of the scaffold, prior to dynamic culture in the bioreactor, in order to avoid dislodging of the cells during mechanical stimulation (Ye *et al.*, 2009). The cells chosen for seeding were SMCs and dermal fibroblasts which expressed a phenotype close to the VICs of the MV leaflets *in vivo* and MSCs due to their relative ease of isolation from the bone marrow of the patient and their differentiation potential towards the VICs phenotype under mechanical stimuli *in vitro.* Following confirmation of cell phenotype, the seeding density and time point for culturing the cells on the scaffolds prior to loading on the bioreactor were investigated. Results obtained with fibroblasts and pSMCs showed the need for a longer culture duration and higher cell density for seeding the scaffold compared to pMSCs, probably due to their limited lifespan, being terminally differentiated. Owing to these results, only pMSCs were used in the subsequent dynamic cultures.

It has been reported that bone marrow derived MSCs have a propensity to default towards an osteogenic lineage (Yoon *et al.*, 2004). This issue could potentially be overcome by careful use of selection methods, such as magnetic-activated cell sorting (MACS) or fluorescence-

activated cell sorting (FACS) (Deschaseaux *et al*., 2003), or using a different source for MSCs, such as adipose tissue, which can be isolated in fairly large quantities using minimally invasive procedures (Pansky *et al*., 2007). Other stem cells which have been reported in the literature for possible use in heart valve tissue engineering are embryonic stem cells and induced pluripotent stem cells (iPCs). These cell types were not chosen for this study due to their limitations. Embryonic stem cells are allogeneic and may be rejected by the patient and undifferentiated embryonic stem cells may be tumorogenic (Forsberg and Hovatta, 2012). In addition there are ethical concerns associated with their harvesting which is embryo-destructive (Forsberg and Hovatta, 2012). Induced pluripotent stem cells, in contrast to embryonic stem cells, do not raise ethical concerns; nevertheless, research using these cells is still at a relatively early stage and there are concerns about their safety in terms of carcinogenic potential of virally or non-virally transduced lines, in the latter case, due to genome instability (Weber *et al*., 2012). Long term animal studies need to be performed to evaluate the safety when using such cells for tissue regeneration.

The bioreactor represents a major component required for the development of tissue engineered heart valves. The bioreactor system used in this study was designed in order to mimic *in vitro* the biaxial strain that the MV leaflets experience *in vivo*, which is mainly characterised by an inflation and deflation of the leaflets during the cardiac cycle (Nolan *et al.,* 1969). During the dynamic cultures, the seeded scaffolds were subjected to biaxial strain amplitude of 10%. This strain level was obtained from previously-developed, near-physiological computational models (fluid-solid-interaction) of the MV apparatus (Roberts, 2012), and represented the maximum strain predicted for the central region of the MV anterior leaflets during the cardiac cycle. To date, the only study reported in the literature on the tissue engineering of MV leaflets was by Flanagan *et al*. (2006). Unfortunately the study of Flanagan *et al*. (2006) did not include any mechanical conditioning of the tissue engineered constructs.
The study progressed to validate the bioreactor system in terms of its ability to maintain cell viability using fresh pericardial patches, which were disinfected using an optimised Cambridge antibiotic protocol and cultured statically for 1 day. Numerous problems were encountered when setting up the pericardium in the bioreactor stations. Initially problems were encountered with air entrapment beneath the pericardium which led to a rapid loss of viability during static culture. This problem was overcome by careful attention to the technique used to fill the stations with medium plus improving the design of the bioreactor stations by adding a stopcock and a tube open to the atmosphere. It would however be useful for future studies to

redesign further aspects of the bioreactor stations. For example, the inlet and the outlet of the lower station consisted of small holes located just below the pericardial membrane; their size should be increased to allow for a better removal of the air during filling with medium. Furthermore, it was observed that while filling the lower station, the medium was partly going towards the lower station and partly towards the upper station, probably due to air entrapment. To overcome this issue, the inlet port of the lower station should be redesigned to guide the flow of medium towards the lower station during filling. Since it was not practicable to make these changes during the course of this study due to time pressure, it was necessary to change the technique for filling the station to solve this issue. Another problem was represented by the soft material of the luer fittings; during initial static experiments a leakage was observed in a bioreactor station, developing at one of the polyvinylidene fluoride (PDVF) luer fittings used to connect the silicone tubing. This problem was resolved by replacing with stronger stainless steel fittings.

Problems were also encountered with loss of tissue viability due to inadequate oxygen and pH control and insufficient passive diffusion of the oxygen through the head volume when the chemostat was not used for physiological control. Unfortunately the bioreactor had been designed to be fed via a 2 L chemostat through which medium conditions were controlled. It was considered wasteful to utilise this volume of expensive medium for short term experiments. This was another design feature that could be improved prior to further studies using the bioreactor. In spite of numerous changes to the methodology used for the culture and analysis of fresh pericardium it was finally concluded that this tissue had an inherent variability in viability that could not be easily overcome. This was most likely related to the quality of the fresh tissue, indeed it has been reported that cell viability of tissue is affected by the deterioration of some cellular organelles shortly after death (Alessandrini *et al*., 1994). The original idea was to culture the fresh pericardial samples statically and also dynamically in the bioreactor in order to optimise the strain value to be used during dynamic experiments with cell-seeded decellularised pericardial samples, in order to maintain the ECM integrity and cell viability during mechanical conditioning in the bioreactor. Unfortunately, it was impossible to further proceed with the dynamic experiments with fresh pericardium, due to the high level of variability in the viability of the tissue that was available. The viability of tissues could possibly be improved if tissues could be immediately submerged in tissue transport medium containing proteinase inhibitors such as aprotinin following removal from the carcases at the abattoir.

Unfortunately, this was not possible during the course of this study due to the reluctance of the abattoir staff to change their working practice.

Studies therefore progressed to utilise pMSC-seeded scaffolds. Initially, the pMSC-seeded scaffolds were seeded statically in bioreactor stations and in tissue holders housed in tissue pots, with the view to investigating potential differences between the two conditions to be used as static controls for the dynamic cultures. After one day, the pMSC-seeded scaffolds in both the bioreactor stations and the tissue holders maintained their viability. Subsequently, pMSC-seeded scaffolds were conditioned under 10% cyclic strain in the bioreactor, whereas additional pMSC-seeded scaffolds were maintained statically in the tissues holders. Again, with dynamic cultures, problems were encountered with air entrapment beneath the scaffolds. Moreover, air was observed underneath the bottom silicone membrane of some stations, causing an unequal volume displacement between the 4 stations. Unfortunately, it was difficult to visualise the level of the medium in the upper stations, with respect to the inlet port due to the small size of the glass window. In addition to this, it was also impossible to visualise the level of the medium in the lower station, and so, it was not possible to observe if the medium was into contact with the bottom surface of samples during the dynamic culture. These issues were finally overcome during the final one day dynamic experiment, by adjusting the flow rate of the medium pumped from the chemostat to the stations so that the level of medium in the upper station was constantly maintained above the inlet port, and by pumping some additional water in the bioreactor chamber, after mounting the stations, until all the air trapped underneath the silicone membranes of the four stations was removed.

The one day dynamic experiment was repeated with the improvements and results showed that cells were viable both after one day dynamic culture in the bioreactor and one day static culture in the tissue holders. Cells started aligning along specific directions when cultured dynamically; unfortunately, it was not possible to define along which direction (circumferential or radial). It has been reported that cell alignment can guide the deposition of ECM proteins, such as collagen and elastin, along specific directions, guiding the formation of specific histoarchitecture (Altman *et al.*, 2002; Mol *et al.,* 2003; Grenier *et al.*, 2005).

In conclusion, prior to future studies the stations should be fabricated using a transparent material to allow for visualisation of the samples. Transparent materials such as polycarbonate, and plexiglass combined with silicone have been used in previous studies (Hoerstrup *et al*., 2000b; Mol *et al*., 2005), these materials allowed for the visualisation of the

engineered valve under culture and can be sterilised using ethylene oxide. Glass could also be used for the fabrication of a large cylindrical window, but it could not be used for the production of more complex components.

In addition to the material used in the fabrication of the bioreactor stations, as indicated above, the design of the bioreactor stations should be changed to make the system more user-friendly. The volumes of the upper and lower parts of the stations could be reduced by half without compromising nutrient supply to the constructs. In addition to using a transparent material, the material of choice would be much lighter than stainless steel. The upper surface of the chamber onto which the bioreactor stations are loaded should be large enough to easily accommodate the many tubing connections of the stations and it should be lower in height. The stations would be easier to incorporate if they did not screw into the rosette, but rather appropriate slots provided with o rings should be designed in the rosette in order to position and "clamp" the stations. The stations should then be connected through a system of pumps to a reservoir for the supply and collection of medium. The whole system could be housed in an incubator to avoid the use of the heaters for the maintenance of the temperature (37ºC) in the stations.

Hoerstrup *et al*. (2000b) created a simple and compact heart valve bioreactor which could be fitted in a standard incubator and which consisted of an air chamber, a reservoir filled with cell culture medium and a perfusion chamber which held the heart valve, sewn inside a transparent silicon tube. A silicon diaphragm was placed between the air chamber and the perfusion chamber, and the air chamber was connected to a respirator pump. The pulsatile flow was achieved by pumping air into the lower chamber and displacing the silicone diaphragm between the liquid chamber and the lower air chamber periodically. The limitation of this system was that it only held one sample; however, this design could be modified to have at least four samples in series.

Further limitations were observed during the use of the chemostat for the monitoring and supply of the oxygen and the 5% (v/v) CO_2. Chemostats were originally developed for the growth of microorganisms. The chemostat was rather complicated to use during the bioreactor experiments; the high number of connections and the long length of the tubes connected to the stations and the reservoir made the chemostat system too bulky and introduced further risks of contamination. The whole set up of the system was not user friendly. In the designs suggested above, the chemostat would be replaced by a reservoir, which could be provided

with an air filter and connected to a gas cylinder with 5% (v/v) CO_2 in air for the continuous supply of oxygen and for the pH control. The culture medium could then be pumped from the reservoir to the stations and then from the stations back to the reservoir in a closed loop system.

Despite the encouraging results from the short-term dynamic cultures of pMSC-seeded decellularised pericardial scaffold, in terms of viability maintenance and cell alignment, future studies need to focus on longer term dynamic cultures, in order to investigate MSC differentiation and phenotype, ECM remodelling and tissue remodelling (Hoerstrup *et al*., 2002; Rabkin *et al*., 2002; Mol *et al*., 2005; Engelmayr *et al*., 2006; Ku *et al*., 2006; Balachandran *et al*., 2009;) as well as on the experimental validation of the strains experienced by the engineered construct during dynamic conditioning (Engelmayr *et al.,* 2003). Seeded constructs could be cultured for one week and 21 days to investigate tissue remodelling over time; similar time points have been used previously, showing ECM production and remodelling at 21 days (Engelmayr *et al*., 2005 and 2006; Weber *et al*., 2013). Biological characterisation of samples should include histology (H&E) for the visualisation of cell distribution and immunohistochemistry for collagen I and III and chondroitin sulphate, to investigate the ECM remodelling and deposition. The qualitative results of the immunohistochemical analysis could be compared to quantitative assays for the measurements of HXP and GAG content. Qualitative and quantitative analysis have been used in previous studies to assess ECM remodelling (Engelmayr *et al*., 2005, 2006; Masoumi *et al*., 2013a, 2013b; Weber *et al*., 2013).

The differentiation of MSCs could be investigated and assessed through immunocytochemical labelling of alpha-SMA, calponin and vimentin to investigate differentiation towards fibroblast or myofibroblast phenotype, and smooth muscle myosin to distinguish between the differentiation towards myofibroblast or SMC phenotype (Perez-Montiel *et al*., 2013). Von Kossa staining as well as osteocalcin could be used as bone marker to investigate potential calcification of the seeded construct as well as potential differentiation of the cells towards an osteoblast phenotype (Mizuno *et al*., 2001; Nakamura *et al*., 2009). Cell differentiation and levels of up-regulation of gene expression after dynamic conditioning of samples could be investigated through reverse-transcriptase polymerase chain reaction (RT-PCR) analysis; in particular the levels of up-regulation mRNA for the alpha-SMA, calponin, vimentin and smooth muscle myosin genes should be studied for cell differentiation, as well as mRNA for COL3A1

gene (type III collagen) and COL1A1 gene (type I collagen) for ECM production, as reported in previous studies (Ku *et al*., 2006). Mechanical tests, such as uniaxial tensile tests, should be performed to investigate the change in the mechanical properties of seeded constructs in comparison to the original scaffold and anisotropic properties of native MV leaflets. In addition, the actual strains experienced by the seeded constructs during mechanical conditioning would require validation as described by Engelmayr *et al.* (2003). The authors developed a cyclic flexure bioreactor system, which involved the recording of images during flexural deformation of samples. Prior to the start of the experiments, they created a calibration grid to couple the data in pixels to the physical dimensions of the sample, in mm. During the experiments, they recorded and calculated the positions and coordinates of some markers positioned on the sample, together with the applied load during one flexure cycle, through a custom C program. They processed all the data using a custom Matlab program to calculate the applied moment and the resulting change in curvature of the sample.

The clinical application of this project to the tissue engineering of the MV would involve the use of xenogeneic porcine pericardial scaffolds that have been treated to remove the immunogenic cells, and then reseeded with the patient's own cells and mechanically conditioned *in vitro*, with a view to producing biological and biomechanical functionality of the graft prior to implantation. Another possible tissue engineering approach would involve the implantation of unseeded scaffolds, with a view to attracting endogenous cell repopulation *in vivo*, after implantation. The potential use of unseeded decellularised scaffolds for MV leaflet reconstruction in the clinic might be limited by the variability of the patient response in terms of recellularisation, especially in the elderly. The ECM proteins would be continuously degraded *in vivo* due to cyclic loading and the presence of functional cells in the scaffold at the time of implantation would create an immediate remodelling potential *in vivo*.

Nevertheless, the clinical translation of cell seeded constructs represents a major challenge. The seeded constructs will need to be tested in a relevant large animal prior to implantation in human. For example, the decellularised porcine pericardium could be seeded with ovine cells, dynamically conditioned in a bioreactor and then, the seeded construct could be implanted into the sheep from which the cells were isolated. This approach would be representative of the homogeneic model of human (autologous) cells seeded to xenogeneic decellularised scaffolds, and physically conditioned in a bioreactor prior to implantation. If the results from the animal study were successful, showing the effective remodelling of the seeded construct

and the maintenance of the valve dynamics *in vivo*, then the same approach could be tested in an initial clinical trial in a small number of patients. If the results from the clinical trial were successful, then this approach could be established in specialist hospitals. In addition, if the bioreactor system was better optimised and simplified, it could be commercialised.

Bioreactors would have to be located in Good Manufacturing Practice (GMP) laboratories in or close to the hospitals, so that cells, isolated from the patient through specific protocols developed for the isolation of the MSCs, could be firstly expanded, using dedicated equipment, and then cultured on the scaffold dynamically up to a specific time point, chosen on the basis of previous studies. The cells would have to be cultured and expanded using specific protocols under ISO standards to ensure quality assurance and safety. These standards and regulations are set by the European Union Tissue and Cells Directives (EUTCD); in particular, in the UK, the Human Tissue Authority, one of the competent authorities under the EUTCD, has responsibility for regulating cells, as well as tissues, and for the registration of the facilities where the expansion and culture of the cells is carried out. Such Authority establishes the regulations for the procurement, testing, processing, storage and distribution of cells and tissues for human application.

In addition, the process would require the use of traceable quality assured reagents and equipment, used during the production process. Quality assurance of the final product (the seeded construct) would also have to be carried out in order to ensure that the whole procedure was safe and that the construct was fit for its intended use and did not place the patient at risk or render the cells harmful or clinically ineffective. It would be necessary to develop non-invasive methods to ensure the quality of the constructs. The implant would also need to be monitored after implantation; echocardiography has been reported as being the method of choice for the evaluation of the function of the valve (Pibarot and Dumesnil, 2009).

To date, no MV leaflets have been produced or commercialised for clinical application, using a tissue engineering approach. A recent interesting example of tissue engineered scaffold reseeded *in vitro* with the patient's autologous cells, and cultured under mechanical stimulation, for clinical application, was described in the study of Macchiarini *et al.* (2008). In this study, a decellularised human trachea free of cells and major histocompatibility complex (MHC) antigens was produced, then the scaffold was cultured with epithelial cells and chondrocytes derived from MSCs, taken from the patient, under mechanical conditioning in a bioreactor. The graft was then used to replace the patient's bronchus. The results were

successful, showing an improved quality of life of the patient, the formation of a functional airway with normal appearance and mechanical properties after 4 months. Also, no immunosuppressive drugs were used. These results are encouraging, showing that by using the appropriate techniques and methodology it could be possible to provide tissue engineered constructs, cultured with the patient's own cells and dynamically conditioned, to successfully treat patients with serious clinical disorders.

In this study, decellularised pericardial scaffolds were seeded dynamically for up to one day *in vitro* in a novel MV leaflet bioreactor. Results were encouraging showing that the viability of cells could be maintained in the system and cells started aligning along preferred directions under dynamic stimulation. Overall the approach used for the mechanical stimulation of the reseeded biological scaffolds has good potential for the development of a tissue engineered construct that could be used in the clinic for the reconstruction of MV leaflets in a limited number of patients.

References

ACAR, C., DE IBARRA, J. S., LANSAC, E. (2004). Anterior leaflet augmentation with autologous pericardium for mitral repair in rheumatic valve insufficiency. *The Journal of heart valve disease*, *13*(5), 741–6.

AKINS, C. W., HILGENBERG, A. D., BUCKLEY, M. J., VLAHAKES, G. J., TORCHIANA, D. F., DAGGETT, W. M., AUSTEN, W. G. (1994). Mitral valve reconstruction versus replacement for degenerative or ischemic mitral regurgitation. *The Annals of thoracic surgery*, *58*(3), 668–75; discussion 675–6.

ALESSANDRINI, F., D'ARMINI, A. M., ROBERTS, C. S., REDDICK, R. L., EGAN, T. M. (1994). When does the lung die? II. Ultrastructural evidence of pulmonary viability after "death". *The Journal of heart and lung transplantation : the official publication of the International Society for Heart Transplantation*, *13*(5), 748–57.

ALFIERI, O., and MAISANO, F. (1999). An effective technique to correct anterior mitral leaflet prolapse. *Journal of cardiac surgery*, *14*(6), 468–70.

ALFIERI, O., DE BONIS, M., LAPENNA, E., REGESTA, T., MAISANO, F., TORRACCA, L., LA CANNA, G. (2004). "Edge-to-edge" repair for anterior mitral leaflet prolapse. *Seminar of Thoracic Cardiovascular Surgery, 16*(2), 182-7.

ALI, M., IUNG, B., LANSAC, E., BRUNEVAL, P., ACAR, C. (2004). Homograft replacement of the mitral valve: eight-year results. *The Journal of thoracic and cardiovascular surgery*, *128*(4), 529–34.

ALTMAN, G. H., HORAN, R. L., MARTIN, I., FARHADI, J., STARK, P. R. H., VOLLOCH, V., VUNJAK-NOVAKOVIC, G., RICHMOND, J., KAPLAN, D. L. (2002). Cell differentiation by

mechanical stress. *FASEB journal : official publication of the Federation of American Societies for Experimental Biology*, *16*(2), 270–2.

ARNETT, E. N., and ROBERTS, W. C. (1976). Active infective endocarditis: a clinicopathologic analysis of 137 necropsy patients. *Current problems in cardiology*, *1*(7), 2–76.

AUBERT, S., BARREDA, T., ACAR, C., LEPRINCE, P., BONNET, N., ECOCHARD, R., PAVIE, A., GANDJBAKHCH, I. (2005). Mitral valve repair for commissural prolapse: surgical techniques and long term results. *European journal of cardio-thoracic surgery : official journal of the European Association for Cardio-thoracic Surgery*, *28*(3), 443–7.

AURICCHIO, F. (2003). Corso di biomeccanica, parte 7: legami costitutivi. Lecture of the Università degli Studi di Pavia, Dipartimento di Meccanica Strutturale. Available from http//www.unipv.it/dms/auricchio (Accessed on 22/11/2013).

BADYLAK, S. F., TULLIUS, R., KOKINI, K., SHELBOURNE, K. D., KLOOTWYK, T., VOYTIK, S. L., Kraine, M. R., SIMMONS, C. (1995). The use of xenogeneic small intestinal submucosa as a biomaterial for Achilles tendon repair in a dog model. *Journal of biomedical materials research*, *29*(8), 977–85.

BAEURLE, S. A., KISELEV, M. G., MAKAROVA, E. S., NOGOVITSIN, E. A. (2009). Effect of the counterion behavior on the frictional–compressive properties of chondroitin sulfate solutions. *Polymer, 50*(7), 1805–1813.

BAIRATI, A., and DEBIASI, S. (1981). Presence of a smooth muscle system in aortic valve leaflets. *Anatomy and embryology*, *161*(3), 329–40.

BALACHANDRAN, K., SUCOSKY, P., JO, H., YOGANATHAN, A. P. (2009). Elevated cyclic stretch alters matrix remodelling in aortic valve cusps: implications for degenerative aortic valve disease. *American journal of physiology. Heart and circulatory physiology*, *296*(3), H756–64.

BANES, A. J., TSUZAKI, M., YAMAMOTO, J., FISCHER, T., BRIGMAN, B., BROWN, T., MILLER, L. (1995). Mechanoreception at the cellular level: the detection, interpretation, and diversity of responses to mechanical signals. *Biochemistry and cell biology = Biochimie et biologie cellulaire*, *73*(7-8), 349–65.

BARBER, J. E., KASPER, F. K., RATLIFF, N. B., COSGROVE, D. M., GRIFFIN, B. P., VESELY, I. (2001a). Mechanical properties of myxomatous mitral valves. *The Journal of thoracic and cardiovascular surgery*, *122*(5), 955–62.

BARBER, J. E., RATLIFF, N. B., COSGROVE, D. M., GRIFFIN, B. P., VESELY, I. (2001b). Myxomatous mitral valve chordae. I: Mechanical properties. *The Journal of heart valve disease*, *10*(3), 320–4.

BENNETT, R. M., GABOR, G. T., MERRITT, M. M. (1985). DNA binding to human leukocytes. Evidence for a receptor-mediated association, internalization, and degradation of DNA. *The Journal of clinical investigation*, *76*(6), 2182–90.

BERRY, J. L., STEEN, J. A., KOUDY WILLIAMS, J., JORDAN, J. E., ATALA, A., YOO, J. J. (2010). Bioreactors for development of tissue engineered heart valves. *Annals of biomedical engineering, 38*(11), 3272–9.

BEVILACQUA, S., CERILLO, A. G., GIANETTI, J., PARADOSSI, U., MARIANI, M., MATTEUCCI, S., KALLUSHI, E., GLAUBER, M. (2003). Mitral valve repair for degenerative disease: is pericardial posterior annuloplasty a durable option? *European journal of cardio-*

thoracic surgery : official journal of the European Association for Cardio-thoracic Surgery, *23*(4), 552–9.

BIANCO, P., and ROBEY, P. G. (2001). Stem cells in tissue engineering. *Nature*, *414*(6859), 118–21.

BILLIAR, K. L., and SACKS, M. S. (2000). Biaxial mechanical properties of the natural and glutaraldehyde treated aortic valve cusp--Part I: Experimental results. *Journal of biomechanical engineering*, *122*(1), 23–30.

BLAU, H. M., BRAZELTON, T. R., WEIMANN, J. M. (2001). The evolving concept of a stem cell: entity or function? *Cell*, *105*(7), 829–41.

BOLLING, S. F., PAGANI, F. D., DEEB, G. M., BACH, D. S. (1998). Intermediate-term outcome of mitral reconstruction in cardiomyopathy. *The Journal of thoracic and cardiovascular surgery*, *115*(2), 381–6; discussion 387–8.

BOOTH, C., KOROSSIS, S. A., WILCOX, H. E., WATTERSON, K. G., KEARNEY, J. N., FISHER, J., INGHAM, E. (2002). Tissue engineering of cardiac valve prostheses I: development and histological characterization of an acellular porcine scaffold. *The Journal of heart valve disease, 11*(4), 457–62.

BORGHETTI, V., CAMPANA, M., SCOTTI, C., DOMENIGHINI, D., TOTARO, P., COLETTI, G., PAGANI, M., LORUSSO, R. (2000). Biological versus prosthetic ring in mitral-valve repair: enhancement of mitral annulus dynamics and left-ventricular function with pericardial annuloplasty at long term. *European Journal of Cardiothoracic Surgery, 17*(4), 431-9.

BOSKEY, A. L. (1981). Current concepts of the physiology and biochemistry of calcification. *Clinical orthopaedics and related research*, (157), 225–57.

BOTH, S. K., VAN DER MUIJSENBERG, A. J. C., VAN BLITTERSWIJK, C. A., DE BOER, J., DE BRUIJN, J. D. (2007). A rapid and efficient method for expansion of human mesenchymal stem cells. *Tissue engineering*, *13*(1), 3–9.

BRAGA/VILELA, A. S., PIMENTEL, E. R., MARANGONI, S., TOYAMA, M. H., DE CAMPOS VIDAL, B. (2008). Extracellular matrix of porcine pericardium: biochemistry and collagen architecture. *The Journal of membrane biology*, *221*(1), 15–25.

BRAUN, J., VAN DE VEIRE, N. R., KLAUTZ, R. J., VERSTEEGH, M. I., HOLMAN, E. R., WESTENBERG, J. J., BOERSMA, E., VAN DER WALL, E. E., BAX, J. J., DION, R. A. (2008). Restrictive mitral annuloplasty cures ischemic mitral regurgitation and heart failure. *The Annals of Thoracic Surgery, 85*(2), 430-6; discussion 436-7.

BRAUNBERGER, E., A. DELOCHE, A. BERREBI, F. ABDALLAH, J. A. CELESTIN, P. MEIMOUN, G. CHATELLIER, S. CHAUVAUD, J. N. FABIANI, A. CARPENTIER (2001). Very long-term results (more than 20 years) of valve repair with Carpentier's techniques in nonrheumatic mitral valve insufficiency. *Circulation*, *104*(12 Suppl 1), I8–11.

BREEN, E. C. (2000). Mechanical strain increases type I collagen expression in pulmonary fibroblasts in vitro. *Journal of applied physiology (Bethesda, Md. : 1985)*, *88*(1), 203–9.

BROWN, A.J., MCCORMICK, L.M., BRAGANZA, D.M., HOOLE, S.P., WEST, N.E. (2013). TCT-571 The impact of predilatation on bioresorbable vascular scaffold expansion *in vivo* - insights from optical coherence tomography. *Journal of the American College of Cardiology*, *62*(18), B172.

BROWN, B., LINDBERG, K., REING, J., STOLZ, D. B., BADYLAK, S. F. (2006). The basement membrane component of biologic scaffolds derived from extracellular matrix. *Tissue engineering*, *12*(3), 519–26.

BUCCIANTE, L. (1975). Istituzioni di anatomia dell'uomo. Piccin-Nuona Libraria edizione, Volume 2.

BUCHBINDER, N. A., and ROBERTS, W. C. (1972). Left-sided valvular active infective endocarditis. *The American Journal of Medicine*, *53*(1), 20–35.

BUCKLEY, M. J., BANES, A. J., LEVIN, L. G., SUMPIO, B. E., SATO, M., JORDAN, R., GILBERT, J., LINK, G. W., TRAN SON TAY, R. (1988). Osteoblasts increase their rate of division and align in response to cyclic, mechanical tension in vitro*. Bone and mineral, 4*(3), 225–36.

BUSCHMANN, M. D., GLUZBAND, Y. A., GRODZINSKY, A. J., HUNZIKER, E. B. (1995). Mechanical compression modulates matrix biosynthesis in chondrocyte/agarose culture. *Journal of cell science, 108*(Pt 4), 1497–508.

BUTCHER, J. T., PENROD, A. M., GARCÍA, A. J., NEREM, R. M. (2004). Unique morphology and focal adhesion development of valvular endothelial cells in static and fluid flow environments. *Arteriosclerosis, thrombosis, and vascular biology*, *24*(8), 1429–34.

BUTCHER, J. T., TRESSEL, S., JOHNSON, T., TURNER, D., SORESCU, G., JO, H., NEREM, R. M. (2006). Transcriptional profiles of valvular and vascular endothelial cells reveal phenotypic differences: influence of shear stress. *Arteriosclerosis, thrombosis, and vascular biology*, *26*(1), 69–77.

BUTT, R. P., and BISHOP, J. E. (1997). Mechanical load enhances the stimulatory effect of serum growth factors on cardiac fibroblast procollagen synthesis. *Journal of molecular and cellular cardiology*, *29*(4), 1141–51.

CARAPETIS, J. R. (2007). Rheumatic heart disease in developing countries. *The New England journal of medicine, 357*(5), 439-41.

CARPENTIER, A. (1983). Cardiac valve surgery--the “French correction”. *The Journal of thoracic and cardiovascular surgery*, *86*(3), 323–37.

CEBOTARI, S., LICHTENBERG, A., TUDORACHE, I., HILFIKER, A., MERTSCHING, H., LEYH, R., BREYMANN, T., KALLENBACH, K., MANIUC, L., BATRINAC, A., REPIN, O., MALIGA, O., CIUBOTARU, A., HAVERICK, A. (2006). Clinical application of tissue engineered human heart valves using autologous progenitor cells. *Circulation, 114*(1 Suppl), 1132-1137.

CHAUVAUD, S., V. JEBARA, CHACHQUES, J. C., EL ASMAR, B., MIHAILEANU, S., PERIER, P., DREYFUS, G., RELLAND, J., COUETIL, J. P. CARPENTIER, A. (1991). Valve extension with glutaraldehyde-preserved autologous pericardium. Results in mitral valve repair. *The Journal of thoracic and cardiovascular surgery*, *102*(2), 171–7; discussion 177–8.

CHAUVAUD, S., FUZELLIER, J. F., HOUEL, R., BERREBI, A., MIHAILEANU, S., CARPENTIER, A. (1998). Reconstructive surgery in congenital mitral valve insufficiency (Carpentier’s techniques): long-term results. *The Journal of thoracic and cardiovascular surgery*, *115*(1), 84–92; discussion 92–3.

CHAUVAUD, S., FUZELLIER, J.-F., BERREBI, A., DELOCHE, A., FABIANI, J.-N., CARPENTIER, A. (2001). Long-Term (29 Years) Results of reconstructive surgery in rheumatic mitral valve insufficiency. *Circulation*, *104*(Supplement 1), I–12–I–15.

CHAUVAUD, S., WALDMANN, T., D’ATTELLIS, N., BRUNEVAL, P., ACAR, C., GEROTA, J., JARRAYA, M., CARPENTIER, A. (2003). Homograft replacement of the mitral valve in young

recipients: mid-term results. *European journal of cardio-thoracic surgery : official journal of the European Association for Cardio-thoracic Surgery*, *23*(4), 560–6.

CHEN, L., MCCULLOCH, A. D., MAY-NEWMAN, K. (2004). Nonhomogeneous deformation in the anterior leaflet of the mitral valve. *Annals of biomedical engineering, 32*(12), 1599–606.

CHESTER, A. H., and TAYLOR, P. M. (2007). Molecular and functional characteristics of heart-valve interstitial cells. *Philosophical transactions of the Royal Society of London. Series B, Biological sciences*, *362*(1484), 1437–43.

CHOCKALINGAM, A., PRABHAKAR, D., DORAIRAJAN, S., PRIYA, C., GNANAVELU, G., VENKATESAN, S., CHOCKALINGAM, V. (2004). Rheumatic heart disease occurrence, patterns and clinical correlates in children aged less than five years. *The Journal of heart valve disease*, *13*(1), 11–14.

CHOQUET, D., FELSENFELD, D. P., SHEETZ, M. P. (1997). Extracellular matrix rigidity causes strengthening of integrin-cytoskeleton linkages. *Cell, 88*(1), 39–48.

CLEARY, E.G., and GIBSON, M.A. (1996). Elastic tissue, elastin and elastin associated microfibrils in Extracellular Matrix. Harwood Academic Publishers.

COLE, W. G., CHAN, D., HICKEY, A. J., WILCKEN, D. E. (1984). Collagen composition of normal and myxomatous human mitral heart valves. *The Biochemical journal*, *219*(2), 451–60.

COURTMAN, D. W., PEREIRA, C. A., KASHEF, V., MCCOMB, D., LEE, J. M., WILSON, G. J. (1994). Development of a pericardial acellular matrix biomaterial: biochemical and mechanical effects of cell extraction. *Journal of biomedical materials research*, *28*(6), 655–66.

COX, B., and EMILI, A. (2006). Tissue subcellular fractionation and protein extraction for use in mass-spectrometry-based proteomics. *Nature protocols, 1*(4), 1872–8.

CULAV, E. M., CLARK, C. H., MERRILEES, M. J. (1999). Connective tissues: matrix composition and its relevance to physical therapy. *Physical Therapy, 79*(3), 308-19.

DA COSTA, F. D. A., SANTOS, L. R., COLLATUSSO, C., MATSUDA, C. N., LOPES, S. A. V, CAUDURO, S., RODERJAN, J. G., INGHAM, E. (2009). Thirteen years' experience with the Ross Operation. *The Journal of heart valve disease, 18*(1), 84–94.

DAHL, S.L., KOH, J., PRABHAKAR, V., NIKLASON, L.E. (2003). Decellularized native and engineered arterial scaffolds for transplantation. *Cell Transplant, 12*(6), 659–66.

DAIMON, M., S. FUKUDA, ADAMS, D. H., MCCARTHY, P. M., GILLINOV, A. M., CARPENTIER, A., FILSOUFI, F., ABASCAL, V. M., RIGOLIN, V. H., SALZBERG, S., HUSKIN, A., LANGENFELD, M., SHIOTA, T. (2006). Mitral valve repair with Carpentier-McCarthy-Adams IMR ETlogix annuloplasty ring for ischemic mitral regurgitation: early echocardiographic results from a multi-center study. *Circulation, 114*(1 Suppl), I588-93.

DAL PAN, F., DONZELLA, G., FUCCI, C., SCHREIBER, M. (2005). Structural effects of an innovative surgical technique to repair heart valve defects. *Journal of Biomechanics, 38*(12), 2460–2471.

DAVID, T. E. (2004). Artificial chordae. *Seminars in thoracic and cardiovascular surgery*, *16*(2), 161–8.

DAVID, T.E., ARMSTRONG, S., IVANOV, J. (2013). Chordal replacement with polytetrafluoroethylene sutures for mitral valve repair: A 25-year experience. *The Journal of Thoracic and Cardiovascular Surgery, 145*(6), 1563–1569.

DEL GAUDIO, C., VIANELLO, A., BELLEZZA, G., MAULÀ, V., SIDONI, A., ZUCCHI, A., BIANCO, A., PORENA, M. (2013). Evaluation of electrospun bioresorbable scaffolds for tissue-engineered urinary bladder augmentation. *Biomedical Materials, 8*(4).

DELOCHE, A., JEBARA, V. A., RELLAND, J. Y., CHAUVAUD, S., FABIANI, J. N., PERIER, P., DREYFUS, G., MIHAILEANU, S., CARPENTIER, A. (1990). Valve repair with Carpentier techniques. The second decade. *The Journal of thoracic and cardiovascular surgery*, *99*(6), 990–1001; discussion 1001–2.

DESCHASEAUX, F., GINDRAUX, F., SAADI, R., OBERT, L., CHALMERS, D., HERVE, P. (2003). Direct selection of human bone marrow mesenchymal stem cells using an anti-CD49a antibody reveals their CD45med,low phenotype. *British journal of haematology*, *122*(3), 506–17.

DILLON, J., YAKUB, M. A., NORDIN, M. N., PAU, K. K., KRISHNA MOORTHY, P. S. (2013). Leaflet extension in rheumatic mitral valve reconstruction. *European journal of cardio-thoracic surgery : official journal of the European Association for Cardio-thoracic Surgery*, *44*(4), 682–9.

DION, R., R. BENETIS, ELIAS, B., GUENNAOUI, T., RAPHAEL, D., VAN DYCK, M., NOIRHOMME, P., VAN OVERSCHELDE, J. L. (1995). Mitral valve procedures in ischemic regurgitation. *The Journal of heart valve disease*, *4 Suppl 2*, S124–9; discussion S129–31.

DOHMEN, P. M., and KONERTZ, W. (2009). Tissue-engineered heart valve scaffolds. *Annals of thoracic and cardiovascular surgery : official journal of the Association of Thoracic and Cardiovascular Surgeons of Asia*, *15*(6), 362–7.

DOHMEN, P. M., LEMBCKE, A., HOLINSKI, S., PRUSS, A., KONERTZ, W. (2011). Ten years of clinical results with a tissue-engineered pulmonary valve. *The Annals of thoracic surgery, 92*(4), 1308–14.

DOTY, D. B., DOTY, J. R., FLORES, J. H., MILLAR, R. C. (2001). Cardiac valve replacement with mitral homograft. *Seminars in thoracic and cardiovascular surgery*, *13*(4 Suppl 1), 35–42.

DREYFUS, G. D., SOUZA NETO, O., AUBERT, S. (2006). Papillary muscle repositioning for repair of anterior leaflet prolapse caused by chordal elongation. *The Journal of Thoracic and Cardiovascular Surgery, 132*(3), 578-84.

DU, L., WU, X., PANG, K., YANG, Y. (2011). Histological evaluation and biomechanical characterisation of an acellular porcine cornea scaffold. *The British journal of ophthalmology, 95*(3), 410–4.

DUMONT, E., GILLINOV, A. M., BLACKSTONE, E. H., SABIK, J. F., SVENSSON, L. G., MIHALJEVIC, T., HOUGHTALING, P. L., LYTLE, B. W. (2007). Reoperation after mitral valve repair for degenerative disease. *The Annals of thoracic surgery*, *84*(2), 444–50; discussion 450.

DUMONT, K., J. YPERMAN, VERBEKEN, E. SEGERS, P. MEURIS, B. VANDENBERGHE, S. FLAMENG, W. VERDONCK, P. R. (2002). Design of a new pulsatile bioreactor for tissue engineered aortic heart valve formation. *Artificials Organs, 26*(8), 710-4.

DURAN, C. M., B. GOMETZA, DE VOL, E. B. (1991). Valve repair in rheumatic mitral disease. *Circulation, 84*(5 Suppl), III125-32.

DURAN, C. G., and GOMETZA, B. (1993). New uses of pericardium for valve surgery. In: D'Allesandro LC editors. Casa Editrice Scientifica Internazionale. Rome.

DURAN, C. M. (1993). Perspectives in reparative surgery for acquired valvular disease. *Advances in cardiac surgery*, *4*, 1–23.

DURAN, C. M. (1999). Surgical techniques for the repair of anterior mitral leaflet prolapse. *Journal of cardiac surgery*, *14*(6), 471–81.

EASTWOOD, M., MCGROUTHER, D. A., BROWN, R. A. (1998). Fibroblast responses to mechanical forces. *Proceedings of the Institution of Mechanical Engineers. Part H, Journal of engineering in medicine*, *212*(2), 85–92.

EDMUNDS, L. H. (1987). Thrombotic and bleeding complications of prosthetic heart valves. *The Annals of thoracic surgery*, *44*(4), 430–45.

EDWARDS, C. A., and O'BRIEN, W. D. (1980). Modified assay for determination of hydroxyproline in a tissue hydrolyzate. *Clinica Chimica Acta*, *104*(2), 161–167.

EINSTEIN, D. R., KUNZELMAN, K. S., REINHALL, P. G., NICOSIA, M. A., COCHRAN, R. P. (2005). The relationship of normal and abnormal microstructural proliferation to the mitral valve closure sound. *Journal of biomechanical engineering, 127*(1), 134–47.

ELKINS, R.C., DAWSON, P.E., GOLDSTEIN, S., WALSH, S.P., BLACK, K.S. (2001). Decellularized human valve allografts. *The Annals of Thoracic Surgery, 71*(5), S428-S432.

ENGELMAYR, G. C., HILDEBRAND, D. K., SUTHERLAND, F. W. H., MAYER, J. E., SACKS, M. S. (2003). A novel bioreactor for the dynamic flexural stimulation of tissue engineered heart valve biomaterials. *Biomaterials*, *24*(14), 2523–32.

ENGELMAYR, G. C., ENGELMAYR, G.C.JR., E. RABKIN, F. W. SUTHERLAND, F. J. SCHOEN, J. E. MAYER, JR., SACKS, M. S. (2005). The independent role of cyclic flexure in the early in vitro development of an engineered heart valve tissue. *Biomaterials*, *26*(2), 175–187.

ENGELMAYR, G. C., SALES, V. L., MAYER, J. E., SACKS, M. S. (2006). Cyclic flexure and laminar flow synergistically accelerate mesenchymal stem cell-mediated engineered tissue formation: Implications for engineered heart valve tissues. *Biomaterials*, *27*(36), 6083–95.

ENGELMAYR, G. C. JR., SOLETTI, L., VIGMOSTAD, S. C., BUDILARTO, S. G., FEDERSPIEL, W. J., CHANDRAN, K. B., VORP, D. A., SACKS, M. S. (2008). A novel flex-stretch-flow bioreactor for the study of engineered heart valve tissue mechanobiology. *Annals of biomedical engineering*, *36*(5), 700–12.

ESCHENHAGEN, T., FINK, C., REMMERS, U., SCHOLZ, H., WATTCHOW, J., WEIL, J., ZIMMERMANN, W., DOHMEN, H.H., SCHAFER, H., BISHOPRIC, N., WAKATSUKI, T., AND ELSON, E.L. (1997). Three-dimensional reconstitution of embryonic cardiomyocytes in a collagen matrix: a new heart muscle model system. *FASEB journal: official publication of the Federation of American Societies for Experimental Biology, 11*(8), 683–94.

ETCHEVERS, H. C., VINCENT, C., LE DOUARIN, N. M., COULY, G. F. (2001). The cephalic neural crest provides pericytes and smooth muscle cells to all blood vessels of the face and forebrain. *Development (Cambridge, England)*, *128*(7), 1059–68.

FEDAK, P. W. M., MCCARTHY, P. M., BONOW, R. O. (2008). Evolving concepts and technologies in mitral valve repair. *Circulation*, *117*(7), 963–74.

FILOVÁ, E., STRAKA, F., MIREJOVSKÝ, T., MASÍN, J., BACÁKOVÁ, L. (2009). Tissue-engineered heart valves. *Physiological research / Academia Scientiarum Bohemoslovaca*, *58 Suppl 2*, S141–58.

FISHER, J., DAVIES, G. A. (1989). Buckling in bioprosthetic valves. *The Annals of Thoracic Surgery*, *48*(1), 147–148.

FISHER, J., BOOTH, C. and INGHAM, E. (2008). Decellularisation of matrices. University of Leeds, UK. Application nmber PCT/GB02/02341.

FLANAGAN, T. C., and PANDIT, A. (2003). Living artificial heart valve alternatives: a review. *European cells & materials*, *6*, 28–45; discussion 45.

FLANAGAN, T. C., WILKINS, B., BLACK, A., JOCKENHOEVEL, S., SMITH, T. J., PANDIT, A. S. (2006). A collagen-glycosaminoglycan co-culture model for heart valve tissue engineering applications. Biomaterials, 27(10), 2233–46.

FLANAGAN, T. C., CORNELISSEN, C., KOCH, S., TSCHOEKE, B., SACHWEH, J. S., SCHMITZ-RODE, T., JOCKENHOEVEL, S. (2007). The in vitro development of autologous fibrin-based tissue-engineered heart valves through optimised dynamic conditioning. *Biomaterials, 28*(23), 3388–97.

FORSBERG, M., and HOVATTA, O. (2012). Challenges for the Therapeutic use of Pluripotent Stem Derived Cells. *Frontiers in physiology, 3*, 19.

FOSSETT, E., and KHAN, W. S. (2012). Optimising human mesenchymal stem cell numbers for clinical application: a literature review. *Stem cells international*, *2012*, 465259.

FRAGA, C. H., TRUE, L. D., KIRK, D. (1998). Enhanced expression of the mesenchymal marker, vimentin, in hyperplastic versus normal human prostatic epithelium. *The Journal of urology, 159*(1), 270–4.

FREED, L. A., LEVY, D., LEVINE, R. A., LARSON, M. G., EVANS, J. C., FULLER, D. L., LEHMAN B., BENJAMIN, E. J. (1999). Prevalence and clinical outcome of mitral-valve prolapse. *The New England journal of medicine*, *341*(1), 1–7.

FREYMAN, T. (2005). Decellularized bone marrow extracellular matrix. US patent. Application number PCT/US2009/030046.

FREYTES, D. O., BADYLAK, S. F., WEBSTER, T. J., GEDDES, L. A., RUNDELL, A. E. (2004). Biaxial strength of multilaminated extracellular matrix scaffolds. *Biomaterials*, *25*(12), 2353–61.

FUCHS, J. R., NASSERI, B. A., VACANTI, J. P. (2001). Tissue engineering: a 21st century solution to surgical reconstruction. *The Annals of thoracic surgery*, *72*(2), 577–91.

FUNG, Y. C. (1984). Biomechanics mechanical properties of living tissues. Springer.

GAEMPERLI, O., BIAGGI, P., GUGELMANN, R., OSRANEK, M., SCHREUDER, J. J., BÜHLER, I., SÜRDER, D., LÜSCHER, T. F., FELIX, C., BETTEX, D., GRÜNENFELDER, J., CORTI, R. (2013). Real-time left ventricular pressure-volume loops during percutaneous mitral valve repair with the MitraClip system. *Circulation*, *127*(9), 1018–27.

GAILIT, J., and RUOSLAHTI, E. (1988). Regulation of the fibronectin receptor affinity by divalent cations. *The Journal of biological chemistry*, *263*(26), 12927–32.

GALLOWAY, A. C., COLVIN, S. B., BAUMANN, F. G., ESPOSITO, R., VOHRA, R., HARTY, S., FREEBERG, R., KRONZON, I., SPENCER, F. C. (1988). Long-term results of mitral valve reconstruction with Carpentier techniques in 148 patients with mitral insufficiency. *Circulation*, *78*(3 Pt 2), I97–105.

GALLOWAY, A. C., COLVIN, S. B., BAUMANN, F. G., GROSSI, E. A., RIBAKOVE, G. H., HARTY, S., SPENCER, F. C. (1989). A comparison of mitral valve reconstruction with mitral valve replacement: intermediate-term results. *The Annals of thoracic surgery*, *47*(5), 655–62.

GILBERT, T. W., SELLARO, T. L., BADYLAK, S. F. (2006). Decellularization of tissues and organs. *Biomaterials*, *27*(19), 3675–83.

GILBERT, T. W., STEWART-AKERS, A. M., SIMMONS-BYRD, A., BADYLAK, S. F. (2007). Degradation and remodeling of small intestinal submucosa in canine Achilles tendon repair. *The Journal of bone and joint surgery. American volume*, *89*(3), 621–30.

GILBERT, T. W., FREUND, J. M., BADYLAK, S. F. (2009). Quantification of DNA in biologic scaffold materials. *The Journal of surgical research*, *152*(1), 135–9.

GILLINOV, A. M., COSGROVE, D. M., BLACKSTONE, E. H., DIAZ, R., ARNOLD, J. H., LYTLE, B. W., SMEDIRA, N. G., SABIK, J. F., MCCARTHY, P. M., LOOP, F. D. (1998). Durability of mitral valve repair for degenerative disease. *The Journal of thoracic and cardiovascular surgery*, *116*(5), 734–43.

GILLINOV, A. M., WIERUP, P. N., BLACKSTONE, E. H., BISHAY, E. S., COSGROVE, D. M., WHITE, J., LYTLE, B. W., MCCARTHY, P. M. (2001). Is repair preferable to replacement for ischemic mitral regurgitation? *The Journal of thoracic and cardiovascular surgery*, *122*(6), 1125–41.

GILLINOV, A. M. (2005a). Chordal transfer for repair of anterior leaflet prolapse. *Multimedia Manual of Cardio-Thoracic Surgery*, *2005*(0118).

GILLINOV, A. M., SHORTT, K. G., COSGROVE, D. M. (2005b). Commissural closure for repair of mitral commissural prolapse. *The Annals of thoracic surgery*, *80*(3), 1135–6.

GOISSIS, G., SUZIGAN, S., PARREIRA, D. R., MANIGLIA, J. V., BRAILE, D. M., RAYMUNDO, S. (2000). Preparation and characterization of collagen-elastin matrices from blood vessels intended as small diameter vascular grafts. *Artificial organs*, *24*(3), 217–23.

GONZALEZ-LAVIN, L., TANDON, A. P., CHI, S., BLAIR, T. C., MCFADDEN, P. M., LEWIS, B., DAUGHTERS, G., IONESCU, M. (1984). The risk of thromboembolism and hemorrhage following mitral valve replacement. A comparative analysis between the porcine xenograft valve and Ionescu-Shiley bovine pericardial valve. *The Journal of thoracic and cardiovascular surgery*, *87*(3), 340–51.

GRANDE-ALLEN, K. J., CALABRO, A., GUPTA, V., WIGHT, T. N., HASCALL, V. C., VESELY, I. (2004). Glycosaminoglycans and proteoglycans in normal mitral valve leaflets and chordae: association with regions of tensile and compressive loading. *Glycobiology*, *14*(7), 621–33.

GRAUSS, R. W., HAZEKAMP, M. G., OPPENHUIZEN, F., VAN MUNSTEREN, C. J., GITTENBERGER-DE GROOT, A. C., DERUITER, M. C. (2005). Histological evaluation of decellularised porcine aortic valves: matrix changes due to different decellularisation methods. *European journal of cardio-thoracic surgery : official journal of the European Association for Cardio-thoracic Surgery, 27(4),* 566–71.

GRAY, H. (2008). Gray's anatomy. 40th edition. Churchill Livingstone Elsevier.

GRAYSON, A. C. R., VOSKERICIAN, G., LYNN, A., ANDERSON, J. M., CIMA, M. J., LANGER, R. (2004). Differential degradation rates in vivo and in vitro of biocompatible poly(lactic acid) and poly(glycolic acid) homo- and co-polymers for a polymeric drug-delivery microchip. *Journal of biomaterials science. Polymer edition, 15*(10), 1281–304.

GRENIER, G., RÉMY-ZOLGHADRI, M., LAROUCHE, D., GAUVIN, R., BAKER, K., BERGERON, F., DUPUIS, D., LANGELIER, E., RANCOURT, D., AUGER, F.A., GERMAIN, L. (2005). Tissue reorganization in response to mechanical load increases functionality. *Tissue engineering*, *11*(1-2), 90–100.

GRINNELL, F. (1994). Fibroblasts, myofibroblasts, and wound contraction. *The Journal of cell biology, 124*(4), 401–4.

GRINNELL, F. (2000). Fibroblast-collagen-matrix contraction: growth-factor signalling and mechanical loading. *Trends in cell biology*, *10*(9), 362–5.

GROSS, L., and KUGEL, M. A. (1931). Topographic anatomy and histology of the valves in the human heart. *The American journal of pathology*, *7*(5), 445–474.7.

GRUNKEMEIER, G. L. and RAHIMTOOLA, S. H. (1990). Artificial heart valves. *Annual Review of Medicine, 41*, 251-63.

GUILAK, F., RATCLIFFE, A., MOW, V. C. (1995). Chondrocyte deformation and local tissue strain in articular cartilage: a confocal microscopy study. *Journal of orthopaedic research: official publication of the Orthopaedic Research Society, 13*(3), 410–21.

GUPTA, V., WERDENBERG, J. A., LAWRENCE, B. D., MENDEZ, J. S., STEPHENS, E. H., GRANDE-ALLEN, K. J. (2008). Reversible secretion of glycosaminoglycans and

proteoglycans by cyclically stretched valvular cells in 3D culture. *Annals of biomedical engineering*, *36*(7), 1092–103.

GUYTON, A.C. (1976). Textbook of Medical Physiology. W.B. Saunders Company. Philadelphia.

HAMMER, W. J., ROBERTS, W. C., DE LEON, A. C. (1978). “Mitral stenosis” secondary to combined “massive” mitral annular calcific deposits and small, hypertrophied left ventricles. *The American Journal of Medicine*, *64*(3), 371–376.

HAMMERMEISTER, K. E., SETHI, G. K., HENDERSON, W. G., OPRIAN, C., KIM, T., RAHIMTOOLA, S. (1993). A comparison of outcomes in men 11 years after heart-valve replacement with a mechanical valve or bioprosthesis. Veterans Affairs Cooperative Study on Valvular Heart Disease. *The New England journal of medicine*, *328*(18), 1289–96.

HAWKINS, J. A., HILLMAN, N. D., LAMBERT, L. M., JONES, J., DI RUSSO, G. B., PROFAIZER, T., FULLER, T. C., MINICH, L. L., WILLIAMS, R. V., SHADDY, R. E. (2003). Immunogenicity of decellularized cryopreserved allografts in pediatric cardiac surgery: comparison with standard cryopreserved allografts. *The Journal of thoracic and cardiovascular surgery, 126*(1), 247–52; discussion 252–3.

HAYEK, E., GRING, C. N., GRIFFIN, B. P. (2005). Mitral valve prolapse. *Lancet*, *365*(9458), 507–18.

HAYFLICK, L. (1965). The limited in vitro lifetime of human diploid cell strains. *Experimental Cell Research*, *37*(3), 614–636.

HE, Z., RITCHIE, J., GRASHOW, J. S., SACKS, M. S., YOGANATHAN, A. P. (2005). In vitro dynamic strain behavior of the mitral valve posterior leaflet. *Journal of biomechanical engineering, 127*(3), 504–11.

HIBINO, N., DUNCAN, D. R., NALBANDIAN, A., YI, T., QYANG, Y., SHINOKA, T., BREUER, C. K. (2012). Evaluation of the use of an induced puripotent stem cell sheet for the construction of tissue-engineered vascular grafts. *The Journal of thoracic and cardiovascular surgery, 143*(3), 696–703.

HILDEBRAND, D. K., WU, Z. J., MAYER, J. E., SACKS, M. S. (2004). Design and hydrodynamic evaluation of a novel pulsatile bioreactor for biologically active heart valves. *Annals of biomedical engineering, 32*(8), 1039–49.

HISHIKAWA, K., and LÜSCHER, T. F. (1997). Pulsatile stretch stimulates superoxide production in human aortic endothelial cells. *Circulation*, *96*(10), 3610–6.

HOCHACHKA, P. W., and MOMMSEN, T. P. (1983). Protons and anaerobiosis. *Science (New York, N.Y.)*, *219*(4591), 1391–7.

HODDE, J. P., BADYLAK, S. F., BRIGHTMAN, A. O., VOYTIK-HARBIN, S. L. (1996). Glycosaminoglycan content of small intestinal submucosa: a bioscaffold for tissue replacement. *Tissue engineering*, *2*(3), 209–17.

HODDE, J., RECORD, R., TULLIUS, R., BADYLAK, S. (2002). Fibronectin peptides mediate HMEC adhesion to porcine-derived extracellular matrix. *Biomaterials*, *23*(8), 1841–8.

HOERSTRUP, S.P., SODIAN, R., DAEBRITZ, S., WANG, J., BACHA, E.A., MARTIN, D.P., MORAN, A.M., GULESERIAN, K.J., SPERLING, J.S., KAUSHAL, S., VACANTI, J.P.,

SCHOEN, F.J., MAYER, J.E. JR. (2000a). Functional living trileaflet heart valves grown in vitro. *Circulation, 102*(19 Suppl 3), III44-9.

HOERSTRUP, S. P., SODIAN, R., SPERLING, J. S., VACANTI, J. P., MAYER, J. E. (2000b). New pulsatile bioreactor for in vitro formation of tissue engineered heart valves. *Tissue engineering, 6*(1), 75–9.

HOERSTRUP, S.P., KADNER, A., MELNITCHOUK, S., TROJAN, A., EID, K., TRACY, J., SODIAN, R., VISJAGER, J.F., KOLB, S.A., GRUNENFELDER, J., ZUND, G., TURINA, M.I. (2002). Tissue engineering of functional trileaflet heart valves from human marrow stromal cells. *Circulation, 106*(12 Suppl 1), I143-I50.

HUBBELL, J. A. (1995). Biomaterials in tissue engineering. *Bio/technology (Nature Publishing Company)*, *13*(6), 565–76.

HUDSON, T.W., LIU, S.Y., SCHMIDT, C.E. (2004a). Engineering an improved acellular nerve graft via optimized chemical processing. *Tissue Engineering,10*(9-10), 1346–58.

HUDSON, T.W., ZAWKO, S., DEISTER, C., LUNDY, S., HU, C.Y., LEE, K., SCHMIDT, C. E. (2004b). Optimized acellular nerve graft is immunologically tolerated and supports regeneration. *Tissue Engineering, 10*(11-12),1641–51.

HUTMACHER, D. W., and SINGH, H. (2008). Computational fluid dynamics for improved bioreactor design and 3D culture. Trends in biotechnology, 26(4), 166–72.

INGBER, D. E. (1997). Tensegrity: the architectural basis of cellular mechanotransduction. *Annual review of physiology, 59*, 575–99.

INGBER, D. E. (2006). Cellular mechanotransduction: putting all the pieces together again. *FASEB journal : official publication of the Federation of American Societies for Experimental Biology, 20*(7), 811–27.

ISHIHARA, T., FERRANS, V. J., JONES, M., BOYCE, S. W., KAWANAMI, O., ROBERTS, W. C. (1980). Histologic and ultrastructural features of normal human parietal pericardium. *The American journal of cardiology*, *46*(5), 744–53.

IYENGAR AKS, SUGIMOTO, H., SMITH, D. B., SACKS, M. S. (2001). Dynamic in vitro quantification of bioprosthetic heart valve leaflet motion using structured light projection. *Annals of biomedical engineering*, *29*(11), 963–73.

JENSEN, A. S., BAANDRUP, U., HASENKAM, J. M., KUNDU, T., JØRGENSEN, C. S. (2006). Distribution of the microelastic properties within the human anterior mitral leaflet. *Ultrasound in medicine & biology*, *32*(12), 1943–8.

JEONG, S., KWON, J. H., LIM, J. I., CHO, S.-W., JUNG, Y., SUNG, W. J., KIM, S. H., KIM, Y. H., MOO, L. Y., KIMA, B.-S., CHOI, C. Y., KIM, S.-J. (2005). Mechano-active tissue engineering of vascular smooth muscle using pulsatile perfusion bioreactors and elastic PLCL scaffolds. *Biomaterials*, *26*(12), 1405–11.

JIMENEZ, J.H., LIOU, S.W., PADALA, M., HE, Z., SACKS, M., GORMAN, R.C., GORMAN, J.H. 3RD, YOGANATHAN, A.P. (2007). A saddle-shaped annulus reduces systolic strain on the central region of the mitral valve anterior leaflet. *The Journal of thoracic and cardiovascular surgery, 134*(6), 1562–8.

JOCKENHOEVEL, S., ZUND, G., HOERSTRUP, S. P., SCHNELL, A., TURINA, M. (2002). Cardiovascular tissue engineering: a new laminar flow chamber for in vitro improvement of

mechanical tissue properties. *ASAIO journal (American Society for Artificial Internal Organs : 1992)*, *48*(1), 8–11.

JOKINEN, J. J., HIPPELÄINEN, M. J., PITKÄNEN, O. A., HARTIKAINEN, J. E. K. (2007). Mitral valve replacement versus repair: propensity-adjusted survival and quality-of-life analysis. *The Annals of thoracic surgery*, *84*(2), 451–8.

KADNER, A., HOERSTRUP, S. P., ZUND, G., EID, K., MAURUS, C., MELNITCHOUK, S., GRUNENFELDER, J., TURINA, M. I. (2002). A new source for cardiovascular tissue engineering: human bone marrow stromal cells. European journal of cardio-thoracic surgery: official journal of the European Association for Cardio-thoracic Surgery, 21(6), 1055–60.

KARIM, N., GOLZ, K., BADER, A. (2006). The cardiovascular tissue-reactor: a novel device for the engineering of heart valves. *Artificial organs*, *30*(10), 809–14.

KASIMIR, M. T., RIEDER, E., SEEBACHER, G., SILBERHUMER, G., WOLNER, E., WEIGEL, G., SIMON, P. (2003). Comparison of different decellularization procedures of porcine heart valves. *The International journal of artificial organs*, *26*(5), 421–7.

KIM, B. S., NIKOLOVSKI, J., BONADIO, J., MOONEY, D. J. (1999). Cyclic mechanical strain regulates the development of engineered smooth muscle tissue. *Nature biotechnology, 17*(10), 979–83.

KLEBE, R. J. (1974). Isolation of a collagen-dependent cell attachment factor. *Nature*, *250*(5463), 248–251.

KLEBE, R. J. (1975). Cell attachment to collagen: the requirement for energy. *Journal of cellular physiology*, *86*(2 Pt 1), 231–6.

KLUES, H. G., MARON, B. J., DOLLAR, A. L., ROBERTS, W. C. (1992). Diversity of structural mitral valve alterations in hypertrophic cardiomyopathy. *Circulation*, *85*(5), 1651–60.

KNIGHT, R. (2003). Tissue engineering vascular solutions: histological, biochemical and biomechanical characterisation of fresh and decellularised porcine pericardium. BSc thesis. School of Biochemistry and Microbiology, University of Leeds.

KOROSSIS, S. (2002). Biomechanics & hydronamics of decellularised aortic valves for tissue engineering. PhD thesis. School of Mechanical Engineering, University of Leeds.

KOROSSIS, S. A., BOOTH, C., WILCOX, H. E., WATTERSON, K. G., KEARNEY, J. N., FISHER, J., INGHAM, E. (2002). Tissue engineering of cardiac valve prostheses II: biomechanical characterization of decellularized porcine aortic heart valves. *The Journal of heart valve disease*, *11*(4), 463–71.

KU, C.-H., JOHNSON, P. H., BATTEN, P., SARATHCHANDRA, P., CHAMBERS, R. C., TAYLOR, P. M., YACOUB, M. H., CHESTER, A. H. (2006). Collagen synthesis by mesenchymal stem cells and aortic valve interstitial cells in response to mechanical stretch. *Cardiovascular research*, *71*(3), 548–56.

KUHN, K. (1987). Structure and Function of Collagen Types. Mayne R, Burgeson R Academic. New York.

KUNZELMAN, K. S., and COCHRAN, R. P. (1992). Stress/strain characteristics of porcine mitral valve tissue: parallel versus perpendicular collagen orientation. *Journal of cardiac surgery*, *7*(1), 71–8.

KUNZELMAN, K. S., COCHRAN, R. P., MURPHREE, S. S., RING, W. S., VERRIER, E. D., EBHERART, R. C. (1993a). Differential collagen distribution in the mitral valve and its influence on biomechanical behaviour. *The Journal of Heart Valve Disease, 2*(2), 236-44.

KUNZELMAN, K. S., COCHRAN, R. P., CHUONG, C., RING, W. S., VERRIER, E. D., EBERHART, R. D. (1993b). Finite element analysis of the mitral valve. *The Journal of heart valve disease*, *2*(3), 326–40.

KUNZELMAN, K. S., COCHRAN, R. P., VERRIER, E. D., EBERHART, R. C. (1994). Anatomic basis for mitral valve modelling. *The Journal of heart valve disease, 3*(5), 491–6.

LANGER, R., and VACANTI, J. P. (1993). Tissue engineering. *Science (New York, N.Y.)*, *260*(5110), 920–6.

LAWRIE, G. M., EARLE, E. A., EARLE, N. R. (2006). Feasibility and intermediate term outcome of repair of prolapsing anterior mitral leaflets with artificial chordal replacement in 152 patients. *The Annals of thoracic surgery*, *81*(3), 849–56; discussion 856.

LEASK, R. L., JAIN, N., BUTANY, J. (2003). Endothelium and valvular diseases of the heart. *Microscopy research and technique*, *60*(2), 129–37.

LEE, M.C., FUNG, Y.C., SHABETAI, R., LEWINTER, M.M. (1987). Biaxial mechanical properties of human pericardium and canine comparisons. *The American journal of physiology*, *253*(1 Pt 2), H75–82.

LEE, D. J., STEEN, J., JORDAN, J. E., KINCAID, E. H., KON, N. D., ATALA, A., BERRY, J., YOO, J. J. (2009). Endothelialization of heart valve matrix using a computer-assisted pulsatile bioreactor. *Tissue engineering. Part A, 15*(4), 807–14.

LEVICK, J. R. (2003). An introduction to Cardiovascular Pysiology. 4th edition. Hodder Arnold.

LEYH, R. ., WILHELMI, M., WALLES, T., KALLENBACH, K., REBE, P., OBERBECK, A., HERDEN, T., HAVERICH, A., MERTSCHING, H. (2003). Acellularized porcine heart valve scaffolds for heart valve tissue engineering and the risk of cross-species transmission of porcine endogenous retrovirus. *The Journal of Thoracic and Cardiovascular Surgery*, *126*(4), 1000–1004.

LICHTENBERG, A., TUDORACHE, I., CEBOTARI, S., RINGES-LICHTENBERG, S., STURZ, G., HOEFFLER, K., HURSCHELER, C., BRANDES, G., HILFIKER, A., HAVERICH, A. (2006). In vitro re-endothelialization of detergent decellularized heart valves under simulated physiological dynamic conditions. *Biomaterials, 27*(23), 4221–9.

LIM, K. H., YEO, J. H., DURAN, C. M. G. (2005). Three-dimensional asymmetrical modeling of the mitral valve: a finite element study with dynamic boundaries. *The Journal of heart valve disease, 14*(3), 386–92.

LIS, Y., BURLEIGH, M. C., PARKER, D. J., CHILD, A. H., HOGG, J., DAVIES, M. J. (1987). Biochemical characterization of individual normal, floppy and rheumatic human mitral valves. *The Biochemical journal*, *244*(3), 597–603.

LIU, X., WU, H., BYRNE, M., KRANE, S., JAENISCH, R. (1997). Type III collagen is crucial for collagen I fibrillogenesis and for normal cardiovascular development. *Proceedings of the National Academy of Sciences of the United States of America*, *94*(5), 1852–6.

LIU, A. C., JOAG, V. R., GOTLIEB, A. I. (2007). The emerging role of valve interstitial cell phenotypes in regulating heart valve pathobiology. *The American journal of pathology*, *171*(5), 1407–18.

LODE, A., BERNHARDT, A., GELINSKY, M. (2008). Cultivation of human bone marrow stromal cells on three-dimensional scaffolds of mineralized collagen: influence of seeding density on colonization, proliferation and osteogenic differentiation. *Journal of tissue engineering and regenerative medicine*, *2*(7), 400–7.

LOVEKAMP, J. J., SIMIONESCU, D. T., MERCURI, J. J., ZUBIATE, B., SACKS, M. S., VYAVAHARE, N. R. (2006). Stability and function of glycosaminoglycans in porcine bioprosthetic heart valves. *Biomaterials*, *27*(8), 1507–18.

MACCHIARINI, P., JUNGEBLUTH, P., GO, T., ASNAGHI, M. A., REES, L. E., COGAN, T. A., DODSON, A., MARTORELL, J., BELLINI, S., PARNIGOTTO, P. P., DICKINSON, S. C., HOLLANDER, A. P., MANTERO, S., CONCONI, M. T., BIRCHALL, M. A. (2008). Clinical transplantation of a tissue-engineered airway. *Lancet*, *372*(9655), 2023–30.

MANASSERO, M., VIATEAU, V., DESCHEPPER, M., OUDINA, K., LOGEART-AVRAMOGLOU, D., PETITE, H., BENSIDHOUM, M. (2013). Bone regeneration in sheep using acropora coral, a natural resorbable scaffold, and autologous mesenchymal stem cells. *Tissue Engineering Part A, 19*(13-14), 1554-1563.

MARANTO, A.R., and SCHOEN, F. (1988). Phosphatase enzyme activity is retained in glutaraldehyde treated bioprosthetic heart valves. *ASAIO transactions / American Society for Artificial Internal Organs, 34*(3), 827–30.

MARCHAND, M., AUPART, M., NORTON, R., GOLDSMITH, I. R., PELLETIER, C., PELLERIN, M., DUBIEL, T., DAENEN, W., CASSELMAN, F., HOLDEN, M., DAVID, T. E., RYBA, E. A. (1998). Twelve-year experience with Carpentier-Edwards PERIMOUNT pericardial valve in the mitral position: a multicenter study. *The Journal of heart valve disease*, *7*(3), 292–8.

MARTINI, F. and NATH, J. L. (2009). Fundamentals of anatomy & physiology. 8th edition. Pearson international.

MARTINS-GREEN, M., and BISSELL, M.J. (1995). Cell–extracellular matrix interactions in development. *Seminars in Cell & Developmental Biology, 6*,149–59.

MASOUMI, N., JOHNSON, K. L., HOWELL, M. C., ENGELMAYR, G. C. (2013a). Valvular interstitial cell seeded poly(glycerol sebacate) scaffolds: Toward a biomimetic in vitro model for heart valve tissue engineering. *Acta Biomaterialia, 9*(4), 5974–5988.

MASOUMI, N., JEAN, A., ZUGATES, J. T., JOHNSON, K. L., ENGELMAYR, G. C. (2013b). Laser microfabricated poly(glycerol sebacate) scaffolds for heart valve tissue engineering. *Journal of biomedical materials research. Part A*, *101*(1), 104–14.

MASTERS, R. G., HADDAD, M., PIPE, A. L., VEINOT, J. P., MESANA, T. (2004). Clinical outcomes with the Hancock II bioprosthetic valve. *The Annals of thoracic surgery*, *78*(3), 832–6.

MAY-NEWMAN, K., and YIN, F. C. (1995). Biaxial mechanical behaviour of excised porcine mitral valve leaflets. *The American journal of physiology*, *269*(4 Pt 2), H1319–27.

MCBEATH, R., PIRONE, D. M., NELSON, C. M., BHADRIRAJU, K., CHEN, C. S. (2004). Cell shape, cytoskeletal tension, and RhoA regulate stem cell lineage commitment. *Developmental cell*, *6*(4), 483–95.

MCCOY, S. L., KURTZ, S. E., HAUSMAN, F. A., TRUNE, D. R., BENNETT, R. M., HEFENEIDER, S. H. (2004). Activation of RAW264.7 macrophages by bacterial DNA and lipopolysaccharide increases cell surface DNA binding and internalization. *The Journal of biological chemistry*, *279*(17), 17217–23.

MEINEL, L., KARAGEORGIOU, V., FAJARDO, R., SNYDER, B., SHINDE-PATIL, V., ZICHNER, L., KAPLAN, D., LANGER, R., VUNJAK-NOVAKOVIC, G. (2004). Bone tissue engineering using human mesenchymal stem cells: effects of scaffold material and medium flow. *Annals of biomedical engineering*, *32*(1), 112–22.

MENDELSON, K., and SCHOEN, F. J. (2006). Heart valve tissue engineering: concepts, approaches, progress, and challenges. *Annals of biomedical engineering*, *34*(12), 1799–819.

MERRETT, K., FAGERHOLM, P., MCLAUGHLIN, C. R., DRAVIDA, S., LAGALI, N., SHINOZAKI, N., WATSKY, M. A., MUNGER, R., KATO, Y., LI, F., MARMO, C. J., GRIFFiTH, M. (2008). Tissue-engineered recombinant human collagen-based corneal substitutes for implantation: performance of type I versus type III collagen. *Investigative ophthalmology & visual science*, *49*(9), 3887–94.

MERRYMAN, W. D., ENGELMAYR, G. C. JR., LIAO, J., SACKS, M. S. (2006). Defining biomechanical endpoint for tissue engineered heart valve leaflets from native leaflet properties. *Progress in Pediatric Cardiology, 21*(2),153-160.

MERRYMAN, W. D., LUKOFF, H. D., LONG, R. A., ENGELMAYR, G. C., HOPKINS, R. A., SACKS, M. S. (2007). Synergistic effects of cyclic tension and transforming growth factor-beta1 on the aortic valve myofibroblast. *Cardiovascular pathology : the official journal of the Society for Cardiovascular Pathology*, *16*(5), 268–76.

MIRSADRAEE, S. (2005). Tissue engineering of pericardium. PhD thesis. School of Medicin, University of Leeds.

MIRSADRAEE, S., WILCOX, H. E., KOROSSIS, S. A., KEARNEY, J. N., WATTERSON, K. G., FISHER, J., INGHAM, E. (2006). Development and characterization of an acellular human pericardial matrix for tissue engineering. *Tissue engineering*, *12*(4), 763–73.

MIRSADRAEE, S., WILCOX, H. E., WATTERSON, K. G., KEARNEY, J. N., HUNT, J., FISHER, J., INGHAM, E. (2007). Biocompatibility of acellular human pericardium. *The Journal of surgical research*, *143*(2), 407–14.

MIZUNO, M., and KUBOKI, Y. (2001). Osteoblast-related gene expression of bone marrow cells during the osteoblastic differentiation induced by type I collagen. *Journal of biochemistry*, *129*(1), 133–8.

MIZRACHI, A. (2009). Tissue Engineering of Mitral Heart Valve leaflets. BSc thesis. School of Biochemistry and Microbiology, University of Leeds.

MOCHIZUKI, T., MUNETA, T., SAKAGUCHI, Y., NIMURA, A., YOKOYAMA, A., KOGA, H., SEKIYA, I. (2006). Higher chondrogenic potential of fibrous synovium- and adipose synovium-derived cells compared with subcutaneous fat-derived cells: distinguishing properties of mesenchymal stem cells in humans. *Arthritis and rheumatism*, *54*(3), 843–53.

MOHLER, E. R., CHAWLA, M. K., CHANG, A. W., VYAVAHARE, N., LEVY, R. J., GRAHAM, L., GANNON, F. H. (1999). Identification and characterization of calcifying valve cells from human and canine aortic valves. *The Journal of heart valve disease*, *8*(3), 254–60.

MOL, A., BOUTEN, C. V. C., ZÜND, G., GÜNTER, C. I., VISJAGER, J. F., TURINA, M. I., BAAIJENS, F. P., HOERSTRUP, S. P. (2003). The relevance of large strains in functional tissue engineering of heart valves. *The Thoracic and cardiovascular surgeon*, *51*(2), 78–83.

MOL, A., DRIESSEN, N. J. B., RUTTEN, M. C. M., HOERSTRUP, S. P., BOUTEN, C. V. C., BAAIJENS, F. P. T. (2005). Tissue engineering of human heart valve leaflets: a novel bioreactor for a strain-based conditioning approach. *Annals of biomedical engineering, 33*(12), 1778–88.

MOON, M. R., MILLER, D. C., MOORE, K. A., OYER, P. E., MITCHELL, R. S., ROBBINS, R. C., STINSON, E. B., SHUMWAY, N. E., REITZ, B. A. (2001). Treatment of endocarditis with valve replacement: the question of tissue versus mechanical prosthesis. *The Annals of thoracic surgery*, *71*(4), 1164–71.

MOONEY, D., HANSEN, L., VACANTI, J., LANGER, R., FARMER, S., INGBER, D. (1992). Switching from differentiation to growth in hepatocytes: control by extracellular matrix. *Journal of cellular physiology, 151*(3), 497–505.

MOORE, R., MADARA, J. L., MACLEOD, R. J. (1994). Enterocytes adhere preferentially to collagen IV in a differentially regulated divalent cation-dependent manner. *The American journal of physiology*, *266*(6 Pt 1), G1099–107.

MOSMANN, T. (1983). Rapid colorimetric assay for cellular growth and survival: application to proliferation and cytotoxicity assays. *Journal of immunological methods*, *65*(1-2), 55–63.

MUEHRCKE, D. D., COSGROVE, D. M., LYTLE, B. W., TAYLOR, P. C., BURGAR, A. M., DURNWALD, C. P., LOOP, F. D. (1997). Is there an advantage to repairing infected mitral valves? *The Annals of thoracic surgery*, *63*(6), 1718–24.

MURATA, K. (1981). Acidic glycosaminoglycans in human heart valves. *Journal of Molecular and Cellular Cardiology, 13*(3), 281–292.

NAKAMURA, A., DOHI, Y., AKAHANE, M., OHGUSHI, H., NAKAJIMA, H., FUNAOKA, H., TAKAKURA, Y. (2009). Osteocalcin secretion as an early marker of in vitro osteogenic differentiation of rat mesenchymal stem cells. *Tissue engineering. Part C, Methods*, *15*(2), 169–80.

NIKLASON, L. E. (1999). Functional arteries grown in vitro. *Science, 284*(5413), 489–493.

NOLAN, S. P., DIXON, S. H., FISHER, R. D., MORROW, A. G. (1969). The influence of atrial contraction and mitral valve mechanics on ventricular filling. *American Heart Journal*, *77*(6), 784–791.

O'BRIEN, M. F., GOLDSTEIN, S., WALSH, S., BLACK, K. S., ELKINS, R., CLARKE, D. (1999). The SynerGraft valve: a new acellular (nonglutaraldehyde-fixed) tissue heart valve for autologous recellularization first experimental studies before clinical implantation. *Seminars in thoracic and cardiovascular surgery*, *11*(4 Suppl 1), 194–200.

ORLIC, D., KAJSTURA, J., CHIMENTI, S., LIMANA, F., JAKONIUK, I., QUAINI, F., NADAL-GINARD, B., BODINE, D. M., LERI, A., ANVERSA, P. (2001). Mobilized bone marrow cells repair the infarcted heart, improving function and survival. *Proceedings of the National Academy of Sciences of the United States of America, 98*(18), 10344–9.

OSWAL, D., KOROSSIS, S., MIRSADRAEE, S., WILCOX, H., WATTERSON, K., FISHER, J., INGHAM, E. (2007). Biomechanical characterization of decellularized and cross-linked bovine pericardium. *The Journal of heart valve disease*, *16*(2), 165–74.

OTTO, C. M., and BONOW, R. O. (2009). Valvular Heart Disease. Elsevier Health Sciences. 3rd edition. Philadelphia.

PANSKY, A., ROITZHEIM, B., TOBIASCH, E. (2007). Differentiation potential of adult human mesenchymal stem cells. *Clinical laboratory*, *53*(1-2), 81–4.

PEREZ-MONTIEL, M. D., PLAZA, J. A., DOMINGUEZ-MALAGON, H., SUSTER, S. (2006). Differential expression of smooth muscle myosin, smooth muscle actin, h-caldesmon, and calponin in the diagnosis of myofibroblastic and smooth muscle lesions of skin and soft tissue. *The American Journal of dermatopathology*, *28*(2), 105–11.

PERIER, P., DELOCHE, A., CHAUVAUD, S., FABIANI, J. N., ROSSANT, P., BESSOU, J. P., RELLAND, J., BOUREZAK, H., GOMEZ, F., BLONDEAU, P. (1984). Comparative evaluation of mitral valve repair and replacement with Starr, Björk, and porcine valve prostheses. *Circulation*, *70*(3 Pt 2), I187–92.

PERIER, P. (2005). Quadrangular resection for repair of posterior leaflet prolapse. *Multimedia Manual of Cardio-Thoracic Surgery*, *2005*(1129).

PETERSEN, T.H., CALLE, E.A., ZHAO, L., LEE, E.J., GUI L., RAREDON, M.B. GAVRILOV, K., YI, T., ZHUANG, Z. W., BREUER, C., HERZOG, E. (2010). Tissue-engineered lungs for in vivo implantation. *Science, 329* (5991), 538–41.

PIBAROT, P., and DUMESNIL, J. G. (2009). Prosthetic heart valves: selection of the optimal prosthesis and long-term management. *Circulation*, *119*(7), 1034–48.

PONTICIELLO, M. S., SCHINAGL, R. M., KADIYALA, S., BARRY, F. P. (2000). Gelatin-based resorbable sponge as a carrier matrix for human mesenchymal stem cells in cartilage regeneration therapy. *Journal of biomedical materials research*, *52*(2), 246–55.

QUIGLEY, R. L. (2005). Prevention of systolic anterior motion after repair of the severely myxomatous mitral valve with an anterior leaflet valvuloplasty. *The Annals of thoracic surgery*, *80*(1), 179–82; discussion 182.

SOKAL, R.R., and ROHLF, F. J. (1995). Biometry: the principles and practice of statistics in biological research. 3rd edition. W. H. Freeman and company. New York.

RABKIN, E., AIKAWA, M., STONE, J. R., FUKUMOTO, Y., LIBBY, P., SCHOEN, F. J. (2001). Activated interstitial myofibroblasts express catabolic enzymes and mediate matrix remodeling in myxomatous heart valves. *Circulation*, *104*(21), 2525–2532.

RABKIN, E. and SCHOEN, F. J. (2002). Cardiovascular tissue engineering. *Cardiovascular Pathology ,11*(6), 305-17.

RABKIN, E., HOERSTRUP, S. P., AIKAWA, M., MAYER, J. E., SCHOEN, F. J. (2002). Evolution of cell phenotype and extracellular matrix in tissue-engineered heart valves during in-vitro maturation and in-vivo remodelling. *The Journal of heart valve disease*, *11*(3), 308–14; discussion 314.

RABKIN-AIKAWA, E., FARBER, M., AIKAWA, M., SCHOEN, F. J. (2004). Dynamic and reversible changes of interstitial cell phenotype during remodelling of cardiac valves. *The Journal of heart valve disease*, *13*(5), 841–7.

RABKIN-AIKAWA, E., MAYER, J. E., SCHOEN, F. J. (2005). Heart valve regeneration. *Advances in biochemical engineering/biotechnology*, *94*, 141–79.

RALPHS, J. R., WAGGETT, A. D., BENJAMIN, M. (2002). Actin stress fibres and cell-cell adhesion molecules in tendons: organisation in vivo and response to mechanical loading of tendon cells *in vitro*. *Matrix biology : journal of the International Society for Matrix Biology, 21*(1), 67–74.

RAMAMURTHI, A., and VESELY, I. (2005). Evaluation of the matrix-synthesis potential of crosslinked hyaluronan gels for tissue engineering of aortic heart valves. *Biomaterials, 26*(9), 999–1010.

REING, J. E., BROWN, B. N., DALY, K. A., FREUND, J. M., GILBERT, T. W., HSIONG, S. X., HUBER, A., KULLAS, K. E., TOTTEY, S., WOLF, M. T., BADYLAK, S. F. (2010). The effects of processing methods upon mechanical and biologic properties of porcine dermal extracellular matrix scaffolds. *Biomaterials*, *31*(33), 8626–33.

RENSEN, S. S. M., DOEVENDANS, P. A. F. M., VAN EYS, G. J. J. M. (2007). Regulation and characteristics of vascular smooth muscle cell phenotypic diversity. *Netherlands heart journal : monthly journal of the Netherlands Society of Cardiology and the Netherlands Heart Foundation*, *15*(3), 100–8.

RHEINWALD, J.G., and GREEN H. (1975). Serial cultivation of strains of human epidermal keratinocytes: the formation of keratinizing colonies from single cells. *Cell, 6 (3),*331–43.

RIEDER, E., SEEBACHER, G., KASIMIR, M.-T., EICHMAIR, E., WINTER, B., DEKAN, B., WOLNER, E., SIMON, P., WEIGEL, G. (2005). Tissue engineering of heart valves: decellularized porcine and human valve scaffolds differ importantly in residual potential to attract monocytic cells. *Circulation, 111*(21), 2792–7.

ROBERTS, N. (2012). Computational Modelling of the Mitral Valve and Pericardium patch Bioreactor for Mitral Valve Repair. PhD thesis. School of Mechanical Engineering, University of Leeds.

ROBERTS, W. C., EWY, G. A., GLANCY, D. L., MARCUS, F. I. (1967). Valvular stenosis produced by active infective endocarditis. *Circulation*, *36*(3), 449–451.

ROBERTS, W. C., BULKLEY, B. H., MORROW, A. G. (1973). Pathologic anatomy of cardiac valve replacement: A study of 224 necropsy patients. *Progress in Cardiovascular Diseases*, *15*(6), 539–587.

ROBERTS, W. C., SIEGEL, R. J., MCMANUS, B. M. (1987). Idiopathic dilated cardiomyopathy: analysis of 152 necropsy patients. *The American journal of cardiology*, *60*(16), 1340–55.

ROBERTS, W. C. (2001). Neoplasms involving the heart, their simulators, and adverse consequences of their therapy. *Proceedings (Baylor University. Medical Center)*, *14*(4), 358–76.

ROSS, E. M., and ROBERTS, W. C. (1986). Severe atherosclerotic coronary arterial narrowing and chronic congestive heart failure without myocardial infarction: analysis of 18 patients studied at necropsy. *The American journal of cardiology*, *57*(1), 51–6.

ROY, R., WEWER, U. M., ZURAKOWSKI, D., PORIES, S. E., MOSES, M. A. (2004). ADAM 12 cleaves extracellular matrix proteins and correlates with cancer status and stage. *The Journal of biological chemistry, 279*(49), 51323–30.

RUGGERI, Z. M., and WARE, J. (1993). von Willebrand factor. *FASEB journal : official publication of the Federation of American Societies for Experimental Biology*, *7*(2), 308–16.

RUOSLAHTI, E. (1981). Fibronectin. *Journal of Oral Pathology and Medicine, 10*(1), 3–13.

RUOSLAHTI, E., and PIERSCHBACHER, M. D. (1987). New perspectives in cell adhesion: RGD and integrins. *Science (New York, N.Y.), 238*(4826), 491–7.

RUSSO, A., GRIGIONI, F., AVIERINOS, J.-F., FREEMAN, W. K., SURI, R., MICHELENA, H., BROWN, R., SUNDT, T. M., ENRIQUEZ-SARANO, M. (2008). Thromboembolic complications after surgical correction of mitral regurgitation incidence, predictors, and clinical implications. *Journal of the American College of Cardiology*, *51*(12), 1203–11.

SACKS, M. S., HE, Z., BAIJENS, L., WANANT, S., SHAH, P., SUGIMOTO, H., & YOGANATHAN, A. P. (2002). Surface strains in the anterior leaflet of the functioning mitral valve. *Annals of biomedical engineering*, *30*(10), 1281–90.

SACKS, M. S., and YOGANATHAN, A. P. (2007). Heart valve function: a biomechanical perspective. *Philosophical transactions of the Royal Society of London. Series B, Biological sciences*, *362*(1484), 1369–91.

SACKS, M. S., DAVID MERRYMAN, W., SCHMIDT, D. E. (2009a). On the biomechanics of heart valve function. *Journal of biomechanics*, *42*(12), 1804–24.

SACKS, M. S., SCHOEN, F. J., MAYER, J. E. (2009b). Bioengineering challenges for heart valve tissue engineering. *Annual review of biomedical engineering*, *11*, 289–313.

SADLER, J. E. (1998). Biochemistry and genetics of von Willebrand factor. *Annual review of biochemistry, 67*, 395–424.

SALATI, M., SCROFANI, R., SANTOLI, C. (1991). Posterior pericardial annuloplasty: a physicological correction? *European journal of cardio-thoracic surgery : official journal of the European Association for Cardio-thoracic Surgery*, *5*(5), 226–9; discussion 229.

SALATI, M., MORIGGIA, S., SCROFANI, R., SANTOLI, C. (1997). Chordal transposition for anterior mitral prolapse: early and long-term results. *European Journal of Cardiothoracic Surgery*, 11(2), 268-73.

SAMUEL, R., DAHERON, L., LIAO, S., VARDAM, T., KAMOUN, W.S., BATISTA, A., BUECKER, C., SCHÄFER, R., HANA, X., AU, P., SCADDEN, D.T., DUDA, D.G., FUKUMURA, D., JAINA, R.K. (2013). Generation of functionally competent and durable engineered blood vessels from human induced pluripotent stem cells. *Proceedings of the National Academy of Sciences of the United States of America, 110*(31), 12774–9.

SAPIRSTEIN, J. S., and SMITH, P. K. (2001). The “ideal” replacement heart valve. *American heart journal*, *141*(5), 856–60.

SATO, M., OHSHIMA, N., NEREM, R. M. (1996). Viscoelastic properties of cultured porcine aortic endothelial cells exposed to shear stress. *Journal of biomechanics*, *29*(4), 461–7.

SCHMITT-GRÄFF, A., DESMOULIÈRE, A., GABBIANI, G. (1994). Heterogeneity of myofibroblast phenotypic features: an example of fibroblastic cell plasticity. *Virchows Archiv : an international journal of pathology*, *425*(1), 3–24.

SCHNELL, A. M., HOERSTRUP, S. P., ZUND, G., KOLB, S., SODIAN, R., VISJAGER, J. F., GRUNENFELDER, J., SUTER, A., TURINA, M. (2001). Optimal cell source for cardiovascular tissue engineering: venous vs. aortic human myofibroblasts. *The Thoracic and cardiovascular surgeon, 49*(4), 221–5.

SCHOEN, F. J., TITUS, J. L., LAWRIE, G. M. (1982). Bioengineering aspects of heart valve replacement. *Annals of biomedical engineering*, *10*(3), 97–128.

SCHOEN, F. J., LEVY, R. J., and PIEHLER, H. R. (1992). Pathological considerations in replacement cardiac valves. *Cardiovascular Pathology, 1*, 29-52.

SCHOEN, F. J., and LEVY, R. J. (2005a). Calcification of tissue heart valve substitutes: progress toward understanding and prevention. *The Annals of thoracic surgery*, *79*(3), 1072–80.

SCHOEN, F. J. (2005b). Cardiac valves and valvular pathology: update on function, disease, repair, and replacement. *Cardiovascular pathology : the official journal of the Society for Cardiovascular Pathology*, *14*(4), 189–94.

SCHOEN, F. J. (2008). Evolving concepts of cardiac valve dynamics: the continuum of development, functional structure, pathobiology, and tissue engineering. *Circulation*, *118*(18), 1864–80.

SCOTT, M., and VESELY, I. (1995). Aortic valve cusp microstructure: the role of elastin. *The Annals of thoracic surgery*, *60*(2 Suppl), S391–4.

SEDDON, A. M., CURNOW, P., BOOTH, P. J. (2004). Membrane proteins, lipids and detergents: not just a soap opera. *Biochimica et biophysica acta, 1666*(1-2), 105–17.

SEGURA, A. M., LUNA, R. E., HORIBA, K., STETLER-STEVENSON, W. G., MCALLISTER, H. A., WILLERSON, J. T., FERRANS, V. J. (1998). Immunohistochemistry of matrix metalloproteinases and their inhibitors in thoracic aortic aneurysms and aortic valves of patients with Marfan's syndrome. *Circulation*, *98*(19 Suppl), II331–7; discussion II337–8.

SELIKTAR, D., BLACK, R. A., VITO, R. P., NEREM, R. M. (2000). Dynamic mechanical conditioning of collagen-gel blood vessel constructs induces remodeling in vitro. *Annals of biomedical engineering, 28*(4), 351–62.

SHAH, S. R., and VYAVAHARE, N. R. (2008). The effect of glycosaminoglycan stabilization on tissue buckling in bioprosthetic heart valves. *Biomaterials*, *29*(11), 1645–53.

SHEKAR, P. S., COUPER, G. S., COHN, L. H. (2005). Mitral valve re-repair. *The Journal of heart valve disease*, *14*(5), 583–7.

SHI, Y., and VESELY, I. (2003). Fabrication of mitral valve chordae by directed collagen gel shrinkage. *Tissue engineering, 9*(6), 1233–42.

SHI, Y., and VESELY, I. (2004). Characterization of statically loaded tissue-engineered mitral valve chordae tendineae. *Journal of biomedical materials research. Part A, 69*(1), 26–39.

SHINOKA, T., BREUER, C. K., TANEL, R. E., ZUND, G., MIURA, T., MA, P. X., LANGER, R., VACANTI, J. P., MAYER, J. E. (1995). Tissue engineering heart valves: valve leaflet replacement study in a lamb model. *The Annals of thoracic surgery, 60*(6 Suppl), S513–6.

SIEVERS, H.-H., STIERLE, U., SCHMIDTKE, C., BECHTEL, M. (2003). Decellularized pulmonary homograft (SynerGraft) for reconstruction of the right ventricular outflow tract: first clinical experience. *Zeitschrift für Kardiologie, 92*(1), 53–9.

SIMON, P., KASIMIR, M. T., SEEBACHER, G., WEIGEL, G., ULLRICH, R., SALZER-MUHAR, U., RIEDER, E., WOLNER, E. (2003). Early failure of the tissue engineered porcine heart valve SYNERGRAFT in pediatric patients. *European journal of cardio-thoracic surgery : official journal of the European Association for Cardio-thoracic Surgery*, *23*(6), 1002–6; discussion 1006.

SIROIS, E., CHARARA, J., RUEL, J., DUSSAULT, J. C., GAGNON, P., DOILLON, C. J. (1998). Endothelial cells exposed to erythrocytes under shear stress: An in vitro study. *Biomaterials*, *19*(21), 1925–1934.

SKALLI, O., PELTE, M. F., PECLET, M. C., GABBIANI, G., GUGLIOTTA, P., BUSSOLATI, G., RAVAZZOLA, M., ORCI, L. (1989). Alpha-smooth muscle actin, a differentiation marker of smooth muscle cells, is present in microfilamentous bundles of pericytes. *The journal of histochemistry and cytochemistry : official journal of the Histochemistry Society, 37*(3), 315–21.

SMEDIRA, N. G., SELMAN, R., COSGROVE, D. M., MCCARTHY, P. M., LYTLE, B. W., TAYLOR, P. C., APPERSON-HANSEN, C., STEWART, R. W., LOOP, F. D. (1996). Repair of anterior leaflet prolapse: chordal transfer is superior to chordal shortening. *The Journal of thoracic and cardiovascular surgery*, *112*(2), 287–91; discussion 291–2.

SODIAN, R., LEMKE, T., LOEBE, M., HOERSTRUP, S. P., POTAPOV, E. V., HAUSMANN, H., MEYER, R., HETZER, R. (2001). New pulsatile bioreactor for fabrication of tissue-engineered patches. *Journal of Biomedical Materials Research*, *58*(4), 401–405.

SPIEGELSTEIN, D., GHOSH, P., STERNIK, L., TAGER, S., SHINFELD, A., RAANANI, E. (2007). Current strategies of mitral valve repair. *The Israel Medical Association journal : IMAJ*, *9*(4), 303–9.

STAPLETON, T. W., INGRAM, J., KATTA, J., KNIGHT, R., KOROSSIS, S., FISHER, J., INGHAM, E. (2008). Development and characterization of an acellular porcine medial meniscus for use in tissue engineering. *Tissue engineering. Part A*, *14*(4), 505–18.

STAUB, F., BAETHMANN, A., PETERS, J., WEIGT, H., KEMPSKI, O. (1990). Effects of lactacidosis on glial cell volume and viability. *Journal of cerebral blood flow and metabolism : official journal of the International Society of Cerebral Blood Flow and Metabolism*, *10*(6), 866–76.

STINSON, E. B., GRIEPP, R. B., OYER, P. E., SHUMWAY, N. E. (1977). Long-term experience with porcine aortic valve xenografts. *The Journal of thoracic and cardiovascular surgery*, *73*(1), 54–63.

STINSON, E. B., GRIEPP, R. B., SHUMWAY, N. E. (1974). Clinical experience with a porcine aortic valve xenograft for mitral valve replacement. *The Annals of Thoracic Surgery*, *18*(4), 391–401.

SUTHERLAND, F. W. H., PERRY, T. E., YU, Y., SHERWOOD, M. C., RABKIN, E., MASUDA, Y., GARCIA, G. A., MCLELLAN, D. L., ENGELMAYR, G. C. JR., SACKS, M. S., SCHOEN, F. J., MAYER, J. E. (2005). From stem cells to viable autologous semilunar heart valve. *Circulation, 111*(21), 2783–91.

SYEDAIN, Z. H., WEINBERG, J. S., TRANQUILLO, R. T. (2008). Cyclic distension of fibrin-based tissue constructs: evidence of adaptation during growth of engineered connective tissue. *Proceedings of the National Academy of Sciences of the United States of America*, *105*(18), 6537–42.

SYEDAIN, Z. H., and TRANQUILLO, R. T. (2009). Controlled cyclic stretch bioreactor for tissue-engineered heart valves. *Biomaterials*, *30*(25), 4078–84.

TAKAHASHI, K., and YAMANAKA, S. (2006). Induction of pluripotent stem cells from mouse embryonic and adult fibroblast cultures by defined factors. *Cell, 126*(4), 663–676.

TARONE, G., GALETTO, G., PRAT, M., COMOGLIO, P. M. (1982). Cell surface molecules and fibronectin-mediated cell adhesion: effect of proteolytic digestion of membrane proteins. *The Journal of cell biology, 94*(1), 179–86.

TAYLOR, P. M., BATTEN, P., BRAND, N. J., THOMAS, P. S., YACOUB, M. H. (2003). The cardiac valve interstitial cell. *The international journal of biochemistry & cell biology*, *35*(2), 113–8.

THELEMAN, K. P., GRAYBURN, P. A., ROBERTS, W. C. (2006). Mitral “annular” calcium forming a complete circle “O” causing mitral stenosis in association with a stenotic congenitally bicuspid aortic valve and severe coronary artery disease. *The American journal of geriatric cardiology*, *15*(1), 58–61.

THEODORIDIS, K., CALISTRU, A., MEYER, T., TUDORACHE, I., CEBOTARI, S., SARIKOUCH, S., BARA, C., BREHM, R., HILFIKER, A., HAVERICH, A. (2013). An analysis of tissue-engineered pulmonary valves implanted in the elderly ovine model. *QScience Proceedings*, 2012, Heart Valve Biology and Tissue Engineering.

THOMAS, D.S., INGHAM, E., FISHER, J., KOROSSIS, S. (2009). Tissue Engineering of the Mitral Heart Valve Leaflet. *Tissue Engineering and Regenerative Medicine Society (TERMIS) conference.*

THUBRIKAR, M., NOLAN, S. P., BOSHER, L. P., DECK, J. D. (1980). The cyclic changes and structure of the base of the aortic valve. *American Heart Journal*, *99*(2), 217–224.

TILL, J. E., and MCCULLOCH, E. A. (1961). A direct measurement of the radiation sensitivity of normal mouse bone marrow cells. *Radiation research*, *14*, 213–22.

TIMPL, R., ROHDE, H., ROBEY, P. G., RENNARD, S. I., FOIDART, J. M., MARTIN, G. R. (1979). Laminin--a glycoprotein from basement membranes. *The Journal of biological chemistry, 254*(19), 9933–7.

TORTORA, G. J. and NELSEN, M. T. (2009). Principles of human anatomy. 11th edition. John Wiley & Sons.

TRANQUILLO, R. T., and GIRTON, T. S (2003). Tissue engineered cardiovascular valve. US patent. Application number 6,666,886.

TULADHAR, S. M. and PUNJABI, P. P. (2006). Surgical reconstruction of the mitral valve. *Heart, 92*(10), 1373-7.

TURI, Z. G. (2004). Cardiology patient page. Mitral valve disease. *Circulation*, *109*(6), e38–41.

TWENTYMAN, P. R., and LUSCOMBE, M. (1987). A study of some variables in a tetrazolium dye (MTT) based assay for cell growth and chemosensitivity. *British journal of cancer*, *56*(3), 279–85.

ULBRICHT, A., EPPLER, F. J., TAPIA, V. E., VAN DER VEN, P. F. M., HAMPE, N., HERSCH, N., VAKEEL, P., STADEL, D., HAAS, A., SAFTIG, P., BEHRENDS, C., FÜRST, C. O., VOLKMER, R., HOFFMANN, B., KOLANUS, W., HÖHFELD, J. (2013). Cellular Mechanotransduction relies on tension-induced and chaperone-assisted autophagy. *Current Biology, 23*(5), 430–435.

VÄÄNÄNEN, H. K. (2005). Mesenchymal stem cells. *Annals of medicine*, *37*(7), 469–79.

VACANTI, J. P., and LANGER, R. (1999). Tissue engineering: the design and fabrication of living replacement devices for surgical reconstruction and transplantation. *The Lancet*, *354*, S32–S34.

VAN DEN BOS, C., SILVERSTETTER, S., MURPHY, M., CONNOLLY, T. (1998). p21(cip1) rescues human mesenchymal stem cells from apoptosis induced by low-density culture. *Cell and tissue research*, *293*(3), 463–70.

VAN DER FLIER, A., and SONNENBERG, A. (2001). Function and interactions of integrins. *Cell and tissue research*, *305*(3), 285–98.

VESELY, I. (2005). Heart valve tissue engineering. *Circulation research, 97*(8), 743–55.

VESELY, I., and BOUGHNER, D. (1989). Analysis of the bending behaviour of porcine xenograft leaflets and of natural aortic valve material: bending stiffness, neutral axis and shear measurements. *Journal of biomechanics, 22*(6-7), 655–71.

VESELY, I., BOUGHNER, D., SONG, T. (1988). Tissue buckling as a mechanism of bioprosthetic valve failure. *The Annals of thoracic surgery*, *46*(3), 302–8.

VINCENTELLI, A., WAUTOT, F., JUTHIER, F., FOUQUET, O., CORSEAUX, D., MARECHAUX, S., LE TOURNEAU, T., FABRE, O., SUSEN, S., VAN BELLE, E., MOUQUET, F., DECOENE, C., PRAT, A., JUDE, B. (2007). In vivo autologous recellularization of a tissue-engineered heart valve: are bone marrow mesenchymal stem cells the best candidates? *The Journal of thoracic and cardiovascular surgery*, *134*(2), 424–32.

VIRMANI, R. (1980). Quantification of coronary arterial narrowing and of left ventricular myocadial scarring in healed myocardial infarction with chronic eventually fatal, congestive cardiac failure. *American Journal of Medicine, 68,* 831-838.

VON OPPELL, U. O., and MOHR, F. W. (2000). Chordal replacement for both minimally invasive and conventional mitral valve surgery using premeasured Gore-Tex loops. *The Annals of thoracic surgery*, *70*(6), 2166–8.

VOTTA, E., CAIANI, E., VERONESI, F., SONCINI, M., MONTEVECCHI, F. M., REDAELLI, A. (2008). Mitral valve finite-element modelling from ultrasound data: a pilot study for a new approach to understand mitral function and clinical scenarios. Philosophical transactions. *Series A, Mathematical, physical, and engineering sciences, 366*(1879), 3411–34.

VYAVAHARE, N., HIRSCH, D., LERNER, E., BASKIN, J. Z., SCHOEN, F. J., BIANCO, R., KRUTH, H. S., ZAND, R., LEVY, R. J. (1997). Prevention of bioprosthetic heart valve calcification by ethanol preincubation. Efficacy and mechanisms. *Circulation*, *95*(2), 479–88.

WANG, N., BUTLER, J. P., INGBER, D. E. (1993). Mechanotransduction across the cell surface and through the cytoskeleton. *Science (New York, N.Y.), 260*(5111), 1124–7.

WANG, Y., KIM, U.-J., BLASIOLI, D. J., KIM, H.-J., KAPLAN, D. L. (2005). In vitro cartilage tissue engineering with 3D porous aqueous-derived silk scaffolds and mesenchymal stem cells. *Biomaterials*, *26*(34), 7082–94.

WATKINS, M. W., and LEWINTER, M. M. (1993). Physiologic role of the normal pericardium. *Annual review of medicine*, *44*, 171–80.

WEBER, E., ROSSI, A., SOLITO, R., SACCHI, G., AGLIANO', M., GERLI, R. (2002). Focal adhesion molecules expression and fibrillin deposition by lymphatic and blood vessel endothelial cells in culture. *Microvascular research*, *64*(1), 47–55.

WEBER, B., EMMERT, M. Y., HOERSTRUP, S. P. (2012). Stem cells for heart valve regeneration. *Swiss medical weekly*, *142*, w13622.

WEBER, M., HETA, E., MOREIRA, R., GESCHE, V. N., SCHERMER, T., FRESE, J., JOCKENHOEVEL, S., MELA, P. (2013). Tissue-engineered fibrin-based heart valve with a tubular leaflet design. *Tissue engineering. Part C, Methods*.

WEINBERG, C. B., and BELL, E. (1986). A blood vessel model constructed from collagen and cultured vascular cells. *Science (New York, N.Y.), 231*(4736), 397–400.

WEISS, R. A. (1998). Transgenic pigs and virus adaptation. *Nature*, *391*(6665), 327–8.

WESTON, M. W., and YOGANATHAN, A. P. (2001). Biosynthetic activity in heart valve leaflets in response to in vitro flow environments. *Annals of biomedical engineering*, *29*(9), 752–63.

WICK, T.M., and FAROOQUE, T. (2009). Bioreactor development for cartilage tissue engineering: computational modelling and experimental results. Seventh International Conference on CFD in the Minerals and Process Industries. Australia.

WILCOX, H.E., KOROSSIS, S.A., BOOTH, C., WATTERSON, K.G., KEARNEY, J.N., FISHER. J., INGHAM, E. (2005). Biocompatibility and recellularization potential of an acelluar porcine heart valve matrix. *The journal of heart valve disease, 14,* 228-237; discussion 236–7.

WILLIAMS, S. F., MARTIN, D. P., HOROWITZ, D. M., PEOPLES, O. P. (1999). PHA applications: addressing the price performance issue. *International Journal of Biological Macromolecules, 25*(1), 111–121.

WILSHAW, S.-P., KEARNEY, J. N., FISHER, J., INGHAM, E. (2006). Production of an acellular amniotic membrane matrix for use in tissue engineering. *Tissue engineering*, *12*(8), 2117–29.

WILSON, C. A., WONG, S., MULLER, J., DAVIDSON, C. E., ROSE, T. M., BURD, P. (1998). Type C retrovirus released from porcine primary peripheral blood mononuclear cells infects human cells. *Journal of virology*, *72*(4), 3082–7.

WONG, T., MCGRATH, J. A., NAVSARIA, H. (2007). The role of fibroblasts in tissue engineering and regeneration. *The British journal of dermatology*, *156*(6), 1149–55.

WOODS, T., and GRATZER, P. F. (2005). Effectiveness of three extraction techniques in the development of a decellularized bone-anterior cruciate ligament-bone graft. *Biomaterials*, *26*(35), 7339–49.

World Health Organisation (2004). World heart organization: Rheumatic fever and rheumatic heart disease. *Tech. Rep. Series, 923*, 1-122.

WURZINGER, L. J., and SCHMID-SCHÖNBEIN, H. (1990). The role of fluid dynamics in triggering and amplifying hemostatic reactions in thrombogenesis. *Monographs on atherosclerosis*, *15*, 215–26.

XU, C. C., CHAN, R. W., TIRUNAGARI, N. (2007). A biodegradable, acellular xenogeneic scaffold for regeneration of the vocal fold lamina propria. *Tissue engineering, 13*(3), 551–66.

YANG, C., HILLAS, P. J., BÁEZ, J. A., NOKELAINEN, M., BALAN, J., TANG, J., SPIRO, R., POLAREK, J. W. (2004). The application of recombinant human collagen in tissue engineering. *BioDrugs : clinical immunotherapeutics, biopharmaceuticals and gene therapy*, *18*(2), 103–19.

YAU, T. M., EL-GHONEIMI, Y. A., ARMSTRONG, S., IVANOV, J., DAVID, T. E. (2000). Mitral valve repair and replacement for rheumatic disease. *The Journal of thoracic and cardiovascular surgery*, *119*(1), 53–60.

YE, Q., ZÜND, G., BENEDIKT, P., JOCKENHOEVEL, S., HOERSTRUP, S. P., SAKYAMA, S., HUBBELL, J. A., TURINA, M. (2000). Fibrin gel as a three dimensional matrix in cardiovascular tissue engineering. *European journal of cardio-thoracic surgery: official journal of the European Association for Cardio-thoracic Surgery, 17*(5), 587–91.

YE, X., ZHAO, Q., SUN, X., LI, H. (2009). Enhancement of mesenchymal stem cell attachment to decellularized porcine aortic valve scaffold by in vitro coating with antibody against CD90: a preliminary study on antibody-modified tissue-engineered heart valve. *Tissue engineering. Part A*, *15*(1), 1–11.

YOON, Y.-S., PARK, J.-S., TKEBUCHAVA, T., LUEDEMAN, C., LOSORDO, D. W. (2004). Unexpected severe calcification after transplantation of bone marrow cells in acute myocardial infarction. *Circulation*, *109*(25), 3154–7.

ZELTINGER, J., LANDEEN, L. K., ALEXANDER, H. G., KIDD, I. D., SIBANDA, B. (2001). Development and characterization of tissue-engineered aortic valves. *Tissue engineering, 7*(1), 9–22.

APPENDIX

Stress-strain behaviour of the leaflet anterior groups

The stress-strain behaviour of the leaflet anterior groups, circumferential and radial, are illustrated in Figure A.1-A.6 and Figure A.7-A.12, respectively.

Only the data corresponding to the final loading ramp to failure, following preconditioning, were used in the subsequent analysis. The recorded force-extension histories of the samples were converted to stress strain in Microsoft Excel XP, as described in Section 2.18.3, and the stress-strain behaviour of the specimens was plotted. The six mechanical parameters were calculated as follows. The ultimate tensile strength (σ_{uts}) and the failure strain corresponded to the Y and X coordinates at the failure point of the curve. All the values of stress and strain from the σ_{uts} and failure strain onwards were discarded. Then, a line was drawn to fit and identify the linear region of the collagen phase and the elastin phase (Figure A.1). The elastin (El-E) and collagen phase slope (Coll-E) were calculated by selecting the stress and strain values correspondent to the linear region of the curve, and then the same interval was selected and processed on Origin Pro 8 to calculate the slope by using the function Fit-Linear. The transition strain corresponded to the X coordinate at which the line of the Coll-E crossed the X axsis, and the transition stress corresponded to the Y coordinate of the projection of the transition strain on the stress-strain curve (Figure A.1). The six parameters for each specimen were finally averaged over the number of specimens in the group, and analysed statistically, as described in Section 2.19.

The same analysis was performed for the leaflet posterior groups and the fresh and decellularised pericardial groups.

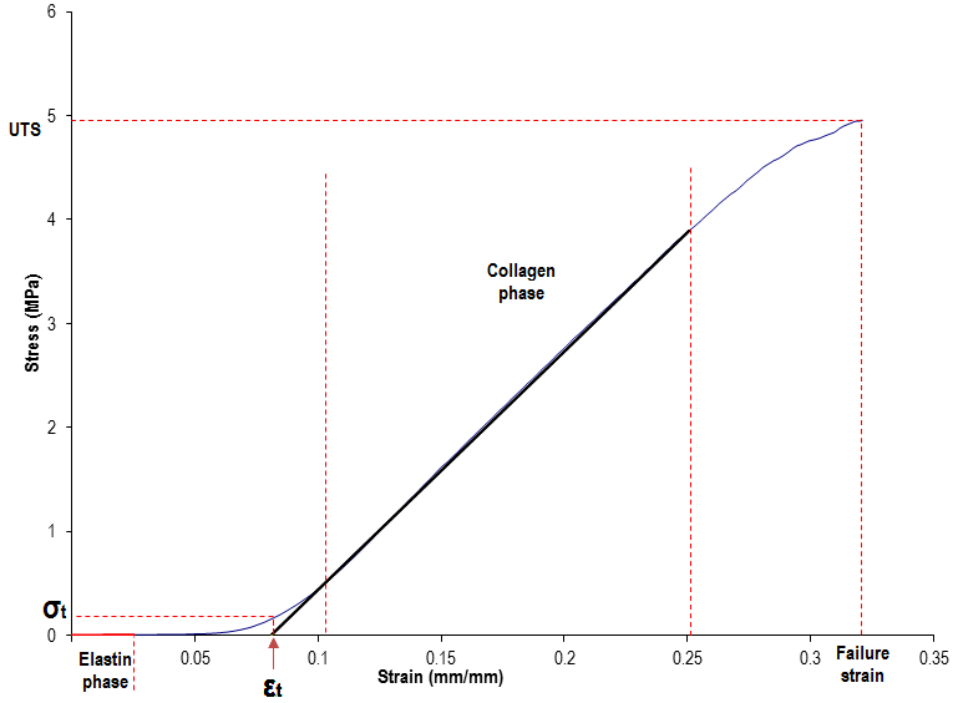

Figure A.1: Leaflet anterior circumferential – sample 1. The red and black lines indicate the elastin and collagen phase region, respectively. σ_t: transition stress; ε_t: transition strain; UTS: ultimate tensile strength.

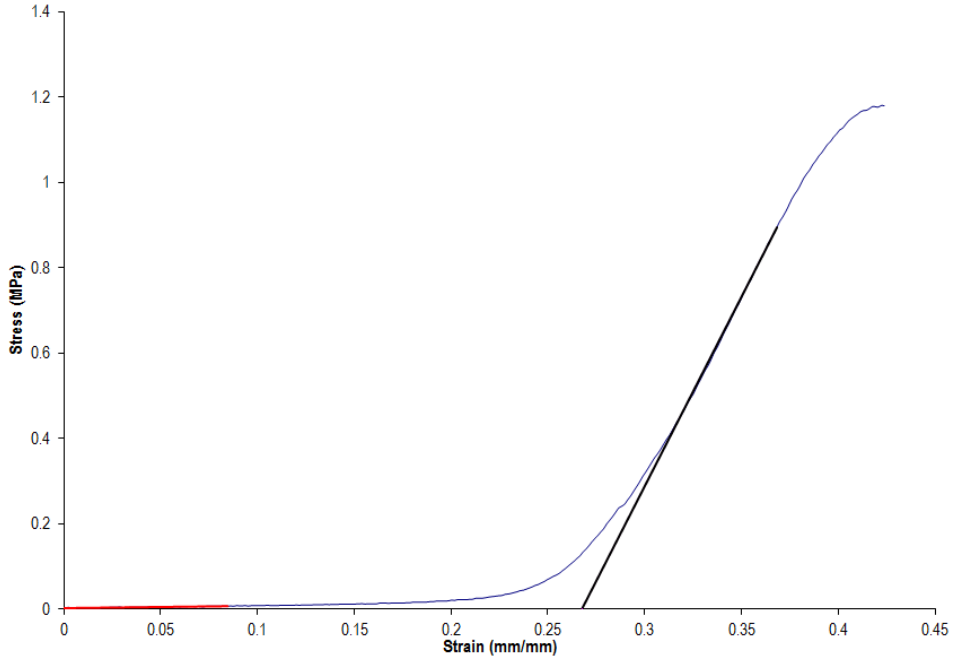

Figure A.2: Leaflet anterior circumferential – sample 2. The red and black lines indicate the elastin and collagen phase region, respectively.

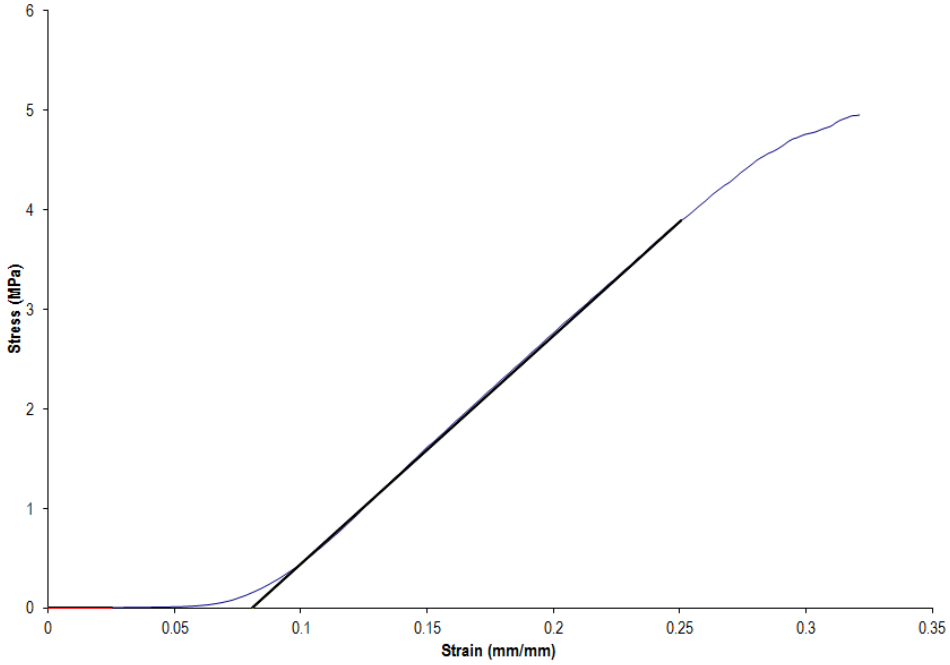

Figure A.3: Leaflet anterior circumferential – sample 3. The red and black lines indicate the elastin and collagen phase region, respectively.

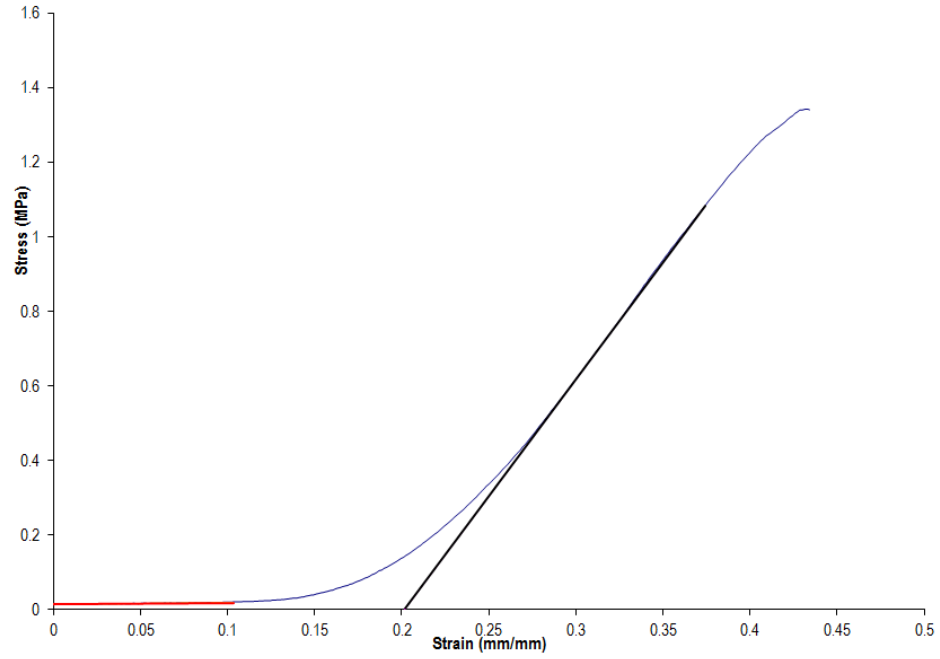

Figure A.4: Leaflet anterior circumferential – sample 4. The red and black lines indicate the elastin and collagen phase region, respectively.

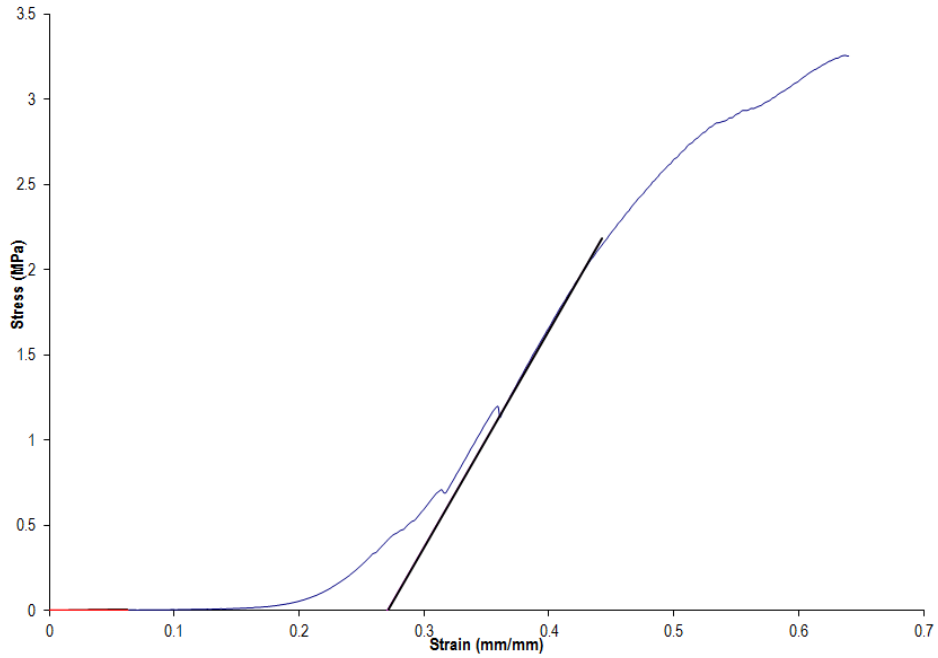

Figure A.5: Leaflet anterior circumferential – sample 5. The red and black lines indicate the elastin and collagen phase region, respectively.

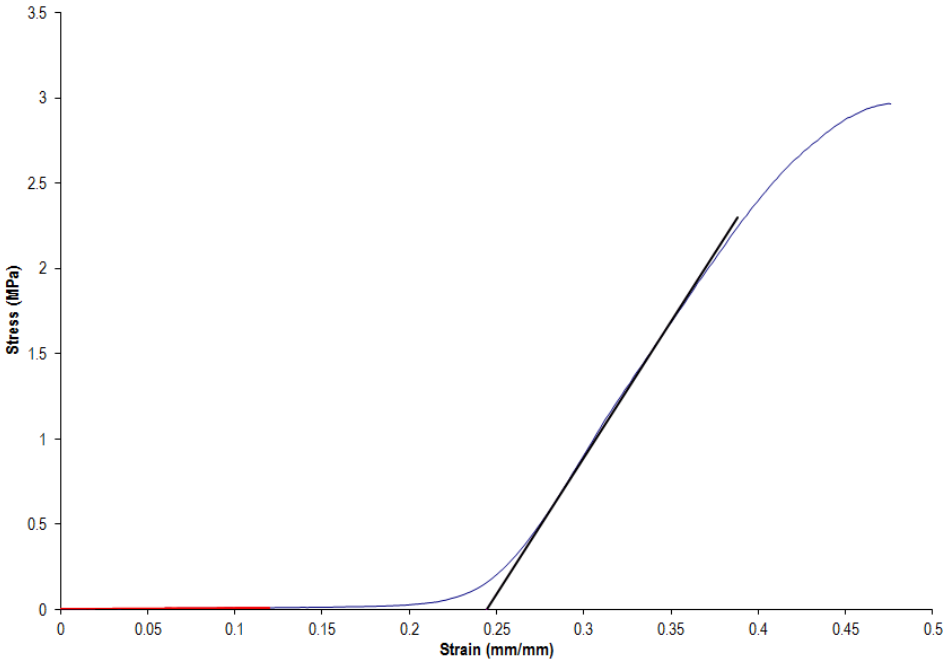

Figure A.6: Leaflet anterior circumferential – sample 6. The red and black lines indicate the elastin and collagen phase region, respectively.

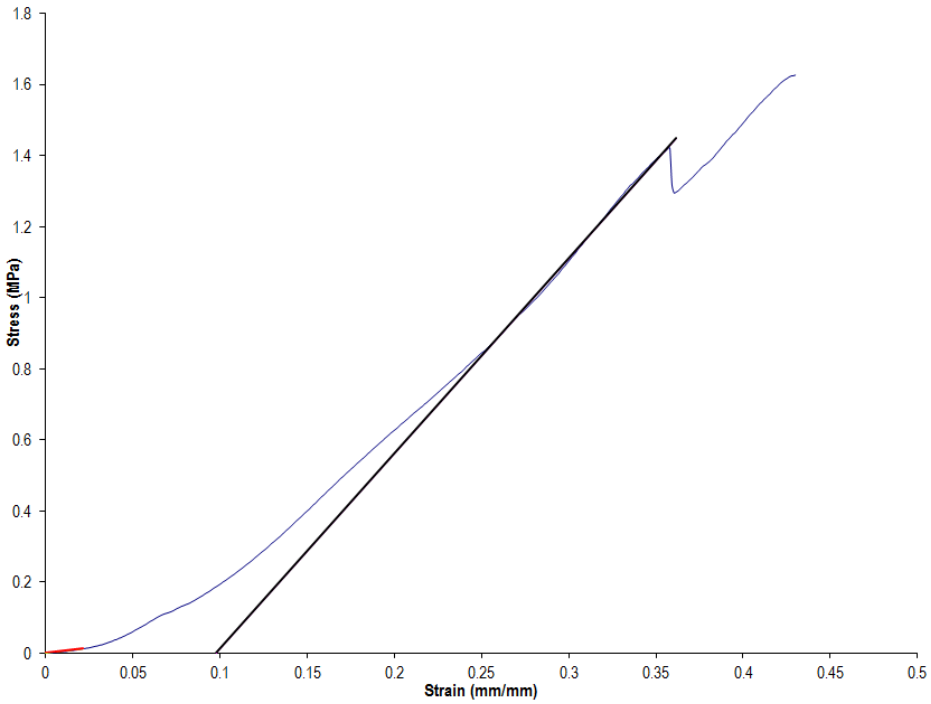

Figure A.7: Leaflet anterior radial – sample 1. The red and black lines indicate the elastin and collagen phase region, respectively.

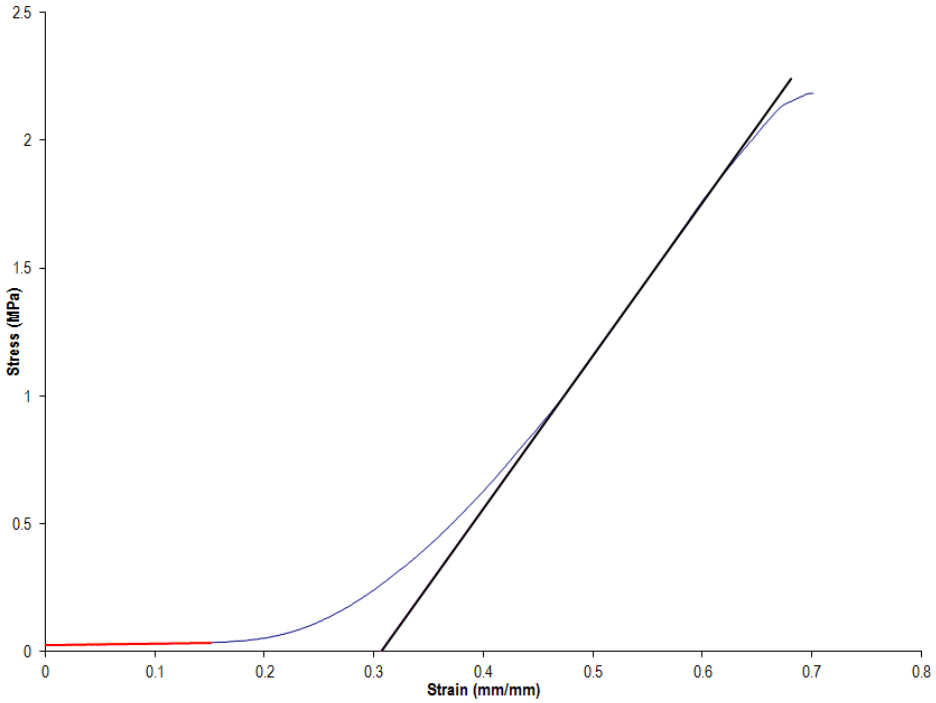

Figure A.8: Leaflet anterior radial – sample 2. The red and black lines indicate the elastin and collagen phase region, respectively.

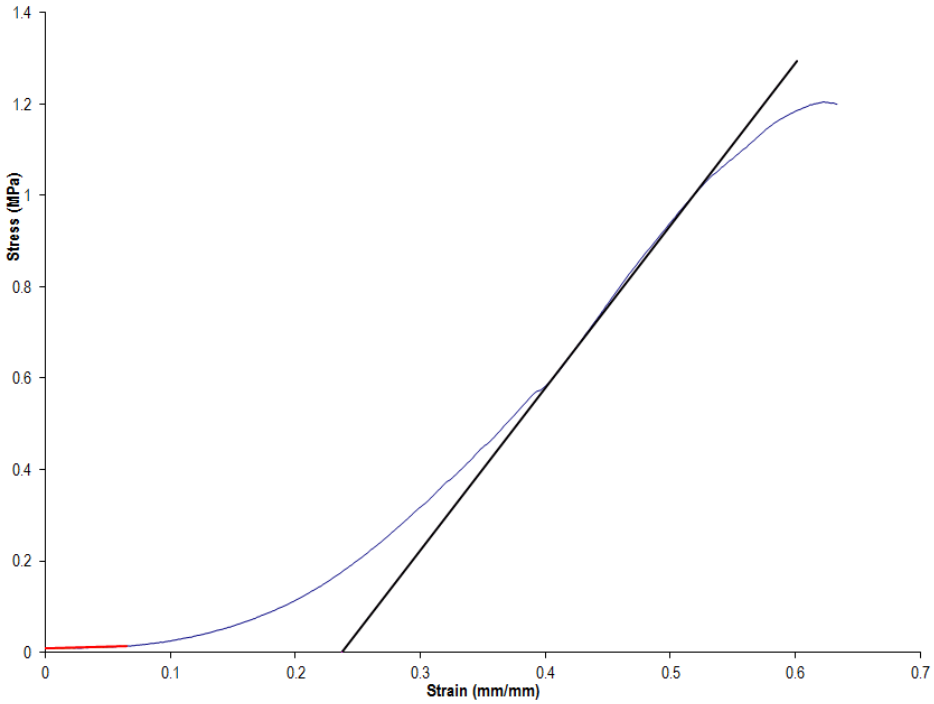

Figure A.9: Leaflet anterior radial – sample 3. The red and black lines indicate the elastin and collagen phase region, respectively.

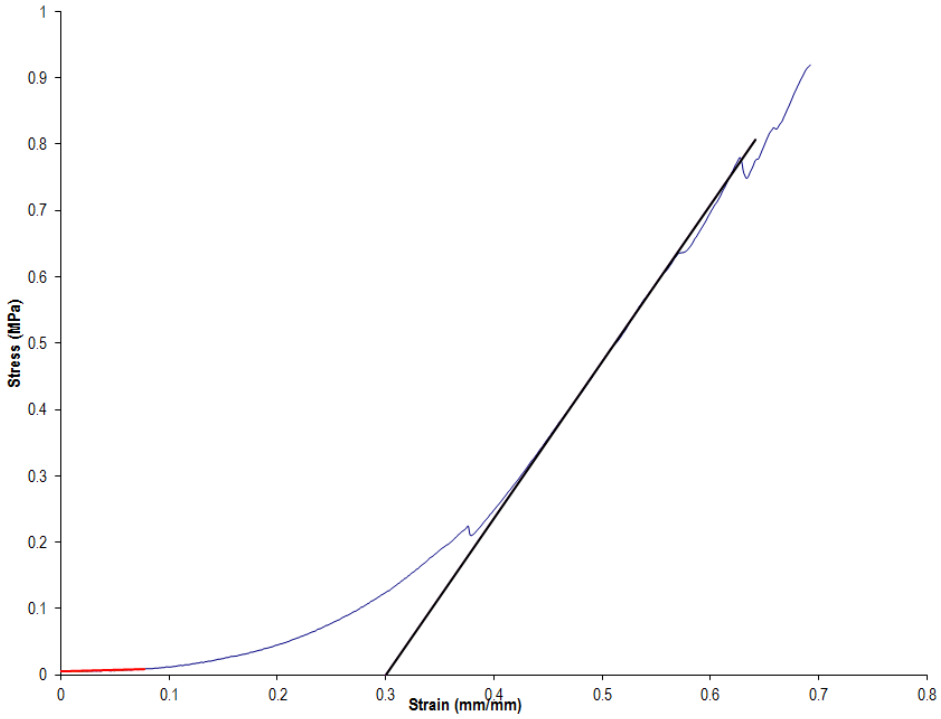

Figure A.10: Leaflet anterior radial – sample 4. The red and black lines indicate the elastin and collagen phase region, respectively.

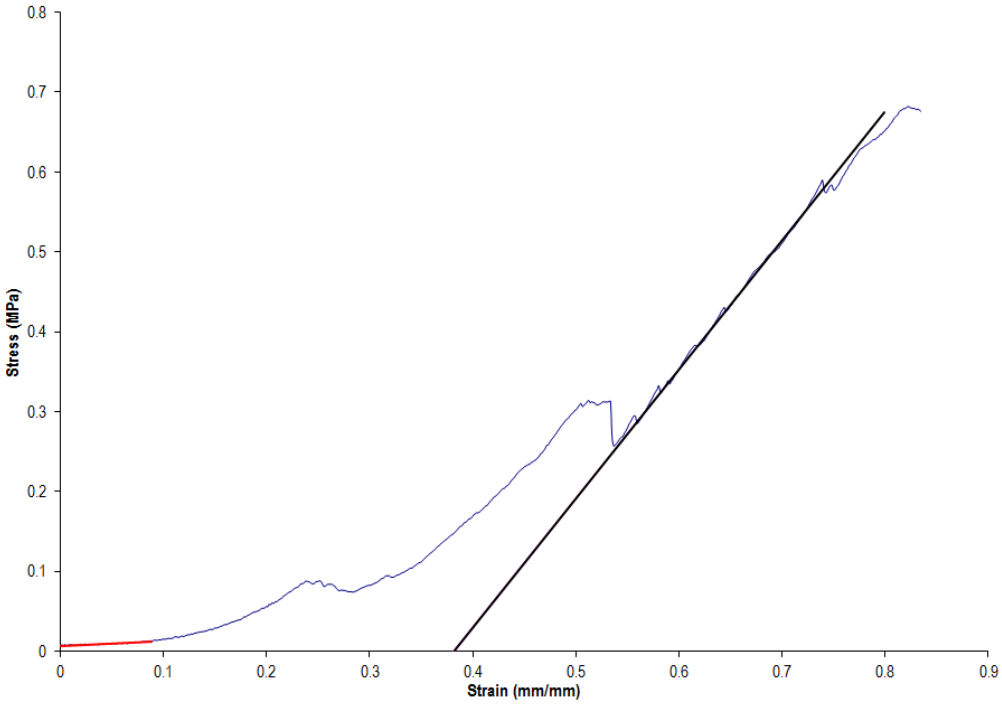

Figure A.11: Leaflet anterior radial – sample 5. The red and black lines indicate the elastin and collagen phase region, respectively.

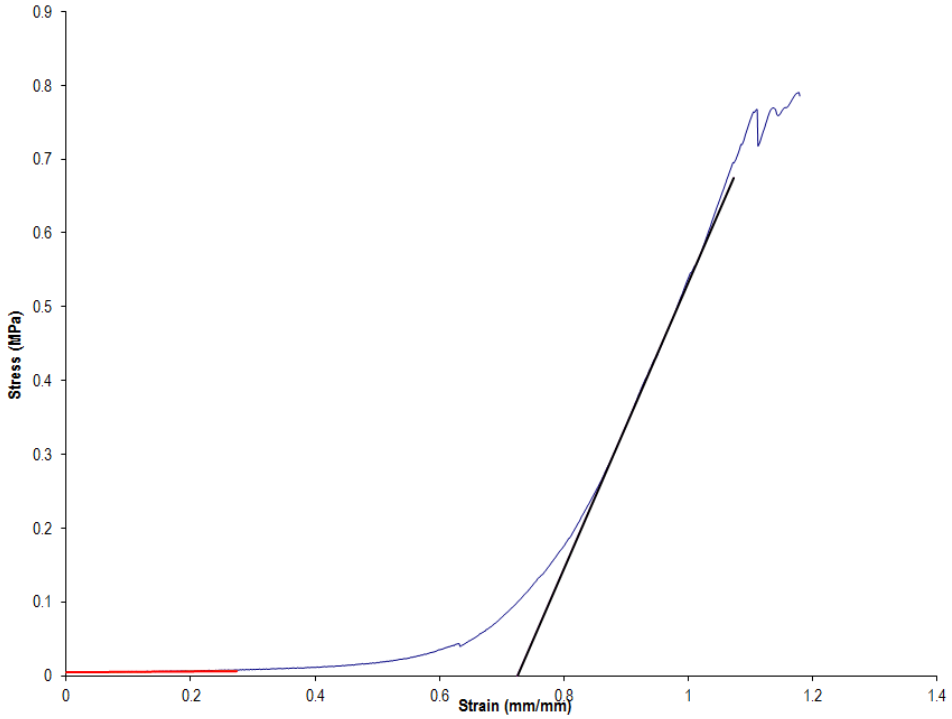

Figure A.12: Leaflet anterior radial – sample 6. The red and black lines indicate the elastin and collagen phase region, respectively.